STUDY ON BUBBLE GENERATION, GROWTH AND DEPARTURE FROM A NUCLEAR FUEL PIN UNDER BOILING CONDITIONS

By
PARUL GOEL

ENGG01201304008

Bhabha Atomic Research Center, Mumbai

A thesis submitted to the

Board of Studies in Engineering Sciences

In partial fulfillment of requirements

for the Degree of

DOCTOR OF PHILOSOPHY

of

HOMI BHABHA NATIONAL INSTITUTE

April, 2019

STATEMENT BY AUTHOR

This dissertation has been submitted in partial fulfillment of requirements for an advanced degree at Homi Bhabha National Institute (HBNI) and is deposited in the Library to be made available to borrowers under rules of the HBNI.

Brief quotations from this dissertation are allowable without special permission, provided that accurate acknowledgement of source is made. Requests for permission for extended quotation from or reproduction of this manuscript in whole or in part may be granted by the Competent Authority of HBNI when in his or her judgment the proposed use of the material is in the interests of scholarship. In all other instances, however, permission must be obtained from the author.

Parul Goel

DECLARATION

I, hereby declare that the investigation presented in the thesis has been carried out by me. The work is original and has not been submitted earlier as a whole or in part for a degree / diploma at this or any other Institution / University.

Parul Goel

List of Publications arising from the thesis

Journal

1. "Experimental study on bubble departure characteristics in subcooled nucleate pool boiling", P. Goel, A.K. Nayak, P. P. Kulkarni, J.B. Joshi, *Int. J. Multiphase Flow*, **2017**, 89, 163-176.
2. "Bubble departure characteristics in a tube bundle under cross flow conditions", P. Goel, A. K. Nayak, M.K. Das, J.B. Joshi, *Int. J. Multiphase Flow*, **2018,** 100, 143-154.
3. "Experimental study of bubble departure characteristics in forced convective subcooled nucleate boiling", P. Goel, A. K. Nayak, P. Ghosh, J.B. Joshi, *Experimental Heat Transfer*, 2018, 31(3), 194-218.
4. "Experimental study of bubble departure characteristics in forced convective nucleate boiling in 4-rod bundle", P. Goel, A. K. Nayak, P. Ghosh, J.B. Joshi, *Int. J. Multiphase Flow*. (Under review).

Conferences

1. P. Goel, A. K. Nayak, J.B. Joshi, M. K. Das, Experimental Study of Vapor Bubble Departure Characteristics for a Cylindrical Heater under Cross Flow Conditions. 6th International and 43rd National Conference on Fluid Mechanics and Fluid Power, Allahabad, U.P., India, December 15-17, 2016.
2. P. Goel, A. K. Nayak, J.B. Joshi, Numerical Study of the Bundle Effect in the Convective Heat Transfer. ICHMT International Symposium on Advances in Computational Heat Transfer, Napoli, Italy, May 28-June 1, 2017.
3. P. Goel, A. K. Nayak, J. B. Joshi, Experimental Study of Bubble Dynamics in Forced Convective Subcooled Nucleate Boiling. Paper 21307, 17th International Topical Meeting on Nuclear Reactor Thermal Hydraulics (NURETH-17), Xi'an, China, September 3-8, 2017.

Parul Goel

All that I am or ever hope to be,

I owe it to my Angel Mother…

-Abraham Lincoln

Dedicated to my mother.

The strength behind my will.

ACKNOWLEDGEMENTS

CONTENTS

LIST OF FIGURES

LIST OF TABLES

Homi Bhabha National Institute

SYNOPSIS OF Ph. D. THESIS

1. **Name of the Student:** Parul Goel
2. **Name of the Constituent Institution:** Bhabha Atomic Research Centre
3. **Enrolment No.:** ENGG01201304008
4. **Title of the Thesis:** Study on bubble generation, growth and departure from a nuclear fuel pin under boiling conditions
5. **Board of Studies:** Engineering Sciences

SYNOPSIS

Nuclear fuel bundle geometry consists of several fuel pins arranged in horizontal or vertical arrays depending on the kind of nuclear reactor. The Boiling Water reactors (BWRs), Pressurized water reactors (PWRs) and the Indian Advanced Heavy Water Reactor (AHWR) have the vertical fuel bundles with the coolant flowing from bottom to top, while the Pressurized Heavy Water Reactors (PHWRs) have horizontal array of fuel bundles where the coolant flows from one end to other. The coolant (water) undergoes boiling in the reactor core under normal operating conditions in a BWR or in AHWR, and under accidental conditions such as in LOCA in PHWR. One of the important boiling regimes observed in the above conditions is *nucleate boiling,* characterised by the bubbles nucleating, growing and departing from the heating surface, due to the surface temperature being higher than the saturation temperature of the coolant at the system pressure. This process is a highly efficient means of heat transfer, although the heat flux needs to be maintained below the critical heat flux level (CHF) to avoid any damage to the fuel pins. Hence, understanding boiling mechanism and predicting the two-phase heat transfer behaviour in nuclear rod bundle is essential for safe design and operation of the nuclear reactors.

Traditionally, 1-D system codes have been used to study the thermal hydraulics of nuclear reactor fuel bundles. But, in the last few years, with the development of computational codes, there has been a thrust for multi-dimensional, multi-scale models for two phase flows. These models, however, are still under development and require closure relations based on phenomenological models for various parameters in the computational models. These models require a good understanding of the flow physics and bubble behaviour for development, and substantial amount of data in the wide range of relevant conditions for validation. The most important input parameters, for which models are required, are the bubble departure diameter, departure frequency, active nucleation site density and bubble growth rate. These parameters are required for closure relations to evaluate the contributions of different heat transfer mechanisms in two-phase conditions, namely, convection and evaporative heat transfer.

From the literature review, we see that a number of correlations exist for bubble departure diameter (Fritz 1935, Unal 1976, Prodanovic et al. 2002) and frequency (Cole 1960) in pool and flow boiling conditions. But an analysis of these data and models show a wide variation among themselves. Besides, these models have been validated with limited data. Further, the bubble characteristics data show contradictory behaviour in different studies in both pool and flow boiling. For example, the bubble departure diameter and frequency are found to increase with heat flux by some authors while other find them to decrease with heat flux. In addition, there are almost no studies for bubble characteristics in cross flow boiling which are of relevant to rod bundles of PHWRs. In natural circulation BWRs like AHWR, during start-up of this reactor, the mass flux is very small. Similar conditions may prevail in PHWRs in accidents involving boiling on horizontal rod bundles with no pumps available. The bubble characteristics under low heat flux and mass flux conditions, have not been studied earlier. Hence, the objective of this thesis is to investigate the bubble departure characteristics in a variety of geometries and operating conditions relevant to different nuclear reactors under pool and forced convective boiling. In addition, experiments have been conducted to generate data considering the influence of heater size, geometry and surface characteristics, and to compare our

data with that available in literature, and develop more suitable models for the bubble departure

parameters which can be adopted for closures in CFD codes.

Thus, the objective of the thesis is to clarify and resolve the following unresolved issues as

described below.

1. <u>Unresolved Issue-1:</u>

Effect of operating conditions, heater surface characteristics and geometry on bubble characteristics

in pool boiling is not clearly understood. The existing correlations have large error bands.

To address this aspect, an extensive set of experiments were carried out in pool boiling. The

schematic of the experimental setup is given in *Figure 1*. Four kinds of heater samples were used, i.e.

three stainless steel (SS 316) rods of different surface roughness and a SS ribbon to study the effect

of surface characteristics and size dependence. The heater rod 2 was also inclined at 45°, and 90° to

the horizontal to study the effect of inclination angle. The details of the heaters are provided in Table

1. The experimental conditions were: bulk liquid subcooling $\Delta T_{sub} = 5\ K, 10\ K, 20\ K$, wall

superheat $\Delta T_{sat} = 0 - 15\ K$ and heat flux $q" = 0 - 300\ kW/m^2$.

Table 1 Properties of heater elements

Heater element	Dimensions (mm)	Surface roughness (μm)	Static contact angle (°)	Inclination angle (°)
SS rod 1	$l = 107$ $d = 4$	0.5	65°	0°
SS rod 2	$l = 93.2$ $d = 4$	1.0	60°	0°, 45°, 90°
SS rod 3	$l = 93.8$ $d = 4$	3.54	54°	0°
SS ribbon	$110.9x11.1x2.9$	1.5	56.5°	0°
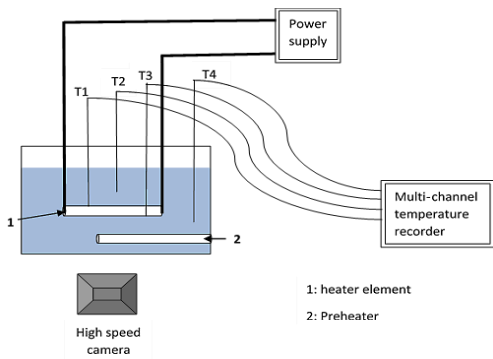
Figure 1 Schematic diagram of the pool boiling setup.

The bubble dynamics was recorded using a Mikrotron Motion BLITZ Cube 4 high speed

camera at a speed of 1000 fps at a spatial resolution of 1280×1024 pixels. A zooming lens of 20-100

mm focal length and a 1000W halogen light source was used for the camera. The image frames from

the high-speed recordings were manually analysed using the ImageJ software to obtain the values of

departure diameters and frequencies. The original grayscale image was processed, i.e. procedures like

contrast enhancement, filtration, thresholding, edge detection were carried out; and then the diameter was measured as shown in *Figure 2*. The bubble diameters could be measured with an accuracy of $\pm 1\ pixel$ which comes to about 4% for a bubble diameter of about 2 mm in addition to 0.1% error of digitalization. The error in time measurement comes from the speed of the camera, and is of nearly $1ms$.
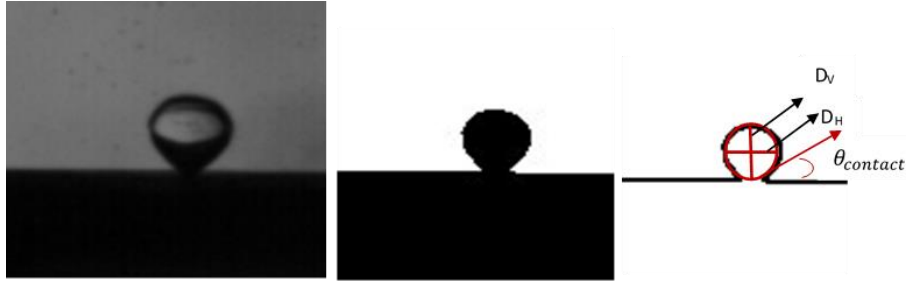
Figure 2 Image processing and bubble dimension measurement

After systematic and repeated experiments, it was concluded that the departure diameter (D) and frequency (f) are increasing functions of the applied heat flux and wall superheat. This implies that $f.D$, which dimensionally represents the velocity of bubble rise in the liquid, is also an increasing function of heat flux. This agrees with the previous experiments but in contradiction to the most widely used models. The diameter decreases with increase in the degree of subcooling due to higher condensation rate on the bubble cap. It was observed that the bubble departure frequency is an increasing function of the degree of subcooling, but can decrease with an increase in subcooling for $\Delta T_{sub} < 5K$. This has been theorised before, but never observed experimentally. The departure diameter was found to decrease as the surface roughness of the heater increased, though the frequency was only affected by the surface roughness for low superheats. The diameter was observed to increase with increase in the heater surface area and the inclination angle of the heater element. While the departure frequency increased with increase in inclination angle, it decreased for a bigger heater surface. Some key results are shown in *Figure 3*. Results of this work has been published in *International Journal of Multiphase Flow*.
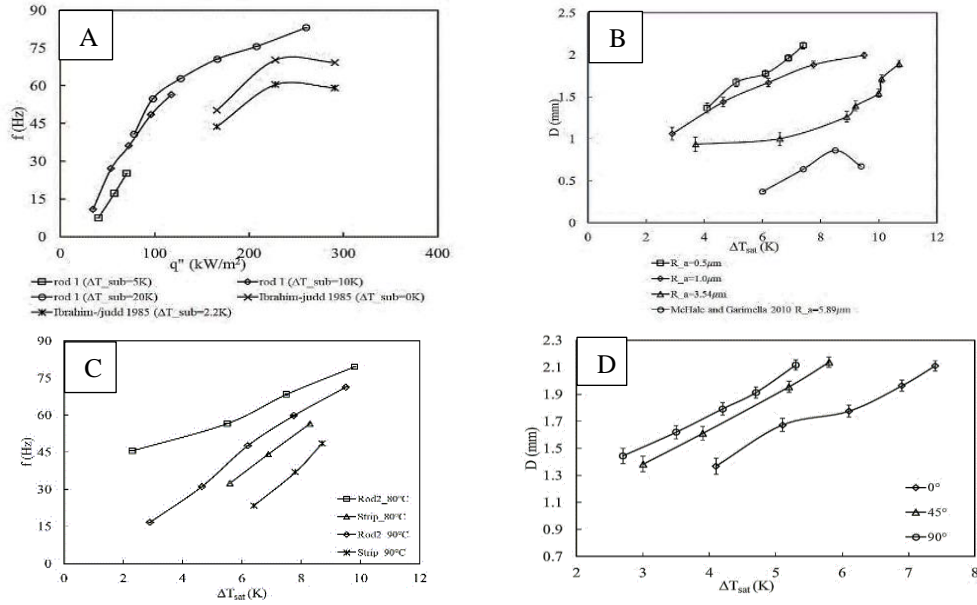
Figure 3 (A) Effect of subcooling on departure frequency. (B) Effect of surface roughness on departure diameter. (C) Effect of heater size of departure frequency; and (D) Effect of heater inclination on departure diameter.

2. Unresolved Issue-2

The bubble dynamics in cross flow conditions in horizontal rod bundle are not known, especially in low liquid mass flux conditions, like those in LOCA or prolonged SBO in PHWR, where the passive coolant flow from bottom to top results in localised boiling with liquid cross flow.

To resolve these issues, large number of experiments were carried out in a cross flow boiling facility. The test section was a cuboidal tank with one side made of removable Teflon sheet into which the heater rods could be screwed in. We first carried out the experiments with a single heated rod, and then with a staggered 5×3 horizontal rod bundle. The heater elements were the SS hollow rods with cartridge heaters inside the hole drilled centrally along the axis of the rods. The schematic of the setup and the details of the heater rods are presented in *Figure 4*. The experiments were carried out for the following conditions: inlet fluid temperature = saturated (373 K); $q'' = 8 - 28 \ kW/m^2$, $\Delta T_{sat} = 7 - 22 \ K$ and inlet liquid mass flux for the single rod was in the range of $G = 59 - 147.5 \ kg/m^2 s$, and for the tube bundle $G = 120 - 303.5 kg/m^2 s$, which corresponded to Re being in the range of $4200 - 11000$. Based on the bundle geometry used, following test cases were considered:

Case 1: An isolated single rod was heated,

Case 2: Only a single rod (row 3; central column) was heated in the rod bundle,

Case 3: Two rods (row 3 and 4; central column) were heated, while the bubble characteristics were measured on the upper rod (row 3), and

Case 4: Three rods (row 2, 3 and 4; central column) were heated, and the bubble characteristics were observed on the middle rod (row 3).
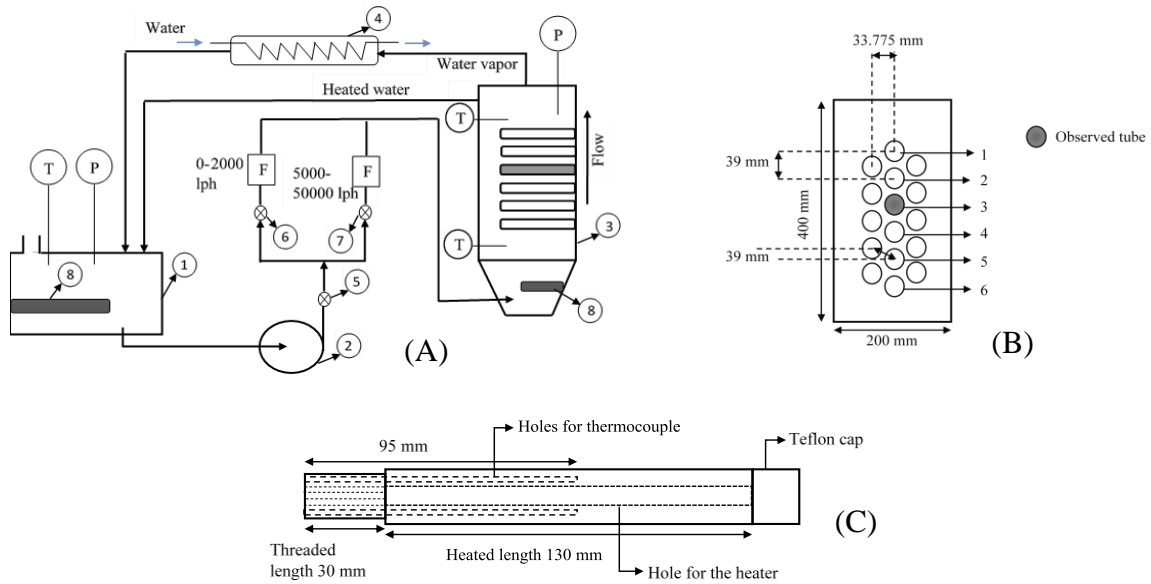
Figure 4 (A) Schematic of the experiment setup. (B) Details of the tube bundle. (C) Details of the heater tube.

After ensuring the repeatability of the experiments, parametric studies concluded that bubble departure diameter and frequency both increase with an increase in applied heat flux and wall superheat, but decrease with an increase in mass flux. The departure diameter of vapor bubbles from a single rod in a bundle were almost equal to that from an isolated single rod, but increased with an increase in the number of heated rods in its neighbourhood. The increase in the bubble departure size can be attributed to the superheated liquid present around the observed rod due to the heating of nearby rods, which increases the evaporation at the wall and reduces the condensation in the surrounding liquid. The departure frequency from a single rod in a bundle was significantly higher compared to that from an isolated single rod. The frequency further increased with the number of heated rods in the bundle. This increase can be explained in terms of the reduced waiting period, due to quicker

recuperation of the superheated boundary layer due to presence of hotter bulk liquid around the rods. These results are presented below in *Figure 5*.
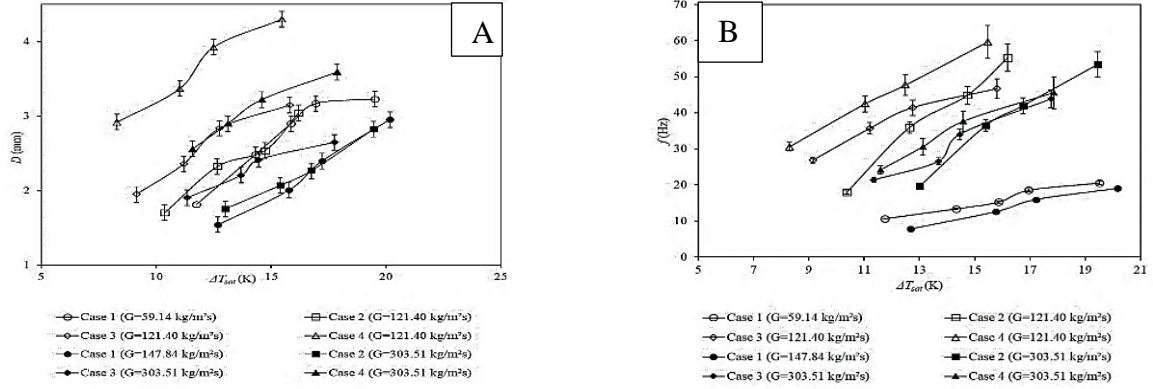
Figure 5 Effect of wall superheat, mass flux and presence of heater tubes on (A) departure diameter and (B) frequency.

Based on the experiments conducted, semi-empirical models for bubble departure diameter and frequency were developed for subcooled pool and cross flow boiling in horizontal heater. Here, the surface roughness and size of the heater was also considered. For pool boiling, we propose the model for diameter in terms of Bond number (*Bo*) as:

$$Bo = \frac{gD^2(\rho_l - \rho_v)}{\sigma} = 0.003(\gamma - 1)^{1.78} \left(\frac{R_a}{L_a}\right)^{0.01} \left(\frac{D_h}{L_a}\right)^{-0.85} Ja^{1.85} Pr^{-2.5} \vartheta^{-0.6} \tag{1}$$

where γ is the surface-liquid interaction parameter, R_a is the surface roughness, D_h is the hydraulic diameter, and L_a is the Laplace length, Ja is the Jakob number, Pr is the Prandtl number and ϑ is the subcooling number, defined as the ratio of $T_w - T_b$ to ΔT_{sat}. This correlation was compared with the data in the literature for pool boiling and the agreement is within ±30% as shown in *Figure 6*. To account for the cross flow and the presence of heater tubes, we introduced Re and a parameter n to account for the number of heated tubes. The final equation thus obtained is

$$Bo = 0.0056\, n^q\, Ja^{1.85} Pr^{-2.5} \vartheta^{-0.6} (1 + Re)^{-0.036} \tag{2}$$

where

$$q = \begin{cases} 0.75, top\ tube \\ 1.005, middle\ tube, \\ 0.255, bottom\ tube \end{cases} \tag{3}$$

The comparison of the correlation with the results obtained for tube 3 for the three cases have been shown in *Figure 7*. The data is predicted by the correlation within $\pm 30\%$.

Following a similar process, model for departure frequency in subcooled pool boiling was obtained as

$$f\sqrt{D} = 0.01\gamma^{-0.51}\left(\frac{R_a}{L_a}\right)^{0.22}\left(\frac{4g(\rho_l-\rho_v)}{3\rho_l}\right)^{\frac{1}{2}}Ja^{2.05}\vartheta^{0.39} \tag{4}$$

Figure 8 shows the comparison of the experimental data with the predictions, and we can see that the correlation agrees with experiments within $\pm 30\%$.
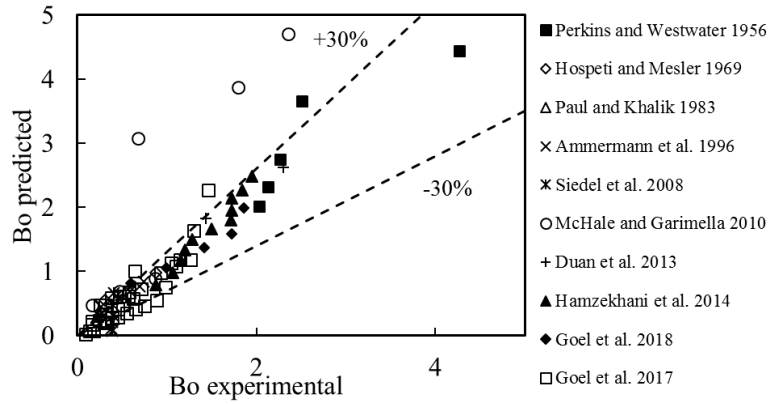
Figure 6 Comparison of predicted Bo with experimental data in pool boiling.
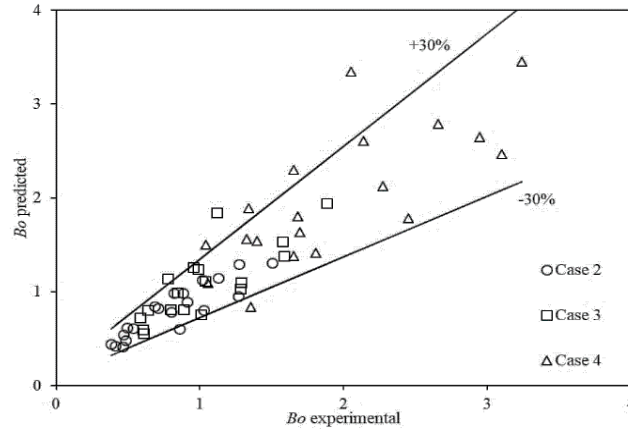
Figure 7 Comparison of predicted Bo with experimental data in pool boiling.

Taking the effect of the fluid flow and the number of heated rods into account, we obtained

$$f\sqrt{D} = 0.0004n^r\left(\frac{4g(\rho_l-\rho_v)}{3\rho_l}\right)^{\frac{1}{2}}Ja^{2.05}(1+Re)^{-0.031} \tag{7}$$

where

$$r = \begin{cases} 0.178, top\ tube \\ 0.356, middle\ tube \\ 0.178, bottom\ tube \end{cases} \tag{8}$$

The comparison of the correlation with the data for the three bundle cases have been given in *Figure 9*, and the predictions were found to be within the acceptable limits. Results of this work has been published in *International Journal of Multiphase Flow*.
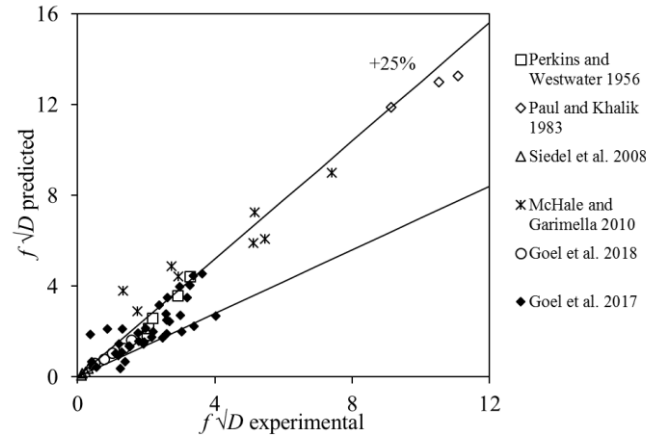
Figure 8 Comparison of experimental and predicted f√D in pool boiling.
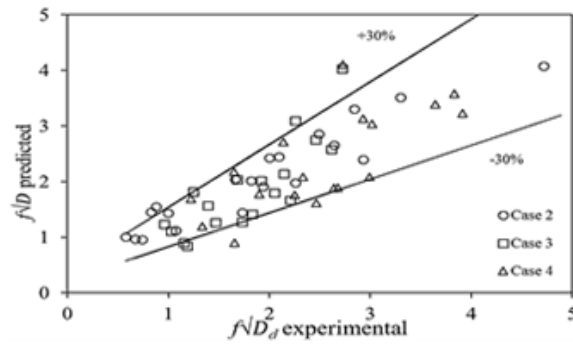
Figure 9 Comparison of experimental and predicted departure frequency in a tube bundle.

3. Unresolved Issue-3

Bubble characteristics in flow boiling under low heat and mass flux conditions in rod bundle like those during start-up of a natural circulation BWR, is not known. The existing correlations for bubble departure characteristics even for a single heated rod show significant scatter.

To resolve this aspect, a series of experiments were carried out to study the effect of operating conditions as well as the size of annulus, along with the effect of rod bundle on bubble characteristics. *Figure 10* shows the schematic of the setup. All of the three kinds of test sections used were annuli. The quartz glass made the outer tube and SS316 heater rod ($O.D. = 12\ mm$) fitted with a nichrome heating element in its core made the inner heater rod. The dimensional details of the three test sections are as follows:

1. <u>The wide annulus</u>: glass tube $I.D. = 45\ mm$. Total length $= 980\ mm$, heated length$= 900\ mm$. $D_h = 33\ mm$.

2. <u>The narrow annulus</u>: glass tube $I.D. = 16\ mm$. Total length $= 1040\ mm$, entry length $= 240\ mm$, exit length $= 240\ mm$, heated length $= 560\ mm$, $D_h = 4\ mm$.

3. <u>The 4-tube bundle</u>: 4 heater rods, glass tube $I.D. = 36\ mm$. Total length $= 1040\ mm$, entry length $= 240\ mm$, exit length $= 240\ mm$, heated length $= 560\ mm$. $D_h = 8.571\ mm$.

The experiments were carried out for the following conditions:

1. <u>For wide annulus</u>: wall heat flux $(q") = $ 40-95 kW/m^2, wall superheat $(\Delta T_{sat}) = 0 - 6\ K$, degree of subcooling $(\Delta T_{sub}) = 10 - 30\ K$, and mass flow rate $(\dot{m}) = 10, 15, 20\ gps$ or mass flux $(G) = 6.7 - 13.3\ kg/m^2 s$.

2. <u>For narrow annulus</u>: $q" = 1 - 30\ kW/m^2$, $\Delta T_{sat} = 0 - 6\ K$, $\Delta T_{sub} = 5,10\ K$ and $\dot{m} = 20,30\ gps$ or $G = 227.27, 340.91\ kg/m^2 s$.

3. <u>For 4 tube bundle</u>: $q" = 1 - 30\ kW/m^2$, $\Delta T_{sat} = 0 - 7\ K$, $\Delta T_{sub} = 5, 10\ K$, and $\dot{m} = 20, 30\ gps$ or $G = 35.37, 53.05\ kg/m^2 s$.
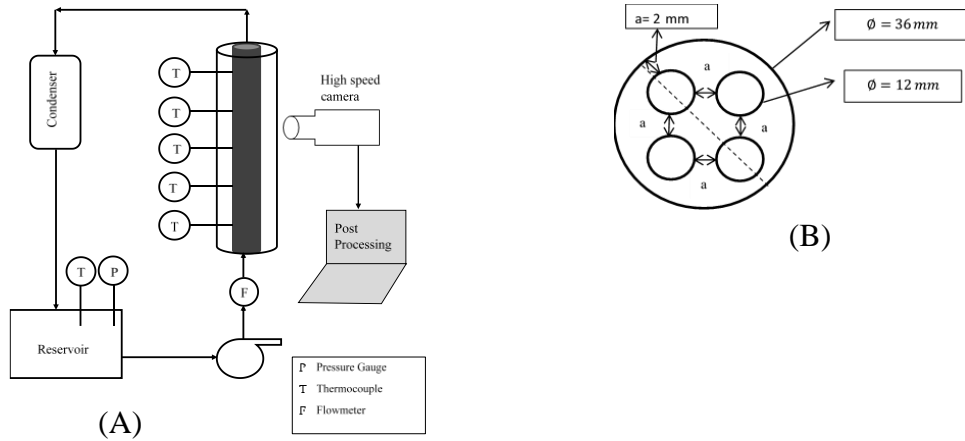
Figure 10 (A) Schematic of vertical flow boiling setup. (B) cross sectional details of the 4-tube bundle.

With repeated experiments, it was observed that maximum, departure and lift-off diameter and the bubble departure frequency, all increase with an increase in heat flux or wall superheat, and decrease with an increase in liquid subcooling or mass flux. These behaviours were found to exist in all three test sections as shown in *Figure 11* below. The diameter was observed to increase in the

narrow annulus and further in the bundle, compared to the wide annulus, under similar conditions. The departure frequency on the other hand, decreases with the decrease in the annular gap.
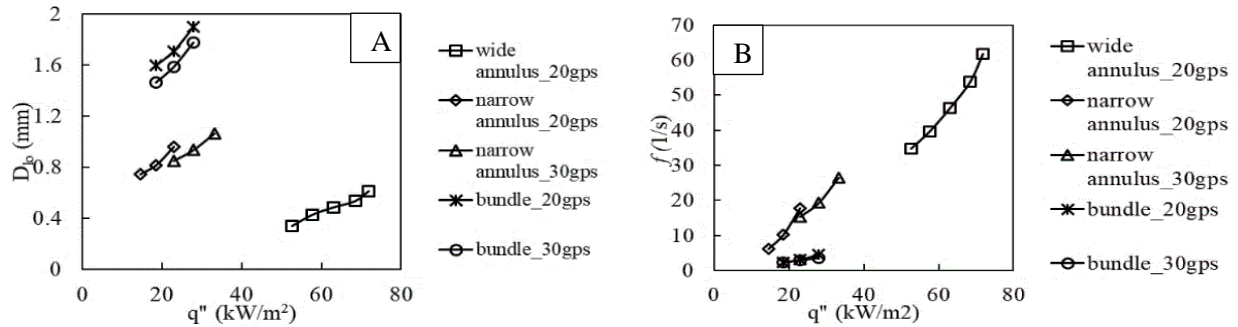
Figure 11 Variation of bubble (A) lift-off diameter and (B) departure frequency with heat flux, mass flux and test sections.

The reason for this increase in diameter are the different growth behaviours in the three test sections. In the narrow annulus, three different kinds of bubble growths could be observed. First, were the *individual bubbles*, that has life cycle similar to the ones observed in the bigger annulus. Second, were the *merged bubbles* - bubbles that nucleated close to each other, and merged to form a single bubble in the early periods of their growth cycles. Third, were the *confined bubbles* – due to the smaller gap between the heater and the glass tube, some bubbles grew to touch the glass surface. These bubbles then elongated rather than growing radially. The bubble growth in both the cases, happened mainly during the sliding phase.

However, in the bundle, it was observed that the heater rods had a large number of nucleation sites with water. The bubble nucleated at their sites, grew to a size, then departed from their nucleation site to merge with a nearby bubble. The coalesced bubble then grew, at its location or while sliding on the heater surface up to a maximum size, after which it started to condense and lifted off soon after to collapse in the bulk liquid. Hence, in the analysis, the departure diameter is taken to be the average size of individual bubbles growing at their own sites, before they leave their site and coalesce with a nearby bubble. The maximum diameter is taken to be the average size, the coalesced bubbles grow to before they start condensing. Finally, lift off diameter is taken to be the average size of the coalesced bubbles that lift from the heater surface.

The existing models for the bubble departure diameter and frequency in flow boiling with a single heater surface, developed in terms of non-dimensional numbers have been validated for limited data sets. They show an error of up to 50% for the data they were validated with, and up to 300% with the other data sets. This can be seen in figure below where parity plots for bubble lift off diameter with Prodanovic et al. (2002) model (*Figure 12(A)*) and bubble departure diameter with Brooks et al. (2015) model(*Figure 12(B)*) are shown as examples. The regression studies with the various parameters in both dimensional and non-dimensional forms were unable to bring all the data together satisfactorily. Hence, efforts have been made in the present work to develop generalized models for bubble departure diameter and frequency for flow boiling geometries using artificial intelligence, that account for large range of operating conditions, heater geometry and orientation, and hence, are able to predict all the data in the published literature as well as that obtained in the present study.
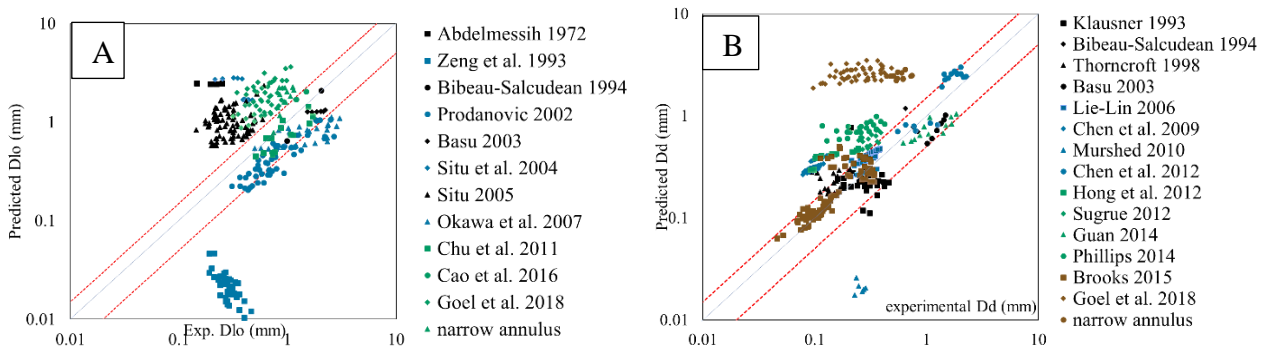
Figure 12 Parity plots for bubble departure diameter in flow boiling with models of (A) Prodanovic et al. 2002, and (B) Brooks et al. 2015.

Closure: Based on the literature review, three major unresolved issues were identified. To address those issues, we carried out extensive experiments in the range of operating conditions, not explored before, but are important to the nuclear reactors under normal and accidental conditions. As a result, we conclude

1. The bubble departure diameter and departure frequency, which are the important parameters in estimating the evaporation and quenching heat flux components in the two-phase heat transfer, are themselves affected by a number of operating parameters. The product of departure diameter and frequency is confirmed to increase with increase in heat flux or wall superheat, which was earlier

assumed to be a constant. An increase in the degree of liquid subcooling significantly decreases the bubble departure diameter, while the frequency may increase (above $\Delta T_{sub} \sim 5K$) or decrease depending on the dominant mechanism of the boundary layer recuperation. An increase in heater surface roughness causes the departure diameter to decrease but frequency to increase. The heater size increase results in an increase in departure diameter but significant decrease in frequency. And lastly, increase in heater inclination angle results in increased diameter and frequency.

2. The nuclear reactors have fuel rod bundles, with multiple heated rods fit together at small pitch-diameter ratio (typically~ 1.2). The effect of such close neighbouring heated rods on the bubble characteristics have been examined in both horizontal cross flow and vertical annular flow geometries. In cross flow conditions, the bubble diameter and frequency for any given condition was found to increase with the increase in number of heated rods below the observed rod, due to the increased temperature in the superheated boundary layer, that increased the growth of the bubbles and reduced the growth and waiting times to give a higher heat transfer. In the annular geometries, the reduced annular gaps caused bubble elongation and coalescence, thereby giving larger departure diameters, while the frequency was found to decrease drastically.

3. The simultaneous measurement of departure diameter and frequency, under a myriad of conditions, have enabled us to develop semi-empirical models for both the variables in horizontal bundle geometry for subcooled pool boiling, which show better agreement with the literature data than existing models. The models for cross flow boiling in a bundle have also been proposed based on the data obtained in this study.

Outline of thesis: Based on work described above, the thesis has been divided into 8 chapters. The first chapter outlines the introduction, literature review and the motivation for the work. The second chapter provides a brief description of visualization technique to measure bubble characteristics. The third and the fourth chapter describe the studies carried out in pool boiling and the cross flow boiling, and the bubble behaviour in nucleate boiling regime. The fifth chapter describes the departure diameter and frequency models for subcooled pool boiling and cross flow boiling in a single heater,

extended to a rod bundle. The sixth chapter explains the vertical flow boiling experiments in all three geometries; and the seventh chapter covers the model development in vertical flow boiling. Important conclusions of the study and future work are outlined in Chapter 8 of the thesis.

1. Chapter 1

Introduction

1.1. Importance

Nuclear reactor core is made of fissile material where fission reaction generates large amounts of heat, which are removed by the coolant (water) to generate steam which in turn is used to generate electricity. The nuclear fuel bundle geometry consists of several fuel pins arranged in horizontal or vertical arrays depending on the kind of nuclear reactor. The Boiling Water reactors (BWRs), Pressurized water reactors (PWRs) and the Indian Advanced Heavy Water Reactor (AHWR) have the vertically aligned fuel bundles with the coolant flowing from bottom to top, while the Pressurized Heavy Water Reactors (PHWRs) have horizontal array of fuel bundles where the coolant flows in bidirectional manner in the normal operating conditions (*Figure 1.1*). The coolant water undergoes boiling in the reactor core – under normal operating conditions in a BWR or in AHWR, and under accidental conditions in a PHWR. The boiling regime observed in these conditions depends on the operating conditions. *Nucleate boiling* regime is one of the most encountered flow regimes in fuel bundles. It is characterised by the bubbles nucleating, growing and departing from the heating surface, due to the surface temperature being higher than the saturation temperature of the coolant at the system pressure. This process is a highly efficient means of heat transfer, but the boiling heat flux also needs to be maintained below the critical heat flux level (CHF), to avoid any burnout or failure of the fuel pins. Hence, understanding boiling mechanism and predicting the total two-phase heat transfer is essential for safe design and operation of the nuclear reactors.
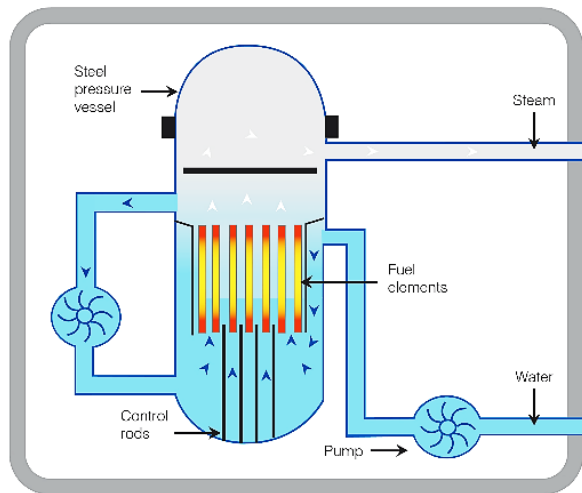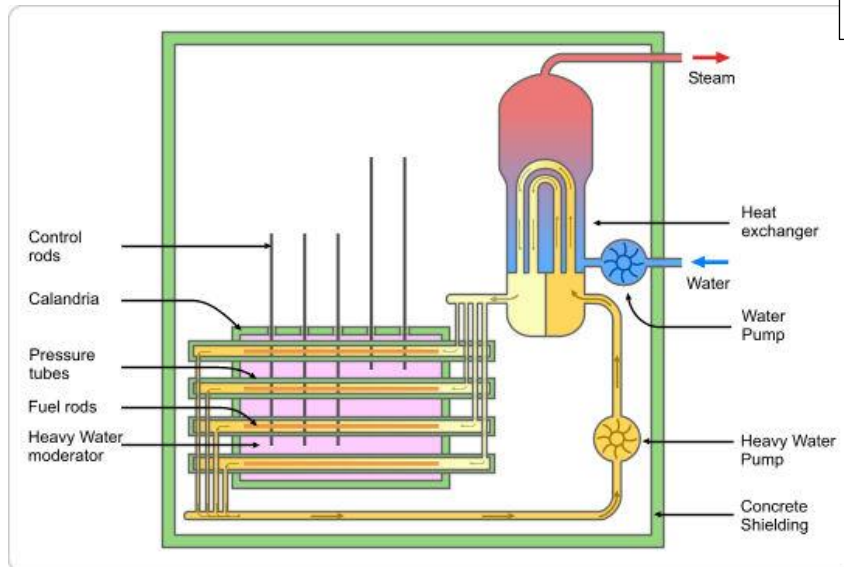
Figure 1.1 Images showing fuel bundle arrangement in (A) BWR and (B) PHWR.

Boiling is the process of phase change of liquid into vapor at a solid-liquid interface when the temperature of the solid surface exceeds the saturation temperature corresponding to the liquid pressure. Heat transferred from the solid surface to the liquid is expressed in form of the Newton's law of cooling:

$$q^{"} = h(T_w - T_{sat}) = h\Delta T_{sat} \tag{1.1}$$

where ΔT_{sat} is the wall superheat, and h is the two-phase heat transfer coefficient. Nukiyama (1934) studied the quantity of heat transferred from a metal wire to the surrounding water, heated in a temperature controlled environment and discovered the different regimes of boiling.

The plot of heat transferred as a function of wall superheat, is now the basis of any boiling discussion, and is given in *Figure 1.2*.
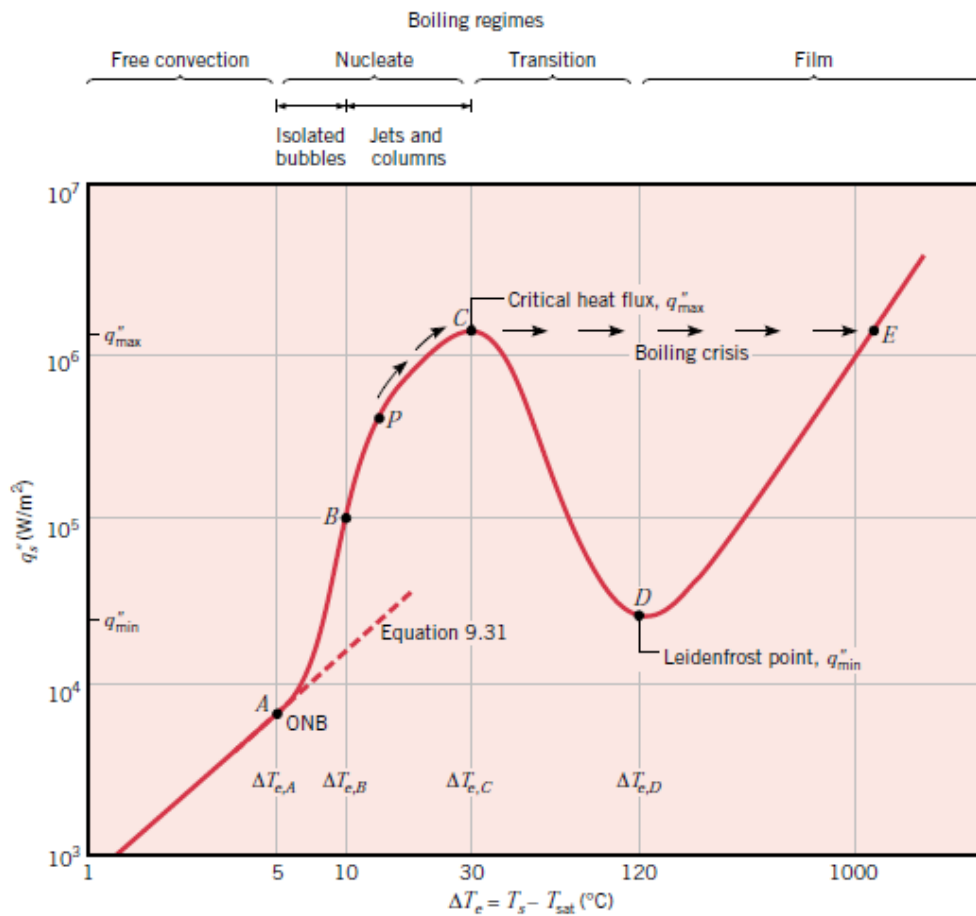
Figure 1.2 Nukiyama Boiling Curve (Image from Incropera *et al.* (2002)).

As the temperature of the heated surface increases, the convective heat transfer starts to take place, until point A, where the surface temperature exceeds the required value for the bubble nucleation to take place. The region between points A to C, referred to as the *nucleate boiling regime* - characterized by the nucleation, growth and departure of vapor bubbles, is a very efficient mechanism to transfer large amount of heat at small degree of superheats. In the region A-B, isolated bubbles grow and depart from the nucleation sites, while in region B-C, the bubble density increases so that they coalesce and leave the surface in form of jets or columns. The bubble departure causes mixing of the fluid and results in enhanced convective heat transfer, in addition to the latent heat transfer. The point P is the point of maximum heat

transfer coefficient in the nucleate boiling regime, beyond which due to the aggregation of bubbles near the surface, the heat transfer coefficient begins to reduce, but the total heat flux still increases. The point C represents the maximum amount of heat flux a surface can transfer beyond which any increase in temperature would result in vapor film not letting the liquid to wet the surface and the heat transfer decreases. In case of the heat flux controlled systems, reaching point C would result in a very quick increase in surface temperature and surface may suffer structural damage due to low heat transfer. This condition is referred to as the *boiling crisis*.

Nucleate boiling can be classified in a number of ways – (1) based on the location of bubble nucleation, (2) based on bulk liquid flow, and (3) based on the bulk liquid temperature compared to the saturation temperature. When the bubble nucleates in the nucleation cavities on a heater surface in contact with the liquid, it is referred to as the *heterogeneous* boiling, while when the liquid itself is superheated (temperature higher than the saturation temperature at the system pressure), the bubbles may nucleate in the liquid far away from the walls. This form of nucleate boiling is called the *homogeneous boiling*. When boiling takes place on a heater surface immersed in a stationary liquid pool, and the only liquid motion is very near to the surface due to the natural convection and bubble generated mixing, it is called *pool boiling*. *Flow boiling*, on the other hand, takes place with a fluid in motion by external means in addition to the convection and bubble induced mixing. Finally, if the bulk liquid temperature away from the surface is maintained below saturation temperature, it is termed as s*ubcooled boiling* while it is called *saturated boiling* when the bulk liquid temperature is also saturated. The bubbles departed from the heater surface can be seen to rise all through the saturated liquid pool height, and at higher temperatures or applied heat flux conditions, a large volume of saturated bulk liquid may be filled with vapor bubbles, giving it the name *bulk boiling*.

1.2. Motivation

Nucleate boiling is known for transferring large amounts of heat at comparatively lower surface temperatures with an extremely high heat transfer efficiency and hence, finds applications in a number of thermal systems, like nuclear reactor core, chemical reactors, boilers, steam generators, evaporators, which correspond to the conventional channels; but more recently in electronic devices, microchips, microelectromechanical systems (MEMS), which correspond to the narrow or so-called micro-channel. The safe and efficient design of these systems require a reliable estimation of two-phase boiling heat transfer.

There are many models available for predicting the boiling heat transfer in the literature, but all of them are based on the basic assumption that the total two-phase heat transfer is composed of two parts – (1) *macro-convection*, the single-phase heat transfer due to the motion (natural or forced) of the coolant liquid, and (2) *micro-convection*, the heat transfer associated with the nucleation and growth of the vapor bubbles. The pool boiling heat transfer is assumed to have only micro-convective component, and the most popularly used are the empirical models given by Forster and Zuber (1955) and Cooper (1984). The earlier models for flow boiling, like proposed by Chen (1966) and others proposed on the same lines assume an asymptotic summation of macro and micro convective heat transfer components. They use the well-known Dittus-Boelter equation for the macro part, while most of the models employ Forster and Zuber (1955) or Cooper (1984) models for the micro-convective parts. These models are all empirical, validated with limited data available at the time, and do not provide the desired accuracy. To reduce the empiricism built in the above mentioned *heat flux partition* scheme, Kurul and Podowski (1990) proposed a 2 dimensional multi-scale model for boiling flows derived from the conservation equations of mass, momentum and energy. Even their initial model showed significant success with the benchmark experiments, and was later further developed by many researchers. The *mechanistic* heat flux partition model states that the total

two-phase heat flux is the sum of (1) convective, (2) evaporative and (3) quenching components.

$$q_w'' = q_{sp}'' + q_q'' + q_e''$$ (1.2)

where the single-phase heat transfer is calculated as

$$q_{sp}'' = h_{sp}(T_w - T_l)(1 - A_b)$$ (1.3)

Here, h_{sp} is the single phase convective heat transfer coefficient, and can again be estimated by Dittus-Boelter or some other correlation, and A_b is the fraction of the heater surface area covered by the bubbles, so $(1 - A_b)$ is the fraction of the surface area covered by fluid. The quenching heat flux is the cyclic average energy transferred to the liquid that rewets the heater surface after every bubble departure, and is calculated as

$$q_q'' = A_b \frac{2k_l(T_w - T_l)}{\sqrt{\pi \alpha_l T_f}}$$ (1.4)

where T_f is the bubble time period, which is the inverse of bubble departure frequency. Finally, the evaporative heat flux is the total latent heat transfer from per unit area of the surface, and is calculated as

$$q_e'' = V_d \rho_v h_{fg} f N_a = \frac{1}{6} \pi D_d^3 \rho_v h_{fg} f N_a$$ (1.5)

where V_d is the bubble departure volume, calculated from the bubble departure diameter, f is the bubble departure frequency from the heater surface and N_a is the bubble active nucleation site density. Further, the calculation of the bubble area of influence A_b is also calculated in terms of the bubble maximum diameter. Hence, as seen from the above relationships, the models for bubble diameters, frequency and nucleation site density are required as closure relations and these parameters have significant effect on the heat transfer behaviour.

With the development of computational power in last few years, there has been a thrust for implementing multi-dimensional, multi-scale models in computational codes. Such codes could play a great role in accurately predicting and hence, in the design and analysis of complex

thermal systems, like boiling in reactor cores or heat removal in MEMS. These models, however are still under development and hence, require empirical or phenomenological models for various input parameters in the codes, like the bubble diameters and frequency. These models require a good understanding of the flow physics and bubble behaviour for development, and substantial amount of data in the wide range of relevant conditions for validation. Hence, it is necessary to conduct studies for deeper understanding of the bubble departure characteristics under a variety of conditions, specifically relevant to the nuclear reactors, and to put forward modified models for bubble departure diameter and frequency which shall be used in computational codes for prediction of performance of heat removal capacity and safety of nuclear reactors.

1.3. Literature Review

As discussed in the previous section, any mechanistic model for predicting boiling heat transfer requires three main parameters as the input for the model:

a. Bubble diameter as a function of time, maximum or departure diameter

b. Bubble period or frequency

c. Active nucleation site density

These three parameters depend on a number of variables like applied heat flux, wall superheat, bulk liquid temperature (subcooling), system pressure, heater conditions like orientation, geometry, surface characteristics and liquid properties. Hence, these are the parameters that formed the basis of experiments carried out over the years. Mainly, visualization experiments involving nucleation on some kind of a heater surface in contact with either stationary or flowing liquid, being recorded on high speed cameras have been conducted. The recording was then played back slowly or the photographs were analyzed to measure the concerned quantities.

1.3.1. Pool boiling

Jakob and Fritz (1931) studied bubble departure behaviour of saturated water on roughened copper plate under atmospheric pressure and postulated the product of departure frequency (f) and diameter (D_d) to be a constant. Jakob (1949) conducted experiments with water and carbon tetrachloride and showed that the departure diameter, frequency and hence, their product remains constant for small heat fluxes (about 20% of CHF). Perkins and Westwater (1956) extended Jakob's work to high fluxes using methanol and concluded that the f, D_d and $f.D_d$ remains constant upto 80% of CHF and increases linearly beyond that. Cole (1960) extended this work with water upto CHF and balancing the buoyancy and drag forces, they found that f and D_d can be related as $f\sqrt{D_d} = 1.15\sqrt{g}$. Ruckenstein (1961) measured bubble departure diameters as a function of wall superheat and proposed a correlation for the same. McFadden and Grassmann (1962) experimentally deduced that the empirical correlation $f.\sqrt{D_d} = 0.56\sqrt{g}$ (constant of heat flux) holds for a wide range of conditions. Zuber (1963) proposed that the heat transfer for isolated bubble regime can be described using the equations for natural convection from a horizontal surface if the vapor void fraction is taken into account to calculate the fluid density. For the high heat flux region, he claimed that the vapor bubbles combine to form vapor columns and hence, latent heat transfer is the main heat transfer process in this region. Based on his theory, he postulated the product $f.D$ to be a function of liquid properties given as $f.D_d = 0.59\left(\frac{g\sigma(\rho_l-\rho_v)}{\rho_l^2}\right)^{1/4}$. Gaertner (1965) in his experiments with saturated water observed that the departure diameter remained almost constant while the departure frequency increased with the heat flux in the isolated bubble regime. He also observed that the frequency of the bubbles was affected by the density of nucleation sites like the isolated sites produced large bubbles with low frequency and vice versa. Cole (1967) re-examined the data generated by Cole and Shulman (1966) and found that

while the product $f.D_d$ was independent of the Jakob number ($Ja = \frac{\rho_l C_p \Delta T_{sat}}{\rho_v h_{fg}}$) in the isolated bubble regime (partially developed boiling region) but was strong function of Ja in fully developed boiling near CHF suggesting that the vapor removal mechanism is quite different in the two regimes. Ivey (1967) studied the correlations proposed by various authors for $f.D_d$ and concluded that the product can be described by three different relations for three separate regions. They suggested (i) $f\sqrt{D_d} = 0.9\sqrt{g}$ for hydrodynamic region, where only buoyancy and drag forces affect the bubble behaviour; (ii) $f.D_d^{3/4} = 0.44\sqrt{g}$ for the transition region, where buoyancy, drag and surface tension are equally important; and lastly, (iii) $f.D_d^2 = constant$ in the thermodynamic region, where the bubble behavior is mainly controlled by the liquid thermo-physical properties. The hydrodynamic and transition region together represent the inertially controlled bubble growth regions while the thermodynamic region represents the thermal diffusion controlled bubble growth region. Williams and Mesler (1967) studied the effect of heater inclination on the contact and waiting period of the bubbles forming in the artificial and natural cavities. They proposed that the vapor completely vacates the nucleation site when it slides away from the site in case of the vertical surface leading to the complete filling of the cavity with the liquid. This changes the thermal boundary layer behaviour and increases the waiting period considerably for the vertical surface compared to the horizontal surface, implying that the departure frequency decreases as the inclination angle increases. Though they also stated that this effect alone cannot explain the increase in waiting time, which was pronounced for artificial sites but not so much for the natural cavities. Cole and Rohsenow (1969) proposed a correlation for calculating bubble departure diameter at low pressures ($0.067 - 1\ bar$) for various fluids by introducing two distinct constants- one for water and other for rest of the fluids, and they also introduced the bubble diameter dependence on Jakob number. Saddy and Jameson (1971) working with uniformly superheated water and acetic acid

deduced $f = AD_d{}^2$. Judd and Hwang (1976) carried out experiments with subcooled dichloromethane at a pressure little higher than atmospheric (1.5 bar) and found that the departure diameter decreased while the frequency increased as the heat flux was increased for each subcooling tested because the nucleation sites per unit area increased. Chen and Chuang (1979) studied the effect of superheat, cavity size and the inclination angle of the heater element on the departure frequency and proposed a single semi-empirical correlation relating all three parameters fixing model constants based on their experimental results. Their results showed that the bubble departure frequency increased with increase in inclination angle and wall superheat. Ali and Judd (1981) studied the waiting period model proposed by Hsu (1962) which considered transient heat conduction as the only mechanism by which the liquid thermal boundary layer thickness increases after a bubble departure, but this model under predicted the experimental results. So, Ali and Judd (1981) proposed that the combined mechanism of transient conduction and convection because of the unsteady velocity field set up in the wake of the departed bubble for the thermal boundary layer formation. Their modified theory was then in agreement with the experiments that the waiting period decreased with increasing heat flux and subcooling. Paul and Abdel-Khalik (1983) working with saturated water boiling on a platinum wire deduced that the expression of the kind $f . D_d{}^a = constant$ is inadequate and suggested that the frequency should rather be expressed as a normal distribution function of departure diameter at each heat flux. They observed that both frequency and diameter increase with heat flux, though the increase was very slow since the wall temperature didn't change much with increase in heat flux. Ibrahim and Judd (1985) carried out experiments with subcooled water and concluded that frequency decreases with increase in subcooling up to a point beyond which it reverses its trend. They explained it as the transient conduction being the dominant mechanism for quenching heat transfer up to a certain subcooling beyond which convection heat transfer becomes dominant. Ammerman *et al.* (1996) conducted experiments

with saturated FC-72 heated on a platinum wire using Laser Doppler Anemometry and deduced that departure diameter and the frequency per unit length increase with increase in heat flux. Demiray and Kim (2004) studied the effect of subcooling on a single bubble heat transfer and observed that the individual bubble departure diameter and energy transfer were higher with low subcooling (high pool temperature) because the bubble gained most of its energy from the superheated liquid layer and not the wall or microlayer under the bubble. The departure frequency increased at high subcooling resulting in higher overall heat transfer. Nimkar *et al.* (2006) prepared special silicon surface with artificially created re-entrant cavities with different cavity spacing and observed the departure characteristics of the bubbles. They concluded that though the departure diameter and frequency both increase with the increasing heat flux and superheat, they are not affected by the change in cavity spacing. Siedel *et al.* (2008) studied boiling of pentane on a single and two adjacent nucleation sites and observed that the bubble departure frequency was almost proportional to the wall superheat. They found that the bubble growth time significantly reduced with increase in wall superheat but the bubble departure volume was almost constant since, the force balance governing the departure remains unaffected by the superheat. Hence, the product $f.D_d$ was proportional to the wall superheat and not a constant as presumed in some previous works. McHale and Garimella (2010) boiled saturated FC-72 on a rough and a smooth surface and observed that both departure diameter and frequency increased with increase in superheat but the surface roughness also played an important role which had not been explained by any model so far. They observed that to the first order, the diameter decreased with surface roughness while the frequency increased, for a given heat flux or wall superheat. Hutter *et al.* (2012) studied boiling on the artificially created micro cavities on a thin silicon wafer and inferred that though the departure diameters tend to increase with increase in cavity spacing, the frequency is unaffected by it. McHale and Garimella (2013) studied the bubble parameters with surface roughness (using 7 different

surfaces with varied finishes) and showed that as a first approximation, departure diameter decreased with increase in surface roughness (R_a value). Duan *et al.* (2013) carried out experiments with synchronized high speed imaging, IR thermometry and PIV measurements and recorded the characteristics of 3 bubbles each in two data sets varying in heat flux and superheat. Hamzekhani *et al.* (2014) observed the bubble departure diameters at saturation conditions for water and binary mixtures and concluded that the diameter increased with increase in heat flux. They proposed a new model to predict bubble departure diameter taking the fluid properties into account in terms of four dimensionless numbers. Continuing their work, Hamzekhani *et al.* (2015) studied the bubble departure frequency for water and NaCl solutions and concluded that the bubble frequency increased with an increase in heat flux, but decreases with an increase in NaCl concentration. Bovard *et al.* (2017) studied bubble departure diameter in the boiling of four different pure liquids – water, ethanol, acetone and methanol, on four kinds of metal surfaces – aluminium, brass, copper and stainless steel. All four surfaces had different surface roughness values. They concluded that the bubble departure diameter increased with an increase heat flux, and decreased with an increase in surface roughness in a limited range of conditions, but is not much affected by surface roughness beyond that.

From the foregoing discussion, it may be noted that the behaviour of the departure diameter and frequency with the heat flux is debatable (constant, increasing or decreasing), amongst different studies and no single consensus has been reached. The experimental studies for pool boiling focussing on saturated boiling, subcooled boiling, the effect of surface roughness and the effect of surface inclination are summarized in *Table 1.1*, *Table 1.2, Table 1.3 and Table 1.4* respectively. It can be clearly seen that most of the subcooled boiling studies are focused on the heat transfer or bubble growth rates but there is almost no data for diameter and frequency under subcooled conditions except for three studies as shown in *Table 1.2*. The effect of surface finish has basically only been studied by McHale and Garimella and more

recently by Bovard *et al.* (2017), while the heater inclination on the two parameters have also not been studied in enough detail. The existing models in the literature for bubble departure diameter and frequency in pool boiling are listed in *Table 1.5* and *Table 1.6* for reference.

Table 1.1 Summary of saturated pool boiling experiments in literature.

S. No.	Reference	Working liquid	Heater element	Heat flux q'' (kW/m^2)	Observations
1.	Perkins and Westwater (1956)	Methanol	Hollow Copper tube	0-378.5	f, D_d and the product $f.D_d$ remain constant with an increase in heat flux up to 80% of CHF and increase linearly with heat flux beyond that.
2.	Gaertner (1965)	Water	Platinum and Copper flat surfaces	33.1-1554.2	The departure diameter remained almost constant while the departure frequency increased with the heat flux.
3.	Ali and Judd (1981)	Dichloromethane	Flat glass plate		Waiting period (t_w) decreased with increasing heat flux and the degree of subcooling. Proposed a new model for waiting period based on the combined mechanism of transient conduction and convection (because of the unsteady velocity field set up in the wake of the departed bubble).

S. No.	Reference	Working liquid	Heater element	Heat flux q'' (kW/m^2)	Observations
4.	Paul and Abdel-Khalik (1983)	Water	Platinum wire	0-600	The departure diameter and frequency both increase very slowly with an increase in heat flux.
5.	Ammerman *et al.* (1996)	FC-72	Platinum wire	19-150	The departure diameter and the frequency per unit length increase with an increase in heat flux.
6.	Siedel *et al.* (2008)	Pentane	Copper plate		The bubble departure frequency was almost proportional to the wall superheat but the bubble departure volume was almost constant since, the force balance governing the departure remains unaffected by the superheat.
7.	McHale and Garimella (2010)	FC-77	Top surface of Aluminium block square	20-110	Both departure diameter and frequency increased with increase in superheat but the surface roughness also played an important role.
8.	McHale and Garimella (2013)	FC-72, FC-77 and water	ITO film on glass substrate	4.7-132.4	The departure diameter decreased with an increase in surface roughness.

S. No.	Reference	Working liquid	Heater element	Heat flux q'' (kW/m^2)	Observations
			with controlled surface roughness (7 surfaces)		
9.	Hamzekhani *et al.* (2014)	Pure and binary mixtures, water	SS rod	0-120	The departure diameter increased with an increase in heat flux.
10.	Hamzekhani *et al.* (2015)	Water, water/NaCl mixture	SS rod	0-120	The departure frequency increased with an increase in heat flux.
11.	Bovard *et al.* (2017)	Water, ethanol, acetone, methanol	Aluminium, brass, copper, SS rods	0-120	The departure diameter increased with an increase in heat flux.

Table 1.2 Summary of subcooled pool boiling experiments in literature.

S. No.	Reference	Heater Element	Working Liquid	q'' (kW/m^2)	Subcooling (K)	D_d	f	Observations
1.	Faneuff *et al.* (1958)	wire	water	-	-			Bubble growth rate follows the Plesset and Zwick (1954)model.
2.	Nishikawa *et al.* (1965)	Flat disc wire	water	38.2-63.7 43.7-2244.6	2.20-14.21 2.1-40.0			Bubble growth and collapse is independent of heat fux. Bubble collapse has significant dependence on subcooling. Bubble growth rate is highly affected by the heater size.

S. No.	Reference	Heater Element	Working Liquid	q'' (kW/m^2)	Subcooling (K)	D_d	f	Observations
3.	Judd and Hwang (1976)	Flat glass plate with stannic oxide film	dichloromethane	20-60	0, 5.3, 11.3	✓	✓	Departure diameter decreased but frequency increased with an increase in heat flux.
4.	Ali and Judd (1981)	Flat glass plate	dichloromethane	25-60	0.9, 8.2, 16.7		✓	Waiting time of bubbles decrease with an increase in subcooling.
5.	Ibrahim and Judd (1985)	Flat Cu surface	water	166, 228, 291	0-15		✓	Bubble growth time is independent of subcooling up to a point, after which growth rate decreases with an increase in subcooling.

S. No.	Reference	Heater Element	Working Liquid	q'' (kW/m^2)	Subcooling (K)	D_d	f	Observations
								Bubble waiting time initially increases with subcooling and reverses trend after a point.
6.	Inoue *et al.* (1998)	wire	R113		0-220			CHF is directly proportional to subcooling. Effect of subcooling on CHF increases with an increase in pressure.
7.	Henry and Kim (2004)	Resistance microheater array	FC-72		2, 12, 22, 29			CHF increased with subcooling. At low gravity, subcooling had negligible impact on

S. No.	Reference	Heater Element	Working Liquid	$q''\ (kW/m^2)$	Subcooling (K)	D_d	f	Observations
								bubble behavior. At high gravity, bubble departure diameter was dominated by surface tension, and departure frequency was very low.
8.	Demiray and Kim (2004)	Resistance microheater array	FC-72		5, 16			Bubble departure diameter was higher at low subcooling but departure frequency increased at high subcooling, hence, higher heat transfer at high subcooling.

S. No.	Reference	Heater Element	Working Liquid	$q''\ (kW/m^2)$	Subcooling (K)	D_d	f	Observations
9.	Wang *et al.* (2005)	Microwire (4-100 μm dia.)	water	550	40-60			They observed two new bubble behaviors in micro wires apart from growth and departure-sweeping (back and forth motion of bubble parallel to wire), and return (bubble moving back to wire after departure into bulk liquid).
10.	Lu and Peng (2006)	Microwire (100 μm dia.)	water	600-1000	55-65			Bubble leaping (periodic up and down motion of the bubble from the wire

S. No.	Reference	Heater Element	Working Liquid	$q''\ (kW/m^2)$	Subcooling (K)	D_d	f	Observations
								surface) and leaping with sweeping (bubble moved away from wire, slipped parallel to wire, reconnected with the wire, slipped on the wire).
11.	Kim *et al.* (2006)	Resistance microheater array	R113		2-9			Bubbles were axisymmetric along axis normal to heater but not along axis parallel to heater. Bubble diameter decreased with an increase in subcooling

S. No.	Reference	Heater Element	Working Liquid	$q''\ (kW/m^2)$	Subcooling (K)	D_d	f	Observations
								above 10 K. Bubble growth time increases with an increase in departure diameter. Waiting period is affected by the amount and temperature of the liquid flowing in to surface after bubble departure.

Table 1.3 Summary of studies for surface roughness effect on boiling.

S. No.	Reference	Heater Element	Working Liquid	q'' (kW/m^2)	R_a (μm)	D_d	f	Observations
1.	Benjamin and Balakrishnan (1997)	Flat surface of a metal block	Water, CCl₄, acetone, n-hexane	100-1000	0.2, 0.52, 0.89, 1.17			At a given heat flux, nucleation site density (N_a) first decreases and then increases as surface micro-roughness increases.
2.	Jones et al. (2009)	Flat plate	Water, FC-77	0-400	0.027, 0.038, 1.08-10			Heat transfer coefficient increased with increase in surface roughness for FC-77 and water, but the effect of surface roughness was more pronounced for FC-77.

S. No.	Reference	Heater Element	Working Liquid	q'' (kW/m^2)	R_a (μm)	D_d	f	Observations
3.	McHale and Garimella (2010)	Flat plate	FC-77	-	0.03, 5.89	✓	✓	D_d increases with an increase in wall superheat, but is dependent on surface roughness also. N_a increases with heat flux and surface roughness. f increases with an increase in heat flux.
4.	McHale and Garimella (2013)	Flat plate	Water, FC-72, FC-77	0-200	0.26-7.5	✓	✓	D_d decreases with an increase in surface roughness as a first approximation.

S. No.	Reference	Heater Element	Working Liquid	q'' (kW/m^2)	R_a (μm)	D_d	f	Observations
5.	Bovard *et al.* (2017)	Cylindrical rod	Water, ethanol, acetone, methanol	0-120	30-430	✓	✓	D_d decreases as surface roughness increases.

Table 1.4 Summary of studies for heater inclination effect on boiling.

S. No.	Reference	Heater Element	Working Liquid	q'' (kW/m^2)	Inclination angle $\phi(°)$	D_d	f	Observations
1.	Githinji and Sabersky (1963)	Strip	Isopropyl alcohol	0-650	0, 90, 180			Boiling curves shift to the left as the heater inclination angle increases.
2.	Marcus and Dropkin (1963)	Flat metal block		16.6-112	0, 22.5, 45, 67.5, 90			Heat transfer coefficient for horizontal heaters is much higher than for vertical heaters in

S. No.	Reference	Heater Element	Working Liquid	q'' (kW/m^2)	Inclination angle $\phi(°)$	D_d	f	Observations
								saturated convection and boiling incipience, but the trend is reversed for vigorous boiling.
3.	Williams and Mesler (1967)	Strip	Water		0, 90			For artificial cavities, horizontal surface produces small spherical bubbles with negligible waiting period, and vertical surfaces produce large hemispherical bubbles with long waiting time. The influence of surface inclination was

S. No.	Reference	Heater Element	Working Liquid	q'' (kW/m^2)	Inclination angle $\phi(°)$	D_d	f	Observations
								observed to be much smaller for natural cavities.
4.	Chen and Chuang (1979)	Flat plate	R11		0, 30, 60, 90		✓	In the isolated bubble regime, f increases with wall superheat and surface inclination angle, but decreases with an increase in cavity radius.
5.	Nishikawa *et al.* (1984)	Flat plate	Water	17-450	0-175			Heat transfer coefficient increases as the surface inclination angle increases at low heat fluxes, but no

S. No.	Reference	Heater Element	Working Liquid	q'' (kW/m^2)	Inclination angle $\phi(°)$	D_d	f	Observations
								effect was observed at high heat fluxes.
6.	Kang (2003)	Tube	Water		0, 15, 30, 45, 60, 75, 90			Heat transfer coefficients were maximum and minimum when the tube was in near horizontal and vertical positions, respectively.

Table 1.5 Existing models for bubble departure diameter in pool boiling.

S. No.	Reference	Correlation Departure Diameter
1.	Fritz (1935)	$D_d = 0.0208 \, \theta \left[\dfrac{\sigma}{g(\rho_l - \rho_v)} \right]^{1/2}$

S. No.	Reference	Correlation Departure Diameter
2.	Ruckenstein (1961)	$D_d = \left[\dfrac{\rho_l \alpha^2}{g(\rho_l - \rho_v)}\right]^{1/3} Ja^{4/3}$
3.	Cole and Rohsenow (1969)	$D_d = C \left[\dfrac{\sigma}{g(\rho_l - \rho_v)}\right]^{1/2} Ja^{5/4}$, $C = 1.5 \times 10^{-4}\ for\ water, C = 4.65 \times 10^{-4}\ for\ other\ liquids.$
4.	Kutateladze and Gogonin (1979)	$D_d = 0.25 \left[\dfrac{\sigma}{g(\rho_l - \rho_v)}\right]^{1/2} (1 + 10^5 K_l)^{1/2}, K_l < 0.06$ $K_l = \left(\dfrac{Ja}{Pr}\right)\left[\left\{\dfrac{g\rho_l(\rho_l - \rho_v)}{\mu_l^2}\right\}\left\{\dfrac{\sigma}{g(\rho_l - \rho_v)}\right\}^{3/2}\right]^{-1}$
5.	Kocamustafaogullari (1983)	$D_d = 0.0012 \left(\dfrac{\rho_l - \rho_v}{\rho_v}\right)^{0.9} \left[\dfrac{\sigma}{g(\rho_l - \rho_v)}\right]^{1/2}$
6.	Jensen and Memmel (1986)	$D_d = 0.19 \left[\dfrac{\sigma}{g(\rho_l - \rho_v)}\right]^{1/2} (1.8 + 10^5 K_l)^{2/3}$
7.	Stephan (1992)	$D_d = 0.25 \left[\dfrac{\sigma}{g(\rho_l - \rho_v)}\right]^{1/2} \left(1 + \left(\dfrac{Ja}{Pr}\right) K_l\right)^{1/2}$

S. No.	Reference	Correlation Departure Diameter
8.	Kim and Kim (2006)	$D_d = 2\left[25\dfrac{\sqrt{27}}{2}\alpha.Ja\sqrt{\dfrac{\rho_l}{\sigma}}\right]^2$
9.	Phan *et al.* (2010)	$D_d = 1.94\left(\dfrac{\rho_v}{\rho_l}\right)^{1/2}\left(\dfrac{\rho_l}{\rho_v}-1\right)^{1/3}tan\theta^{-1/6}\left[\dfrac{\sigma}{g(\rho_l-\rho_v)}\right]^{1/2}$
10.	Hamzekhani *et al.* (2014)	$D_d = \left[\left\{\dfrac{\sigma}{g(\rho_l-\rho_v)}\right\}\left\{\dfrac{\mu_v v}{\sigma cos\theta}\right\}^{0.25}Ja^{0.75}\left\{\dfrac{g\rho_l(\rho_l-\rho_v)}{\mu_l^2}\left\{\dfrac{\sigma}{g(\rho_l-\rho_v)}\right\}^{3/2}\right\}^{0.5}\right]^{1/2}$
11.	Bovard *et al.* (2017)	$D_d = 17.952177\left(0.0172742+Ja^{1.285607}Ca^{0.661205}\left(\dfrac{\alpha_l}{\alpha_w}\right)^{0.025346}\right)\sqrt{\dfrac{\sigma}{g(\rho_l-\rho_v)}}$

Table 1.6 The models for bubble departure frequency in pool boiling.

S. No.	Reference	Correlation
1.	Jakob and Fritz (1931)	$f.D_d = 0.078$
2.	Peebles and Garber (1953)	$f.D_d = 1.18 \left[\dfrac{t_g}{t_g + t_w}\right]\left[\dfrac{\sigma g(\rho_l - \rho_v)}{\rho_l^2}\right]^{1/4}$
3.	Cole (1960)	$f^2 D_d = \dfrac{4g(\rho_l - \rho_v)}{3C_D \rho_l}$ $C_D = 1$ for water @ 1atm
4.	McFadden and Grassmann (1962)	$f.\sqrt{D_d} = 0.56\sqrt{g}$
5.	Zuber (1963)	$f.D_d = 0.59 \left[\dfrac{\sigma g(\rho_l - \rho_v)}{\rho_l^2}\right]^{1/4}$
6.	Hatton and Hall (1966)	$f.D_d^2 = 284.7\alpha_l$
7.	Ivey (1967)	$f^2 D_d = 0.9g$, hydrodynamic region $fD_d^{0.75} = 0.44g^{0.25}$, transition region $(cm^{0.25})$
8.	Mikic and Rohsenow (1969)	$f^{1/2}D_d = 0.83Ja\sqrt{\pi\alpha_l}, \quad 0.15 < \dfrac{t_g}{t_g + t_w} < 0.8$
9.	Stephan (1992)	$fD_d = \dfrac{1}{\pi}\left[\dfrac{g}{2}\left(D_d + \dfrac{4\sigma}{\rho_l g D_d}\right)\right]^{0.5}$

1.3.2. Flow Boiling

1.3.2.1. Cross Flow Boiling

Leong and Cornwell (1979) working with a horizontal tube bundle (reboiler with pitch-to-diameter ratio, $P/D = 1.34$) in R113 at atmospheric pressure observed a significant increase in the two-phase heat transfer in the upper tubes of the bundle compared to that of the lowest tubes. Cornwell and Schuller (1982) carried out photographic studies on the same setup

and observed a large number of bubbles originating in the lower tubes, which rise and impinge on the upper tubes to increase the intensity of turbulence to increase the heat transfer coefficient in the higher tubes. They also observed these bubbles grow and slide along the sides of the upper tubes. They measured the bubble mean diameter and height of two bubbles sliding on a heater tube, to estimate the thickness of the microlayer drying under them, and made an order of magnitude calculation for the contribution of these sliding bubbles to the increase in heat transfer. Their results showed that the bubbles sliding and growing on the sides of the upper tubes, take up enough energy to reduce the wall temperature and result in the increase of heat transfer coefficient by a factor of about 4 over that of the lower tubes at the same input heat flux. Singh *et al.* (1983) gave a correlation for heat transfer coefficient based on their experiments in cross flow boiling of water across a single tube. Singh *et al.* (1985) carried out similar experiments with R-12 at atmospheric pressure and proposed an asymptotic correlation for heat transfer coefficient with the underlying reasoning that the bulk flow velocity enhances the superficial velocity of the vapor bubbles to increase the heat transfer coefficient in cross flow boiling over that of pool boiling. Hwang and Yao (1986) studied the heat transfer across a single tube in a channel, a tube in a non-heated bundle and a heated bundle. In all the three cases, at low heat flux, heat transfer significantly increased with an increase in flow velocity, but at higher heat flux the velocity was found not to affect the heat transfer. Also, the heat transfer increased with an increase in the flow quality, but the increase was dependent on value of heat flux. At low heat flux, the bubbles coming from below impinge and slide on upper tubes to increase turbulence and hence, the enhanced heat transfer, but at the high heat flux, the upstream vapor bubbles become too big, that instead of impinging the upper tubes, they coalesce with bubbles of upper tubes to form a vapor blanket decreasing the heat transfer. The heat transfer for a tube in the bundle was higher than a single tube and the heat transfer in the heated and non-heated bundle were almost the same at high heat fluxes. They suggested the

combined effects of the enhanced bubble coalescence and circulation on the lower side of the heated tube lead to a higher quality distribution, and a higher effective velocity in the tube spacing due to the "quality boundary layer" formation on the heated tubes, which resulted in higher heat transfer coefficients for the bundle cases over a single tube in a channel. Jensen and Hsu (1988) studied the cross flow boiling heat transfer in a 27×5 inline tube bundle with a P/D ratio of 1.3. They also reported that the increase in heat and mass flux resulted in the increase of heat transfer coefficient, but only at low heat flux values. The increase in local heat transfer coefficient from bottom to top was also very small except at low heat fluxes. They compared their data to the model proposed by Hwang and Yao (1986), and found 20% over prediction, which according to them could be improved with better estimations of factors S and F. Gupta *et al.* (1995) studied the heat transfer in a horizontal tube bundle with varying pitch-to-diameter ratios ($P/D = 1.5 - 6$), and with tubes arranged in a vertical column ($n \times 1$ bundle). They concluded that the vapor bubbles rising from lower tubes and impinging on the upper tube surface enhance the turbulence which leads to increased heat transfer on the upper tubes compared to a single tube geometry. This increase was observed to decrease with an increase in flow velocity, possibly due to suppression of nucleation in the lower tubes under these conditions, which would lead to reduction of generated turbulence around the upper tubes. They also found that the heat transfer of a given tube increased with a decrease in P/D ratio. They proposed a correlation for the heat transfer coefficient for each tube in the bundle. Here, the total heat transfer coefficient is summation of Fh_{sp}, the heat transfer due to the bulk motion of the liquid and h_{mic}, the micro-convective component due to the growth and departure of the vapor bubbles. F is the enhancement factor that accounts for the increase in single phase heat transfer due to the turbulence created by vapor bubbles, and N is the row number counted from the bottom. Kumar *et al.* (2002) measured the two-phase heat transfer of the individual tubes in a vertical stack of two copper tubes. They reported that when both the tubes were

simultaneously heated, the heat transfer of the lower tube was same as when it was heated alone. However, the bubbles rising from the lower tube come in contact with the upper tube and increase the intensity of turbulence there to cause higher heat transfer coefficient. This causes enhanced convective heat transfer thereby reducing the wall temperature of the upper tube proportionally. This also results in reduced bubble population on the upper tube. They suggested that since the upper tube in the tube bank provided a higher heat transfer at a given heat flux, it can be considered to be working as a single tube at a higher effective heat flux ($q"_{upper}$ + a fraction of $q"_{lower}$). Gupta (2005) observed heat transfer of saturated water under atmospheric conditions in an 5×3 inline horizontal tube bundle ($P/D = 1.5$). He found that the heat transfer coefficient for the lower tube, like that for a single tube, increased with an increase in heat flux and cross flow velocity. The effect of velocity decreases as the heat flux increases, probably due to more developed nucleate boiling at higher heat flux values, with large number of bubbles generating greater intensity of turbulence, and the contribution of velocity in increasing turbulence further may be insignificant. He observed that the heat transfer coefficient was minimum for the lowest row tubes increasing in the upward direction reaching maximum at the topmost row. Higher the location of tube in the bundle, more the number of vapor bubbles reaching it from bottom tubes, causing higher its heat transfer coefficient. Further, the upper tubes showed a maxima in the heat transfer coefficient curve with the heat flux; the maxima occurred at lower heat flux values for upper tubes compared to the lower tubes. At high enough heat fluxes, the upper tubes are surrounded by a large number of vapor bubbles and do not have exposure to sufficient liquid, thereby reducing the heat transfer. Furthermore, they observed that the heat transfer coefficient could decrease with an increase in cross flow velocity for the upper tubes at low heat fluxes. At low heat fluxes, nucleation is small and the effects of velocity would supress nucleation on all the tubes, reducing the amount of vapor bubbles reaching the upper tubes, resulting in a fall in heat

transfer coefficient. Ribatski *et al.* (2008) studied boiling heat transfer of refrigerant R123 on a vertical array of horizontal tubes and found that the heat transfer increased in the upward direction of the bank, only for heat fluxes in the partial nucleate boiling region and remained constant beyond that. They also observed that the P/D ratio and the tube positioning in the array did not have a significant effect on the heat transfer in the fully developed nucleate boiling region. They observed that the ratio of heat transfer coefficient of second tube to that of the first tube (h_2/h_1), counting from the bottom, initially increases with heat flux to reach a peak and then decreases asymptotically in the range of higher heat fluxes. The peak of the ratio of heat transfer coefficients of the third and the first tube (h_3/h_1) was always higher than the ratio for second and first tubes, suggesting that h_N/h_1 increases with N upto a maximum value and remains constant after that. Based on their experiments, they proposed a generalised correlation for predicting h_N in a given tube bundle. Swain and Das (2017) studied the cross flow boiling heat transfer of water in a 5×3 bundle and found that varying the applied wall heat flux in a decreasing order from lowest to topmost tube, resulted in a higher overall heat transfer coefficient compared to when same heat flux is supplied to all the tubes. This is because of a larger number of bubbles being released from the lower tubes at higher power which then slide and contribute to increasing heat transfer coefficient in the upper tubes. Similarly varying the heat flux in an increasing order from bottom to top resulted in a lower overall heat transfer coefficient compared to uniform heat flux case, because of the vapor rising from the lower tubes coalesces with the vapor bubbles produced in the upper tubes to form a vapor blanket, resulting in a decrease in heat transfer coefficient. The heat transfer models for cross flow boiling conditions have been summarized in *Table 1.7* for reference.

Table 1.7 Heat transfer models for cross flow boiling in literature.

S. No.	Reference	Model equations	Application
1.	Singh *et al.* (1983)	$h = h_{sp}\left[1 + \left(\frac{h_{mic}}{sp}\right)^{0.86}\right]^{1.163}$ $h_{sp} = \left(\frac{k_l}{D}\right)Pr^{0.3}\left[0.35 + 0.56\left(\frac{DG}{\mu_l}\right)^{0.52}\right]$ $h_{mic} = \frac{q"}{T_w - T_l}$ (experimentally measured)	Cross flow boiling across a single horizontal tube.
2.	Singh *et al.* (1985)	$h = \left(1 + \frac{bv}{v_{su}}\right)^{0.67} h_{mic} + h_{sp}$ ($b = 0.4$, empirical constant) $h_{sp} = \left(\frac{k_l}{D}\right)Pr^{0.3}\left[0.35 + 0.56\left(\frac{DG}{\mu_l}\right)^{0.52}\right]$ $h_{mic} = \frac{1}{C_{sf}}\frac{k_l}{D}\left(\frac{DG}{\mu_l}\right)^{0.67} Pr^{-0.7}$ (Rohsenow (1952))	Cross flow boiling across a single horizontal tube.
3.	Hwang and Yao (1986)	$h = Sh_{mic} + Fh_{sp}$ $h_{mic} = \begin{cases} 0.16q"^{0.77}, & non\ heated\ bundle \\ 0.2086q"^{0.75}, & heated\ bundle \end{cases}$ $S = \frac{k_l}{Fh_{sp}Y}\left[1 - \exp(-\frac{Fh_{sp}Y}{k_l})\right]$	Cross flow boiling across a single horizontal tube, bundle.

S. No.	Reference	Model equations	Application
		$Y = 0.0205(D/Bo)$	
		$h_{sp} = h'_{sp}(1 - x_{loc})^{0.6}$	
		$h'_{sp} = \left(\frac{k_l}{D}\right) 0.366 Re_d^{0.6} Pr^{1/3}$, $\quad 4000 < Re_d < 2{\times}10^5$	
		$F = \left(\frac{1}{1-\alpha_m}\right)^{0.744}$	
		$\alpha_m = \frac{0.833 x_{loc}}{x_{loc}+(1-x_{loc})(\rho_v/\rho_l)}$	
4.	Gupta *et al.* (1995)	For the isolated single tube or lowest heated tube of the bundle:	Cross flow boiling heat transfer coefficient of each individual tube in the bundle.
		$h = h_{sp}\left[1 + \left(\frac{h_{mic}}{h_{sp}}\right)\right]$	
		$h_{sp} = \left(\frac{k_l}{D}\right)\left(0.4 Re^{1/2} + 0.06 Re^{2/3}\right) Pr^{0.36} \left(\frac{\mu_l}{\mu_v}\right)^{0.25}$ (Whitaker (1972))	
		$h_{mic} = 13.035(T_w - T_{sat})^{2.881}$	
		For the upper tubes of the bundle	
		$h = F h_{sp} + h_{mic}$	
		$F = 851.38 Bg^{0.707}(P/D)^{-0.245} N^{0.577}$	

S. No.	Reference	Model equations	Application
5.	Shah (2005)	$\psi = h/h_{sp}$ $\psi = \psi_0$ at $\Delta T_{sub} = 0$ $\psi = \psi_0 + \frac{\Delta T_{sub}}{\Delta T_{sat}}$ at $\Delta T_{sub} > 0$ $\psi_0 = 1 + \frac{Bg}{(0.000216 + 0.041Bg - 1.53Bg^2)}$ $h_{sp} = \begin{cases} \left(\frac{k_l}{D}\right)0.21Re^{0.62}Pr^{0.4}, Re > 700 \\ \left(\frac{k_l}{D}\right)0.615Re^{0.466}Pr^{1/3}, Re < 700 \end{cases}$ (Shah (1984)) (Holman (1968))	Subcooled cross flow boiling across a single horizontal tube.
6.	Gupta (2005)	Same as Gupta *et al.* (1995) only with $F = 134.24Bg^{0.469}(P/D)^{-0.311}N^{0.946}C^{0.304}$ C: column factor ($C = 2\ and\ 3$, for side and central column tubes)	Cross flow boiling in $n \times c$ bundle.
7.	Shah (2007)	$h = F_{mic}h_{cooper}, \ Y_{IB} > 0.0008$ $\psi = \psi_0, \ 0.00021 < Y_{IB} \le 0.0008$ $\psi = \frac{2.3}{Z^{0.08}Fr^{0.22}}, \ Y_{IB} \le 0.00021$	Cross flow boiling heat transfer coefficient of each

S. No.	Reference	Model equations	Application
		$F_{mic} = \dfrac{h_{mic,actual}}{h_{cooper}}$ $h_{cooper} = 55.1 q''^{0.67} p_r^{0.12} (-\log_{10} p_r)^{-0.55} M^{-0.55}$ $Y_{IB} = F_{mic} Bg. Fr^{0.3}$ $Z = \left(\dfrac{1-x}{x}\right)^{0.8} Pr^{0.4}$ $\psi_0 = max\{443 Bg^{0.65} F_{mic}, 31 Bg^{0.33} F_{mic}, 1\}$ *Use $\psi = \psi_0$, when $x = 0$ and $Y_{IB} \leq 0.00021$ $h_{sp} = \left(\dfrac{k_l}{D}\right) 0.21 Re^{0.62} Pr^{0.4}$ (Shah (1984))	individual tube in the bundle.

Hence, it can be seen that a lot of work has been done to understand the enhancement of heat transfer in a horizontal tube bank under cross flow conditions, but even though many authors have attributed the increase to the vapor bubbles, there have been almost no efforts to measure the bubble size or departure frequency in tube bundles. Also, no models have been developed for predicting departure diameter and frequency under cross flow conditions.

1.3.2.2. Forced convective upward boiling

In convective boiling, the bubble size can be characterized by: (1) maximum diameter (D_{max}), the maximum size a bubble attains before condensation starts dominating the evaporation; (2) departure diameter (D_d), the bubble size when it leaves its nucleation site and starts to slide along the heater surface; (3) lift-off diameter (D_{lo}), the bubble size when it leaves the heater surface and moves in the bulk liquid. Bubble departure frequency is defined as the inverse of the time period between two consecutive bubble departures from a given nucleation site. Gunther (1951) and Tolubinsky and Kostanchuk (1970) studied the bubble growth and collapse in highly subcooled water. Their measurements of the bubble maximum diameter showed that it increases with an increase in the heat flux, but decreases with an increase in the subcooling. Abdelmessih *et al.* (1972) studied the growth and collapse of vapor bubbles nucleating from an artificial site created on a stainless-steel heating strip in slightly subcooled water. They observed that in the beginning, bubbles were hemispherical in shape but as the bubbles grow, they become oblate due to the shearing effect of the flow. They form an inverted pear shape while sliding on the heater surface and assume an ellipsoidal shape upon lift-off from the surface. They found that the bubble population, maximum diameter and lifespan decreases with an increase in the flow velocity but increases with an increase in the heat flux. They observed that as the liquid velocity increases, the growth time decreases but waiting period increases at low heat flux values; while at high heat fluxes, both growth and waiting period tend to remain independent of the liquid velocity, resulting the frequency to be

unaffected by the liquid velocity under all conditions. The frequency of bubble formation was found to increase with an increase in the heat flux up to a point and became constant after that. Ünal (1976) experimentally observed the bubble growth rate and maximum diameters for subcooled water at very high heat flux, mass flux and pressures. He observed the maximum diameter to increase with an increase in heat flux and a decrease in the subcooling. He proposed a semi-empirical equation for bubble growth and maximum diameter derived from a heat transfer controlled bubble model, which is valid for $1 < P < 177\ bar$. But, the assumptions on which the model is based have mostly been derived from the studies in pool boiling. Del Valle and Kenning (1985) studied subcooled flow boiling at high heat fluxes (~70-95% of CHF) and found that for the conditions of their study, total applied heat flux could be expressed as a simple superposition of the convective and nucleate boiling heat flux. Calculating the nucleate boiling heat transfer coefficient, they found it to increase with an increase in the degree of subcooling. Their experiments showed that the bubble maximum diameter increases with heat flux at small values, but at high values of heat flux, bubble size tends to decrease. They measured growth and waiting times to conclude that frequency increases with heat flux since the waiting time decreased with an increase in heat flux.

Bibeau and Salcudean (1994) observed bubble growth and collapse at different degrees of subcooling at atmospheric pressure and found that under identical conditions, bubble growth rate remains the same but the bubble maximum diameter and the lifetime can vary from bubble to bubble. They observed that the bubbles departed from their sites almost immediately after nucleation and slide along the heater surface, growing and then condensing up to the lift-off. They found two regions of bubble sliding behaviour for constant velocity and subcooling; at low heat fluxes, close to onset of nucleate boiling, bubbles slide for distances ∼8-50 mm; while at higher heat fluxes, bubble slide up to an average distance of 2 mm. Zeitoun and Shoukri (1996) examined the effect of heat flux, mass flux and inlet subcooling on the vapor bubbles

at near atmospheric pressure. They measured the sauter mean diameter of the bubbles using heat speed photography and found that the bubble growth and condensation cycle remains similar upstream and downstream of the Net Vapor Generation (NVG) point. They identified NVG as the point after which large coalesced bubbles are formed thereby entering the fully developed nucleate boiling regime. They observed that the mean bubble size and the lifetime decreased with an increase in mass flux for high subcooling, but as the subcooling decreased (less than 10 K), the trend reversed as the enhanced mass flux enhanced the coalescence. The mean bubble diameter and lifetime increased with an increase in the heat flux and decrease in the liquid subcooling. Thorncroft *et al.* (1998) carried out experiments with slightly subcooled FC-87 in both upward and downward flow conditions and observed that the bubble dynamics differ significantly in the two scenarios. In their experiments, the vapor bubbles did not lift-off in the upflow condition, except the rare ones due to random fluctuations, while the bubbles regularly lifted off in downflow. The bubble growth rate, departure diameter and lift-off diameters increased with an increase in heat flux and decreased with an increase in subcooling or mass flux for both upflow and downflow. They recorded a decrease in waiting period with an increase in heat flux, meaning the departure frequency would increase with heat flux. They also noted that waiting period and departure diameter were directly correlated, implying that departure diameter and frequency would be inversely related. Prodanovic *et al.* (2002) in continuation of Bibeau and Salcudean (1994) work, parametrically studied bubble growth and collapse measuring the bubble maximum and lift-off diameters at pressure of 2 and 3 bar. They found three flux regions: (1) low flux region which is characterized by the low bubble population and spherical bubbles that seldom lift from the surface, (2) isolated bubble region, where individual bubbles grow and slide on heater surface getting elongated in the process, and eventually lift-off from the surface, (3) bubble coalescence region, where bubbles coalesce due to high population resulting in large bubbles of various shapes and sizes. Their parametric

studies showed that the bubble maximum diameter and lifespan decreased with an increase in heat flux (more noticeable at low heat flux values), liquid velocity, degree of subcooling and pressure (1-3 bar).

Situ *et al.* (2004) and Situ *et al.* (2005) measured lift-off diameters of the vapor bubbles in an annular geometry and concluded that higher values of inlet liquid temperature, heat flux and lower values of liquid flow velocity would result in higher surface temperatures and hence, higher bubble lift-off diameters. Also, they observed that lift-off diameter might first increase and then decrease with an increase in bubble departure frequency. They observed two kinds of nucleation sites, one with almost negligible waiting period and the other with significantly longer waiting periods, while the growth period remained similar for all sites. Their measurements showed that bubble departure frequency increased with an increase in heat flux at first (due to fall in the waiting period), but it saturated after a point which was characterized by bubble coalescence at the nucleation site corresponding to the zero-waiting period. Similar trends were observed by Okawa *et al.* (2007) in their experiments in a tube with a transparent ITO film as heater surface. They measured departure frequency under different conditions and observed that the departure frequency increased with an increase in the heat flux and the pressure, and decreased with an increase in the liquid velocity and degree of subcooling. Situ *et al.* (2008) measured bubble departure frequency in the same setup as used by Situ *et al.* (2005) under varied conditions. They performed non-dimensional analysis of their own data along with that obtained by Basu *et al.* (2005b) and Thorncroft *et al.* (1998), and compared it with different available models (both pool and flow boiling). They found that the pool boiling models do not satisfactorily predict the flow boiling data, and the flow boiling models were also not working well. They proposed a new correlation for non-dimensional departure frequency in terms of dimensionless nucleate boiling heat flux. Murshed *et al.* (2010) conducted experiments with refrigerant R-134a and studied the effect of heat flux and system

pressure on the bubble behaviour. They concluded that the departure diameter increased non-linearly with heat flux since higher heat flux means higher surface temperature. They also observed the departure diameter to increase with an increase in system pressure, but noted that this may not be true for all experiments. They also measured departure frequency under different conditions and observed that the departure frequency increased with an increase in heat flux and pressure, and decreased with an increase in liquid velocity. Euh *et al.* (2010) measured bubble departure frequency under different thermal conditions for water and observed that the departure frequency increased with an increase in the heat flux and the pressure, and decreased with an increase in the liquid velocity and the degree of subcooling.

Chen *et al.* (2011) studied bubble growth and collapse under different system pressures (1-10 bar) and observed that bubble growth rates and bubble sizes decreased as the system pressure increased. They proposed a power growth curve equation for dimensionless bubble growth rate for the thermally controlled growth region, which would be valid for a wide range of pressures. Yuan *et al.* (2011) working on the same setup observed that the bubble growth rates are significantly higher for low pressures compared to high pressures. Also for low pressures (1-3 bar), the bubbles grew at nucleation sites and collapsed without sliding, while at higher pressures, the bubbles grew while sliding instead of collapsing. Their parametric studies showed that the maximum bubble diameter decreased with an increase in the degree of subcooling and the mass flux, but with an increase in heat flux, it first increased and reversed the trend after a point. Chu *et al.* (2011) studied the subcooled boiling with water in an annulus and observed that the lift-off diameter or bubble departure frequency (f) do not follow any general trend independently and show competition in removing thermal energy from the surface. Rather, the product $f.D_{lo}^2$ increases with an increase in the heat flux and decreases with an increase in subcooling or liquid mass flux. Ahmadi *et al.* (2012) studied bubble dynamics in the subcooled flow boiling of water under a wide range of pressure (0.9- 9 bar).

They observed two kinds of bubble behaviours, one where bubbles lifted off the heater surface without sliding, and second where bubbles were seen sliding along the heater surface for long distances. Based on their experiments, they suggested that the boundary between these behaviours to be given by Jakob number (Ja): when $Ja > 35$, the bubbles would lift off directly; for $Ja < 15$, the bubbles would slide, and the bubbles would show both behaviours for the Jakob numbers between 15 and 35. Sugrue (2012) studied the effect of heater orientation angle, subcooling, heat flux, mass flux and pressure on bubble departure diameter and compared the results with the mechanistic model of Klausner *et al.* (1993). He observed that the departure diameter increased with increasing heat flux, decreasing degree of subcooling, decreasing mass flux and decreasing pressure. His observations also showed that the largest bubbles departed from the downward facing horizontal heater (inclination angle of 0°) and smallest bubbles from a vertical heater (angle 90°). They compared their results with the Klausner model which gave good qualitative agreement with reference to behaviour of diameter with thermal conditions but showed substantial quantitative errors. Phillips (2014) studied subcooled flow boiling using synchronized high-speed videography, IR thermography and PIV imaging techniques on a similar setup. He recorded that the heat transfer coefficient increased with an increase in mass flux in the single-phase region, but was less affected by heat flux at a given mass flux. When boiling began, the heat transfer coefficient increased considerably and the different mass flux curves merged for high heat flux values. The bubble departure diameter trends with heat flux, mass flux, pressure and subcooling were like those observed by Sugrue (2012). He measured departure frequency under different conditions and observed that the departure frequency increased with an increase in the heat flux, degree of subcooling and pressure, and decreased with an increase in the liquid velocity. He compared the experimental results for departure frequency with the models of Podowski and Podowski (2009), Yeoh *et al.* (2011) and Basu *et al.* (2005a) and found that the models could predict the

growth time adequately but not the waiting time, and hence, the frequency was over predicted. Guan *et al.* (2015) in their subcooled boiling experiments at atmospheric pressure observed that the bubble departure diameter increased with an increase in heat flux, albeit slightly, but decreased with an increase in the degree of subcooling or mass flux. Based on their experiments, they proposed bubble contact diameter as a logarithmic function of bubble diameter, since the contact diameter of the bubble would change with bubble growth. Ahmadi and Okawa (2015) studied the effect of surface wettability on vapor bubble growth and departure. They observed that the bubbles tend to grow and condense at their nucleation sites for hydrophobic surfaces (contact angle$>70°$) while for the hydrophilic surfaces, the bubbles either lift off from the surface or slide along the heater depending on the system pressure and Ja. Further, their results showed that while the nucleation site density decreases with an increase in surface wettability, the mean bubble diameter and wall superheat increases. Cao *et al.* (2016) studied the effect of subcooling and mass flux on the bubble growth and deformation in subcooled flow boiling. They found that for low subcoolings ($\sim 10\,K$), small spherical bubbles grow regularly without any significant deformation at low as well as high flow rates. Also, the departure diameter is very close to maximum diameter and can be effectively treated the same for low subcoolings. At medium subcoolings ($\sim 15 - 30\,K$), low flow rates, the bubble suffered condensation and deformation at the upstream side due to the incoming cold fluid. While at high flow rates, the upstream deformation was coupled with the bubble rolling and sliding on the heater surface due to additional shear. At high subcoolings ($\sim 30 - 50\,K$) and low flow rates, thin superheated boundary layer and liquid entrainment due to bubble motion resulted in a two-sided deformation of the bubble resulting in a very long necking of the bubble. At high flow rates, the bubble shows a concave shape during necking due to the force of the incoming liquid. Guan *et al.* (2016) measured the bubble contact and departure diameters under varied conditions of subcooled flow boiling and showed that bubble departure

diameter is directly dependent on the contact diameter. Yoo *et al.* (2016) focused on the bubble behaviour after departure from the nucleation site in the subcooled flow boiling of water. They observed a bouncing phenomenon shown by the bubbles just after departing from nucleation sites and before start of the sliding, where the bubble attains a bouncing maximum size. They found that higher the wall superheat, more prominent is the bouncing. During the sliding, the bubbles were observed to shrink and then grow again for low mass fluxes, while for the high mass fluxes, bubbles grew more steadily. Also, the bubble sliding velocity was found to be greater than the local liquid velocity for low mass fluxes while the trend reversed for high mass fluxes. They also observed that the mean bubble diameter decreased with an increase in subcooling or mass flux, while no consistent trends could be observed for the bubble departure frequency. Setoodeh *et al.* (2016) measured the subcooled flow boiling heat transfer coefficient in a channel for varying surface roughness, inlet mass flux and channel inclination angle. They compared their data with Chen's correlation, but found significant deviations. Hence, they proposed empirical correlations for forced convection and subcooled flow boiling heat transfer based on their data in the thermodynamically underdeveloped region. The details of the various experiments from literature are summarized in *Table 1.8*.

Based on the understanding developed with the visualization experiments, a number of empirical and analytical models have been proposed for bubble maximum, departure and lift-off diameter, and bubble departure frequency. The analytical models for bubble diameters are based on the balance of all the forces acting on a bubble. The basic assumption of these models is that all the forces in x- (direction parallel to the flow) and y-direction (perpendicular to the flow) are in balance while the bubble is growing at the surface. When the forces in the x-direction unbalance, the bubble leaves its nucleation site and starts to slide along the surface, and when the forces in the y-direction are no longer in balance, the bubble lifts from the heater surface. The models are solely based on the physical description of the individual forces and

hence, departure and lift-off do not necessarily have a temporal order. The major forces involved in bubble growth at a surface are surface tension force F_s, quasi-steady drag force F_{qs}, buoyancy force F_b, shear lift force F_{SL}, unsteady drag force due to asymmetrical bubble growth F_{du}, hydrodynamic pressure F_h and contact pressure forces F_{cp}. A graphical representation of all the acting forces in given in *Figure 1.3* for reference.
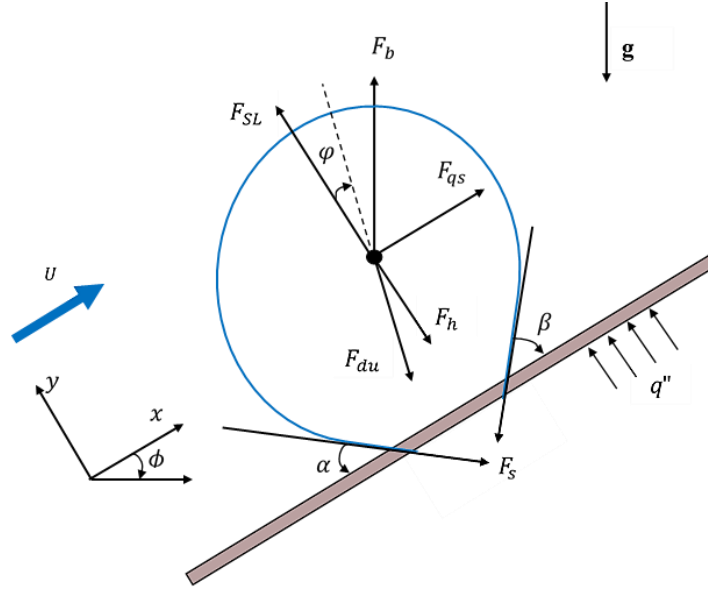
Figure 1.3 Diagram for all the forces acting on a bubble.

The empirical models for bubble diameter is usually expressed as a parametric relationship between diameter and various variables like heat flux, wall superheat, subcooling, mass flux and liquid properties, all expressed in terms of dimensionless numbers. The most widely used empirical and analytical models for bubble diameters are summarized in *Table 1.9* and *Table 1.10*, respectively. Regarding the bubble departure frequency, a few empirical models have been proposed over the years, based on the limited data available in the literature. Again, as in pool boiling, the bubble frequency is found to be significantly affected by the value of bubble departure or lift-off diameter. Hence, the models proposed reflect this observation, and express frequency parametrically as a function of bubble diameter, wall superheat, heat flux, subcooling, liquid properties, etc. The available models for bubble departure frequency are tabulated in *Table 1.11* for reference.

Table 1.8 Summary of vertical flow boiling experiments in literature.

S. No.	Reference	Working liquid	$q''(\frac{kW}{m^2})$	ΔT_{sat} (K)	ΔT_{sub} (K)	P (bar)	G (kg/m²s)	D_{max}	D_d	D_{lo}	f	Remarks
1.	Gunther (1951)	Water	4500-6140		20-86	1, 1.7	77.76-6087.8	✓				D_{max} increases with an increase in heat flux and a decrease in degree of subcooling.
2.	Tolubinsky and Kostanchuk (1970)	Water	470		5-60	1	192.4-198.4	✓				D_{max} increases with an increase in heat flux and a decrease in degree of subcooling.
3.	Abdelmessih *et al.* (1972)	Water	187.26-460.26	6.8	1.85	1	796.1-1274.1	✓			✓	D_{max} increases with an increase in heat flux and a decrease in flow velocity. f increases with an

S. No.	Reference	Working liquid	$q"(\frac{kW}{m^2})$	ΔT_{sat} (K)	ΔT_{sub} (K)	P (bar)	G (kg/m²s)	D_{max}	D_d	D_{lo}	f	Remarks
												increase in heat flux up to a point and is constant thereafter, and is independent of flow velocity.
4.	Ünal (1976)	Water	380-550		3-6	139-177	3139.2-3600	✓				D_{max} increases with an increase in heat flux and a decrease in degree of subcooling.
5.	Del Valle and Kenning (1985)	Water	3444-4683	21-24	84	1	1698.2	✓			✓	D_{max} increases with an increase in heat flux at low values, but behaviour is opposite at high flux values.

S. No.	Reference	Working liquid	$q''(\frac{kW}{m^2})$	ΔT_{sat} (K)	ΔT_{sub} (K)	P (bar)	G (kg/m²s)	D_{max}	D_d	D_{lo}	f	Remarks
												f increases with an increase in heat flux.
6.	Bibeau and Salcudean (1994)	Water	100-1200		10-60	1.05	81.06-395.65	✓				D_{max} decreases with an increase in heat flux, flow velocity and degree of subcooling.
7.	Zeitoun and Shoukri (1996)	Water	286.5-705.5		11.6-31.1	1.17-1.68	150-412					Axial distribution of sauter mean diameter was studied. NVG point was found to be independent of bubble departure.
8.	Thorncroft, Klausner and Mei (1998)	FC-87	2.8-11.8 (up) 1.3-14.6	0.54-7 (up) 0.05-	1.9-3.3 (up) 3.9-5	1	192-319 (up) 192-666		✓		✓	No lift-off in upflow, while regular lift-off in downflow.

S. No.	Reference	Working liquid	$q''(\frac{kW}{m^2})$	ΔT_{sat} (K)	ΔT_{sub} (K)	P (bar)	G (kg/m²s)	D_{max}	D_d	D_{lo}	f	Remarks
			(down)	7.17 (down)	(down)		(down)					Bubble growth rate, D_d and D_{lo} increase with an increase in heat flux, decrease in subcooling and flow velocity. f increases with an increase in heat flux.
9.	Prodanovic *et al.* (2002)	Water	200-1000		10, 20, 30	1.05, 2, 3	77.2-791.5	✓		✓		D_{max}, D_{lo} and bubble lifetime decreases with an increase in heat flux, flow velocity, degree of subcooling and pressure.
10.	Situ *et al.* (2004),	Water	61.8-108		2-20	1	478.8-905.4			✓	✓	D_{lo} increases with an increase in heat flux and

S. No.	Reference	Working liquid	$q"(\frac{kW}{m^2})$	ΔT_{sat} (K)	ΔT_{sub} (K)	P (bar)	G (kg/m²s)	D_{max}	D_d	D_{lo}	f	Remarks
	(2005), (2008)											decrease in flow velocity and subcooling. It may first increase and then decrease with an increase in frequency. f increases with an increase in heat flux at first, but saturates later.
11.	Okawa et al. (2007)	Water	67-550	6-21	9-21	1.23	86.57-1443.24			✓	✓	D_{lo} increases with an increase in heat flux and decrease in flow velocity and subcooling. f increases with an increase in heat flux and

S. No.	Reference	Working liquid	$q''(\frac{kW}{m^2})$	ΔT_{sat} (K)	ΔT_{sub} (K)	P (bar)	G ($kg/m^2 s$)	D_{max}	D_d	D_{lo}	f	Remarks
												pressure, and with decrease in flow velocity. f decreases with an increase in subcooling.
12.	Murshed *et al.* (2010)	R-134a	134, 194-360	4-10	Sat	6.9,7.6, 8.27	1206		✓		✓	D_d increases with an increase in heat flux and pressure (not for all cases). f increases with an increase in heat flux and pressure, and with decrease in flow velocity.

55

S. No.	Reference	Working liquid	$q''(\frac{kW}{m^2})$	ΔT_{sat} (K)	ΔT_{sub} (K)	P (bar)	G ($kg/m^2 s$)	D_{max}	D_d	D_{lo}	f	Remarks
13.	Euh *et al.* (2010)	Water	61.3-238		7.5-23.4	1.7-2 3.3-3.5	226.6-953.9				✓	*f* increases with an increase in heat flux and pressure, and with decrease in flow velocity. No distinct behavior with subcooling could be inferred.
14.	Chen *et al.* (2011)	Water	83.6-188.6		15-30	1-10	86-400					Bubble growth rates and mean bubble sizes decrease with an increase in system pressure.

S. No.	Reference	Working liquid	$q"(\frac{kW}{m^2})$	ΔT_{sat} (K)	ΔT_{sub} (K)	P (bar)	G ($kg/m^2 s$)	D_{max}	D_d	D_{lo}	f	Remarks
15.	Yuan et al. (2011)	Water	84-350	1.4-12.6	20-36	1.2-10.4	76.6-602.7	✓				Bubble growth rates much higher at low pressures. D_{max} decreases with an increase in flow velocity and degree of subcooling. It increases with an increase in heat flux first and then reverses trend after a point.
16.	Chu et al. (2011)	Water	140, 200		4, 12, 22	1.39-1.52	300, 500, 700			✓	✓	The product $f.D_{lo}^2$ increases with an increase in heat flux,

S. No.	Reference	Working liquid	$q''(\frac{kW}{m^2})$	ΔT_{sat} (K)	ΔT_{sub} (K)	P (bar)	G (kg/m²s)	D_{max}	D_d	D_{lo}	f	Remarks
												decrease in subcooling or flow velocity.
17.	Ahmadi et al. (2012)	Water	80-611	3.5-18.4	4-30	0.96-8.6	169-1170					Determined the boundary between the sliding and non-sliding bubbles in terms of Ja. $Ja < 15$: bubbles slide $Ja > 35$: lift off $15 < Ja < 35$: both
18.	Sugrue (2012)	Water	50,100		10,20	1.01	250- 400		✓			D_d increases with an increase in heat flux, decrease in subcooling, flow velocity and pressure.

S. No.	Reference	Working liquid	$q"(\frac{kW}{m^2})$	ΔT_{sat} (K)	ΔT_{sub} (K)	P (bar)	G (kg/m²s)	D_{max}	D_d	D_{lo}	f	Remarks
												Good qualitative agreement with Klausner *et al.* (1993) model, but large quantitative errors.
19.	Phillips (2014)	Water	100-400	1.-15	5-15	1.05	150-750	✓			✓	h increases with flow velocity in single phase region, less affected by heat flux. In two phase region, h unaffected by flow velocity. D_d increases with an increase in heat flux, decrease in subcooling, flow velocity and

S. No.	Reference	Working liquid	$q''(\frac{kW}{m^2})$	ΔT_{sat} (K)	ΔT_{sub} (K)	P (bar)	G (kg/m²s)	D_{max}	D_d	D_{lo}	f	Remarks
												pressure.
												f increases with an increase in heat flux and pressure, and with decrease in flow velocity.
												f increases with an increase in subcooling.
20.	Guan *et al.* (2015)	Water	68.2-101.4		8.5-10.5	1	87.3-319.2				✓	D_d increases with an increase in heat flux, decrease in subcooling and flow velocity. Contact diameter changes as bubble grows, proposed D_w as log

S. No.	Reference	Working liquid	$q"(\frac{kW}{m^2})$	ΔT_{sat} (K)	ΔT_{sub} (K)	P (bar)	G (kg/m^2s)	D_{max}	D_d	D_{lo}	f	Remarks
												function of bubble diameter.
21.	Ahmadi and Okawa (2015)	Water	~200	4-15	3.7-16.8	1, 2, 4	~400					Bubbles grow and depart at nucleation sites for hydrophobic surfaces, but bubbles slide and lift off from surface for hydrophilic surfaces.
22.	Cao et al. (2016)	Water	92-490		5-50	1	100-800					Divided the bubble growth and deformation and sliding behaviour into three categories based on the degree of subcooling.
23.	Guan et al.	Water	68.2-104.3		9	1	87.3-319.2		✓			Bubble departure

S. No.	Reference	Working liquid	$q''(\frac{kW}{m^2})$	ΔT_{sat} (K)	ΔT_{sub} (K)	P (bar)	G (kg/m^2s)	D_{max}	D_d	D_{lo}	f	Remarks
	(2016)											diameter is directly related to contact diameter.
24.	Yoo *et al.* (2016)	HFE-301	8-35		4.5-13.6	1	140-700				✓	Bounce in the bubble just after departure and before it starts sliding was noted, and found more significant at higher wall temperatures. Mean bubble diameter decreased with an increase in subcooling or mass flux but frequency shoed no consistent

S. No.	Reference	Working liquid	$q''(\frac{kW}{m^2})$	ΔT_{sat} (K)	ΔT_{sub} (K)	P (bar)	G (kg/m²s)	D_{max}	D_d	D_{lo}	f	Remarks
												trends.
25.	Setoodeh *et al.* (2016)	Water	0-160	0-35	20	1.4	486-875				✓	Heat transfer increase with increase in surface roughness and mass flux. Heat transfer increases with increase in surface inclination for smooth surface, but decreases for rough surfaces.

Table 1.9 Empirical models for bubble diameter in flow boiling.

S. No.	Reference	Empirical correlation
1.	Ünal (1976)	$$D_{max} = \frac{1.21a\alpha}{\sqrt{bC\Phi}}$$ $$a = \frac{(q''-h\Delta T_{sub})^{1/3}k_l Y}{2C_1^{1/3}\rho_v h_{fg}\sqrt{\pi\alpha_l}}, \quad b = \frac{\Delta T_{sub}}{2(1-(\rho_v/\rho_l))}, \quad \Phi = \begin{cases} (\frac{U}{U_0})^{0.47}, U > 0.61\ m/s \\ 1, U \leq 0.61\ m/s \end{cases}, v_0 = 0.61 m/s$$ $$\alpha = \begin{cases} (2\times10^{-5})P^{0.709}[65-(5.69\times10^{-5})(P-10^5)]^{0.5}, & 0.1 \leq P\ (MN/m^2) \leq 1 \\ 1, & 1 < P(MN/m^2) < 17.7 \end{cases}$$ $$C = \begin{cases} 65-(5.69\times10^{-5})(P-10^5), & 0.1 \leq P\ (MN/m^2) \leq 1 \\ 0.25\times10^{10}P^{-1.418}, & 1 < P(MN/m^2) < 17.7 \end{cases}$$
2.	Tolubinsky and Kostanchuk (1970)	$$D_d = min\left[0.0014, 0.0006exp\left(-\frac{\Delta T_{sat}}{45}\right)\right]$$
3.	Farajisarir (1993)	$$D_{max}^+ = 10.02Ja^{-1.65}\vartheta^{-1.65}$$ $$D^+ = \frac{\sigma D}{\rho_l \alpha_l^2}$$
4.	Prodanovic *et al.* (2002)	$$D_{max}^+ = 236.749Ja^{-0.581}\vartheta^{-0.8843}\left(\frac{\rho_l}{\rho_v}\right)^{1.772}Bg^{0.138}$$ $$D_{lo}^+ = 440.98Ja^{-0.708}\vartheta^{-1.112}\left(\frac{\rho_l}{\rho_v}\right)^{1.747}Bg^{0.124}$$

S. No.	Reference	Empirical correlation
5.	Basu *et al.* (2005)a, (2005)b	$D_d^* = 1.3(\sin\theta)^{0.4}[0.13\exp(-1.75\times10^{-4}Re_l) + 0.005]Ja_{sup}^{0.45}\exp(-0.0065Ja_{sub})$
		$D_{lo}^* = 1.3(\sin\theta)^{0.4}[0.2\exp(-1.28\times10^{-4}Re_l) + 0.005]Ja_{sup}^{0.45}\exp(-0.0065Ja_{sub})$
		$$D^* = \frac{D}{L_c}, L_c = \sqrt{\frac{\sigma}{g(\rho_l - \rho_v)}}$$
6.	Chu *et al.* (2011)	$D_{lo}^+ = 12788.5Ja^{-0.28}\vartheta^{-1.07}\left(\frac{\rho_l}{\rho_v}\right)^{1.36}Bg^{0.35}$
7.	Brooks and Hibiki (2015)	$D_d^* = C_D Ja_T^{-0.49}\left(\frac{\rho_l}{\rho_v}\right)^{0.78}Bg^{0.44}Pr^{1.72}$
		$C_D = \begin{cases} 0.00211, conventional\ channels \\ 0.0136, mini-channels \end{cases}$
8.	Yang *et al.* (2016)	$D_d^* = 0.0058\exp(-0.0001Re_l)Ja_{sup}^{1.45}\exp(-0.015Ja_{sub})$

Table 1.10 Mechanistic models for bubble departure diameter in flow boiling.

S. No.	Reference	Equations
1.	Klausner *et al.* (1993)	$$\sum F_x = F_{sx} + F_{qs} + F_{du}\sin\varphi$$ $$\sum F_y = F_{sy} + F_{sL} + F_b + F_h + F_{cp} + F_{du}\cos\varphi \qquad \varphi\text{: bubble inclination angle with y}$$ $$F_{sx} = -1.25 d_w \sigma \frac{\pi(\alpha-\beta)}{\pi^2-(\alpha-\beta)^2}(\sin\alpha + \sin\beta)$$ $$F_{sy} = -d_w \sigma \frac{\pi}{(\alpha-\beta)}(\cos\beta - \cos\alpha); \qquad d_w = 0.09mm, \alpha = \pi/4, \beta = \pi/5$$ $$F_{qs} = 6\pi\rho_l \nu \Delta U R \left[\left(\tfrac{2}{3}\right) + \left\{(\tfrac{12}{Re_b})^{0.65} + 0.862\right\}^{-1.54}\right], \quad Re_b = 2UR/\nu$$ $$F_{du} = -\rho_l \pi R^2 (\tfrac{3}{2}\dot{R}^2 + R\ddot{R}),$$ $$F_{sL} = 0.5\rho_l \Delta U^2 \pi R^2 \left[3.877 G_s^{1/2}\{Re_b^{-2} + 0.014 G_s^2\}^{1/4}\right]$$ $$G_s = \left|\frac{dU}{dy}\right|\frac{R}{\Delta U}, \Delta U = U - u_b$$ $$F_b = -\frac{4}{3}\pi R^3 (\rho_l - \rho_v)g$$ $$F_h = \frac{9}{8}\rho_l \Delta U^2 \frac{\pi d_w^2}{4}$$ $$F_{cp} = \frac{\pi d_w^2}{4}\frac{2\sigma}{r_c}, r_r \approx 5R$$ $$U(y) = u^*\left[\frac{1}{\kappa}\ln\left(1 + \kappa\frac{yu^*}{\nu}\right) + c\left\{1 + \exp\left(-\frac{\frac{yu^*}{\nu}}{\chi}\right) - \frac{\frac{yu^*}{\nu}}{\chi}\exp\left(-0.33\frac{yu^*}{\nu}\right)\right\}\right]$$

S. No.	Reference	Equations
		$\kappa = 0.4, \chi = 11, c = 7.4, u^* = 0.04u_l , u_l = \dfrac{G(1-X)D}{\rho_l \delta} , X = 0.106,\ \delta = 6.5mm$
		$R = \dfrac{2B^2}{3A}\left[(t^+ + 1)^{3/2} - (t^+)^{\frac{3}{2}} - 1\right], t^+ = A^2 t/B^2,$
		$A = \left(\dfrac{\pi \rho_v h_{fg}\Delta T_{sat}}{\rho_l T_{sat}}\right)^{1/2}, B = \sqrt{\dfrac{12\alpha}{\pi}}\,\dfrac{\Delta T_{sat}C_{p,l}\rho_l}{\rho_v h_{fg}}$
2.	Zeng et al. (1993)	$F_{qs} + F_{du}\sin\phi = 0$ and $F_{sL} + F_b + F_{du}\cos\varphi = 0$
		$F_b + F_{du} = 0 , \varphi = 0$
		$u^* = 0.05u_l, d_w \approx 0$
		$F_{du} = -\rho_l \pi R^2\left(\dfrac{3}{2}C_s \dot{R}^2 + R\ddot{R}\right), \qquad C_s = 20/3$
		$b = 1.0$ (growth constant)
		$R = \dfrac{2b}{\sqrt{\pi}}Ja\sqrt{\alpha t}$
3.	Thorncroft et al. (2001)	For a heater inclined at an angle ϕ to horizontal
		For departure:
		$F_{Bb}\sin\phi + F_{qs} + F_{du}\sin\varphi + F_{growth} + F_{sx}{\sim}0$
		Sliding bubble:
		$F_b\sin\phi + F_{qs} + F_{AM,x}{\sim}0$
		Lift-off of a sliding and growing bubble:
		$F_b\cos\phi + F_{SL} + F_{du}\cos\varphi + F_{s,}{\sim}0$

S. No.	Reference	Equations

$$F_b = -\frac{4}{3}\pi R^3 (\rho_l - \rho_v)g$$

$$\vec{F}_{qs} = 6\pi\rho_l \nu (\vec{U} - \overrightarrow{U_b})R \left[\left(\frac{2}{3}\right) + \left\{\frac{12}{Re_b} + 0.75\left(1 + \frac{3.315}{Re_b^{1/2}}\right)\right\}^{-1}\right], Re_b = 2R(t)\left|\overrightarrow{U(t)} - \overrightarrow{U_b(t)}\right|/\nu,$$

$$F_{du} = -\frac{2}{3}\rho_l \pi R^2 (3\dot{R}^2 + R\ddot{R})$$

$$F_{growth} = 2\pi\rho_l R^2 U\dot{R}$$

$$F_{AM,x} = -\frac{2}{3}\rho_l \pi R^3 \frac{dU_{b,x}}{dt} + 2\pi\rho_l R^2 (U - U_{b,x})\dot{R} \quad \text{(sliding bubble, upright: } \varphi = 0)$$

$$F_{SL} = \frac{1}{2}|U - U_b|(\vec{U} - \overrightarrow{U_b})\pi\rho_l R^2 \Gamma^{1/2}\left\{\left[\frac{1.146J(\varepsilon)}{Re_b^{\frac{1}{2}}}\right]^2 + \left(\frac{3}{4}\Gamma^{1/2}\right)^2\right\}^{1/2} \quad \text{where } \Gamma \text{ is dimensionless shear rate}$$

$$\Gamma = G_s = \left|\frac{dU}{dy}\right|\frac{R}{|U - U_b|}$$

$$J(\varepsilon) = \begin{cases} 0.6765\{1 + \tanh(2.5\log_{10}\varepsilon + 0.191)\}\{0.667 + \tanh(6(\varepsilon - 0.32))\}, & 0.1 \leq \varepsilon \leq 20 \\ 2.225, \varepsilon > 20 \end{cases}$$

$$\varepsilon = \sqrt{2\Gamma/Re_b}$$

$$F_{sx} = -1.25d_w\sigma\frac{\pi(\alpha-\beta)}{\pi^2-(\alpha-\beta)^2}(\sin\alpha + \sin\beta) \quad d_w = 0.09mm,$$

$$F_{sy} = -d_w\sigma\frac{\pi}{(\alpha-\beta)}(\cos\beta - \cos\alpha); \quad \alpha = \pi/4, \beta = \pi/5$$

$$U(y) = u^*\left[\frac{1}{\kappa}\ln\left(1 + \kappa\frac{yu^*}{\nu}\right) + c\left\{1 + \exp\left(-\frac{\frac{yu^*}{\nu}}{\chi}\right) - \frac{\frac{yu^*}{\nu}}{\chi}\exp\left(-0.33\frac{yu^*}{\nu}\right)\right\}\right],$$

S. No.	Reference	Equations
4.	Situ *et al.* (2005)	$\kappa = 0.4, \chi = 11, c = 7.4, u^* = u_l\sqrt{\dfrac{C_f}{2}}, u_l = \dfrac{G(1-X)D}{\rho_l\delta}, X = 0.106, \delta = 6.5mm$

$$C_f = 2(2.236\ln(Re) - 4.639)^{-2},$$

$$R = \frac{2b}{\sqrt{\pi}}Ja\sqrt{\alpha t}, b = 0.9$$

$$\sum F_x = F_{sx} + F_{qs} + F_{du}sin\varphi + F_b$$

$$\sum F_y = F_{sy} + F_{sL} + F_{du}cos\varphi$$

$$F_{sx} = -1.25d_w\sigma\frac{\pi(\alpha - \beta)}{\pi^2 - (\alpha - \beta)^2}(\sin\alpha + \sin\beta)$$

$$F_{sy} = -d_w\sigma\frac{\pi}{(\alpha-\beta)}(\cos\beta - \cos\alpha);$$

$$F_{du} = -\rho_l\pi R^2(\frac{11}{2}\dot{R}^2 + \frac{11}{6}R\ddot{R})$$

$$F_{sL} = 0.5\rho_l C_L \Delta U^2 \pi R^2, C_L = 3.877G_s^{1/2}\{Re_b^{-2} + 0.014G_s^2\}^{1/4}$$

$$F_P + F_g = F_B = -\frac{4}{3}\pi R^3(\rho_l - \rho_v)g$$

$$F_{qs} = 6\pi\rho_l\nu UR\left[\left(\frac{2}{3}\right) + \left\{(\frac{12}{Re_b})^{0.65} + 0.862\right\}^{-1.54}\right]$$

$$u^+ = u/u^*, y^+ = yu^*/\nu_l, u^* = \sqrt{\tau_w/\rho_l},$$

$$G_s = \frac{1}{C_r k^+ u^+}, C_r = 0.5$$

S. No.	Reference	Equations

$$u^+ = \frac{1}{k^+} \ln y^+ + C^+, \quad k^+ = \begin{cases} \frac{\ln 5}{4}, & x^+ \leq 5 \\ 1/5, & 5 < x^+ < 30 \\ 1/2.5, & x^+ \geq 30 \end{cases}$$

$$\tau_w = \frac{C_f}{2}\rho_l v_l^2, \quad C_f = \lambda/4,$$

$$\text{For smooth surfaces, } \lambda = \begin{cases} 64/Re, & Re, 2320 \\ 0.3164/Re^{0.25}, & 4e3 < Re < 1e5 \\ 0.0032 + 0.221 Re^{-0.237}, & 1e5 < Re < 3e6 \end{cases}$$

$$R = \frac{2b}{\sqrt{\pi}} Ja_e \sqrt{\alpha t}$$

Balancing growth and shear lift forces at lift-off,

$$t_{lo} = \frac{\pi R_{lo}^2}{4b^2 Ja^2 \alpha_l} \quad \text{(lift-off time)}$$

$$D_{lo} = \frac{4}{\pi}\sqrt{\frac{22}{3}}\left(\frac{v_l}{\sqrt{C_l}\Delta U}\right) b^2 Ja_e^2 Pr_l^2, \quad \text{(b=1.73 Zeng et al. 1993)}$$

$$Ja_e = S \times Ja, \quad S = \frac{1}{1 + 2.53 \times 10^{-6} Re_{TP}^{1.17}}$$

5. Yeoh and Tu (2005)

$$\sum F_x = F_{sx} + F_{qs} + F_{du}\sin\varphi + F_b$$

$$\sum F_y = F_{sy} + F_{sL} + F_h + F_{cp} + F_{du}\cos\varphi$$

$$F_{sx} = -1.25 d_w \sigma \frac{\pi(\alpha - \beta)}{\pi^2 - (\alpha - \beta)^2}(\sin\alpha + \sin\beta) \qquad \theta = 45°, \varphi = 10°$$

S. No.	Reference	Equations

$$F_{sy} = -d_w \sigma \frac{\pi}{(\alpha-\beta)}(\cos\beta - \cos\alpha); \qquad d_w = 0.09mm, \alpha = \theta + 10 = 55°, \beta = \theta - 10 = 35°$$

$$F_{qs} = 0.5 C_D \rho_l \Delta U^2 \pi R^2 , \quad C_D = \begin{cases} \frac{24}{Re}(1 + 0.1Re^{0.75}), Re \leq 500 \\ \frac{2}{3}\left(\frac{g(\rho_l-\rho_v)d^2}{\sigma}\right)^{0.5}, 500 \leq Re \leq 2\times10^5 \end{cases}$$

$$F_{du} = -\rho_l \pi R^2 (\frac{3}{2}\frac{20}{3}\dot{R}^2 + R\ddot{R}),$$

$$F_{sL} = 0.5\rho_l C_L \Delta U^2 \pi R^2 , \quad C_L = 0.8G_s , \quad G_s = \left|\frac{dU}{dy}\right|\frac{R}{\Delta U}$$

$$F_b = -\frac{4}{3}\pi R^3 (\rho_l - \rho_v)g$$

$$F_h = \frac{9}{8}\rho_l \Delta U^2 \frac{\pi d_w^2}{4}$$

$$F_{cp} = \frac{\pi d_w^2}{4}\frac{2\sigma}{r_c} , r_c \approx 5R$$

$$U = u^*[2.5\ln(y^+) + 5.5]$$

$$R = \frac{2b}{\sqrt{\pi}}Ja\sqrt{\alpha t}, b = 1$$

6.	Chen and Pan (2010)	$k_w = \frac{d_w}{2R} = 1 - exp\left[-a_w\left(\frac{dR^+/dt^+}{R^+}\right)^{n_w}\right], R^+ = R/R_d, t^+ = t/t_d$
7.	Yun *et al.* (2010)	$\sum F_x = F_{sx} + F_{qs} + F_{du}sin\varphi + F_b$ $\sum F_y = F_{sy} + F_{sL} + F_h + F_{cp} + F_{du}cos\varphi$

S. No.	Reference	Equations
		$$d_w = {d_b}/{15} \, , \, C_s = 1$$ $$b = 1.56$$ $$R(t) = \frac{2b}{\sqrt{\pi}} Ja\sqrt{\alpha t} - \frac{bq_i^{''} t}{s\rho_v h_{fg}} \, , \, q_{sp}^{''} = h_{sp}(T_{sat} - T_l) \, , \, h_{sp} = \frac{k}{d_b}(2 + 0.6Re_b^{0.5} Pr^{0.3}), s = 2$$ $$F_{SL} = 0.5\rho_l U_l^2 \pi R^2 \left[3.877 G_s^{1/2} \{Re_b^{-2} + 0.118 G_s^2\}^{1/4}\right] , G_s = \left|\frac{dU}{dy}\right| \frac{R}{U}$$
8.	Colombo and Fairweather (2015)	$$\sum F_x = F_{sx} + F_{qs} + F_{du}\sin\varphi + F_b \sin\phi$$ $$\sum F_y = F_{sy} + F_{SL} + F_h + F_{cp} + F_{du}\cos\varphi + F_b \cos\phi$$ $$d_w = {d_b}/{15} \, , \, \alpha = \pi/4, \beta = \pi/5, \varphi = 10° \, , \, C_s = 1$$ $$R(t) = \frac{2}{1.78} Ja\sqrt{\frac{\alpha t}{Pr}} + 2\sqrt{\frac{3}{\pi}}(1-b)Ja\sqrt{\alpha t} - \frac{h_{sp}(T_{sat} - T_l)bt}{\rho_v h_{fg}}$$ b is the ratio of the bubble surface in contact of the subcooled liquid using the wall temperature and the location of T_{sat} using the temperature profile: $$\theta^+ = Pr.y^+ e^{-\Gamma} + \left\{2.12\ln\left[(1+y^+)\frac{2.5(2 - {y}/{\delta})}{1 + 4(y-\delta)^2}\right] + \beta(Pr)\right\} e^{-1/\Gamma}$$ $$\beta(Pr) = (3.85Pr^{\frac{1}{3}} - 1.3)^2 + 2.12\ln(Pr)$$ $$\Gamma = \frac{0.01(Pr.y^+)^4}{1+5Pr^3 y^+}, \theta^+ = \frac{T_w - T}{T^*}, T^* = \frac{q''}{\rho C_p u^*}, y^+ = \frac{yu^*}{v}$$

S. No.	Reference	Equations

| 9. | Guan *et al.* (2015) |

$$\sum F_x = F_{sx} + F_{qs} + F_{du}sin\varphi + F_b + F_{growth}$$

$$\sum F_y = F_{sy} + F_{sL} + F_{cp} + F_{du}cos\varphi$$

$$F_{du} = -\rho_l\pi R^2\left(\frac{3}{2}\dot{R}^2 + R\ddot{R}\right)$$

$$F_{growth} = 2\pi\rho_l R^2 U\dot{R}$$

$$R(t) = \frac{2b}{\sqrt{\pi}}Ja\sqrt{\alpha t}\ , b = 1.73$$

$$\phi = 15°\ , \alpha = 75°, \beta = 30°$$

$$X = \frac{1}{h_{fg}}\left[\frac{q"LH}{GA} + C_{p,l}(T_{in} - T_{sat})\right]$$

$$d_w = 0.0002611lnD_b + 0.0021535$$

| 10. | Hoang *et al.* (2016) |

$$D_{max} = 1.21ab^{-1/2}$$

$$a = 2(1-m)Ja\sqrt{\frac{\alpha_l}{\pi}\frac{\Delta T_y}{\Delta T_{sat}}}\ , \quad b = \frac{mC\varphi\Delta T_{sub}}{1-(\rho_v/\rho_v)}$$

$$\Delta T_y = \frac{T_w - T_{sat}}{2}$$

$$C = \begin{cases} 65 - (5.69\times10^{-5})(P - 10^5), & 0.1 \le P\ (MN/m^2) \le 1 \\ 0.25\times10^{10}P^{-1.418}, & 1 < P(MN/m^2) < 17.7 \end{cases}$$

$$\varphi = \max[1, \left(u_l/_{0.61}\right)^{0.47}, m = 0.3$$

S. No.	Reference	Equations
11.	Sugrue and Buongiorno (2016)	$$\sum F_x = F_{sx} + F_{qs} + F_{du}\sin\varphi + F_b \sin\phi$$ $$\sum F_y = F_{sy} + F_{sL} + F_h + F_{cp} + F_{du}\cos\varphi + F_b \cos\phi$$ $$d_w = 0.025 D_b$$ $$R(t) = \frac{2b}{\sqrt{\pi}} Ja\sqrt{\alpha t}$$

Table 1.11 Models for bubble departure frequency in flow boiling.

S. No.	Reference	Equations
1.	Podowski *et al.* (1997)	$$f = \frac{1}{t_g + t_w}$$ $$t_w = \left[\left(-C_2 + \sqrt{C_2^2 - 4C_1 C_3}\right)/2C_1\right]^2$$ $$C_1 = \frac{2q"}{\pi}\left(\frac{k_w}{\sqrt{\pi\alpha_w}} + \frac{k_l}{\sqrt{\pi\alpha_l}}\right)^{-1}$$

S. No.	Reference	Equations

$$C_2 = \left[\frac{\left(\frac{k_w T_w}{\sqrt{\alpha_w}} + \frac{k_l T_l}{\sqrt{\alpha_l}}\right)}{\frac{k_w}{\sqrt{\alpha_w}} + \frac{k_l}{\sqrt{\alpha_l}}}\right] - T_{sat} - \frac{q'' r_c}{\pi\sqrt{\alpha_l}}\left(\frac{k_w}{\sqrt{\pi\alpha_w}} + \frac{k_l}{\sqrt{\pi\alpha_l}}\right)^{-1} - \frac{2\sigma}{r_c}\frac{T_{sat}(1/\rho_v - 1/\rho_l)}{h_{fg}}$$

$$C_3 = \left[\frac{\left(\frac{k_w T_w}{\sqrt{\alpha_w}} + \frac{k_l T_l}{\sqrt{\alpha_l}}\right)}{\frac{k_w}{\sqrt{\alpha_w}} + \frac{k_l}{\sqrt{\alpha_l}}} - T_l\right]\frac{r_c}{\sqrt{\pi\alpha_l}}$$

$$t_g = \left[\left(-A_2 + \sqrt{A_2^2 - 4A_1 A_3}\right)/2A_1\right]^2$$

$$A_1 = \frac{q''}{k_w}$$

$$A_2 = 2\left[\frac{\left(\frac{k_w T_w}{\sqrt{\alpha_w}} + \frac{k_l T_l}{\sqrt{\alpha_l}}\right)}{\frac{k_w}{\sqrt{\alpha_w}} + \frac{k_l}{\sqrt{\alpha_l}}} + \frac{2q''\sqrt{t_w}}{\left(\frac{k_w}{\sqrt{\pi\alpha_w}} + \frac{k_l}{\sqrt{\pi\alpha_l}}\right)\pi - T_{sat}}\right]\frac{1}{\sqrt{\pi\alpha_w}}$$

$$A_3 = \frac{D_d \rho_v h_{fg}}{2k_w}$$

S. No.	Reference	Equations
2.	Basu *et al.* (2005)a	$$f = \frac{1}{t_g + t_w}$$ $$t_g = \frac{D_d^2}{45\alpha_l Ja_{sup}\exp(-0.02Ja_{sub})}$$ $$t_w = 139.1(\Delta T_{sat})^{-4.1}$$
3.	Situ *et al.* (2008)	$$fD_{lo}^2 = 10.7\alpha_l\left(\frac{q''_{nb}D_{lo}}{\alpha_l\rho_v h_{fg}}\right)^{0.634}$$
4.	Euh *et al.* (2010)	$$fD_{lo}^2 = 1.6\alpha_l\left(\frac{q''_{nb}D_{lo}}{\alpha_l\rho_v h_{fg}}\right)^{1.3}$$
5.	Brooks and Hibiki (2015)	$$fD_d^2 = 5.5\alpha_l Ja^{2.28}Ja_T^{-1.46}\left(\frac{\rho_l}{\rho_v}\right)^{0.93}Pr^{2.36}$$

The bubble characteristics have also been studied in narrow (mini or micro) channels or annuli; such channel dimensions are found in nuclear reactor bundles, shell and tube evaporators, electronic devices heat sinks. A number of studies have shown that the flow regimes and heat transfer in narrow channels are significantly different from those in conventional sized channels. The channels or annuli are considered narrow when the gap is less than 3 mm. Limited studies have been carried out to study the bubble dynamics in such narrow channels. Sheng and Palm (2000) studied bubble dynamics for water in a single small glass tube and observed that the mass flow rate had a major effect on the bubble departure diameter. Lee *et al.* (2004) studied the bubble behaviour in a microchannel ($D_h = 41.3 \ \mu m$), and found that the bubble departure diameter is mainly governed by surface tension and drag forces and can be correlated by a modified form of Levy (1967) equation. They found the departure frequency to be similar to that in a conventional channel, however, the traditional relationship of $f D_d$ did not seem to hold in their experiments. Lie and Lin (2006) studied bubble characteristics for the boiling of R-134a in horizontal narrow annular geometries. Their visualization experiments showed that bubbles were suppressed to be smaller and less dense with an increase in mass flux and inlet subcooling, while an increase in heat flux resulted in an increase of bubble population and coalescence, and bubble departure frequency. Chen *et al.* (2009) carried out similar experiments in the same geometry using R-207C and found similar conclusions. Both the authors proposed correlations for bubble departure diameter and frequency in terms of non-dimensional numbers. Chen *et al.* (2012) studied the bubble contact diameter and departure diameter in a narrow channel. They found that for a bigger departure diameter, the bubble had a wider contact diameter at the heater surface. They analysed the various forces acting on a vapor bubble using a model for contact diameter that they proposed and concluded that the contact diameter has significant effect on the forces, specially growth force and surface tension forces. Hong *et al.* (2012) carried out bubble visualization study in a

mini-channel of gap 2 mm and concluded that the decreasing mass flux and increasing heat flux result in an increase in bubble departure diameter, under static conditions. Yang *et al.* (2016) studied subcooled flow boiling characteristics in a vertical flow channel and measured the bubble departure diameter, departure frequency and nucleation site density. They found that the bubble departure diameter follows a normal distribution, while the growth period being much less than the waiting period can be neglected in the estimation of departure frequency. They proposed empirical correlations for departure diameter and frequency based on their experiments, which would be valid for wall superheat less than 12℃.

Studying heat transfer in a vertical rod bundle, Weisman (1959) proposed a correlation for predicting single phase convective heat transfer coefficient by introducing a pitch-to-diameter (P/D) dependent constant in the Colburn (1933) equation. Sung-Ho and El-Genk (1989) studied the single phase heat transfer coefficients in natural and forced convection in a 7-rod bundle and found that the critical Reynolds number for transition from laminar to turbulent in forced convection increases linearly with P/D. Their results in the turbulent range agreed with the Weisman (1959) correlation very well, but the heat transfer coefficient had a weaker dependence on Reynolds number in the laminar range. In natural convection, the rod spacing in the bundle had negligible effect on the heat transfer. Anklam and Miller (1982) measured volume averaged void fraction for high pressure, low heat flux conditions and showed that the data could be fitted to a drift-flux equation with a single drift velocity. This velocity decreased with an increase in pressure and was independent of void fraction. Mitsutake *et al.* (1990) developed a three fluid model for estimation of void fraction in dispersed-annular flow regime and validated it with measurements in a 4 rod bundle. Kumamaru *et al.* (1994) measured void fraction in a simulated PWR 17×17 fuel bundle and found that Chexal-Lellouche model predicted the volume averaged void fraction with good accuracy. Their observations showed that volume averaged void fractions were systematically smaller than

chordally averaged void fractions. Inoue *et al.* (1995) measured volume averaged void fraction in a BWR simulated rod bundle to verify the BWR void fraction prediction model at that time. Gupta, *et al.* (2010) measured pool boiling heat transfer in a vertical rod bundle at low heat fluxes at atmospheric pressure. They observed that the heat transfer coefficient increased in the direction of bubbles flow, and the ratio of local heat transfer at tube of the rod and bottom of the rod was higher at the lower heat flux. They proposed a correlation to predict boiling heat transfer coefficient as a function of the rod height. Zhang *et al.* (2017) measured single phase convective and two phase flow boiling heat transfer coefficient in a 7-rod bundle at ow mass flux conditions. The proposed new models for predicting single phase heat transfer coefficient for laminar and transition to turbulent regime, while they confirmed that Weisman (1959) model words well for the turbulent regime. The flow boiling heat transfer coefficient was observed to be higher in a rod bundle compared to a single rod or in a tube. The boiling heat transfer coefficient increased with an increase with mass flux; first increased and then decreased with an increase in quality for a given mas flux. Hence, the few studies carried out with axial flow in rod bundles concern themselves with the measurements of heat transfer coefficient or void fraction, however, to the best of author's knowledge, no studies have been carried out to study the bubble behaviour in a horizontal or vertical rod bundle, with axial flow boiling.

1.4. Unresolved Issues

From the in-depth study of the literature as discussed in the previous section, we can see that there are a number of inconsistencies even after six decades of studies. The major unresolved issues can be stated as:

a) The behaviour of bubble departure diameter and frequency with the applied heat flux or wall superheat is unclear, with different studies inferring increasing, decreasing or constant variations. Also, the effect of liquid subcooling, heater surface characteristics,

like shape, size, inclination angle and surface roughness is limited in both pool and flow boiling cases.

b) There are a good number of studies for departure frequency in pool boiling but very limited studies exist in flow boiling. It has been shown that the mechanisms of bubble departure in pool and flow boiling are quite different. There is not sufficient data for its behaviour with heat flux, mass flux and liquid subcooling to clearly understand the departure mechanism of bubbles in flow boiling conditions, which significantly differs from that in pool boiling.

c) Further, the departure frequency has been found to be dependent on the departure diameter. Hence, the simultaneous measurement of departure diameter and frequency warrant merit. However, such measurements are limited, which limit the accuracy of the frequency correlations due to its dependency on the diameter.

d) At low heat and mass flux conditions, such as the ones encountered in start-up of a natural circulation Boiling Water Reactor (BWR) like Advanced Heavy Water Reactor (AHWR), or accidental conditions in a Pressurized Heavy Water Reactor (PHWR), where passive safety systems are in play, have not been studied in detail. There are almost no bubble behaviour studies corresponding to horizontal rod bundles in PHWRs with cross flow or vertical rod bundles of BWR or AHWR with flow from bottom to top.

e) There are a number of models proposed for bubble departure diameter and frequency in pool and flow boiling conditions. The pool boiling models have been developed with saturated boiling data, and hence, are unable to account for the effects of subcooling, and have significant error bands even for saturated pool boiling data. The flow boiling models are based on force balance; are mechanistic but do not give a desired level of accuracy. The empirical models are mostly developed for limited range of conditions and are poorly

validated. There is no model for bubble departure characteristics for cross flow boiling in horizontal rod bundles and for boiling in flows parallel to heater rod bundles.

1.5. Objective

The main aim of this study is to be propose new models for bubble departure diameter and frequency that can be applicable over a wide range of conditions, and can be incorporated in the multiphase multidimensional CFD models for wall boiling. For that purpose, we would study the process of nucleation, growth and detachment of vapor bubbles on the surface of a single fuel pin and rod bundles in various conditions pertaining to a nuclear reactor. The following objectives were set to achieve that goal:

1. To study the effect of operating conditions, and heated rod properties on the bubble characteristics in pool boiling conditions.

2. To study the bubble characteristics in a horizontal rod bundle under cross flow conditions.

3. To study the bubble characteristics in vertical flow boiling in a conventional sized annulus, a narrow annulus and a 4-rod bundle.

4. To develop new models for bubble departure diameter and frequency for subcooled pool and flow boiling conditions, after carrying out detailed analysis of the existing models.

1.6. Outline of the thesis

The above objectives are accomplished in the following 8 chapters of the thesis:

Chapter 1 outlines the introduction, literature review and the motivation for the work.

Chapter 2 provides a brief description of visualization technique to measure bubble characteristics.

Chapter 3 describes the visualization experiments carried out in pool boiling. It discusses the parametric studies of heat transfer, bubble departure diameter and frequency with various operating variables.

Chapter 4 details the experiments carried out in a 5×3 rod bundle under cross-flow boiling conditions. Here, we discuss the bubble behaviour in a single rod in a rectangular channel, single rod in a non-heated bundle and with successive rods heated in the bundle.

Chapter 5 describes the development of semi-empirical models for bubble departure diameter and frequency models for subcooled pool boiling and cross flow boiling in a single horizontal heater. These models are then extended for the rod bundle, validated for conditions of present study.

Chapter 6 communicates the observations of the vertical subcooled flow boiling experiments conducted in annulus and a four-rod bundle.

Chapter 7 covers the development of AI based correlations for bubble diameters and frequency in subcooled flow boiling.

Chapter 8 includes the conclusions of the thesis and some suggestions for future work.

1.7. Closure

Nucleate boiling is a complicated but an extremely efficient means of heat transfer with a wide range of applications, like nuclear reactor core cooling, evaporators, boilers, cooling of electronic equipment, etc. However, modelling the nucleate boiling phenomena is a complex problem because the phenomena depends on several parameters, such as bubble departure characteristics like departure diameter, frequency, nucleation site density, apart from the geometry of the heated section. There has been a lot of work to understand and model these characteristics in the last six decades, but there still exists several inconsistencies in the parametric behaviour of bubble departure characteristics with various operating variables. Also, there is scarce data for bubble departure characteristics in rod bundle geometries for

nuclear reactor applications. Hence, in this work, targeted set of experiments have been carried out to study the bubble departure diameter and frequency in various conditions, applicable for nuclear reactor core cooling, i.e. pool boiling, cross flow boiling across horizontal rod bundles and axial flow boiling in vertical rod bundle. The data obtained in this study and from the literature have been compared with the models available in the literature. New models for bubble departure diameter and frequency have been proposed by considering various variables not considered before.

2. Chapter 2

Measurement of Bubble Characteristics using High Speed Videography Technique

2.1. Introduction

From the discussion in previous chapter, we understand that the boiling heat transfer has been a subject of interest for nearly six decades. It has numerous applications not only in nuclear reactors, chemical reactors, boilers, heat exchangers, which correspond to the conventional channels; but more recently in electronic devices, microchips, microelectromechanical systems (MEMS), which correspond to the narrow or so-called micro-channels. In order to understand the physics of two-phase flow, it is essential to measure the growth and departure of vapor bubbles and their effect on the flow and heat transfer through direct optical observations. The generation, growth and departure of bubbles is a phenomenon that occurs over the scale of millimetres and over a time scale of milliseconds, making it impossible for the naked eye to make reliable observations. Hence, majority of the experimental techniques to study two phase flow characteristics employ high speed imaging, either independently or in conjunction with other techniques like IR thermography, laser interferometry, or liquid crystallography.

Jawurek (1969) and Judd and Hwang (1976) used laser interferometry in synchronisation with high speed videography (HSV) to study the microlayer evaporation under the growing vapor bubbles. They used glass surface with an electrically conducting, transparent coating, e.g. stannic oxide, as the heating surface. The laser interferometer and HSV was then used to record the instantaneous variation in the liquid film beneath a growing vapor bubble. These measurements were then used to estimate the thickness and rate of evaporation of the

microlayer, to evaluate the contribution of microlayer evaporation to the total two phase heat transfer. Raad and Myers (1971) and Bergez (1995) used liquid crystal coating on one side of the thin metal sheets, with liquid boiling on the other side of the sheets. The liquid crystal coating exhibited the colour fluctuations with temperature changes which were recorded using the high-speed imaging. This technique is advantageous in identifying the active nucleation sites and to study the temperature cycle at any given site, which in turn helps estimate the bubble period. Ibrahim and Judd (1985) used a bubble detection probe in a pool boiling setup to detect active nucleation site density. The probe was moved over the heating surface in small increments in the heater plane, and the probe's output voltage indicated the conductance of water or vapor in the small gap between the probe tip and the heater surface. Sgheiza and Myers (1985), Gerardi *et al.* (2010), Duan *et al.* (2013) and Petkovsek *et al.* (2016) used InfraRed thermography in conjunction with the HSV to measure the bubble departure parameters. All of the techniques have their advantages and limitations; the most important one being their applicability to certain specific geometries. Most of the above techniques require direct access to one side of the heating surface to be able to make measurements. But with the geometries like fuel pins of a nuclear reactor, where the fuel rod is immersed in the working liquid, it is not possible to use IR thermography or liquid crystals or interferometry. The bubble detection probes are not practical for conditions of flow boiling or even pool boiling in narrow spaces. Hence, with the goal of studying the bubble growth and departure characteristics, and with the fuel bundle geometry in mind, we decided to use the direct visualisation technique with high speed camera as used by a number of earlier investigators.

2.2. Image Processing

In the experiments carried out in this study, we used the Mikrotron Motion BLITZ Cube 4 high speed camera at various frame rates to record the bubble dynamics in real time. The camera could go as high as $20000\ fps$, with compromised resolution. A zooming lens of $20-$

100 mm focal length and a 1000 W halogen light source was used for the camera. For any given set of conditions, multiple high-speed recordings of the bubble dynamics lasting for a few seconds were made to record the bubble growth and departure. The image frames from the high-speed recordings were then manually analysed using the ImageJ software (Eliceiri *et al.* (2012)) to obtain the values of departure diameters and frequencies.

The image frames obtained from the above-mentioned videos needed to be processed before measurements of bubble diameters could be made. For the image processing, the grayscale images were uploaded in the ImageJ software and following steps were carried out:

(1) Cropping of the region of interest – a bubble in this case.

(2) Contrast enhancement.

(3) Thresholding to convert the image into binary image.

(4) Fill holes – to fill the vacant spaces inside the bubbles.

(5) Edge detection to obtain the bubble shape.

Figure 2.1 shows the above-mentioned steps as performed for a bubble. The cropped grayscale image (a) was improved via contrast enhancement and filtration (b). Then a threshold value of the pixel intensity was selected, to segregate the image into bubble and the background even further. This converted the grayscale image into a binary image of black and white (c), where the black pixels represent the bubble and the white pixels represent the background. The holes in the bubbles are filled (d) and finally, the edge detection is used to get the periphery of the bubble shape (e), which was then used to measure the bubble horizontal and vertical diameters. A pre-decided calibration scale was used to set scale in the software to convert the pixel length into *mm* scale length for the diameter measurements.
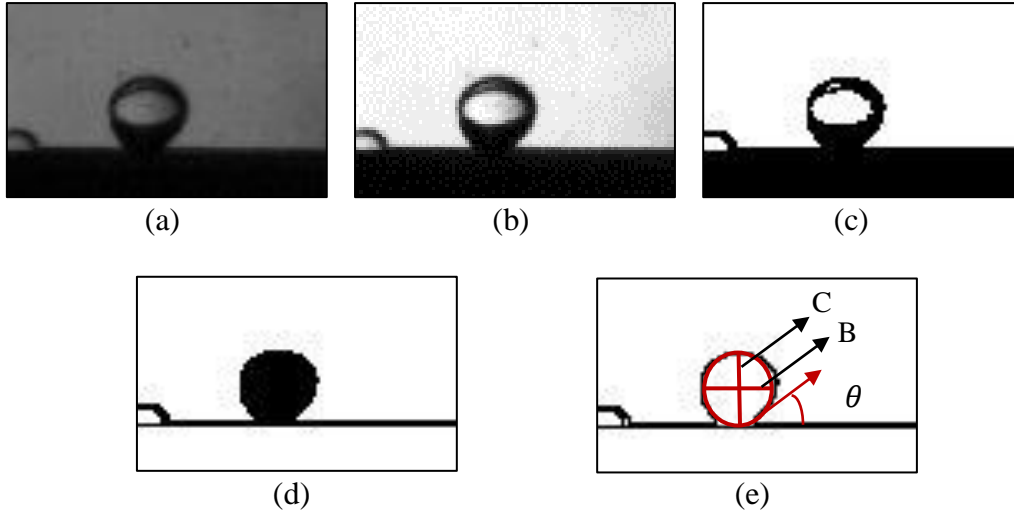
Figure 2.1 Measurements made on a typical bubble.

The equivalent departure diameter of the bubble was defined as the diameter of the sphere with volume equal to that of the spheroidal bubble (shown in *Figure 2.2*).

$$V_{sph} = \frac{\pi}{6}D^3 = \frac{\pi}{6}B^2C = V_b \tag{2.1}$$

$$D = \sqrt[3]{B^2C} \tag{2.2}$$

where B is the measured horizontal bubble diameter parallel to surface and C is the measured bubble diameter perpendicular to heater surface. The departure frequency was defined as the inverse of the time period between two consecutive bubble departures.

$$f = \frac{1}{t_2 - t_1} \tag{2.3}$$

where t_1 and t_2 are the departure times of two consecutive bubbles.
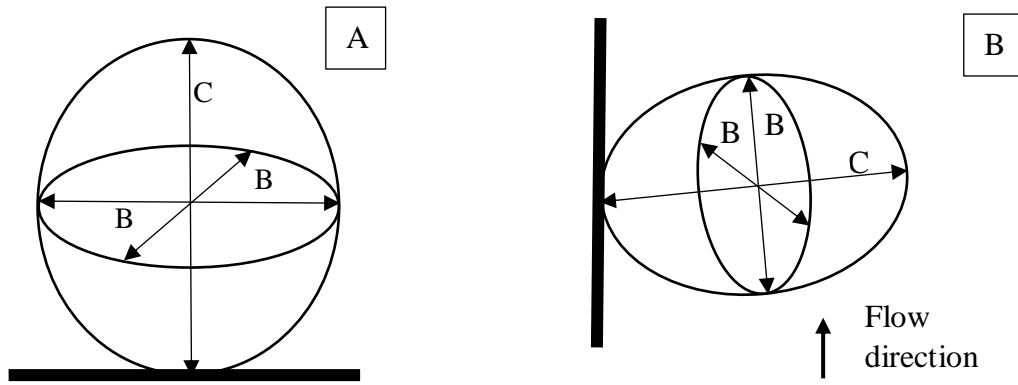
Figure 2.2 Spheroid with its dimensions in (A) pool or horizontal flow condition and (B) vertical flow conditions.

2.3. Statistical Averaging Procedure

Since we were observing the naturally occurring sites, hence for the measurement purposes, a few nucleation sites, which were fairly regular in their bubble ebullition cycle, were selected. The departure diameter and frequency vary for each bubble for a given nucleation site, and, for different nucleation sites, for any given set of conditions. For any given condition, the bubble departure diameter and frequency were measured for about 70-80 bubbles for each selected nucleation site. Then, the final average value of diameter and frequency used in the parametric studies, was obtained by averaging the values over all the nucleation sites. The statistical average of the diameter and frequency for a particular case, taking all the regular sites into account were used in the parametric study plots. The standard deviation and 95% confidence intervals were calculated for each case population in addition to the mean values. These values have been tabulated with the results in each of the experiments and have been presented in forthcoming chapters.

2.4. Measurement Uncertainties

There always are some level of uncertainties associated with any measurement technique, and hence, it is necessary to evaluate the error in each step to be able to state the level of confidence in the final observations. Here, we have converted the 3D bubble behaviour

into 2D images which introduced a digitisation error which on calculation as per method described by Santo *et al.* (2000), comes to about 0.1%. Then, it can be said that the bubble diameters could be measured with an accuracy of $\pm\,1\,pixel$, which would vary with the resolution used in the experiment. The relative error in any bubble measurement can be estimated as

$$D^3 = B^2 C \implies \frac{\Delta D}{D} = \frac{2}{3}\frac{\Delta B}{B} + \frac{\Delta C}{C} \tag{2.4}$$

where $\Delta B = \Delta C = \pm 1\,pixel$ as discussed above. These relative errors have been quoted in the respective experiments in the forthcoming chapters and have also been plotted as the error bars in the graphs. The error in frequency measurement comes from the error in the time difference between the two consecutive frames. Since, frequency is the inverse of time difference between departure of two consecutive bubbles, i.e. from equation (2.3)

$$f = \frac{1}{T_f} \implies \frac{df}{dT_f} = \frac{1}{T_f{}^2} \implies \frac{\Delta f}{f} = f \times \Delta T_f \tag{2.5}$$

Hence, the error in frequency is also proportional to the square of the measured value and the error in time difference ΔT_f, which is basically twice the time resolution of the camera. Some other errors like change in refractive index of water with temperature, error due to camera zoom, errors due to the curvature of the experimental test section, and human errors might have occurred which cannot be quantified in this work.

2.5. Closure

High speed videography is a versatile technique that works well with transparent test sections to observe the bubble growth, departure and further movement along the test sections, without any constraints on the heater geometry or working liquid. The procedure of recording bubble dynamics in experiments has been described here, along with the brief explanation of

the method of image processing. The process of selecting the bubbles and the estimation of associated errors has been discussed which will be presented in the relevant chapters ahead.

3. Chapter 3

Study of Bubble Departure Characteristics in Subcooled Nucleate Pool Boiling

3.1. Introduction

Nucleate pool boiling takes place when a stationary liquid is in contact with a heated surface at a temperature above the liquid saturation temperature. Here, only the liquid very near to the surface is in motion due to the natural convection and due to the mixing introduced by the bubble dynamics. Hence, it makes for a convenient configuration for laboratory experiments and helps understanding the basics of bubble dynamics without the added complication of fluid flow. Apart from being a starting step to understand the complex process of nucleate boiling for optimal design of heat transfer systems, pool boiling itself has numerous applications, like vapor chambers for the cooling of microelectronic devices, flooded evaporators in heat pumps, refrigeration, air-conditioning industry, fuel handling and control systems in nuclear reactors systems, to name a few. Hence, several studies have been carried out in pool boiling over the years, but the understanding of boiling heat transfer and bubble dynamics is still limited. From the discussion in Chapter 1, we could see that the behaviour of bubble departure diameter and frequency with heat flux or wall superheat is in contradiction with each other. The effect of the liquid subcooling, heater surface characteristics or heater inclination angle have not been paid enough attention. Also, most of the pool boiling studies have been carried out with flat plate or ribbon-like heater geometries, even though Nishikawa et al. (1965) showed that the heater geometry and size play an important role in bubble dynamics. Hence, a comprehensive set of experiments were conducted to systematically study

the effect of various parameters on the heat transfer and bubble departure characteristics in subcooled nucleate pool boiling conditions.

3.2. Experimental Description

3.2.1. Setup
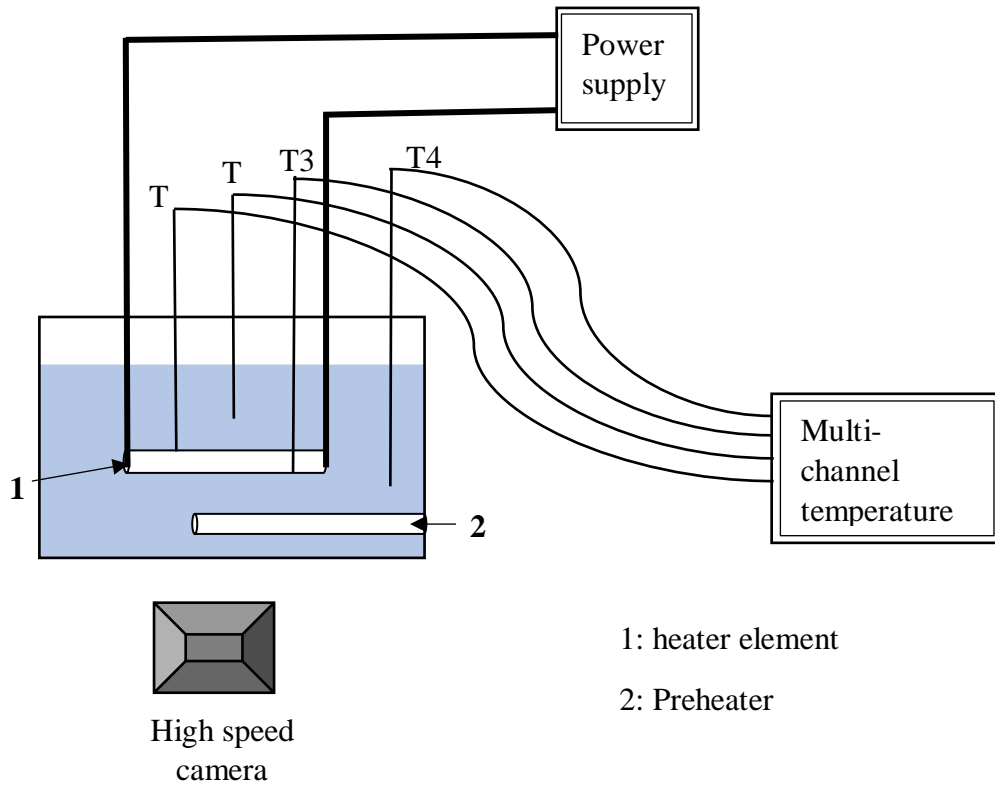
Figure 3.1 Schematic diagram of experimental set-up.

Figure 3.1 shows the schematic of the experimental setup used for the current studies. The container was a $300mm \times 135mm \times 250mm$ cuboidal tank made of stainless steel on the three sides, while the front and back sides were made of polycarbonate sheets to allow for light and photography. The vapor was released through the open top of the tank to maintain atmospheric conditions. An auxiliary cartridge heater of rating of 1000 W was used to heat the water to the required temperature before starting the boiling experiment. Two different kinds of heater elements were used in the studies, i.e. three solid SS316 rods ($D = 3.95mm$) and a flat SS ribbon ($110.9mm \, x \, 11.1mm \, x \, 2.9mm$). The three SS rods were polished with

different grades of silicon carbide emery paper to achieve the required surface roughness values and hence, differed in their surface finish. The average surface roughness (R_a) values for the samples were obtained using a digital stylus profilometer and the details of all the elements are given in *Table 3.1*. The SEM images for the three rods and the surface contours obtained by analysing the same are shown in *Figure 3.2*.

Table 3.1 Properties of heater elements

Heater element	Dimensions (mm)	Surface roughness R_a (μm)	Static contact angle θ (°)	Inclination angle ϕ (°)
SS rod 1	$l = 107$ $D = 4$	0.5	65°	0°
SS rod 2	$l = 93.2$ $D = 4$	1.0	60°	0°, 45°, 90°
SS rod 3	$l = 93.8$ $D = 4$	3.54	54°	0°
SS ribbon	$110.9x11.1x2.9$	1.5	56.5°	0°

(A)

(B)

(C)

Figure 3.2 SEM images at 500X and corresponding surface plot. (A) rod 1(R_a =0.5μm). (B)

rod 2 (R_a =1.0μm). (C) rod 3 (R_a =3.54μm).

3.2.2. Procedure

Each heating element, placed approximately at the centre of the tank was heated electrically by an AC rectified DC high current power supply. The average heat flux applied to the element was obtained from the product of voltage and the current applied to it divided by the total heater surface area. The surface temperature was measured by the 0.5 mm K-type Chromel-Alumel thermocouples (T1 and T3 in *Figure 3.1*) brazed on its surface. Also, the bulk liquid temperature was measured using similar K-type thermocouples (T2 and T4 in *Figure 3.1*). The temperatures were recorded using a six-channel digital recorder. The bubble dynamics was recorded using the high-speed camera at a speed of 1000 *fps* (time resolution of 1 *ms*) at a spatial resolution of 1280 ×1024 pixels as described in the previous chapter.

The container along with the auxiliary and main heater elements were thoroughly cleaned first. Then the demineralized water was poured in the tank and was boiled for about 30 minutes to let the trapped gases escape. Then, after the system cooled a little, a homogeneous bulk liquid temperature was achieved and maintained using the auxiliary heater. The auxiliary heater was then switched off and after a few minutes, the power was applied to the test heater surface and the flux was then increased stepwise. Since the auxiliary heater was switched off a few minutes prior to giving power to the test heater, the liquid motion due to the auxiliary heater does not affect the bubbles. The system was allowed to achieve steady state, which took about 2-3 minutes and then the bubble behaviour was observed for the natural cavities existing on the surface. Similar experimental procedure for maintaining the bulk liquid temperature has been used by Petkovsek *et al.* (2016). The experiment was carried out for the following conditions: bulk liquid subcooling $\Delta T_{sub} = 5\ K$, $10\ K$, $20\ K$, wall superheat $\Delta T_{sat} = 0 - 15\ K$ and heat flux q'' in the range of $5 - 250\ kW/m^2$ for each heater element. For the study of inclination angle, special clamps were used with the SS rod to incline it at an angle of 45° and 90° to the horizontal. The static contact angles mentioned in *Table 3.1* were the average

95

value of the contact angle measured for several bubbles from the images captured in the experiments. Such heat conditions are in the range of normal operating conditions in a boiling water reactor.

High speed recordings of the bubble dynamics lasting for about 3 seconds were made to estimate the departure size and frequencies of the vapor bubbles under various conditions. Recordings for several conditions were repeated to make the sure of the repeatability of the results. The image frames from the high-speed recordings were manually analysed using the ImageJ software to obtain the values of departure diameters and frequencies as explained in the previous chapter. The time variation of the wall temperature, bulk temperature and the near wall temperature were also recorded simultaneously. Since the temperature values fluctuated in each frame, the average values of the temperatures were used for the analysis for all conditions. A ruler was placed in the boiler tank and calibration images were taken before starting the experiment.

The measurement of voltage V_o and current I involve the least count errors of the $\pm 0.01\ V$ and $\pm 1\ A$ respectively. Since, the boiler tank was not insulated, the maximum loss of heat from the conducting walls was estimated to be $\sim 7\%$ of the total applied heat; and the evaporative heat loss to the atmosphere from the open top was between $15 - 24\%$ (Appendix A). The error in temperature gauging is $\pm 0.75\%$ of the measured value up to $400\ ℃$. The bubble diameters could be measured with an accuracy of $\pm\ 1\ pixel$ which comes to about 4% for a bubble diameter of about $2\ mm$ in addition to 0.1% error of digitalization. The error in time measurement comes from the speed of the camera, and is of nearly $1\ ms$. The frequency having been calculated as per equation (2.5), gives a maximum error of 15%. Some other errors like change in refractive index of water with temperature, error due to camera zoom etc. might have occurred which cannot be quantified in this work.

3.3. Results and Discussion

The vapor bubble departure diameter and frequencies were measured using the high-speed images. A typical vapor bubble growing on the heater surface with time is shown in *Figure 3.4*. It can be seen that the bubble grows from a tiny nucleus at $1\ ms$ to a full-grown bubble at $11\ ms$ at which instant it departs from the surface. As explained in section 2.3, few nucleating sites which were regular in their activity were selected to measure the bubble departure diameters and frequencies. The statistical average of the diameter and frequency for a particular case, taking all the regular sites into account were used in the parametric study plots. *Table 3.2* gives the average values of all the bubble departure diameter and frequency measurements made in the study. The surface plots for the bubble departure diameter and frequency with heat flux, wall superheat and liquid subcooling for the four kinds of heaters and for different inclinations are also presented in *Figure 3.3*. The standard deviation and 95% confidence intervals were calculated for each case population in addition to the mean values. *Table 3.3* enlists some typical values for various heater elements used in the study.

Table 3.2 Bubble departure diameter and frequency measurements for pool boiling (additional details are given in Table 3.1).

Heater sample	Heat flux q'' (kW/m^2)	Wall superheat ΔT_{sat} (K)	Liquid subcooling ΔT_{sub} (K)	Departure diameter D_d (mm)	Departure frequency f $(1/s)$
Rod 1	78.380	4.9	17.9	0.998	40.652
(horizontal)	98.260	5.7	19.6	1.231	54.871
	127.428	6.2	20.5	1.542	62.823
	166.373	6.8	19.9	1.851	68.624
	207.678	7.3	19.4	2.001	73.593
	260.227	8.2	17.4	2.34	80.083
Rod 1	34.368	4.1	9.8	1.368	10.889
(horizontal)	53.661	5.1	11.4	1.673	27.078
	72.570	6.1	9.5	1.775	36.119
	96.228	6.9	10.9	1.964	48.647
	117.330	7.4	10.3	2.111	56.483

Heater sample	Heat flux $q"$ (kW/m^2)	Wall superheat ΔT_{sat} (K)	Liquid subcooling ΔT_{sub} (K)	Departure diameter D_d (mm)	Departure frequency f $(1/s)$
Rod 1	24.456	3.9	5	1.726	4.159
(horizontal)	32.536	5.9	5	1.967	7.587
	40.281	6.7	7	2.413	13.652
	57.147	7.5	6.4	2.554	25.213
	70.069	7.95	5.3	2.675	31.334
	99.736	8.25	5.5	2.821	39.651
Rod 2	66.836	2.3	21.9	0.745	45.625
(horizontal)	89.184	5.5	18.9	0.992	56.594
	127.949	7.5	20.2	1.417	71.359
	180.720	9.8	19.9	1.798	82.648
Rod 2	28.492	1.9	11.7	1.062	16.73
(horizontal)	43.914	4.65	8.3	1.439	31.146
	66.484	6.2	8.0	1.67	43.68

Heater sample	Heat flux q'' (kW/m^2)	Wall superheat ΔT_{sat} (K)	Liquid subcooling ΔT_{sub} (K)	Departure diameter D_d (mm)	Departure frequency f $(1/s)$
	95.777	7.75	9.9	1.881	56.764
	136.312	9.5	8.3	1.995	71.256
Rod 2	15.224	1.6	5.0	1.216	6.337
(horizontal)	27.182	3.7	5.8	1.437	11.514
	45.702	7.3	6.3	1.949	22.135
	70.750	9.1	6.1	2.106	39.165
	107.289	10.9	5.1	2.315	50.394
Rod 3	68.832	4.15	19.7	0.677	54.627
(horizontal)	92.795	5.1	20.2	0.831	63.154
	115.510	6.95	21	0.993	71.823
	145.611	7.95	17.3	1.085	75.338
	175.957	8.8	18.5	1.136	79.761
	215.434	9.15	17.3	1.238	83.614

Heater sample	Heat flux q'' (kW/m^2)	Wall superheat ΔT_{sat} (K)	Liquid subcooling ΔT_{sub} (K)	Departure diameter D_d (mm)	Departure frequency f ($1/s$)
Rod 3	45.110	3.7	11.4	0.934	45.235
(horizontal)	67.647	6.6	12.6	1.002	55.651
	86.285	8.9	11.4	1.263	66.784
	105.479	9.2	11.4	1.392	69.974
	125.656	10	10.2	1.545	75.498
	161.043	10.1	10	1.716	79.106
	218.391	10.7	10.5	1.895	83.518
Rod 3	26.889	2.9	5.9	1.055	14.658
(horizontal)	46.672	6.5	4.9	1.334	23.482
	61.758	9.7	5.8	1.571	40.667
	85.231	10.3	5.2	1.736	43.619
	112.170	10.9	5.5	2.095	48.164
	140.351	11.5	5.5	2.277	51.284

Heater sample	Heat flux q'' (kW/m^2)	Wall superheat ΔT_{sat} (K)	Liquid subcooling ΔT_{sub} (K)	Departure diameter D_d (mm)	Departure frequency f $(1/s)$
Ribbon	198.910	5.6	21.5	2.156	32.54
(horizontal)	235.215	6.9	21.3	2.468	44.264
	286.384	8.3	20.3	2.795	56.486
Ribbon	165.666	6.4	9.8	2.616	23.497
(horizontal)	198.753	7.8	10.9	2.846	36.975
	239.287	8.7	9.9	3.015	48.591
Ribbon	120.860	7.2	5.5	2.931	11.648
(horizontal)	149.527	7.7	4.8	3.058	19.169
	189.406	8.5	5.8	3.211	26.732
	238.917	9.0	5.2	3.364	32.723
Rod 2	74.972	3.0	9.7	1.384	27.247
(45° inclined)	113.850	3.9	10.2	1.612	37.135
	170.722	5.2	9.8	1.956	48.264

Heater sample	Heat flux $q"$ (kW/m^2)	Wall superheat ΔT_{sat} (K)	Liquid subcooling ΔT_{sub} (K)	Departure diameter D_d (mm)	Departure frequency f $(1/s)$
	223.592	5.8	8.8	2.137	58.612
Rod 2	72.835	2.7	9.0	1.444	44.176
(vertical)	118.720	3.5	8.7	1.619	51.89
	142.924	4.2	9.8	1.792	59.645
	191.828	4.7	9.1	1.912	65.432
	268.223	5.3	9.8	2.116	71.846
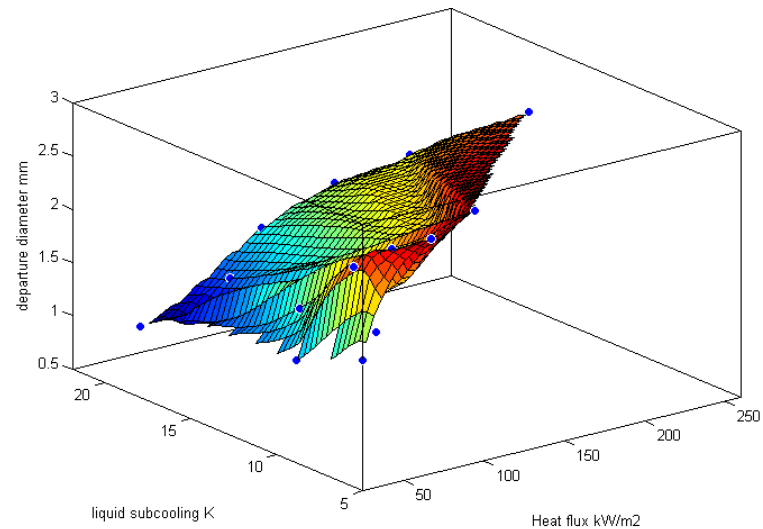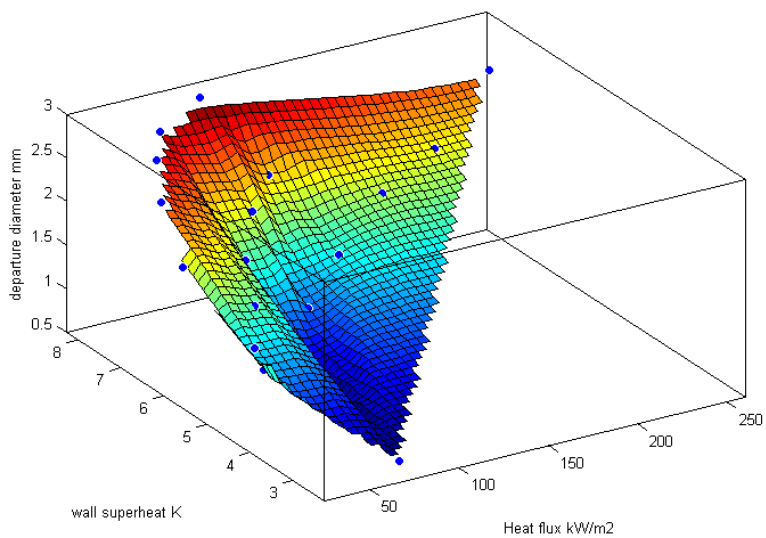
(i)
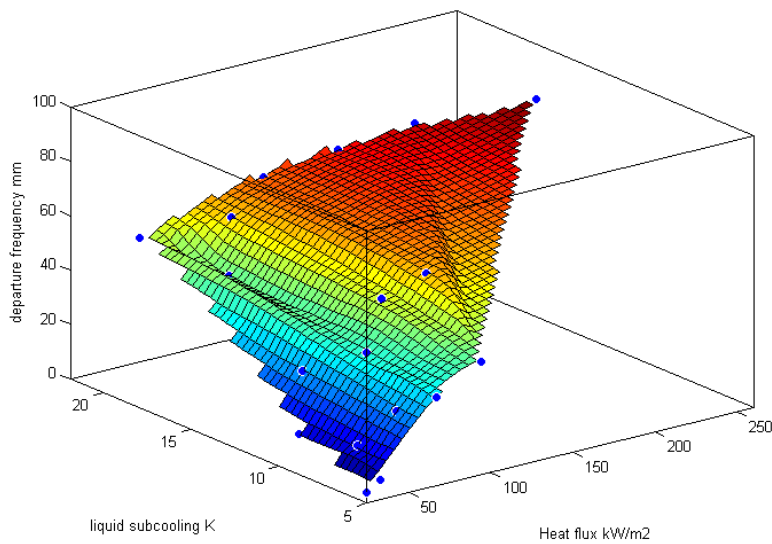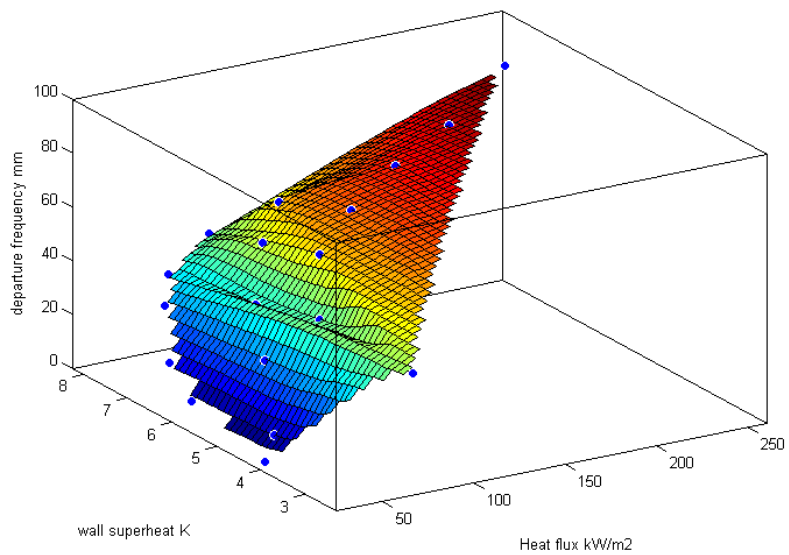
(ii)

(A)
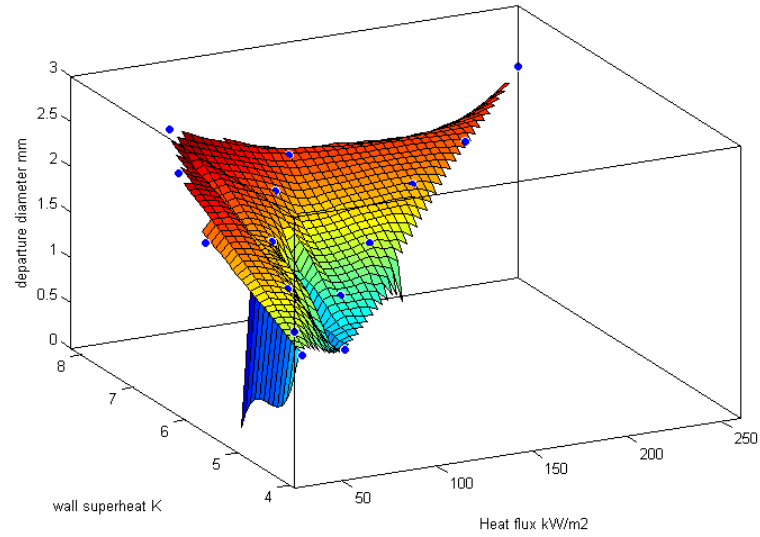
(i)
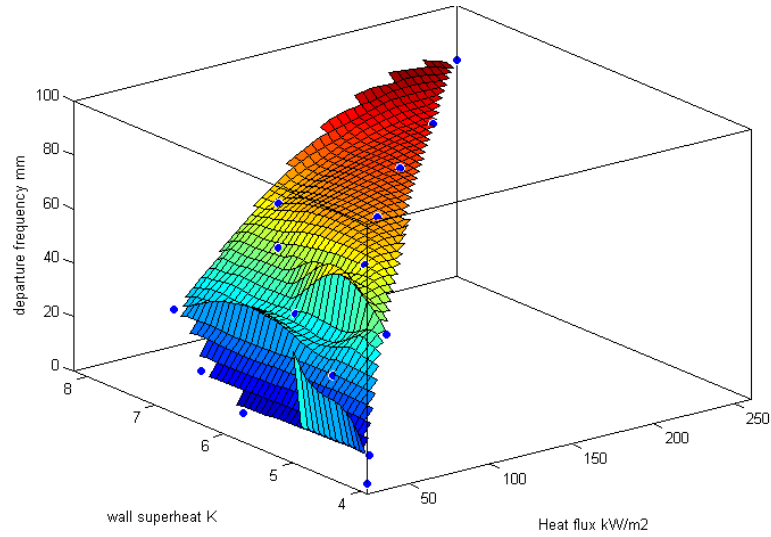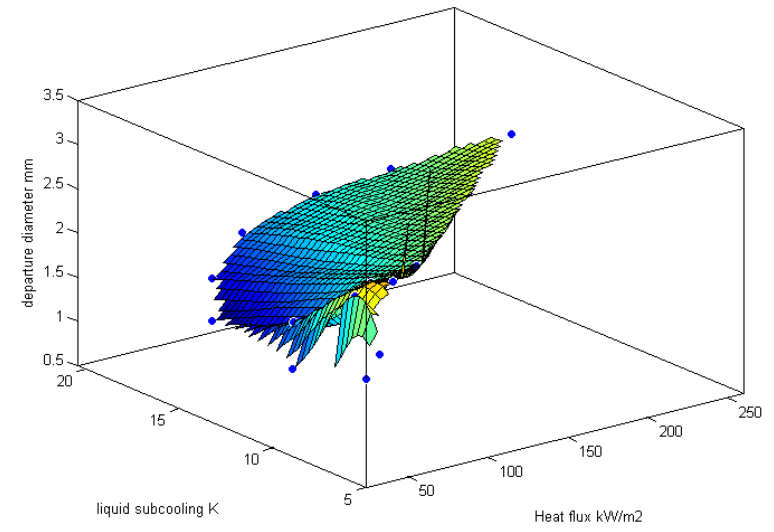
(ii)
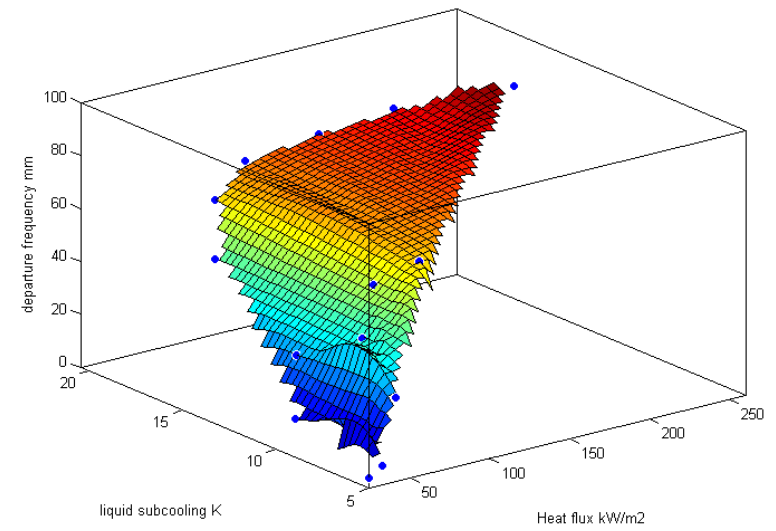
(B)
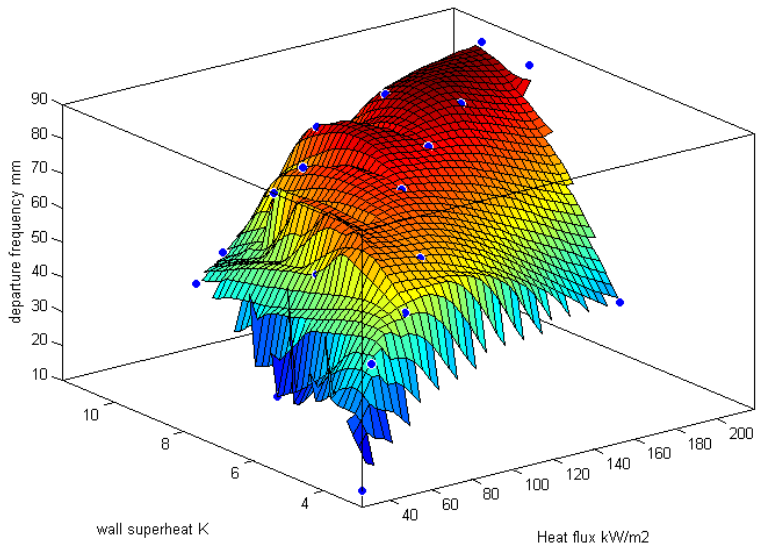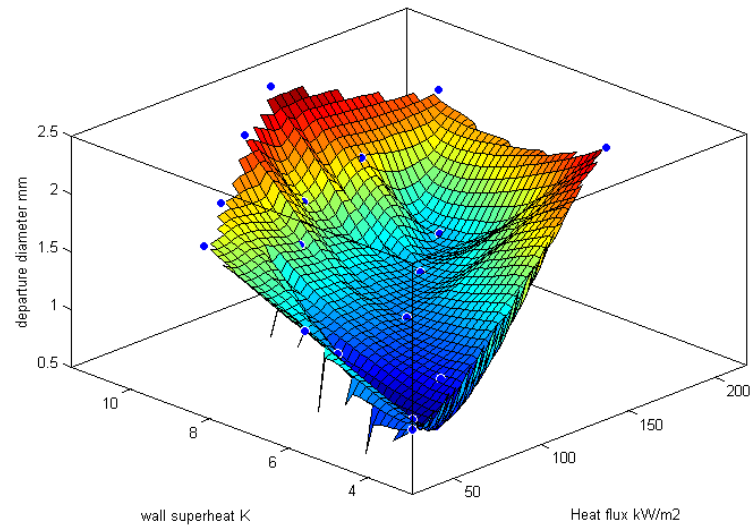
(i)
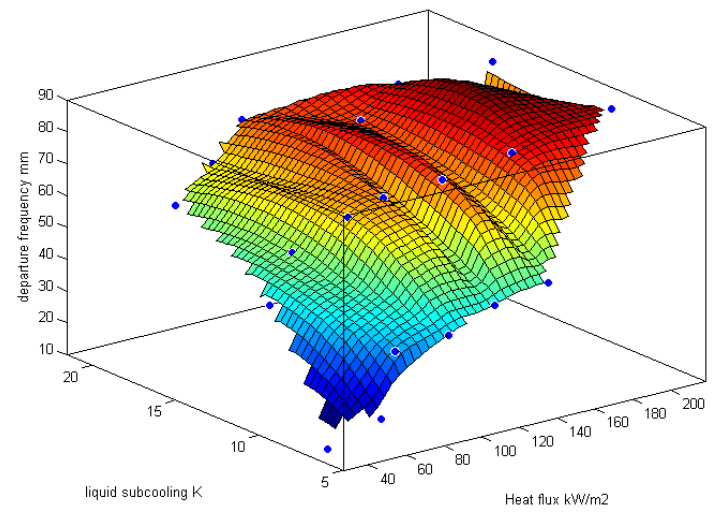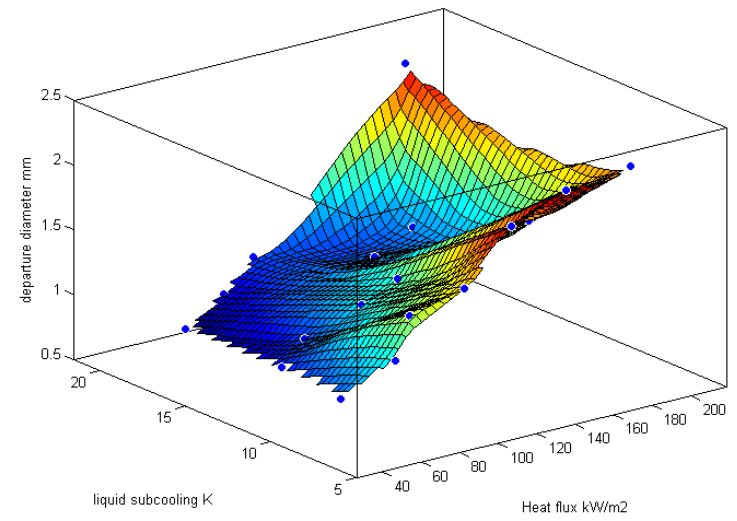
(ii)

(C)
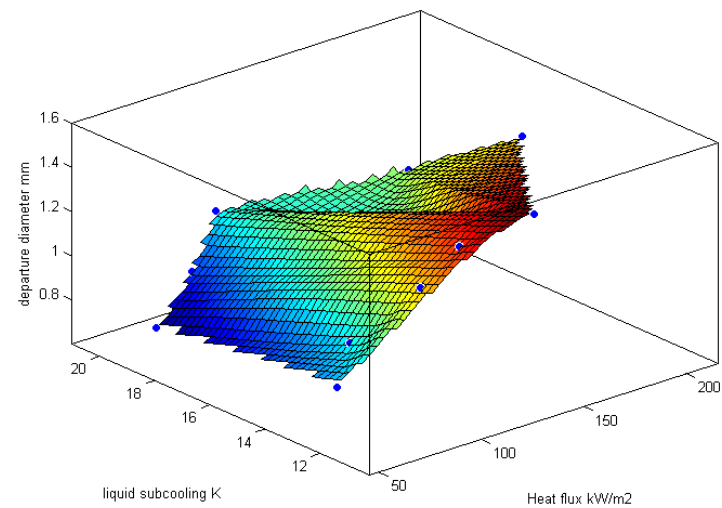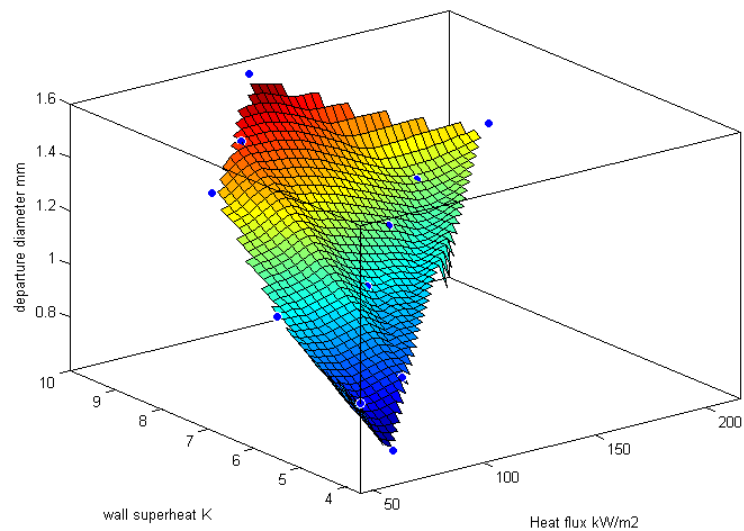
(i)
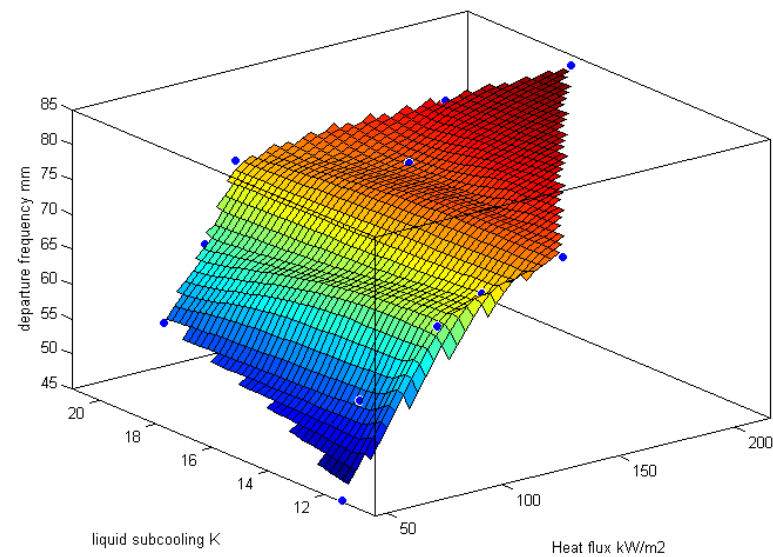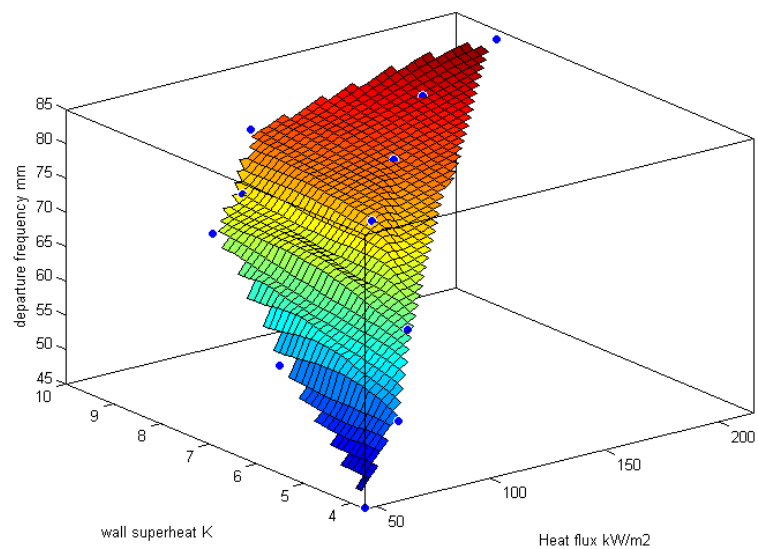
(ii)

(D)
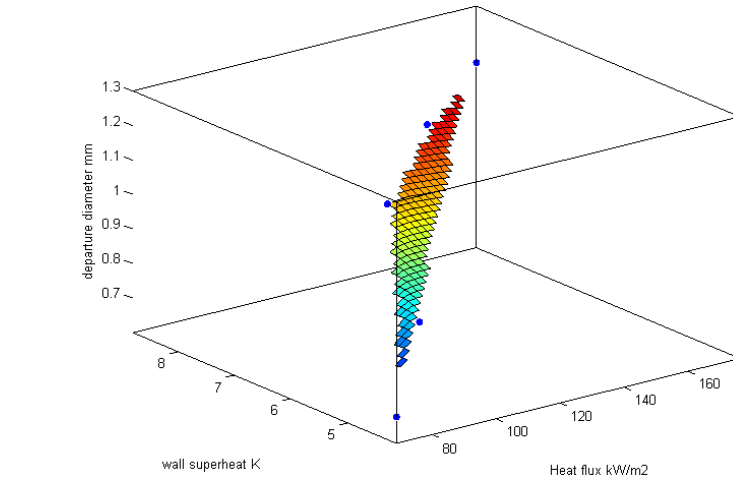
(i)
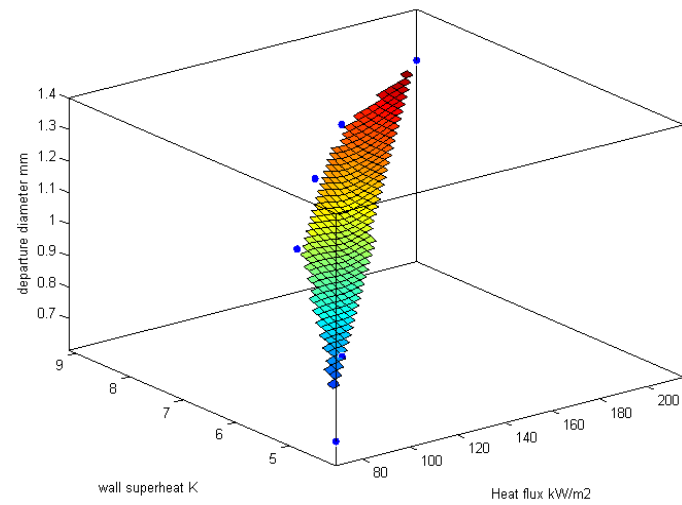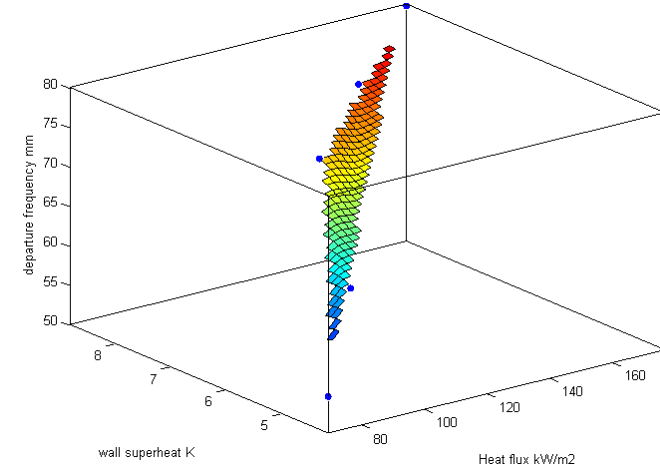
(ii)
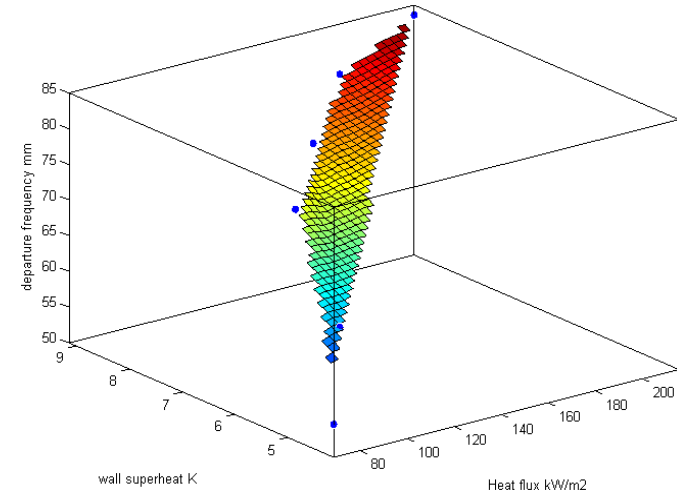
(E)

Figure 3.3 Surface plots for (i) departure diameter and (ii) departure frequency for (A) rod 1, (B) rod 2, (C) rod3, (D) ribbon. (E) Surface plots for rod 2 in (i) 45° inclination and (ii) 90° inclination.

Table 3.3 Statistical analysis of experimental data.

Case		Mean	Standard Deviation	Variance	95% confidence interval
Rod 1, $T_l = 90°C$, $\Delta T_{sat} = 4.1°C$	Diameter	1.368	0.201	0.040	0.057
	Frequency	10.889	0.327	0.107	0.092
Rod 2, $T_l = 90°C$, $\Delta T_{sat} = 4.65°C$	Diameter	1.439	0.158	0.025	0.046
	Frequency	31.146	1.559	2.432	0.456
Rod 3, $T_l = 90°C$, $\Delta T_{sat} = 8.9°C$	Diameter	1.263	0.186	0.035	0.058
	Frequency	66.784	1.944	3.779	0.602
Strip, $T_l = 90°C$, $\Delta T_{sat} = 6.4°C$	Diameter	2.616	0.213	0.045	0.064
	Frequency	23.497	2.157	4.652	0.652
Rod 1 ($\phi = 45°$), $T_l = 90°C$, $\Delta T_{sat} = 3.9°C$	Diameter	1.612	0.437	0.191	0.126
	Frequency	37.135	1.745	3.045	0.504
Rod 1 ($\phi = 90°$), $T_l = 90°C$, $\Delta T_{sat} = 4.2°C$	Diameter	1.792	0.665	0.442	0.190
	Frequency	59.645	5.563	30.946	1.627

1ms

3ms

5ms

7ms

9ms

11ms

10 mm

Scale

12ms
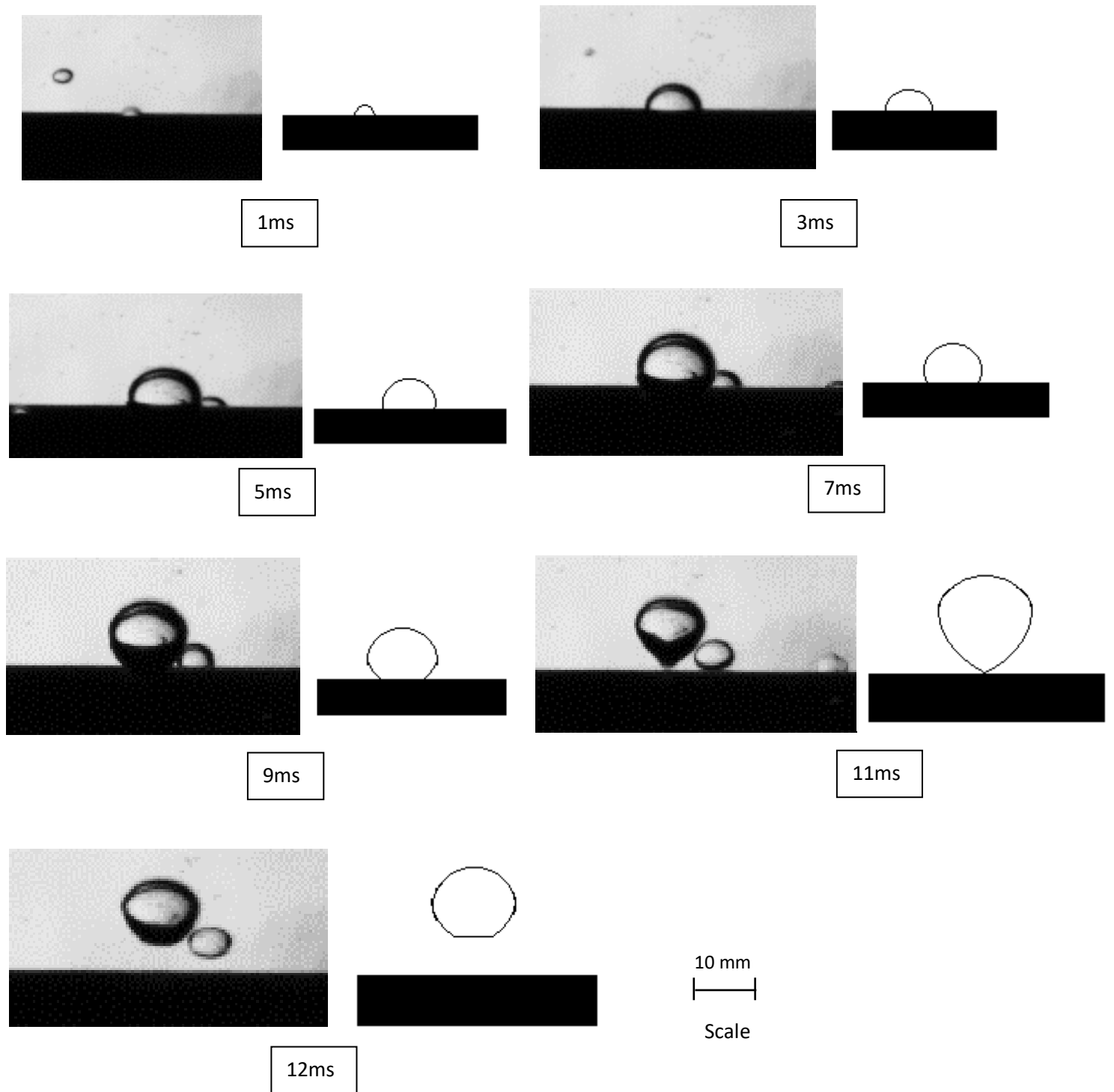
Figure 3.4 Growth and departure of a typical vapor bubble

3.3.1. *Heat Transfer Coefficient*

The boiling curves and heat transfer coefficient curves for different cases are shown in *Figure 3.5* through *Figure 3.7*. The heat transfer coefficient was calculated as

$$h = \frac{q''}{T_w - T_l} = \frac{q''}{\Delta T_{sat} + \Delta T_{sub}}$$

(3.1)

110

where q'' is the applied heat flux, T_w and T_l are the wall and liquid temperatures respectively, ΔT_{sat} is the wall superheat and ΔT_{sub} is the degree of liquid subcooling.

Figure 3.5(A) shows that the boiling curves shift towards the left as the degree of subcooling increases, implying that at any given heat flux, lower bulk temperature results in lower surface superheat values. For instance, at $q'' = 100\ kW/m^2$, wall superheat decreases from ~8.25 K at $\Delta T_{sub} = 5\ K$, to ~6.9 K at $\Delta T_{sub} = 10\ K$, to ~5.7 K at $\Delta T_{sub} = 20\ K$. This is a decrease of about 16% in wall temperature on decreasing the bulk temperature from 95 ℃ to 90 ℃, and similarly, a 17% decrease for the bulk temperature decrease from 90 ℃ to 80 ℃. Also, it can be seen that the onset of nucleate boiling (solid points in the figure) also shifts to lower values with decrease in subcooling, implying that higher bulk temperatures facilitate faster initiation of boiling. For instance, the value of Onset of Nucleate Boiling wall superheat (ONB) decreases by 8% when the degree of subcooling decreases from 10 K to 5 K (4.1 K to 3.8 K), and by 20% when degree of subcooling decreases from 20 K to 10 K (4.9 K to 4.1 K). However, the fall in wall superheat is small compared to the increase in the subcooling, thereby in accordance with equation (3.1), resulting in a reduced heat transfer coefficient with an increase in the degree of subcooling as shown in *Figure 3.5*(B). Consider, at $q'' = 100\ kW/m^2$, the heat transfer coefficient value decreases from 7.25 $kW/m^2\ K$ to 5.41 $kW/m^2\ K$ to 3.88 $kW/m^2\ K$ as the degree of subcooling increases from 5 K to 10 K to 20 K, respectively. This means a decrease of 25% and 28% for an increase in subcooling of 5 K to 10 K and from 10 K to 20 K, respectively. These results are in contrast with the results obtained by Judd and Hwang (1976). Rohsenow (1971) showed that the effect of subcooling on boiling is dependent on the geometry of the heater and that could explain the different results for the rod used in present study and the flat plate type heater in latter case. However, the literature shows that contradictory results can be obtained even for the same geometry. For instance, Duke and Schrock (1961) and Judd and Hwang (1976), both used flat plate type

heaters and obtained opposite results. The reason for discrepancies with same geometry might be attributed to the difference in surface roughness and the preparation of the heater surface. The heat transfer coefficients obtained in this study, using equation (3.1) are compared with the predictions from the two most widely stated correlations for pool boiling heat transfer, namely Forster and Zuber (1955) and Cooper (1984) as given in equations (3.2) and (3.3) below, respectively.

$$h = 0.00122 \left(\frac{k_L^{0.79} C_{p,L}^{0.45} \rho_L^{0.49}}{\sigma^{0.5} \mu_L^{0.29} h_{fg}^{0.24} \rho_v^{0.24}} \right) (\Delta T)^{0.24} (\Delta P)^{0.75} \tag{3.2}$$

$$h = 55 p_r^{0.12} (-log_{10} p_r)^{-0.55} M^{-0.5} q''^{0.67} \tag{3.3}$$

where k_L is the liquid thermal conductivity, $C_{p,L}$ is the specific heat capacity of the liquid, ρ_L is the liquid density, σ is surface tension, μ_L is liquid dynamic viscosity, h_{fg} is the latent heat of vaporization, ρ_v is the vapor density, ΔT is the difference between the wall temperature and liquid temperature, ΔP is the difference between the saturation pressure at wall temperature and the saturation pressure at the liquid temperature; p_r is the reduced pressure (system pressure/critical pressure), and M is the molar mass of the liquid.
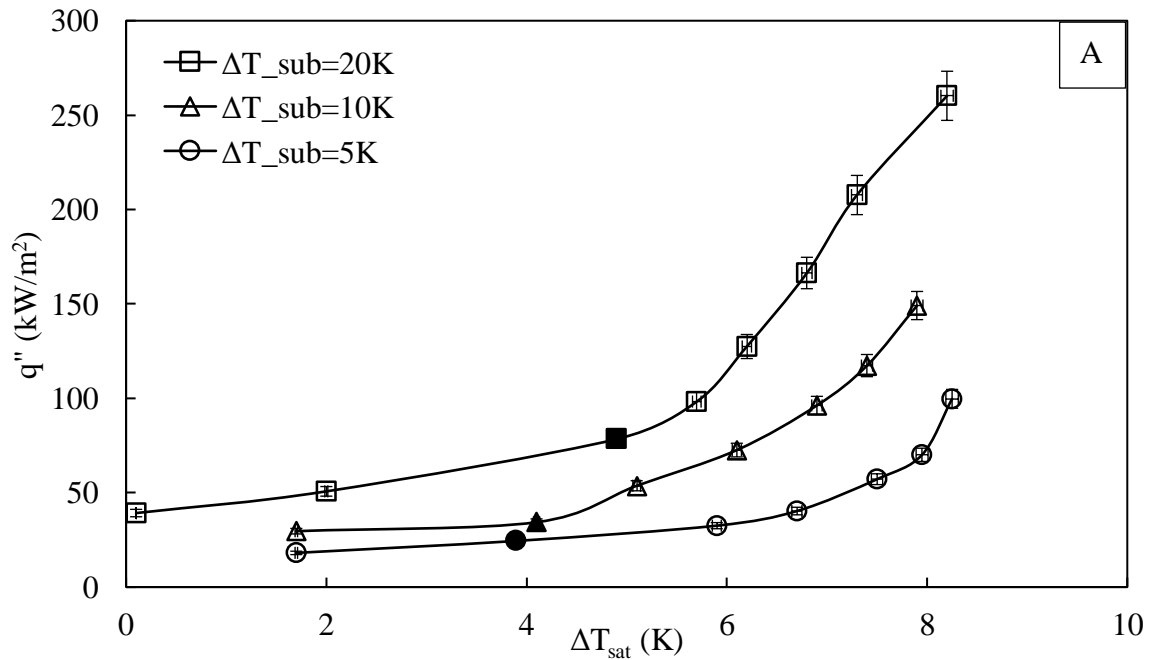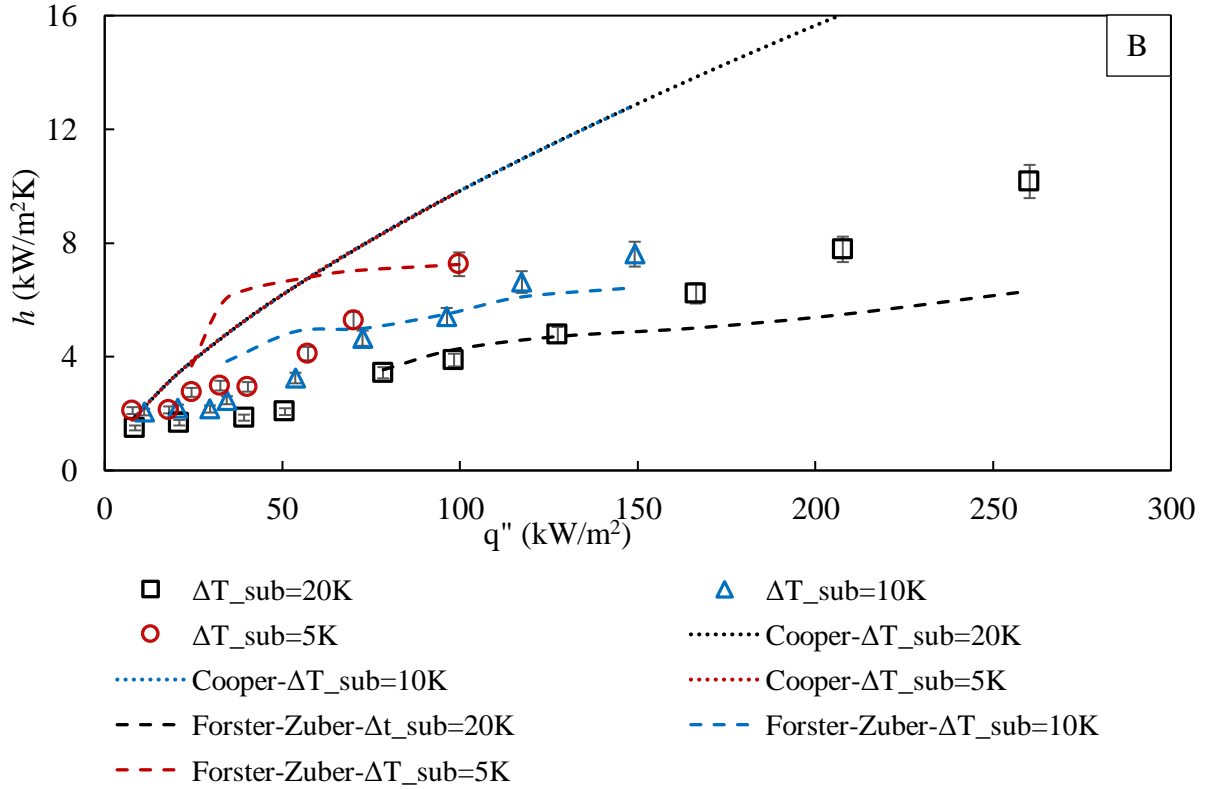
Figure 3.5 Effect of liquid subcooling – (A) boiling curves, (B) heat transfer coefficient (rod 1).

It can be seen in the *Figure 3.5*(B), that the experimentally measured heat transfer coefficient values lie in the range of the predicted values. However, the Cooper (1984) correlation predicts the data correctly only at very low heat fluxes and overpredicts at higher values of heat flux. Also, it does not take the liquid subcooling into account and hence, all three lines overlap one another. On the other hand, Forster and Zuber (1955) correlation takes the liquid subcooling into account in form of $\Delta T = T_w - T_l$, and hence, is able to predict the fall in heat transfer coefficient with increase in liquid subcooling.

Figure 3.6(A) shows that at a given heat flux input, the wall superheat required for nucleation increases as the heater surface roughness (R_a) increases. Although, within the experimental error, the curves appear to merge for the low heat fluxes (below $100 \; kW/m^2$). Similar results were observed by Benjamin and Balakrishnan (1997) also. This result contrasts with the classical nucleation model proposed by Rohsenow (1971). The nucleation model equation is expressed as

$$\Delta T_{sat} = \frac{2v_{fg}\sigma}{h_{fg}r} \qquad (3.4)$$

where r is the radius of the bubble nuclei, v_{fg} is the specific volume change in phase change, σ is surface tension, and h_{fg} is the latent heat of vaporization. The radius of the bubble nuclei can be considered almost equal to the radial size of the nucleating cavity. This model implies that at a given heat flux, the required superheat for bubble nucleation should decrease with an increase in the surface roughness, when an increase in the surface roughness increases the radial size of the cavity. Also, this model assumes that the cavity mouth is circular in shape and the cavity is conical. This assumption may not hold true for surfaces prepared by polishing using emery paper, as in the present case. From *Figure 3.2*, it may be seen that the number and the depth of the cavities increase with increase in R_a rather than the radial size of the cavities. The increased depth of the cavity mouth and number of cavities could result in a higher wall temperature requirement for the bubble formation. At heat fluxes less than $100 \ kW/m^2$, it was mostly natural convection which is independent of the surface roughness of the heater surface. *Figure 3.6*(B) shows the effect of surface roughness on the two-phase heat transfer coefficient, along with the predictions from Forster and Zuber (1955) and Cooper (1984). And again in accordance with equation (3.1), the increase in wall superheat at a given heat flux with an increase in surface roughness, results in a reduced heat transfer coefficient, albeit slightly.
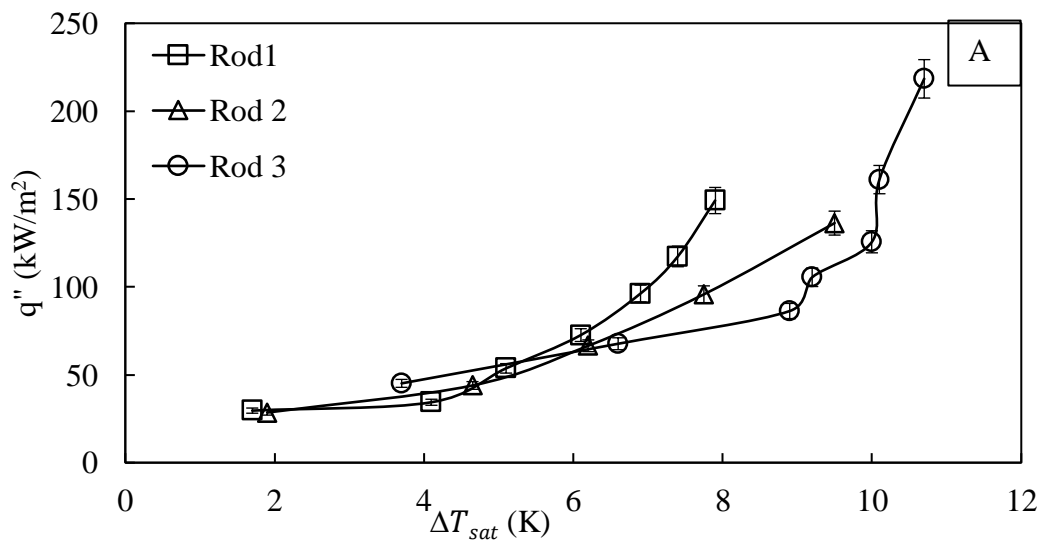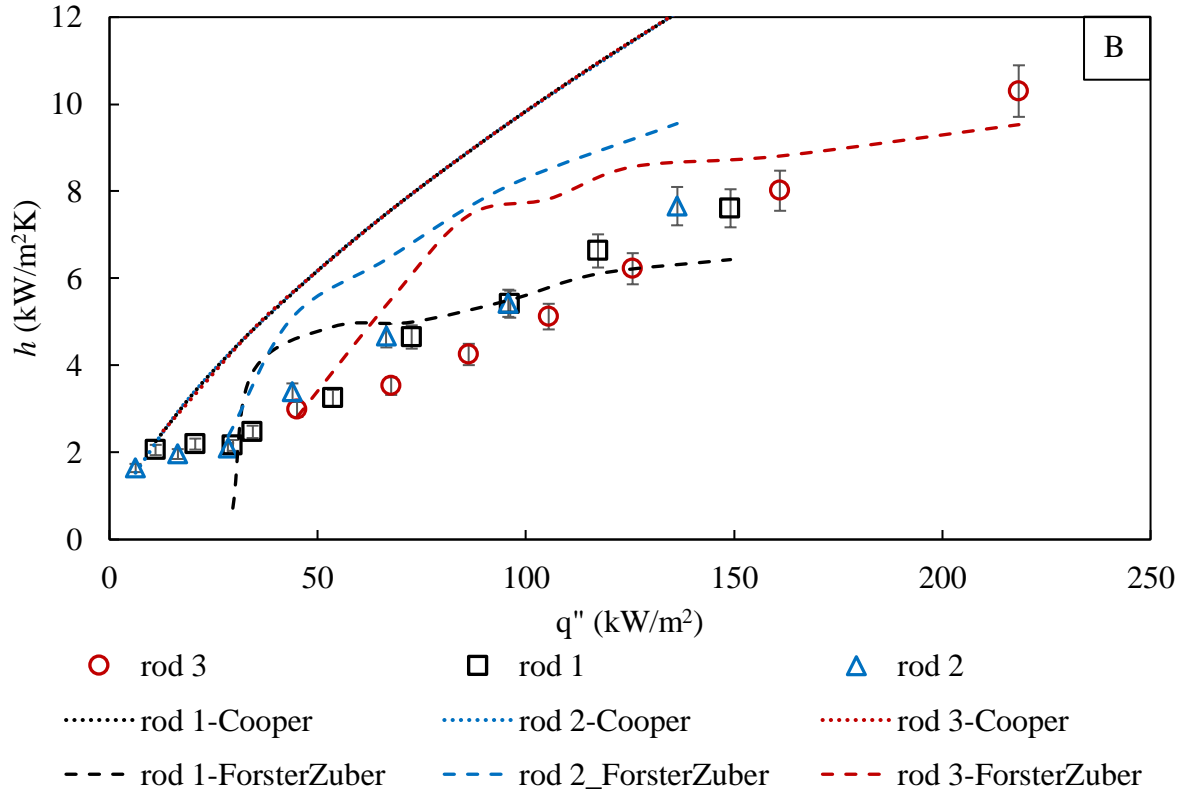
Figure 3.6 Effect of wall surface roughness - (A) Boiling curves, (B) heat transfer coefficient

$$\Delta T_{sub} = 10K.$$

Figure 3.7(A) shows the effect of the heater inclination angle on heat transfer for the same value for liquid subcooling. The nucleate boiling curves shift to their left as the heater inclination goes from horizontal ($\phi = 0°$) to vertical ($\phi = 90°$). This decrease in the wall temperature as the inclination of the heater rod increases can be attributed to the enhanced natural convection for the inclined rods as compared to the horizontal rod due to the increase in the characteristic length or the depth of the fluid involved in convection. More convective heat transfer causes cooling of the heater rods to result in lower surface temperatures. The increase in the nucleate boiling heat transfer with increase in the inclination angle, as seen in *Figure 3.7*(B), can be attributed to two factors – (1) the enhanced convection due to higher depth of convective fluid and higher degree of fluid stirring caused by the bubbles as they slide along the heater surface, and (2) the bubbles sliding along the heater surface also cause the

cooling of the heater surface by evaporative heat transfer while sliding. The heat transfer coefficient is observed to increase about 26% as the heater rod inclination changes from horizontal to $\phi = 45°$, while the increase in heat transfer coefficient for inclination change from $\phi = 45°$ to vertical is only 5%. This can be explained as follows: the convection and bubble sliding motion can occur only along the diameter of the heater rod in the horizontal position, however the convective fluid depth increases about 75% in the $45°$ inclined position (the characteristic length having changed from D to $Lcos\phi$). Also, the bubbles can slide along the length of the heater as well as the along the diameter of the rod. This dual effect brings about a significant increase in heat transfer coefficient. When the rod is inclined vertically, the depth of the convective fluid increases from $Lcos\phi$ to L (abut 40% increase for the value of $L = 10\ mm$) and the bubble sliding is also possible only along the length of the heater. All these factors contribute to a lower increase in heat transfer in changing the inclination from $45°$ to $90°$. *Figure 3.7*(B) shows that both the pool boiling heat transfer coefficient models do not take the inclination angle into account and hence, do not predict the trend of increasing heat transfer coefficient with the inclination angle correctly.
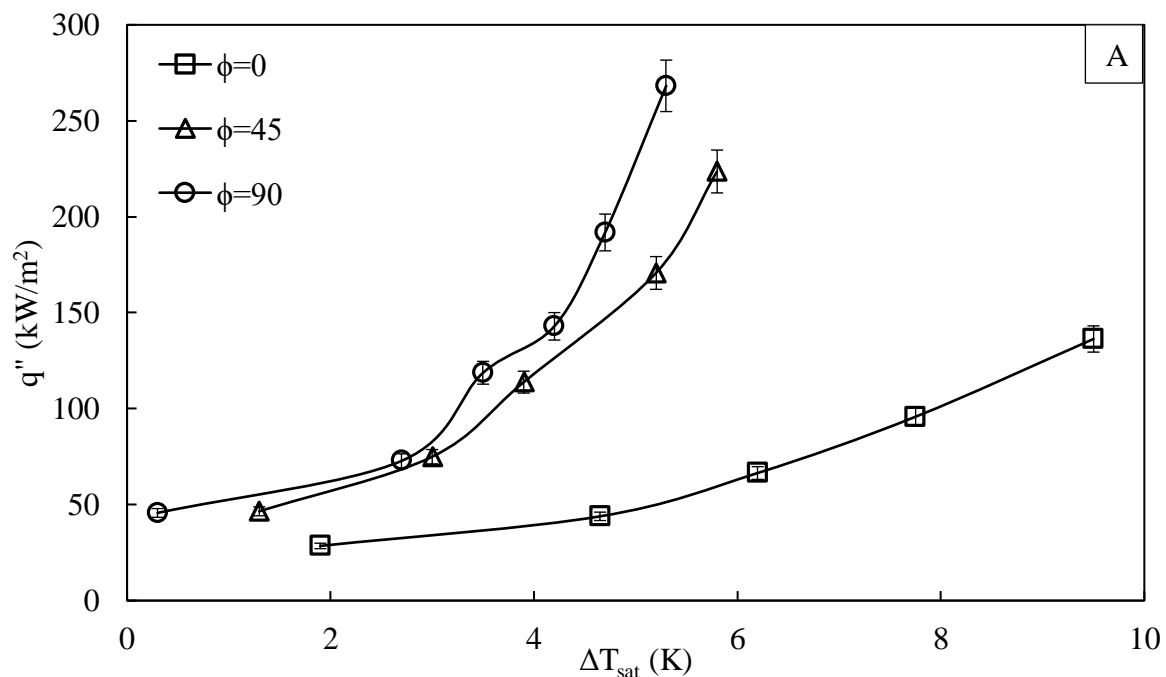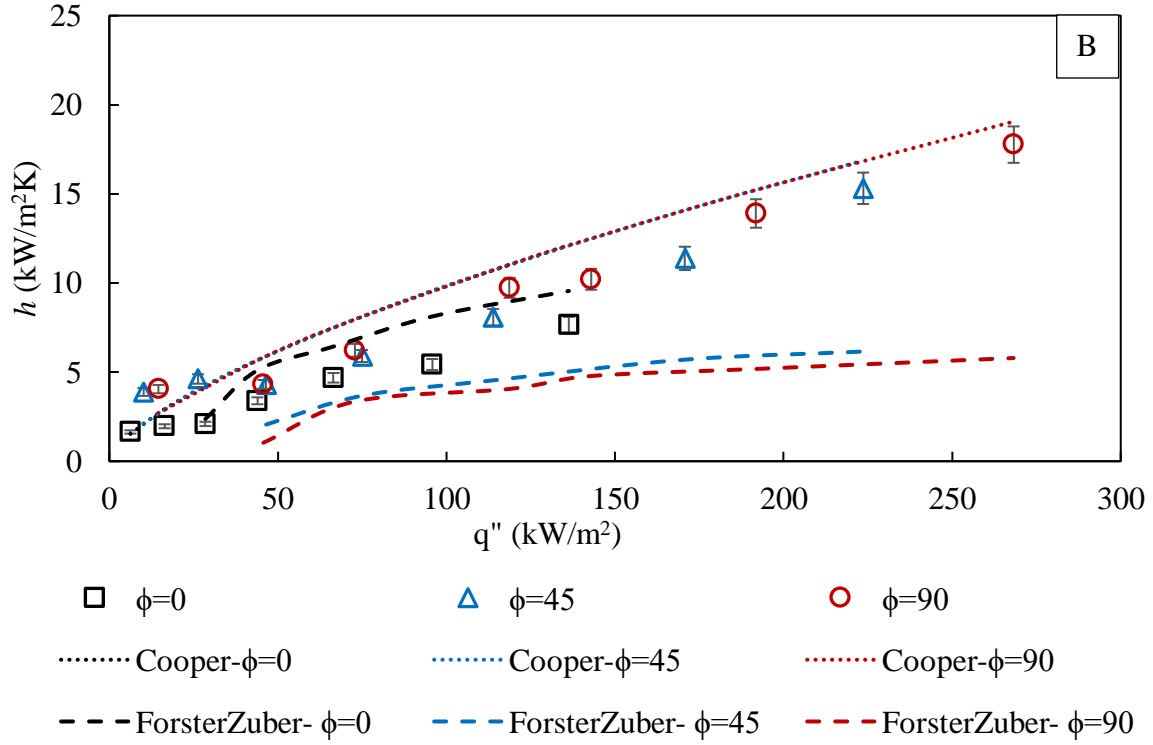
Figure 3.7 Effect of heater inclination angle - (A) Boiling curves, (B) heat transfer coefficient

$$\Delta T_{sub} = 10K.$$

Comparing the effects of degree of subcooling, surface roughness and heater inclination angle on the wall superheat or the heat transfer coefficient, we observe that the effect of heater inclination angle (~56%) is much more pronounced compared to the other two factors (~32%). As the bulk liquid temperature decreases (degree of subcooling increases), the convection heat transfer between the heater wall and the liquid starts at the lower wall temperatures. Hence, at higher subcooling, this wall cooling results in the heater wall achieving a lower temperature for any given heat flux, which would subsequently decrease the bubble sizes and hence, lower overall heat transfer. The effect of increased surface roughness is brought about by the increased density of active nucleation sites. As the surface roughness increases, the number of bubbles growing on the surface increases, and these bubbles form a vapor layer not allowing the liquid to come into contact with surface, especially at the high heat fluxes, thereby increasing the wall temperature and decreasing the heat transfer coefficient. Lastly, as

discussed previously, the enhanced convective fluid depth and the bubble sliding motion causes the decrease in wall temperature and increase in heat transfer coefficient for the variation of inclination angle. Hence, we can say that for the inclination angle, both the convection and bubble dynamics contribute to the change in heat transfer, making its effect more pronounced compared to the other two factors, where convection or the bubble dynamics contribute to the change in heat transfer.

3.3.2. Bubble departure diameter and frequency

3.3.2.1. Effect of heat flux

The bubble departure diameter (D_d) was observed to increase by $\sim 1mm$ (40%) as flux increased from $30\ kW/m^2$ to $120\ kW/m^2$ as shown in *Figure 3.8*(A). However, the obtained results are in contrast with those of Judd and Hwang (1976) as shown in the figure. From the saturated boiling literature, it can be seen that for any given nucleation site, irrespective of the fluid and heater surface, the bubble departure size qualitatively increases with the increase in heat flux, however slowly, due to an enhanced evaporative heat transfer rate in the superheated layer. Nevertheless, the fluid-surface combination and heater surface characteristics do affect the quantitative values significantly. This is further substantiated by the increase in departure frequency (f) with increase in the heat flux (*Figure 3.8*(B)). As the heat flux increases, the temperature gradients in the superheated layer increase, thereby enhancing the evaporative heat transfer and speeding up the bubble cycle. The product of the bubble departure diameter and frequency dimensionally represents the velocity of the bubbles departing from the heater surface. With both f and D_d increasing with an increase in heat flux or wall superheat, the product is also an increasing function of the heat flux.

Judd and Hwang (1976) found the diameter to be a decreasing function of the heat flux for subcooled boiling and explained the increased nucleation site density to be a cause of it. Their results were obtained by boiling dichloromethane on a flat glass plate heater with a thin

stannic oxide film. They explained the decrease of departure diameter saying that, as the nucleation site density increases with the heat flux, it leads to smaller bubbles departing from the surface. But Lee *et al.* (2003) used a similar flat glass plate with an ITO film for heater surface and found that the bubble departure diameter is directly proportional to the Jakob number, implying that the diameter increases with wall superheat and heat flux. Also, Gaertner (1965), Nishikawa *et al.* (1965), Siedel *et al.* (2008) and McHale and Garimella (2010) used flat plate type heater geometry using water, pentane and refrigerant FC-77 as working fluids. They all obtained increase in the departure diameter with an increase in the imposed heat flux. Hence, it can be inferred that the discrepancies in the results obtained by Judd and Hwang cannot be attributed to the difference in fluid or heater surface. The difference in their results can be explained however, in terms of the diameter definition used. They used interferometry in sync with high speed videography to record the bubble growth from the bottom of the heater glass. Hence, it can be understood that they measured the bubble maximum *contact diameter* as opposed to the equivalent diameter. Hence, with increase in heat flux, as explained by them, the nucleation site density increases, which results in competition for the heat energy amongst the neighbouring sites, reducing the maximum possible contact diameter of the bubbles.
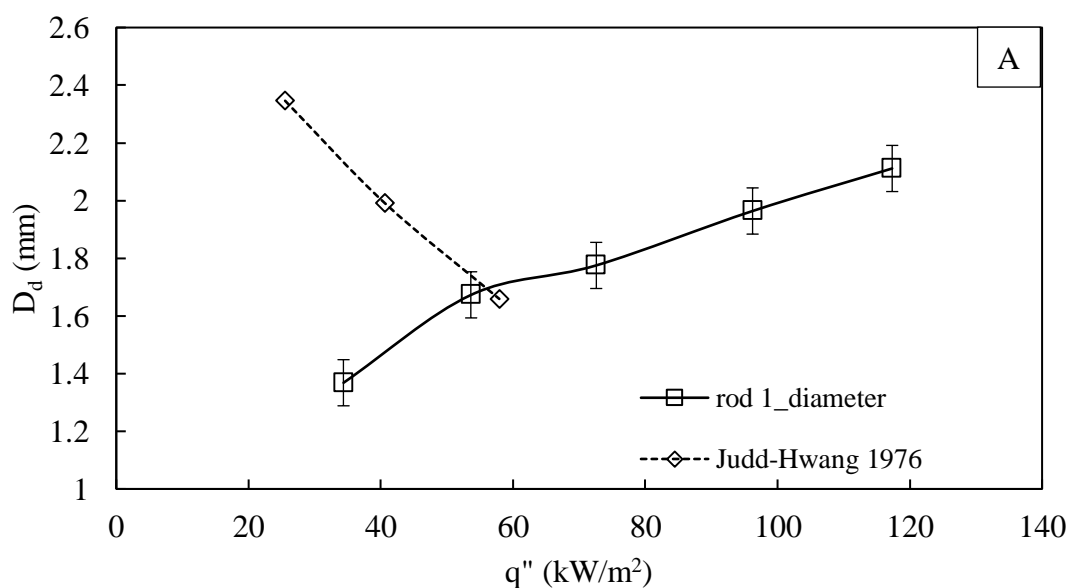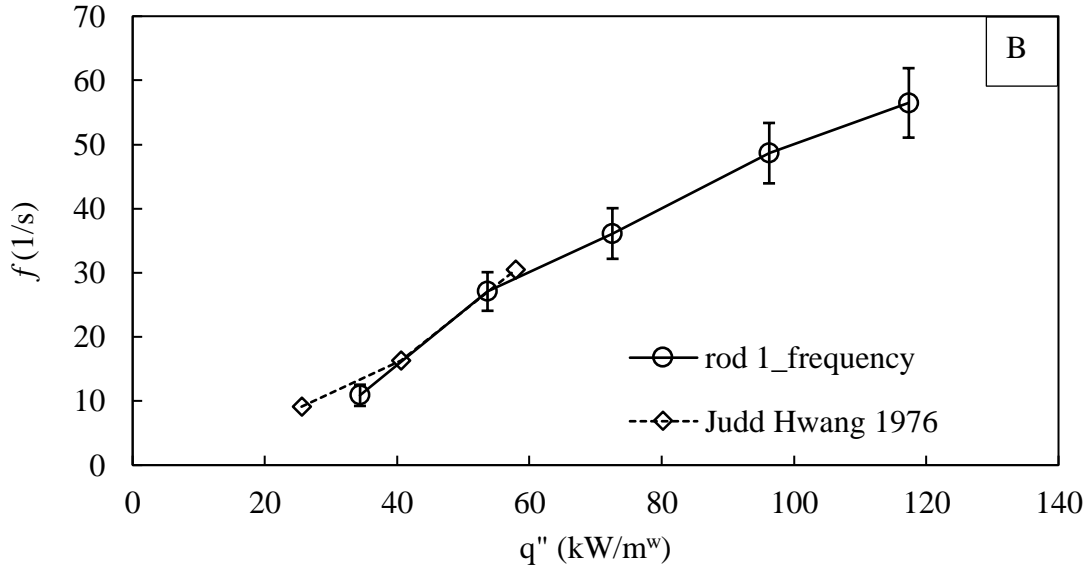
Figure 3.8 (A) Departure diameter, and (B) frequency as a function of wall heat flux (Rod 1,

$$\Delta T_{sub} = 10K).$$

3.3.2.2. Effect of degree of subcooling

To study the effect of subcooling on bubble departure characteristics, three different levels of subcooling, i.e. $5\,K, 10\,K\,and\,20\,K$ were considered. As shown in *Figure 3.9*, it was observed that the departure diameter decreases as the degree of subcooling increases, while the frequency of departure tends to increase (*Figure 3.10*). Here, it is essential to remember that each data set shows the variation of diameter or frequency with the degree of subcooling keeping all other factors constant. So, comparing the data sets amongst each other, which have multiple factors (heat flux, surface roughness, wall superheat) varied from each other would lead us to incorrect inferences. There is very little data for the departure diameter for subcooled liquid under constant flux conditions. The data from Judd and Hwang (1976) and Kim and Kim (2006) has been included in *Figure 3.9* for comparison. Both the data sets show similar parametric behaviour as observed in the present study. The very low values of diameter obtained by Kim and Kim (2006) are because of their use of microheater array of $2.7{\times}2.7\,mm^2$ surface area as their heater element. Also, it can be seen in *Figure 3.11* that at an applied heat flux of $\sim 100\,kW/m^2$, for higher subcooling, the bubbles departed from the heater and were

quickly condensed in 3-4 *ms* from departure moment. While as the subcooling decreases, the rate of condensation slows down, which means that the bubble departed from the heater surface travels up farther in the liquid. At higher bulk temperatures, small bubbles coalesce and depart as a big single bubble, which on being acted upon by the subcooled liquid changes its shape to a flattened disc (*Figure 3.11*(C)). For a given amount of heat input, increase in liquid subcooling has two effects: enhancement in condensation at the bubble cap and the reduction in the evaporation at the bubble base because of the thinning superheated liquid layer. Both these effects result in a smaller departure size of the bubbles. Demiray and Kim (2004) also pointed out that the slimmer superheated liquid layer also slows down the bubble growth rate since the microlayer trapped between the bubble and the heater surface is also reduced.
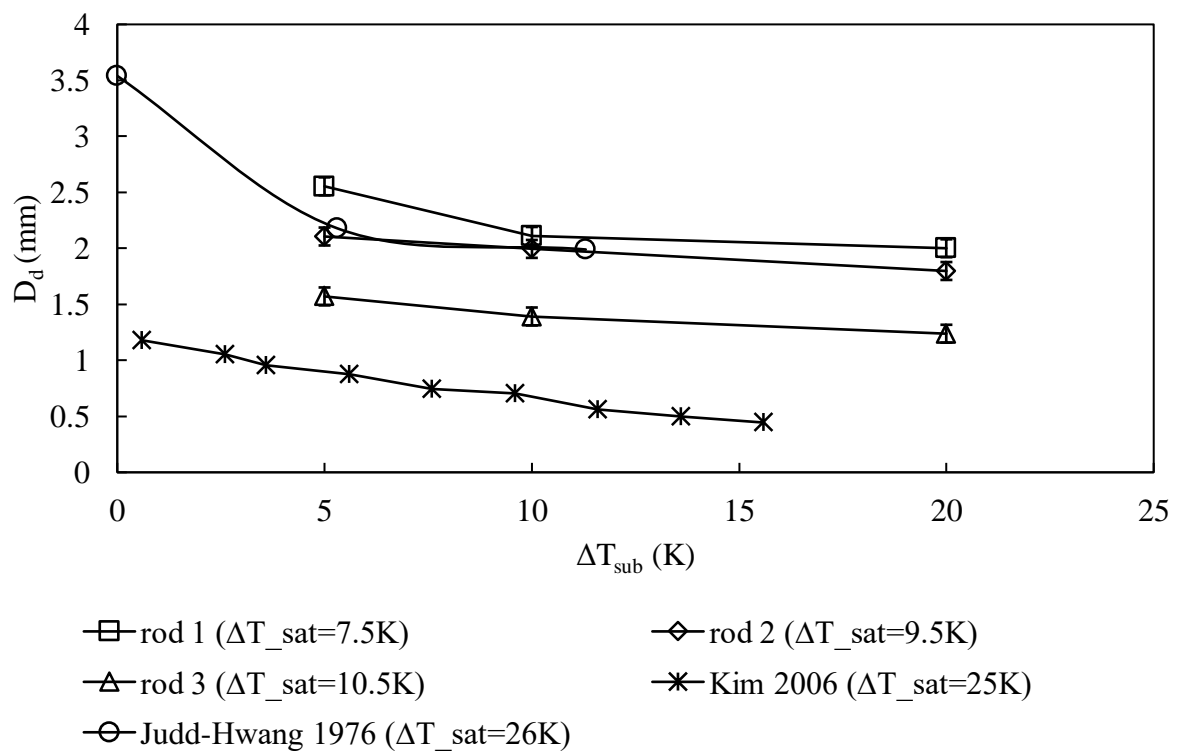
Figure 3.9 Effect of subcooling on bubble departure diameter.
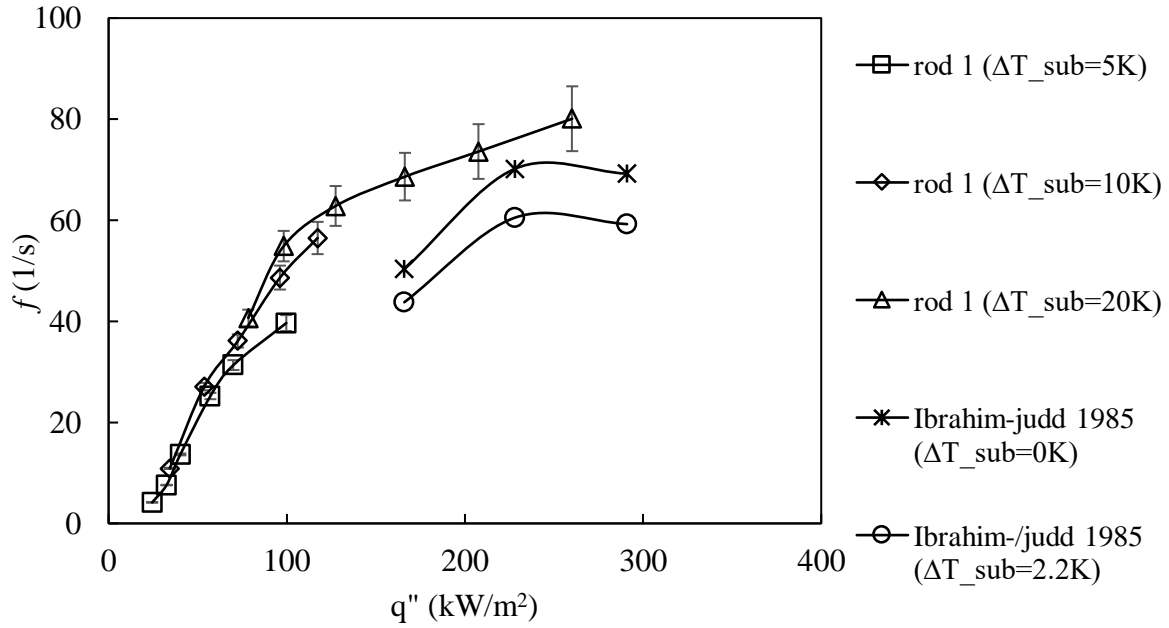
Figure 3.10 Effect of subcooling on departure frequency.

Further, it is conclusively accepted that the bubble growth period $(t_g) \ll$ waiting period (t_w), hence, the value of departure frequency is mainly dependent on the waiting period. The waiting period is governed by the time it takes for the thermal boundary layer to recuperate itself after a bubble has left the site. Ali and Judd (1981) proposed that the recovery of the thermal boundary layer occurs predominantly by transient conduction heat transfer for near saturated liquid $\Delta T_{sub} < 5\ K$, while the mechanism is a combination of transient conduction and convection heat transfer for liquid with higher degree of subcooling. Hence, while the transient conduction causes the waiting time to increase with an increase in subcooling, the higher temperature gradient $(T_w - T_l)$ for higher subcooling, results in a higher convection heat transfer leading to a faster recovery of thermal boundary layer. This considerably reduces the waiting period, thus giving higher departure frequency. However, since there are two competing effects at play, the increase in frequency with an increase in subcooling is less prominent compared to the decrease in departure diameter. Comparing with the results of Ibrahim and Judd (1985), the behaviour was confirmed. Also, for the subcooling $<5\ K$, since the transient conduction alone is responsible for recovery of thermal boundary layer, the

waiting period is found to increase and hence, the frequency may decrease with increase in the degree of subcooling. Also, we observe a tendency of frequency saturating with heat flux towards higher values of heat flux. This can be attributed to the fact that in the nucleate boiling region, the change in wall temperature with an increase in the heat flux is small and the wall temperature tends to saturate in the higher values of heat fluxes. Since, the frequency is largely governed by the convection $(T_w - T_l)$ in the quenching heat transfer, the frequency would saturate as the wall temperature saturates for a given bulk liquid temperature.

C

| t=0 ms | t=1 ms | t=3 | t=5 ms | t=8 | t=12 ms | t=16 ms | t=22 |
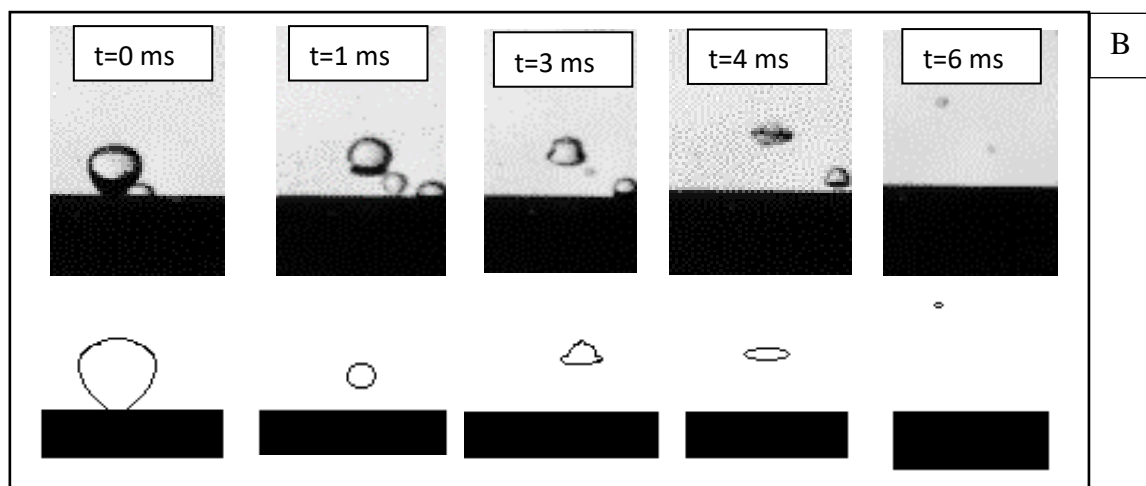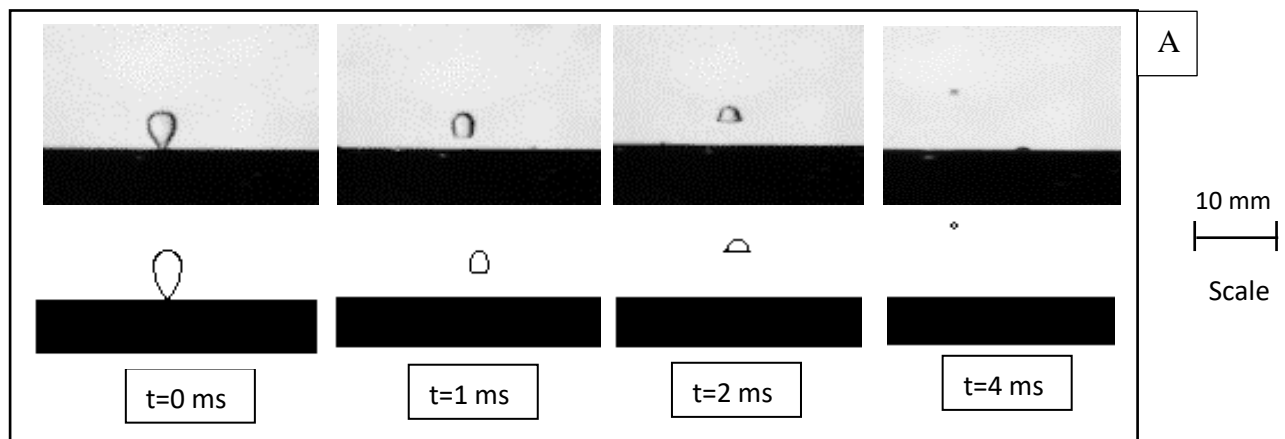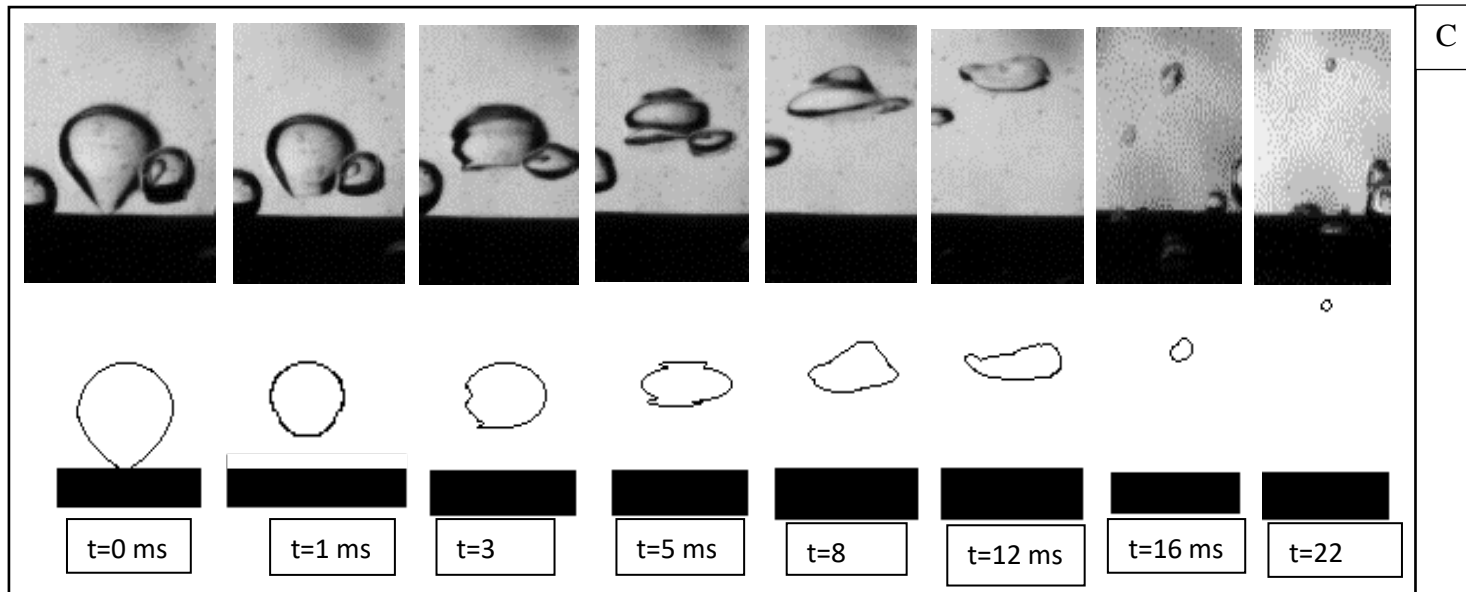
Figure 3.11 Bubble behaviour at different subcooling levels (A) $\Delta T_{sub} = 20°C$, (B) $\Delta T_{sub} = 10°C$, (C) $\Delta T_{sub} = 5°C$.

3.3.2.3. *Effect of heater surface roughness*

The effect of surface characteristics on the departure behaviour of the bubbles was studied by analysing the changes in f and D_d with the average surface roughness R_a values. *Figure 3.12* shows that for a given value of wall superheat, the bubble departure diameter decreases as the heater surface roughness increases, and the results from McHale and Garimella (2010) are also presented for comparison. These results are in qualitative agreement with the work by McHale and Garimella (2010) and McHale and Garimella (2013) who also found similar trends for the departure size variation with surface characteristics. McHale and Garimella (2010) found a general decrease in departure diameter with an increase in surface roughness, however their experiments had a standard deviation of 26%. Further, they calculated departure diameter as the average of diameter measurements of ±5 frames of calculated departure time for each bubble which introduced a measurement uncertainty of about 15%. *Figure 3.13* shows that the departure frequency increases as the heater surface roughness increases for low superheat. However, beyond wall superheat of $8\,K$, all the three curves can be seen to merge, implying that surface roughness does not have any influence on the departure frequency for higher superheats. Quantitatively, at wall superheat of 6 K, when the surface roughness increases from $0.5\,\mu m$ to $3.54\,\mu m$, bubble departure diameter decreases by 43%, and the departure frequency increases by 54%. Higher surface roughness means more number of nucleation sites but smaller in size, which then yield smaller bubbles sizes. Further, the rougher surfaces have a higher number of active nucleation sites, the waves of high temperature from these sites can help augment nucleation and hence, give a higher wall temperature for a given heat flux (Sultan and Judd (1983)). This means that the quenching heat transfer at the surface after the bubble departure, which is proportional to $(T_w - T_l)$, will also be higher for rougher surfaces. Hence, the rougher surfaces facilitate a quicker recovery of the thermal boundary layer after a bubble departure by enhanced convection, thereby reducing the waiting

period. But at high superheats, the temperature gradient $(T_w - T_l)$ becomes almost independent of the surface roughness.
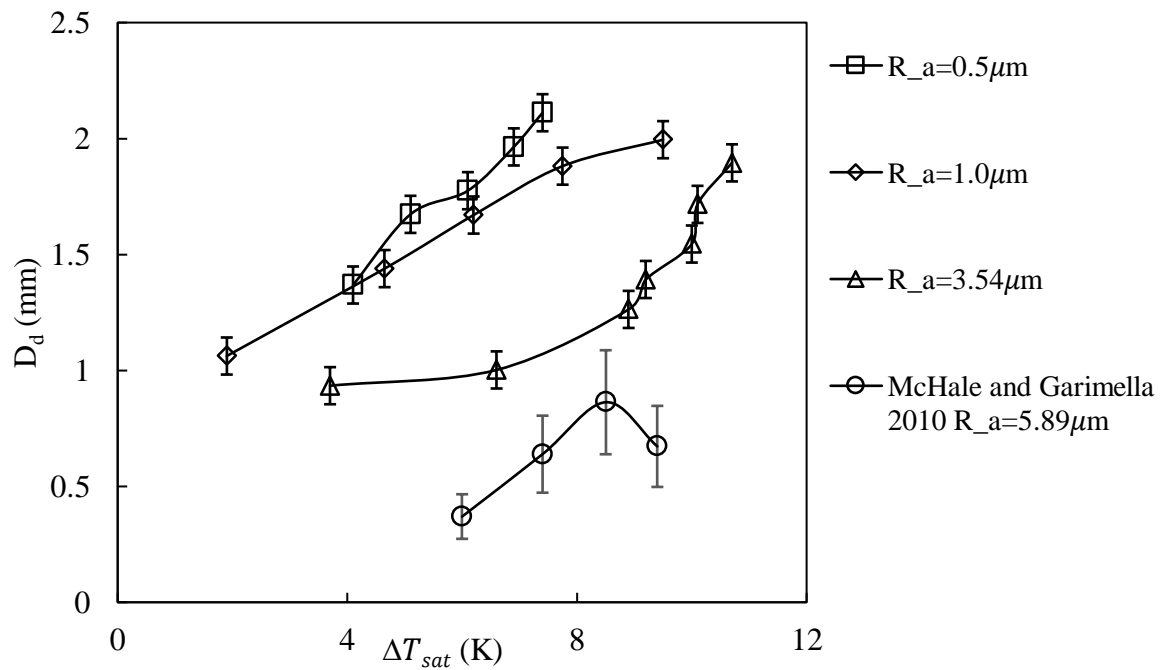
Figure 3.12 Effect of surface roughness of the heater element on the departure diameter ($T_l = 90\ °C$).
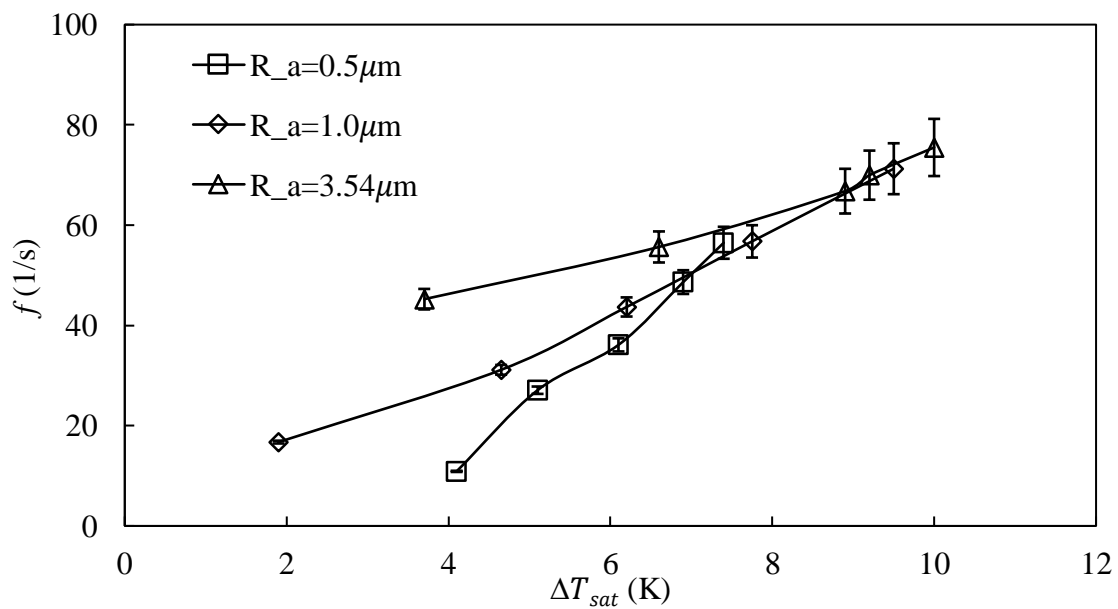
Figure 3.13 Effect of surface roughness on departure frequency ($T_l = 90\ °C$).

3.3.2.4. *Effect of heater inclination angle*

The inclination angle of the heater element (SS rod 2) was varied to study its effect on the bubble departure characteristics. The inclination angles studied were 0°, 45° and 90° with respect to the horizontal. *Figure 3.14* and *Figure 3.15* show that the departure diameter and the departure frequency both increase as the inclination angle increases. The reason for this can be attributed to the sliding of the growing bubble on the inclined surface before lifting off the heater surface. This sliding motion enhances the growth rate of the bubble and hence, bigger bubbles depart from the heater surface with a higher frequency resulting in a higher heat transfer for inclined heater elements. The vertical heater showed very large variations in the bubble waiting periods giving wide fluctuations in the frequency which is apparent in the large standard deviation for the case (*Table 3.3*). The sliding motion of the bubble was observed to be more prominent for the 90° case compared to the 45° case as shown in *Figure 3.16*.
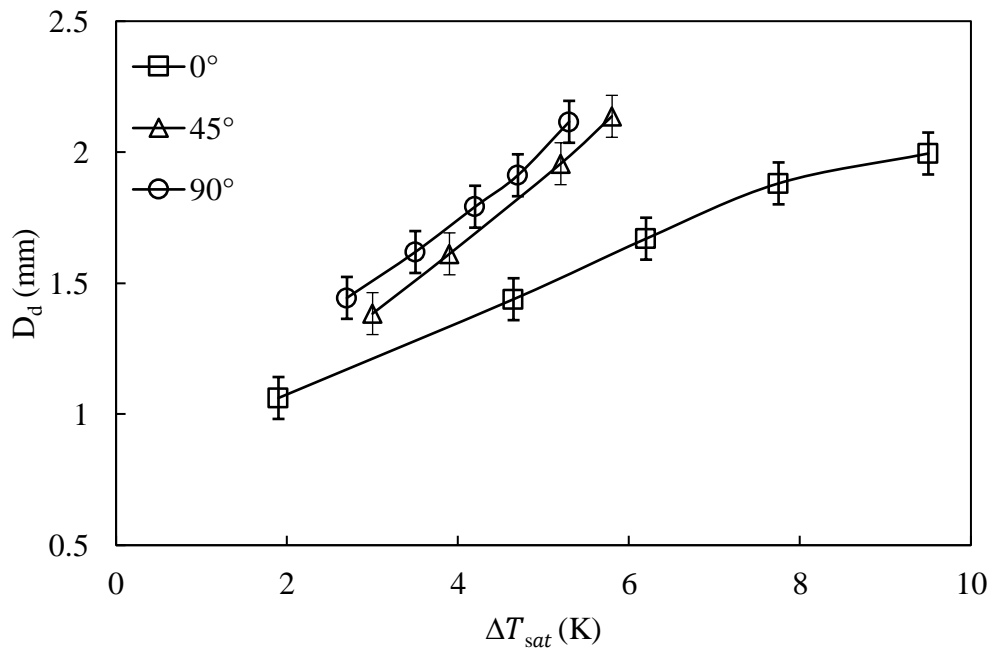
Figure 3.14 Effect of heater inclination angle on departure diameter ($\Delta T_{sub} = 10K$).
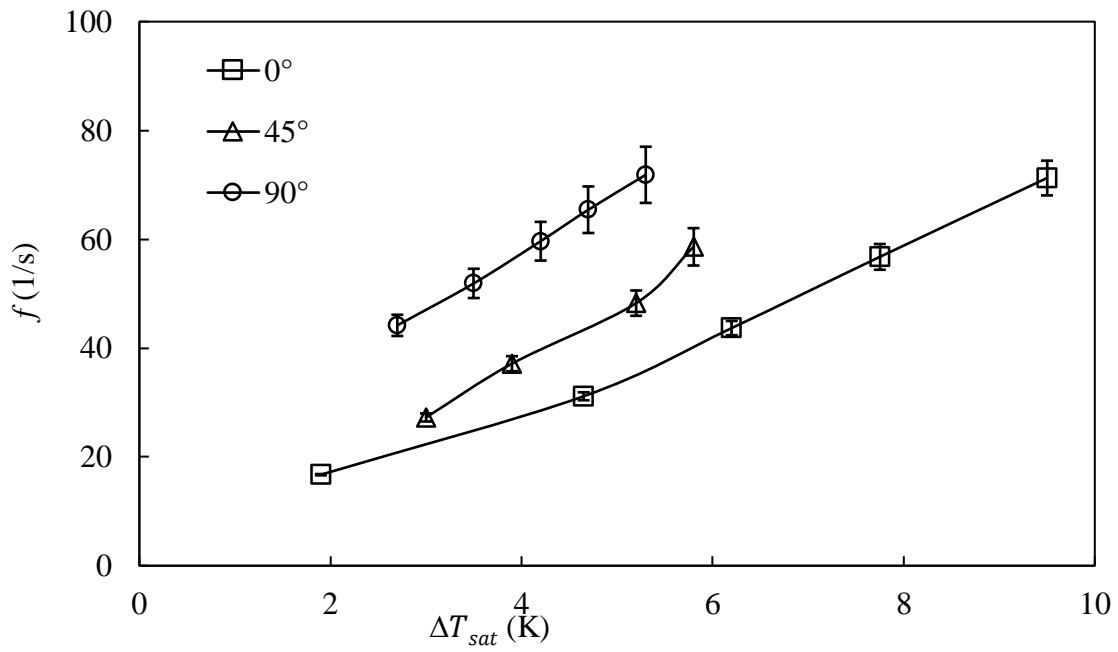
Figure 3.15 Effect of heater inclination angle on departure frequency ($\Delta T_{sub} = 10K$).
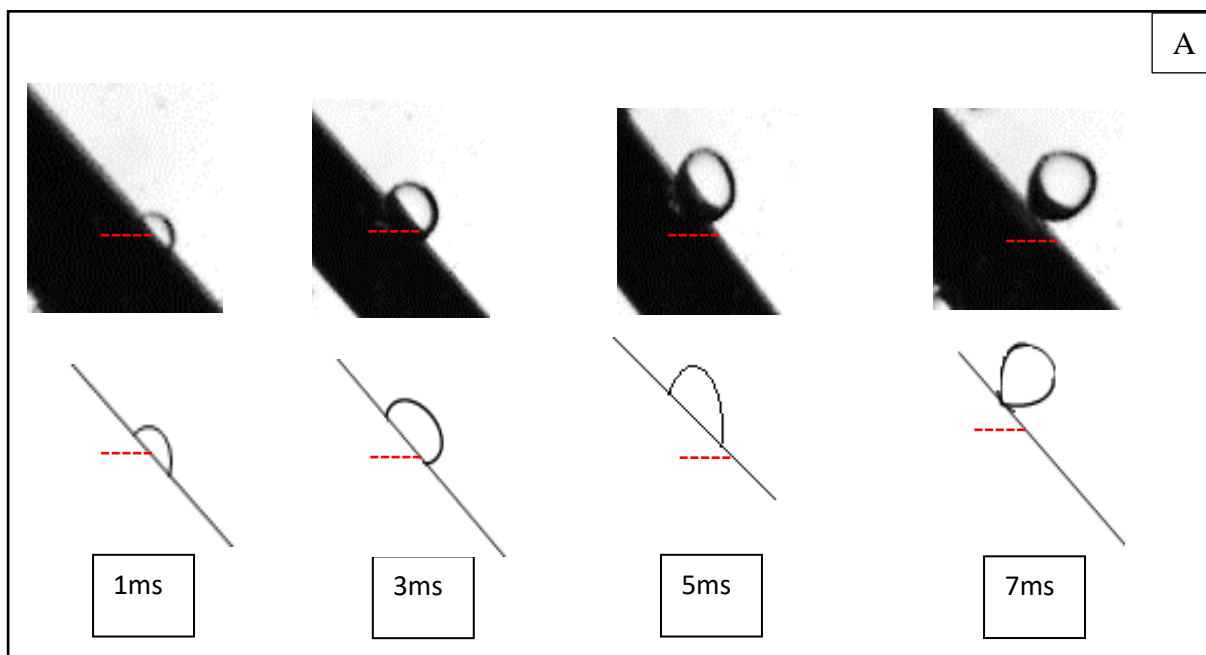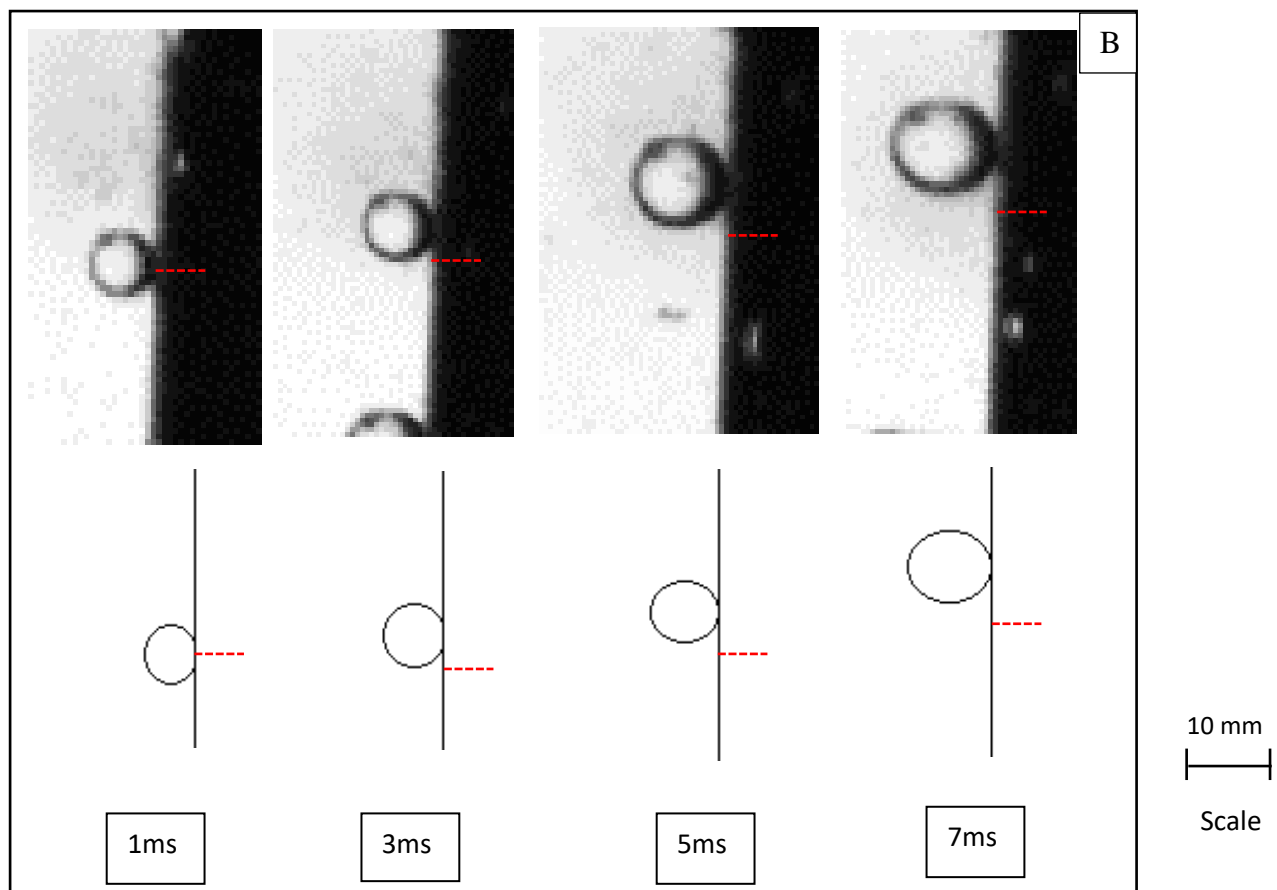
Figure 3.16 The growth of bubble in (A) 45° inclined and (B) vertical heater with sliding

motion (red line marks the nucleation site).

3.3.2.5. Effect of heater geometry

Looking at the effect of the heater shape and size, the data was compared between the rod and the flat ribbon, both of which had similar surface roughness in the range of $1.0 - 1.5 \ \mu m$. As shown in *Figure 3.17*, at a given wall superheat, the bubbles were seen to depart with much larger diameters from the ribbon compared to the rod. The departure frequency, on the other hand, was much lower for the ribbon as shown in *Figure 3.18*. The required heat flux to achieve the superheat values comparable to the rod were quite higher for the ribbon. This can be explained by the availability of larger surface area in the ribbon compared to the rod. This is in accordance with the findings of Nishikawa *et al.* (1965) who found that the growth rate as well as the departure size of the vapor bubbles increased as the size of the heater element increased. Larger bubble departure diameters on the flat ribbon can be attributed to the larger

contact area available resulting in higher evaporation at the bubble base. There is a large wake region formation on the upper side of the ribbon due to boundary layer separation. This leads to the $(T_w - T_l)$ being lower for the ribbon than that for the rod, and hence it takes much longer for the superheated layer to reform after bubble departure due to reduced quenching heat transfer for the ribbon, resulting in a lower bubble frequency.
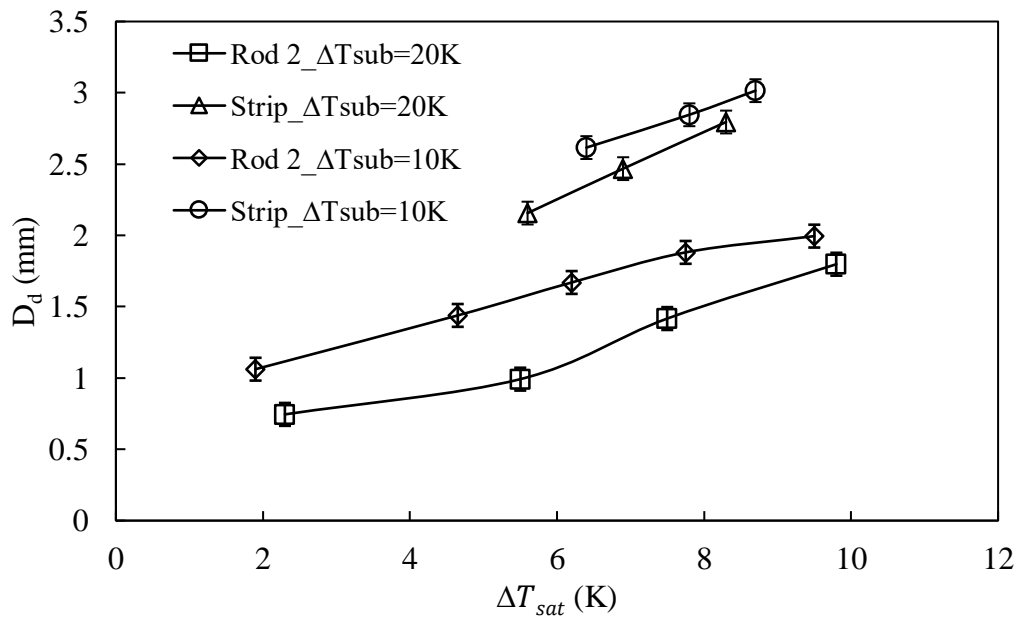
Figure 3.17 Effect of heater geometry on departure diameter at 80 ℃ and 90 ℃ bulk
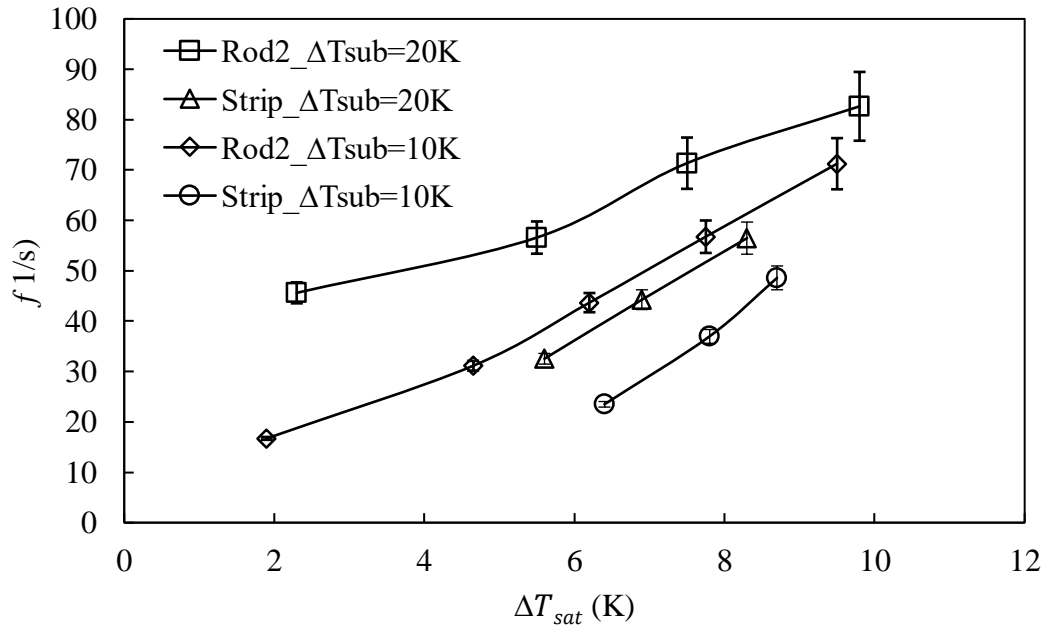
temperature.

Figure 3.18 Effect of heater geometry on departure frequency at 80 ℃ and 90 ℃ bulk temperature.

3.4. Conclusions

A systematic set of visualization experiments were carried out to study vapor bubble departure diameter and frequency under a wide range of operating conditions in the subcooled nucleate pool boiling under atmospheric conditions. The quantitative behaviour of the departure frequency and diameters were studied with the wall heat flux and the degree of subcooling along with the effects of the surface characteristics, heater geometry and the heater inclination angle in the isolated nucleate boiling regime. The main inferences drawn from the study are as follows:

a)   The boiling curves and hence, the heat transfer coefficients are substantially affected by the liquid subcooling, heater inclination angle, and the surface finish. An increase in the degree of liquid subcooling results in a lower wall temperature and a lower heat transfer coefficient. Depending on the method of surface preparation, an increase in average surface roughness could either result in an increased cavity diameter, or an increased

number of cavities with higher depths. Our samples fell in the latter category and an increase in surface roughness meant a higher wall superheat required for nucleation, thereby reducing the heat transfer coefficient. The heater inclination facilitated the bubble sliding, which increases the bubble generated turbulence near the heater wall, resulting in an enhanced heat transfer coefficient.

b) The departure diameter and frequency are increasing functions of the applied heat flux and wall superheat. An increase in the wall heat flux or wall superheat increases the evaporative heat transfer, and reduces the waiting period of the bubbles, resulting in higher bubble departure diameters and frequencies. This implies that $f. D_d$, which dimensionally represents the velocity of bubble rise in the liquid, is also an increasing function of heat flux. This would make sense, as the higher heat flux would cause more intense natural circulation giving the departing bubble a higher thrust. However, most of the widely accepted models assume this product to be a constant of heat flux as shown in *Table 1.6*.

c) The departure diameter decreases with increase in the degree of subcooling due to larger condensation rate on the bubble cap. The bubble departure frequency is an increasing function of the degree of subcooling, but can decrease with subcooling for $\Delta T_{sub} < 5K$.

d)   The departure diameter was found to decrease as the surface roughness of the heater increased, though the frequency was only affected by the surface roughness for low superheats. As the surface roughness increased, the number of nucleation sites increased, and hence, at any given heat flux, the heater energy was being distributed amongst higher number of sites, thereby reducing the amount of energy of any individual site. This resulted in overall smaller bubble departure diameters. However, the heat waves amongst the higher number of sites aid in a faster recuperation of superheated boundary layer after a bubble departure, increasing the bubble departure frequency.

e) The diameter was observed to increase with increase in the heater surface area and the inclination angle of the heater element. While the departure frequency increased with increase in inclination angle, it decreased for a bigger heater surface. The heater inclination enabled the bubble sliding which helped the bubbles to grow while sliding on the heater surface and departing of bigger bubbles. Also, the higher mixing of the fluid due to bubble sliding helps in faster recovery of thermal boundary layer giving a higher departure frequency.

4. Chapter 4

Study of Bubble Departure Characteristics in a Horizontal Rod Bundle under Cross Flow Conditions

4.1. Introduction

When the liquid flows in a direction transverse to the heater surface maintained at temperatures higher than liquid saturation, the condition is referred to as the cross-flow boiling. The passive flow of the coolant from bottom to top inside the rod bundle during accidental conditions in a PHWR due to buoyancy, is an example of the cross flow boiling in a horizontal rod bundle. Some other applications of this kind of over the tube cross flow boiling are flooded evaporators in refrigeration systems, reboilers, tube type steam generators. There are a number of studies measuring heat transfer coefficient in such geometry, but to the best of author's knowledge, no study reports the bubble characteristics in cross flow, on a single heater rod or a rod bundle. There is no understanding of the effect of such flow on the bubble departure characteristics and hence, no models to predict bubble departure diameter and frequency under such conditions exist.

A large number of studies have been carried out to study the effect of tube spacing or pitch to diameter ratio (P/D) on the local and overall heat transfer behaviour in a rod bundle. Some of the studies attribute the enhanced heat transfer to the bubbles sliding along the sides of the upper rods, having been originated on the lower heated rods. Also, the heating of the lower rods increases the liquid velocity adding to the convective heat transfer of the upper rods. However, there has been an overlook of the bubble behaviour on the individual rods under the bundle effect as discussed in Chapter 1. The bubble growth and departure on each rod in the bundle would be affected by the other heated neighbouring rods, which would significantly

contribute to the local heat transfer. In this study, experiments have been carried out to understand the vapor bubble departure characteristics under the effect of the presence of other heated rods in the bundle in addition to the effects of the operating conditions like, applied heat flux, wall superheat and liquid flow velocity.

4.2. Experimental description

4.2.1. Setup

The experimental setup used was same as used by Swain and Das (2017). *Figure 4.1*(A) shows the schematic of the experimental loop used for the present study. The loop mainly consists of a reservoir (1), a centrifugal pump (2), a test vessel (3) and a condenser (4). The test vessel and the reservoir were well insulated and were connected by insulated metal pipes. The reservoir was used to store the distilled water and to collect the condensate from the condenser. The test vessel was a $400\,mm \times 200\,mm \times 180\,mm$ cuboidal channel made up of stainless steel, with toughened glass viewing windows provided on the front and back sides to allow for light and photography. One side of the tank was fitted with a removable $28\,mm$ thick Teflon sheet with threaded holes to hold the heating rods. Hence, the rod system in the test section could be changed as and when required. We used two such sheets, one for a single rod study and another for the study on rod bundle (5×3 staggered) with an equilateral triangular P/D value of 1.95. The centrifugal pump was used to propel the pre-heated distilled water from the reservoir tank into the loop. The safety valve (5) and the control valves [(6), and (7)] were provided to control the flow rate through the test vessel. The water vapor was passed through the shell side of the shell and tube type condenser and then fed back to the reservoir to maintain a closed loop. The reservoir had a valve to release excess steam to maintain atmospheric pressure in the loop. A $1000\,W$ auxiliary cartridge heater (8) was provided in the reservoir to heat up the distilled water to about $90℃$ to avoid any possibility of cavitation in the centrifugal pump. Also, the pump was kept on the ground so that the NPSH of the pump was always

positive. Another cartridge heater was placed at the inlet of the test vessel to heat up the incoming hot liquid to its saturation temperature before it entered the channel. The stainless steel (SS 304) test rods had an average surface roughness of $0.5\ \mu m$ and were $20\ mm$ in diameter and $130\ mm$ in heated length. Each rod was fitted with a cartridge heater placed in the hole drilled centrally along the length of the heating rod. The details of the heater rod and the rod bundle arrangement are shown in *Figure 4.1*(B) and *Figure 4.1*(C) respectively. Each cartridge heater was electrically heated by an AC power supply.
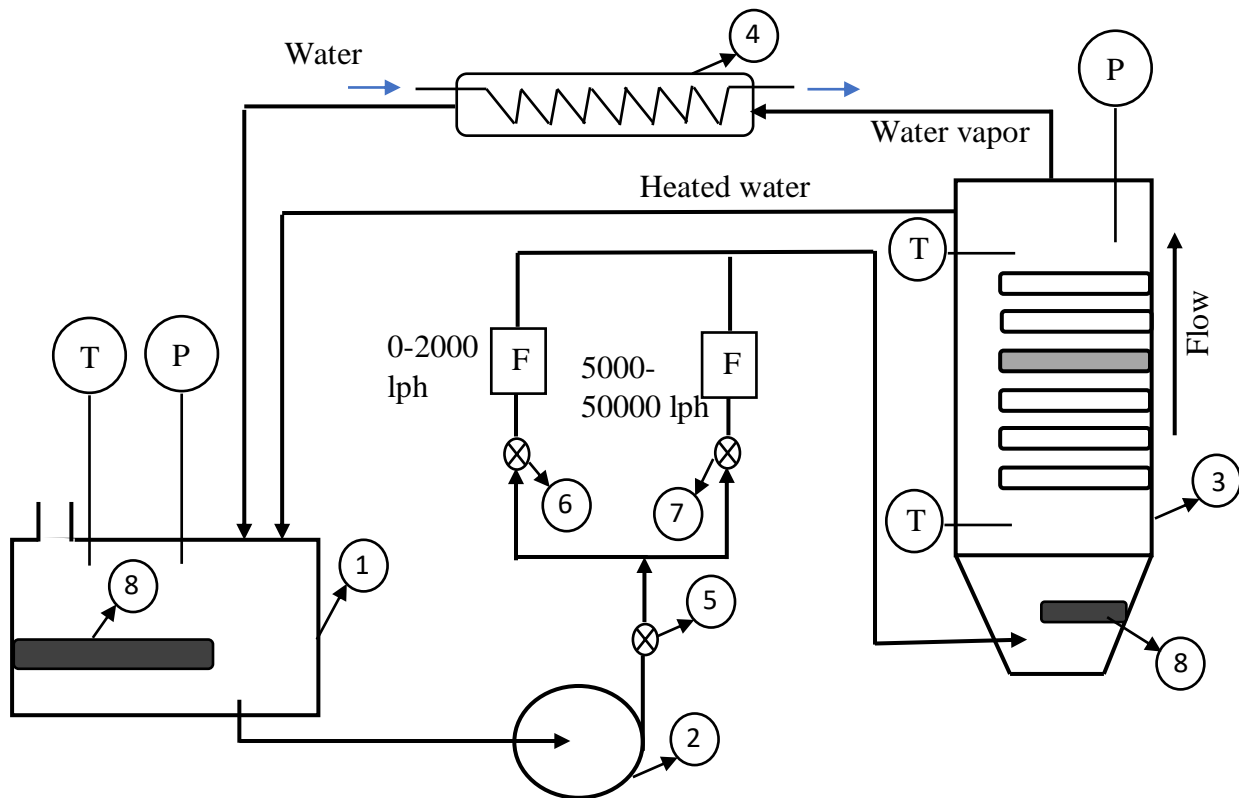
(1) Reservoir   (5) safety valve

(2) centrifugal pump   (6) control valve

(3) test vessel   (7) control valve

(4) condenser   (8) auxiliary cartridge heater

(A)

Rod wall ($D = 20\ mm$)

Thermocouple distance from center ($D = 12\ mm$)

Cartridge Heater ($D = 6\ mm$)

O Holes for thermocouples ($D = 2\ mm$)

Cross sectional view of the heater rod

Holes for thermocouple

Teflon cap

95 mm

Threaded length 30 mm

Heated length 130 mm

Hole for the heater
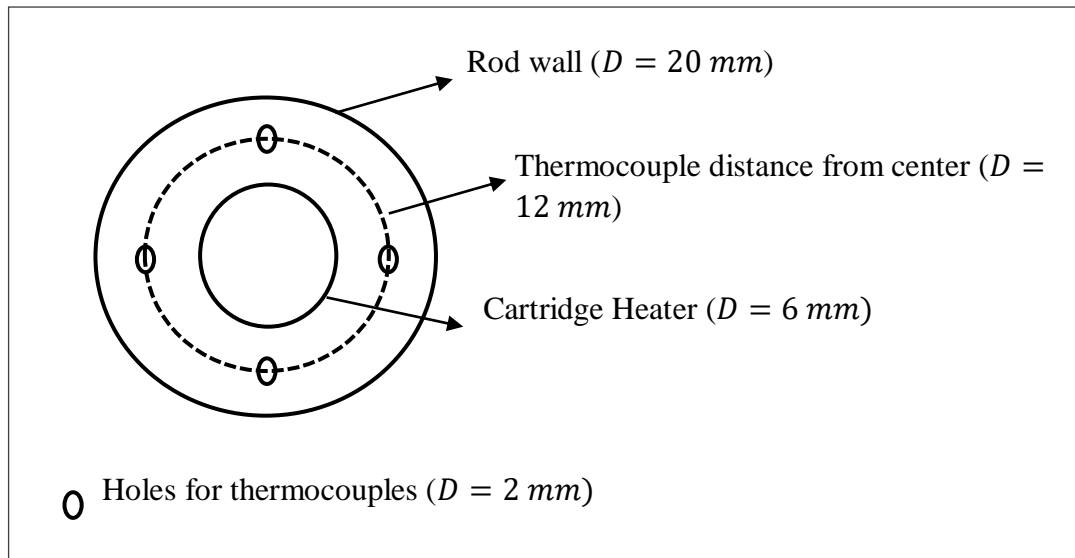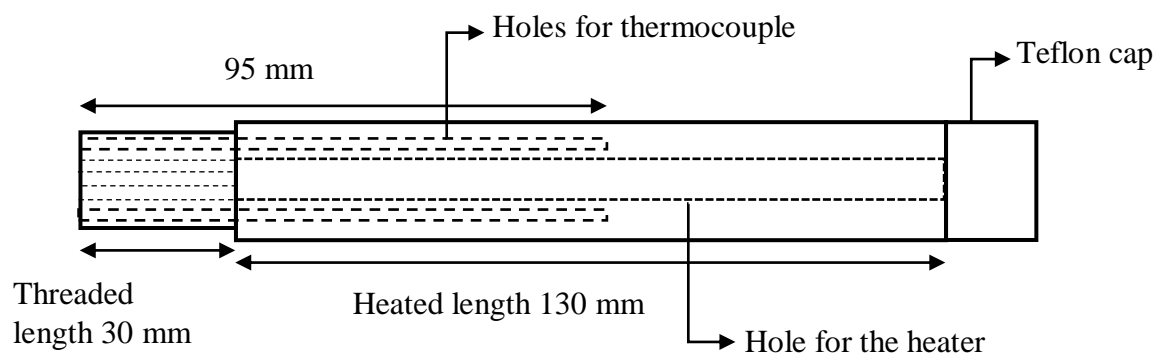
Axial view of the heater rod

(B)
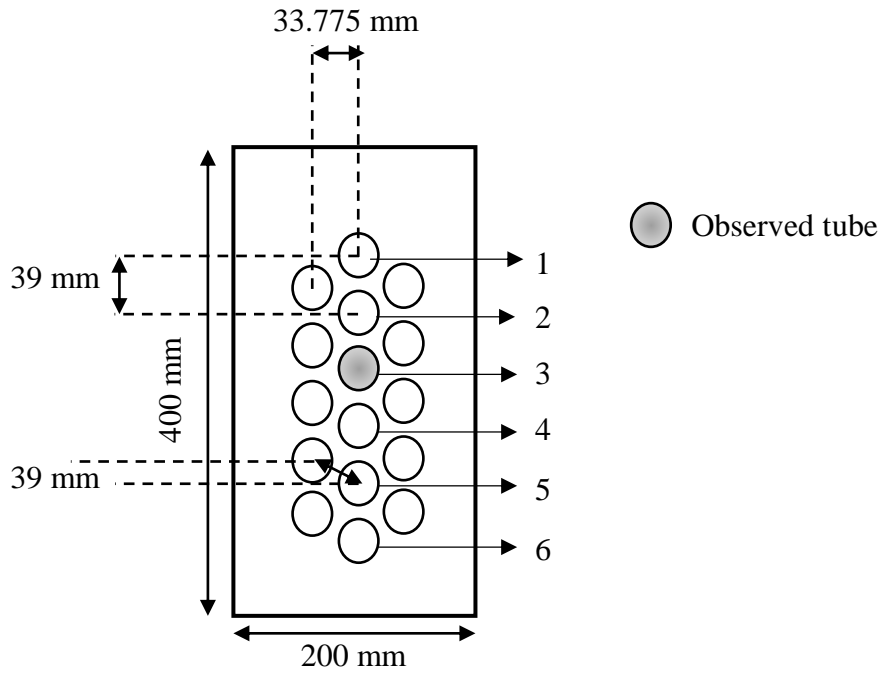
Figure 4.1 (A) Schematic of the experimental setup. (B) Details of the heater rod (Swain and Das (2017)). (C) rod bundle arrangement.

The setup was also equipped with various measuring instruments like rotameters for flow rate measurement, Burdon pressure gauges for measuring pressure at the reservoir and test vessel, thermocouples for measuring liquid and the rod surface temperatures, and a VAW (Voltage, Ampere and Wattage) meter for measuring power input to the heaters in the rod. The average heat flux to the heating rod was obtained from the product of the voltage and the current applied to it divided by the effective heated surface area. Four 2 mm T-type thermocouples were inserted in four holes made in the wall thickness along the circumference, on the top, bottom and two sides of the rod. The average of the four values was then taken as the average wall temperature (after correcting for the loss in the wall thickness between thermocouple and rod surface (refer Appendix B)). Also, similar thermocouples were placed in the reservoir near the inlet and the outlet, to measure the bulk liquid temperature. The temperatures were recorded using a NI digital data acquisition system. The bubble dynamics was recorded using the high-

speed camera at a speed of $1600\ fps$ (time resolution of $617\ \mu s$) at a spatial resolution of 640×640 pixels. A zooming lens of $20 - 100\ mm$ focal length and a $1000\ W$ halogen light source was used for the camera as detailed in chapter 2 earlier.

4.2.2. Procedure

Distilled water in the reservoir was heated using the auxiliary heaters to bring up the temperature to saturation. The heated water was then allowed to circulate in the loop at desired flow rate for about $30\ min$ before the heater elements in the test section were switched on. The system was allowed to boil for about two hours to let any trapped gases escape. The auxiliary heaters were switched off and the power to the heater elements was then increased stepwise. The system was allowed to achieve steady state at each power level, which took about $15 - 20\ min$, before the bubble behaviour was observed for the natural cavities existing on the surface. The experiments were carried out for the following operating conditions: inlet fluid temperature $=$ saturated ($373.15\ K$); applied heat flux $q'' = 8 - 28\ kW/m^2$ and wall superheat $\Delta T_{sat} = 7 - 22\ K$. The inlet volumetric flow rates Q used were from $8 - 20\ m^3/hr$. The liquid mass flux calculated from the inlet velocity for the single rod was in the range of $G = 59 - 147.5\ kg/m^2 s$. The mass flux for the rod bundle has been calculated using the maximum velocity (U_{max}) which occurs at the minimum flow area (A_c) as suggested in the literature for tube banks (Khan *et al.* (2006), Kumar *et al.* (2015), (2016)), and was in the range of $120 - 303.5\ kg/m^2 s$. Based on the bundle geometry used, following test cases (*Table 4.1*) were considered:

Case 1: A single rod was heated,
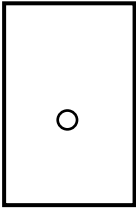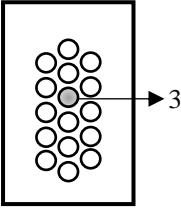
Case 2: Only a single rod (row 3; central column) was heated in the rod bundle,
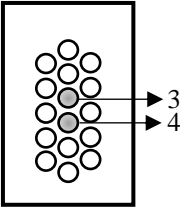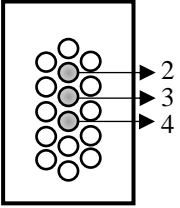
Case 3: Two rods (row 3 and 4; central column) were heated, while the bubble characteristics were measured on the upper rod (row 3), and

Case 4: Three rods (row 2, 3 and 4; central column) were heated, and the bubble characteristics were observed on the middle rod (row 3).

Here the row number was counted from the top as shown in *Figure 4.1*(C). High speed recordings of the bubble dynamics lasting for about 3 seconds each were made to estimate the departure size and frequencies of the vapor bubbles under various conditions. Recordings for several conditions were repeated to confirm the reproducibility of the results. The image frames from the high-speed recordings were manually analysed using the ImageJ software to obtain the values of departure diameters and frequencies as explained in chapter 2. Since the temperature values fluctuated in each frame, average values of the temperatures were used for the analysis for all conditions.

Table 4.1 Experimental matrix

Case No.	Geometry	Graphic representation	Heat flux q'' (kW/m^2)	Vol. flow rate Q (m^3/hr)	Mass flux G ($kg/m^2 s$)
1	Single rod in the channel		$8.13 - 27.72$	8	59.14
				11	81.31
				15	110.88
				20	147.84
2	Single rod in bundle heated		$8.13 - 27.72$	8	121.40
				11	166.93
				15	227.64
				20	303.51

Case No.	Geometry	Graphic representation	Heat flux q'' (kW/m^2)	Vol. flow rate Q (m^3/hr)	Mass flux G (kg/m^2s)
3	Two rods in the bundle heated		$8.13 - 27.72$	8	121.40
				11	166.93
				15	227.64
				20	303.51
4	Three rods in the bundle heated		$8.13 - 27.72$	8	121.40
				11	166.93
				15	227.64
				20	303.51

The measurement of voltage V_o and current I involve the least count errors of the $\pm 0.1\ V$ and $\pm 0.1\ A$ respectively. The error in temperature gauging was $\pm 0.75\%$ of the measured value up to $400\ ℃$. The flow meters gave the volumetric flow rate with a least count of $500\ lph$, which led to an error of about $3.7\ kg/m^2 s$ in the calculation of mass flux. The bubble diameters could be measured with an accuracy of $\pm 1\ pixel$ which comes to about 5% for a bubble diameter of about $2\ mm$ in addition to 0.1% error of digitalization. The error in time measurement comes from the speed of the camera, and is of nearly $617\ \mu s$. The frequency has been calculated as per equation (2.5) and gave a maximum error of 9%. Since, the test vessel and all the pipes were well insulated, we assume negligible heat loss from the system. Some other errors like change in refractive index of water with temperature, error due to camera zoom etc. might have occurred which cannot be quantified in this work.

4.3. Results and Discussion

4.3.1. Heat Transfer Coefficient

The boiling curves and heat transfer coefficients for the single rod in the channel (Case 1) are presented in *Figure 4.2*. We observe that the heat transfer coefficient increases with heat flux as expected. The heat transfer coefficient increases for cross flow conditions compared to pool boiling due to a marginal decrease in wall superheat with the enhanced heat transfer with forced convection compared to the natural convection in pool boiling. However, there was no significant effect of the increase of flow rate in the observed range of heat flux ($8 - 27\ kW/m^2$) which is considered in the intermediate to high range of heat flux for such geometries. These results are in agreement with the literature (Hwang and Yao (1986), Jensen and Hsu (1988), Gupta (2005)) where the increase in mass flux velocity does not have effect on the heat transfer at sufficiently high heat flux values, because of the nucleate boiling being the dominant mechanism at high heat fluxes while the major influence of the enhanced mass flux is to enhance the convection heat transfer. Further, the heat transfer coefficient behaviour

with heat and mass flux was found to be similar for the single heated rod in the bundle (Case 2). However, the heat transfer coefficient for Case 2 was systematically higher than that for Case 1 as shown in *Figure 4.3*. As explained by Hwang and Yao (1986), the increase in the heat transfer is due to the combination of two effects – (1) the wake from the lower rod, causes the vapor bubbles growing on the lower part of the upper heated rod to coalesce and circulate in that region increasing the turbulence, and (2) the higher effective velocity experienced by the upper heated rod in Case 2 even for the same inlet mass flow rate.
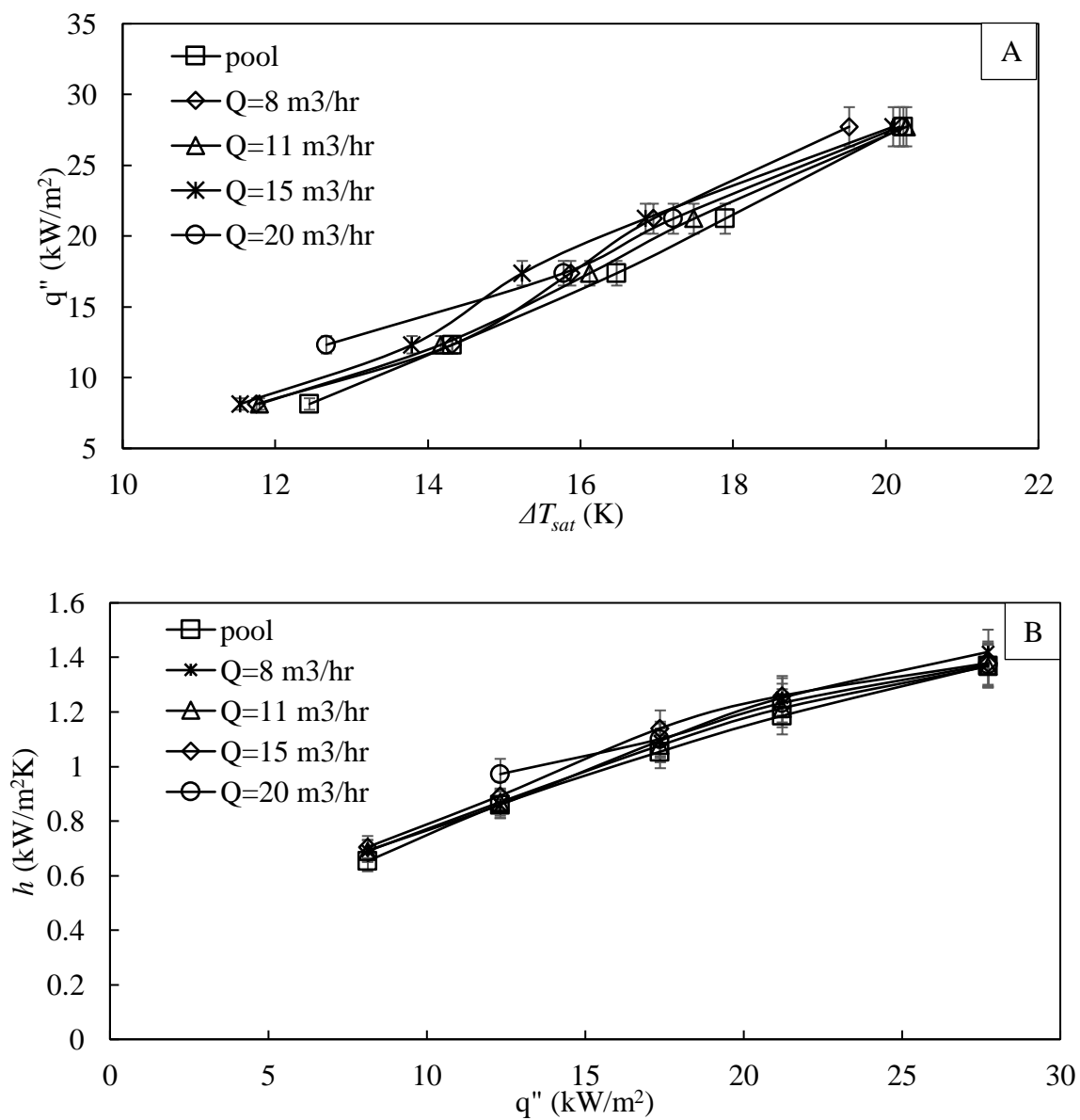
Figure 4.2 Effect of mass flux - (A) boiling curves and, (B) heat transfer coefficient for a single rod in the channel.
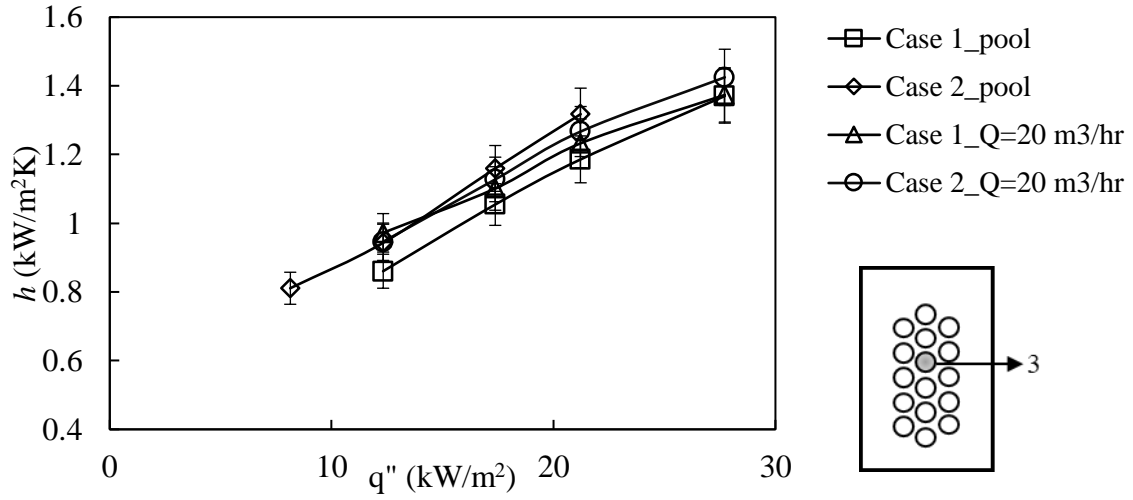
Figure 4.3 Comparison of heat transfer coefficient for Case 1 and 2 for inlet mass flow rate of

0 and 20 m^3/hr.

Further comparing the boiling curves and heat transfer coefficients for Cases 2, 3 and 4, the heat transfer is found to increase when the rod (rod 4) below the observed rod (rod 3) is heated (Case 3), but the heating of the rod (rod 2) above the observed rod (Case 4) has no effect on the local heat transfer coefficient as shown in *Figure 4.4*, for the inlet mass flow rate of 8 m^3/hr (59.14 kg/m^2s for single rod in the channel, and 121.4 kg/m^2s for rod bundle cases). When the rod no. 4 below the observed rod (rod no. 3) was heated, the bubbles rising from the lower rod grow and slide along the sides of the observed rod reducing its average wall temperature. This in addition to the two factors discussed above for the non-heated bundle cause the increase in heat transfer from Case 2 to 3. However, when the three rods were heated (Case 4), the observed rod (rod no. 3) in the middle had the heat transfer almost identical to that it had in the Case 3 scenario. This is because the wake or vapor bubbles produced on rod no. 2 would not travel downward and hence, cannot influence the heat transfer at rod below it. The heat transfer in the experiments were calculated as

$$h = \frac{q^{"}}{T_w - T_l} = \frac{q^{"}}{T_w - T_{sat}} \tag{4.1}$$
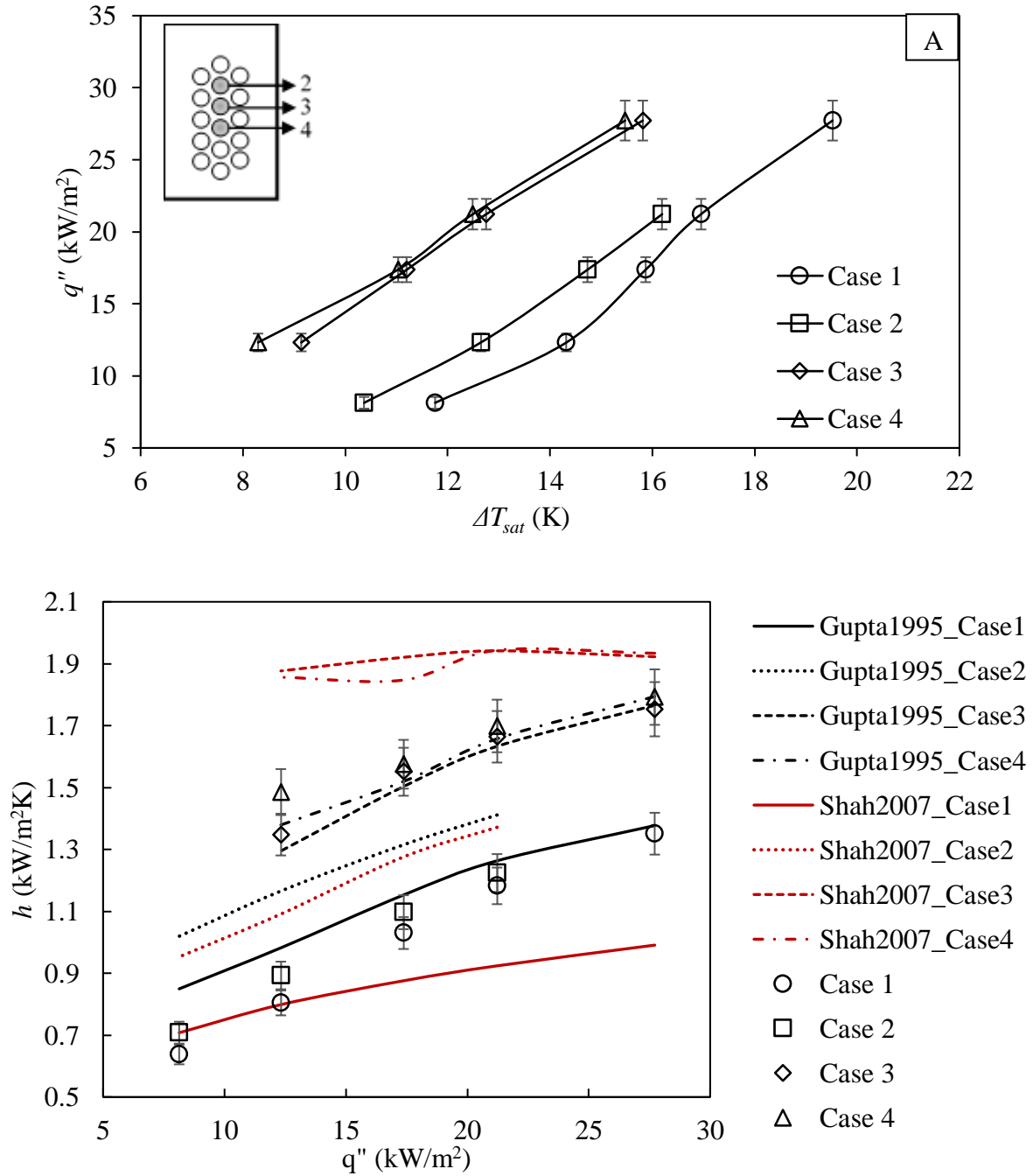
Figure 4.4 (A) Boiling curves and (B) heat transfer coefficient for the rod 3 under different

cases for $Q = 8 \ m^3/hr$.

Figure 4.4(B) also shows the experimental heat transfer compared with that predicted

by the correlation proposed by Gupta *et al.* (1995) and Shah (2007) for calculating heat transfer

coefficient of individual rods in a bundle. It can be seen that the presently obtained

experimental results are within the predicted range of conditions. The Gupta *et al.* (1995)

correlation predictions are closer to the experimental data, with the exception for the Case 2 data, where it is overpredicts. Shah (2007) model severely over predicts the data for all cases, except Case 1 where it under-predicts the data, possibly because it was not validated for a single rod in a channel. The two models have been described in *Table 1.7* in chapter 1. Gupta *et al.* (1995) used an empirical correlation for pool boiling heat transfer coefficient based on their data, which was not generally applicable, hence, the model developed by Hameed et al. (2013) has been used here.

$$h_{mic} = 4944.28 \left(\frac{k_l}{D}\right) \left(\frac{\Delta p}{\rho_l}\right)^{-0.65} Pe^{0.82} \left(\frac{\rho_v}{\rho_l}\right)^{1.1} Pr^{-0.47} \tag{4.2}$$

In the cases 1 and 2, the heat transfer coefficient increases for cross flow conditions compared to pool boiling due to a marginal decrease in wall superheat (~1- 4%) with the enhanced heat transfer with forced convection compared to the natural convection in pool boiling. But in the Case3 and 4, with more rods heated, the increase in velocity suppresses nucleate activity due to lower contact time of the rising fluid with the heated rods. Hence, the wall temperatures are seen to increase (~1-5%) when we switch from pool to flow boiling, and with increase in velocity for a given case. This results in a corresponding 1-5% decrease in the heat transfer coefficient as shown in *Figure 4.5*.
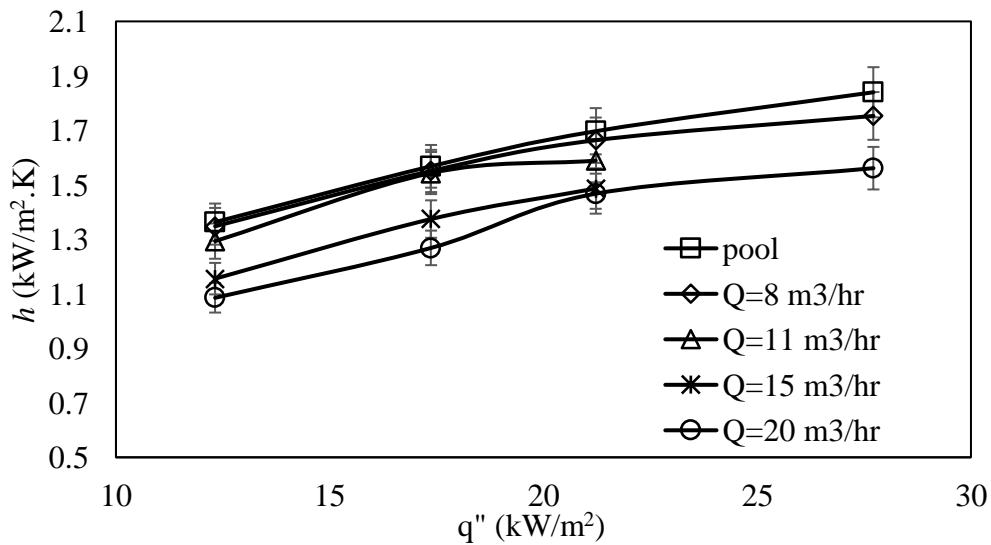
Figure 4.5 Heat transfer coefficient for Case 3.

4.3.2. Single rod in the channel

The departure characteristics of water vapor bubbles were first observed for a single rod in the channel and have been shown in *Figure 4.6*. The departure diameter and departure frequency of the bubbles increased with an increase in the applied heat flux or the wall superheat as expected. An increase in the heat flux or wall superheat would increase the evaporative heat transfer, resulting in a larger bubble diameter. Also, it was observed that, for any given active nucleation site, the growth period of a bubble slowly increased as the applied power increased, but it was accompanied by a sharp fall in the waiting period between the two consecutive bubbles. The mean values of departure diameter and frequency measured for all the cases are given in *Table 4.2*. The standard deviation and 95% confidence intervals were calculated for each case, and are given in *Table 4.3* for a representative case. The departure diameter was also observed to decrease with an increase in mass flux or the flow velocity. This is because the increase in flow velocity would result in the lower contact time between the rising liquid and the heater rod, which would result in thinner superheated layer reducing the evaporative heat transfer and hence, the bubble sizes. Also, it was observed that the bubble departure frequency decreased with an increase in flow rate. This can also be explained as the increase in the waiting time to recuperate the superheated boundary layer because of the lower contact time between the liquid and the heated rods, with an increase in flow velocity.
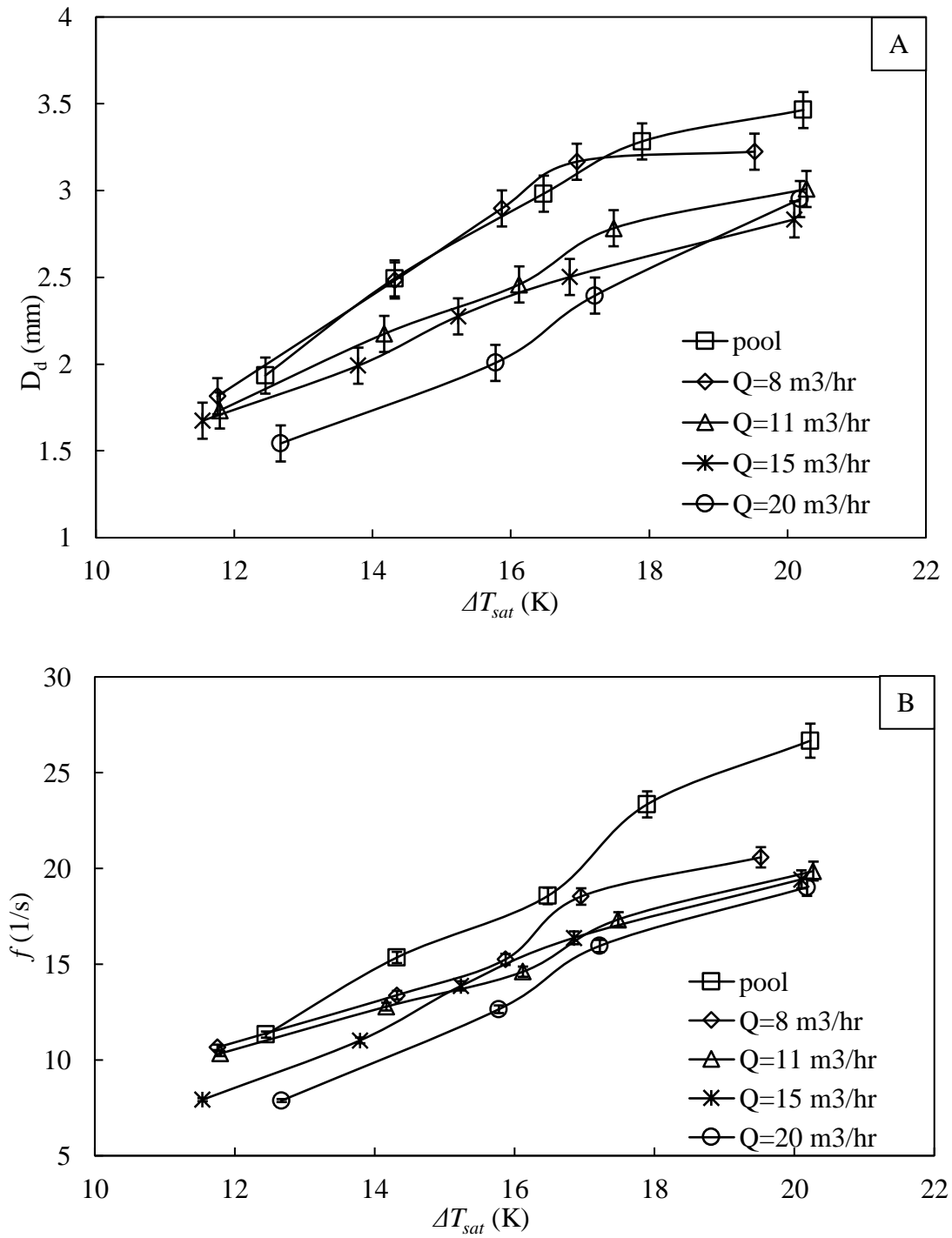
Figure 4.6 (A) Departure diameter and (B) departure frequency for a single rod in the

channel.

Table 4.2 Bubble departure diameter and frequency measurements for cross flow boiling (additional details are given in *Table 4.1*).

Case	Heat flux $q"$ (kW/m^2)	Wall superheat ΔT_{sat} (K)	Vol. Flow rate Q (m^3/hr)	Departure diameter D_d (mm)	Departure frequency f $(1/s)$
Case 1	27.719	20.2	0 (pool)	3.464	26.67
	21.222	17.9	0 (pool)	3.283	23.344
	17.373	16.5	0 (pool)	2.982	18.563
	12.319	14.3	0 (pool)	2.494	15.351
	8.133	12.4	0 (pool)	1.934	11.325
Case 1	27.719	19.5	8	3.224	20.581
	21.222	16.9	8	3.166	18.534
	17.373	15.9	8	2.897	15.251
	12.319	14.3	8	2.482	13.384
	8.133	11.8	8	1.815	10.658
Case 1	27.719	20.3	11	3.009	19.862
	21.222	17.5	11	2.783	17.339
	17.373	16.1	11	2.459	14.608

Case	Heat flux q'' (kW/m^2)	Wall superheat ΔT_{sat} (K)	Vol. Flow rate Q (m^3/hr)	Departure diameter D_d (mm)	Departure frequency f $(1/s)$
	12.319	14.2	11	2.174	12.786
	8.133	11.8	11	1.733	10.335
Case 1	27.719	20.1	15	2.834	19.428
	21.222	16.8	15	2.502	16.377
	17.373	15.2	15	2.275	13.868
	12.319	13.8	15	1.991	11.023
	8.133	11.5	15	1.674	7.926
Case 1	27.719	20.2	20	2.951	19.019
	21.222	17.2	20	2.395	15.951
	17.373	15.8	20	2.007	12.648
	12.319	12.7	20	1.543	7.881
Case 2	21.222	16.1	0 (pool)	3.069	85.106
	17.373	14.9	0 (pool)	2.657	63.97
	12.319	13.1	0 (pool)	2.391	53.943

Case	Heat flux $q"$ (kW/m^2)	Wall superheat ΔT_{sat} (K)	Vol. Flow rate Q (m^3/hr)	Departure diameter D_d (mm)	Departure frequency f $(1/s)$
	8.133	10.0	0 (pool)	1.718	21.192
Case 2	21.222	16.2	8	3.041	55.216
	17.373	14.7	8	2.538	44.83
	12.319	12.6	8	2.321	35.96
	8.133	10.4	8	1.702	17.921
Case 2	24.146	17.8	11	2.527	49.506
	17.373	14.4	11	2.239	40.986
	12.319	11.2	11	1.736	25.702
	8.133	10.5	11	1.607	16.657
Case 2	21.222	16.6	15	2.35	43.161
	17.373	15.2	15	2.11	39.587
	12.319	12.8	15	1.834	23.243
	8.133	10.8	15	1.545	14.644
Case 2	27.719	19.4	20	2.824	53.421

Case	Heat flux $q"$ (kW/m^2)	Wall superheat ΔT_{sat} (K)	Vol. Flow rate Q (m^3/hr)	Departure diameter D_d (mm)	Departure frequency f ($1/s$)
	21.222	16.7	20	2.267	41.979
	17.373	15.4	20	2.071	36.458
	12.319	13.0	20	1.755	19.716
Case 3	27.719	15.1	0 (pool)	3.436	46.434
	21.222	12.5	0 (pool)	3.154	43.794
	17.373	11.1	0 (pool)	2.843	40.171
	12.319	9.0	0 (pool)	2.512	36.569
Case 3	27.719	15.8	8	3.145	46.667
	21.222	12.8	8	2.835	41.414
	17.373	11.2	8	2.359	35.671
	12.319	9.1	8	1.951	26.879
Case 3	21.222	13.4	11	2.549	40.626
	17.373	11.2	11	2.235	31.026
	12.319	9.5	11	1.942	26.194

Case	Heat flux q'' (kW/m^2)	Wall superheat ΔT_{sat} (K)	Vol. Flow rate Q (m^3/hr)	Departure diameter D_d (mm)	Departure frequency f (1/s)
Case 3	21.222	14.3	15	2.489	38.415
	17.373	12.6	15	2.301	28.965
	12.319	10.6	15	1.914	23.461
Case 3	27.719	17.8	20	2.647	43.864
	21.222	14.4	20	2.414	34.044
	17.373	13.7	20	2.205	26.576
	12.319	11.3	20	1.903	21.388
Case 4	27.719	14.9	0 (pool)	4.508	72.752
	21.222	12.5	0 (pool)	4.411	57.705
	17.373	11.5	0 (pool)	3.775	49.115
	12.319	9.1	0 (pool)	3.217	47.233
Case 4	27.719	15.5	8	4.298	59.706
	21.222	12.5	8	3.922	47.736
	17.373	11.0	8	3.367	42.499

Case	Heat flux q'' (kW/m^2)	Wall superheat ΔT_{sat} (K)	Vol. Flow rate Q (m^3/hr)	Departure diameter D_d (mm)	Departure frequency f $(1/s)$
	12.319	8.3	8	2.916	30.595
Case 4	27.719	16.0	11	4.081	56.994
	21.222	12.0	11	3.261	46.203
	17.373	11.6	11	2.962	41.402
Case 4	27.719	15.5	15	3.661	48.427
	21.222	12.7	15	3.248	40.888
	17.373	11.8	15	2.884	35.378
	12.319	9.7	15	2.572	26.296
Case 4	27.719	17.9	20	3.588	45.566
	21.222	14.6	20	3.219	37.625
	17.373	13.1	20	2.897	30.589
	12.319	11.6	20	2.558	24.173

Table 4.3 Departure diameter, growth time, waiting time and frequency for a typical nucleation site.

Heat flux	D_d (mm)			f (1/s)		
q'' (kW/m²)	mean	Std. deviation	95% confidence interval	mean	Std. deviation	95% confidence interval
8.13	1.934	0.031	0.077	11.2	0.195	0.109
12.32	2.365	0.067	0.062	21.8	0.272	0.625
17.37	2.721	0.272	0.178	26.8	0.243	0.613
21.22	3.201	0.271	0.109	30.3	0.237	0.703
27.72	3.610	0.278	0.115	51.5	0.477	0.705

4.3.3. Rod Bundle

The departure diameter and departure frequency of the bubbles for each of the bundle cases show similar behaviour with heat flux, wall superheat and mass flux as for the single rod. The departure diameters and frequencies measured for Case 3 are shown in *Figure 4.7* and *Figure 4.8* respectively, as an example. The comparison of bubble departure diameter in the four cases is presented in *Figure 4.9*. The departure size of the bubbles for a single heated rod in the bundle (case 2) is almost identical to that for an isolated rod (case 1). It was observed that the departure size of the bubbles on the given rod, kept increasing with an increase in the number of its neighbouring rods being heated. So, the departure diameter for case 4 was higher than that for case 3, which in turn was larger than that for case 2. It is known from the literature (Gupta *et al.* (1995), Kumar *et al.* (2002), Gupta (2005)) that a lower heated rod enhances the heat transfer around the heated rod just above it. This is because of the turbulence created by the bubbles rising from the lower rod, and these bubbles sliding along the sides of the upper rod. Further, with the lower rod (rod 4) heated, although the wall temperature of the above rod (rod 3) decreased a little, but the liquid coming in contact with the rod 3 would be hotter than the water at the inlet, helping the bubble growth around its base. This would lead to larger bubble sizes for the case 3 in comparison to case 1 and 2. For the case 4, our observed rod (rod 3) lies in the middle and we noted that its wall temperatures in case 4 is nearly equal to that of it in case 3. Usually, a bubble's growth takes place due to the evaporation at the base within the superheated layer. The bubble cap either undergoes condensation in the subcooled bulk liquid or is unaffected in the saturated bulk liquid. But, when the rod above (rod 2) the observed rod is heated, the bulk liquid temperature in the space between rods 2 and 3 would also be superheated. This superheated liquid could augment the evaporation at the bubble cap, resulting in bubble sizes bigger than those in Case 3. However, since the bulk temperatures within the bundle could not be measured, this postulate cannot be verified.

Departure diameter and frequency both decrease when we go from pool boiling to cross flow boiling in each of the four cases, keeping their behaviour with heat flux and wall superheat the same.
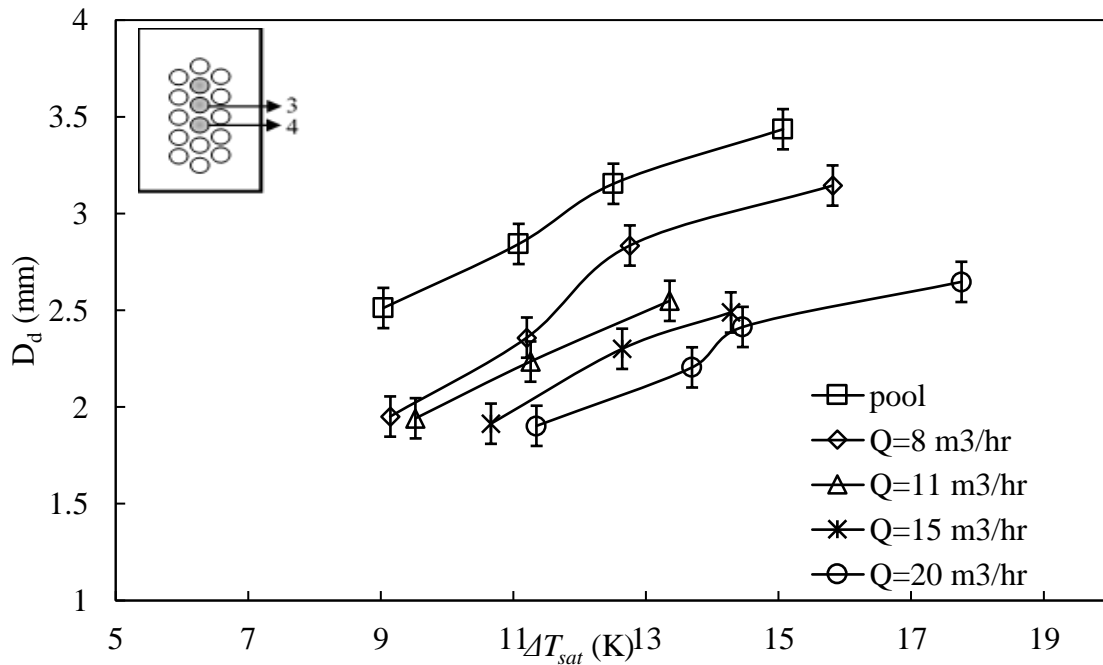
Figure 4.7 Effect of wall superheat and mass flux on departure diameter (Case 3).
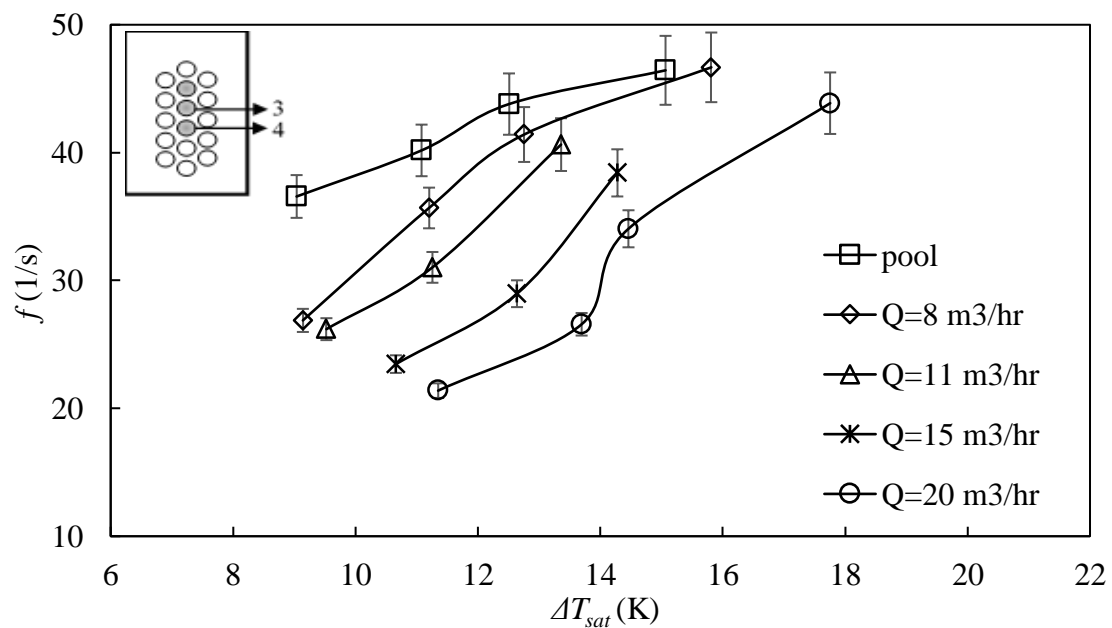
Figure 4.8 Effect of wall superheat and mass flux on bubble departure frequency (Case 3).
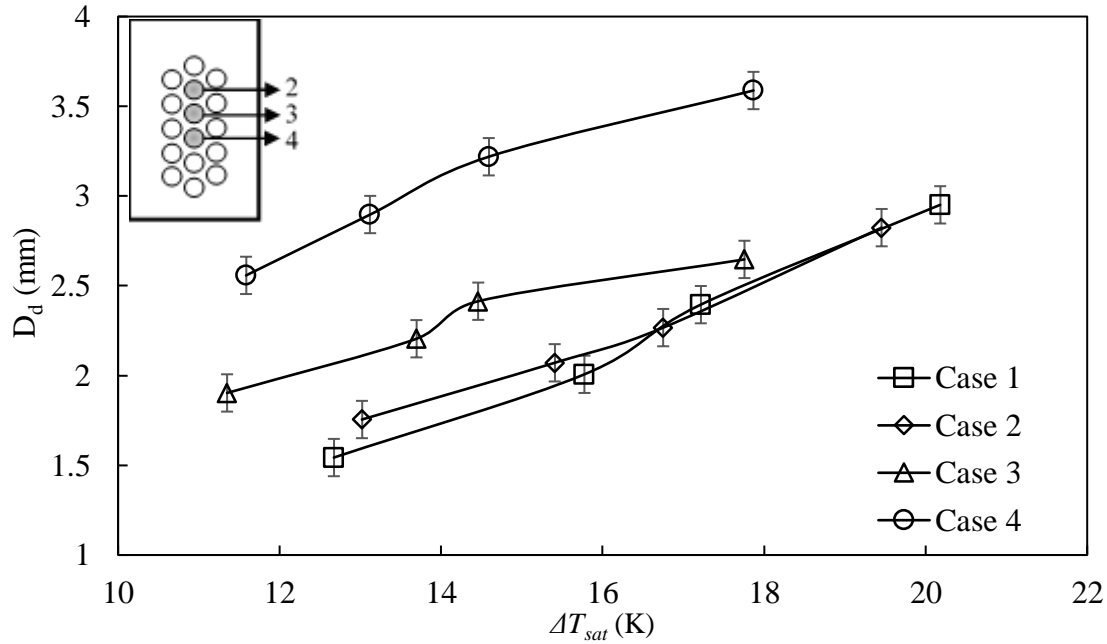
Figure 4.9 Effect of neighbouring heated rods on bubble departure diameter.

The behaviour of the departure frequency for the different cases has been shown in *Figure 4.10*. It was observed that the frequency was substantially higher for the bundle cases, with values in the range of $10 - 20 \; s^{-1}$ for the single rod and $20 - 60 \; s^{-1}$ for the single rod in the bundle. So, it can be said that one of the reasons for the enhancement in the heat transfer for case 2 over case 1 was the higher bubble departure frequency. Further, the departure frequency for cases 3 and 4 were observed to be successively higher than those for case 2. This increase in frequency could be explained as follows: the bubble cycle comprises of the bubble growth time and the waiting time (duration between a bubble departure and the next bubble nucleation at the same site). The growth time is much less than the waiting period, and hence, this waiting period required for the re-establishment of the thermal boundary layer, after the bubble departure largely governs the bubble departure frequency. Ali and Judd (1981) showed that, for near saturated boiling, the recuperation of the thermal boundary layer takes place by the process of transient conduction. For the single rod in the channel, the liquid rushing in to replace the damaged boundary layer is the saturated liquid near the heater. However, in the bundle, the convective plume rising from the heated rod is obstructed by the rod above it, and

159

hence, the local liquid temperature around the heated rod (rod 3), in this case would be a bit higher than average bulk temperature. Hence, this hotter liquid replacing the damaged boundary layer would hasten the recuperation, increasing the departure frequency significantly. Similarly, for the cases 3 and 4, the local bulk liquid temperature would be successively somewhat higher, further reducing the waiting period and driving the departure frequency higher. Also, it was noted that the difference between the values of frequency for the three cases decreased with an increase in liquid flow rate, which is expected as the higher liquid velocity would reduce the frequency in each case and the hotter liquid recuperating the boundary layer in the bundle would increase the frequency, thereby bringing the curves closer together.
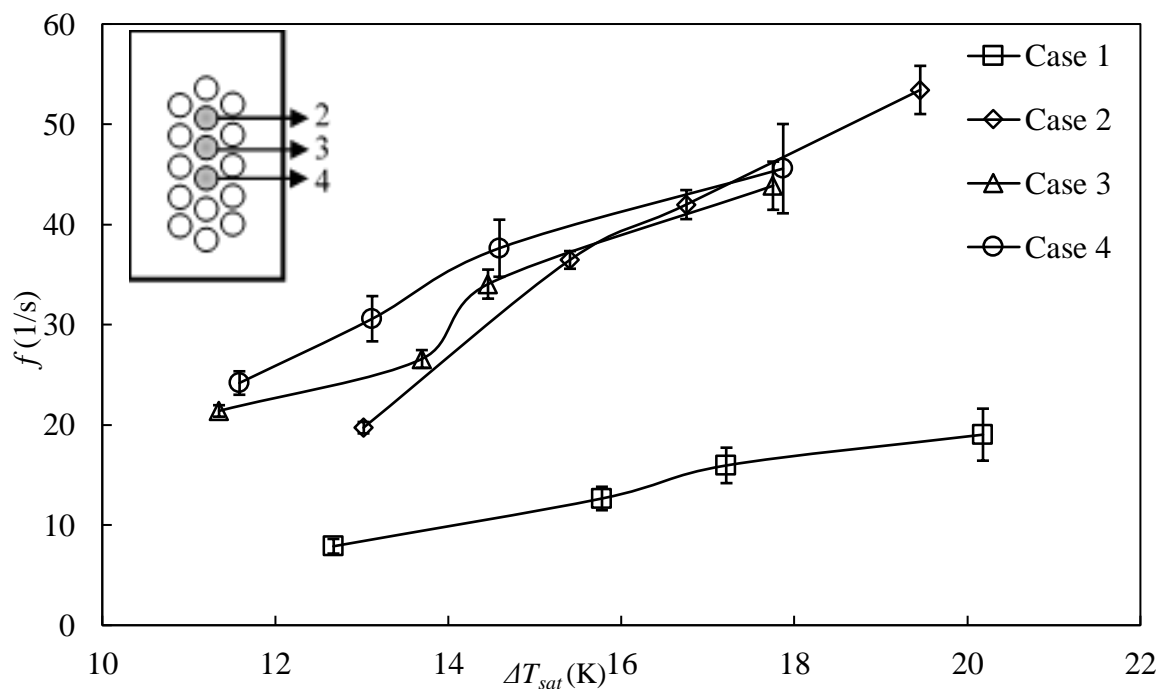
Figure 4.10 Effect of neighbouring heated rods on bubble departure frequency.

4.4. Conclusions

The bubble departure characteristics were experimentally studied on a single rod in a channel (Case 1) and in a rod bundle with different number of heated rods, i.e. only rod no. 3 was heated (Case 2), rod no. 3 and 4 were heated and observations were made on rod 3 (Case

3), and rod 2, 3 and 4 were heated, while observations were made on rod 3 (Case 4). The study enabled us to understand the effect of neighbouring heated rods on the bubble departure characteristics in a rod bundle, and to collect bubble departure diameter and frequency data under such conditions, which does not exist in the open literature to the best author's knowledge. The following conclusions were drawn from the experiments:

a) The heat transfer coefficient for the single rod in the channel was the lowest and increased as the number of heated rods in the bundle increased. The heat transfer coefficient increased up to 20% from case 1 to case 2, the heat transfer coefficient of rod no. 3 increased about 40-60% from case 2 to case 3 and 4. The vapor rising from the lower heated rod increased the turbulence around the observed rod and bubble sliding decreased the average wall temperature leading to an enhanced heat transfer coefficient in case 3 over case 2. However, the heating of a rod above the observed tube did not have any effect on the observed heat transfer.

b) The departure diameter and frequency both were observed to increase with an increase in applied heat flux and wall superheat, but decreased with an increase in inlet flow rate. An increase in heat flux, causing the increased wall temperature results in the enhanced evaporative heat transfer giving larger bubble sizes, while an increased heat flux, results in a faster recuperation of the thermal boundary layer after a bubble departure, reducing the waiting period and hence, increasing the departure frequency. On the other hand, an increase in mass velocity causes lower contact time between the rising fluid and the heater rods, which results in thinner superheated layer and hence, smaller departure diameters, and longer waiting periods for reformation of boundary layer, and thus, lower departure frequencies.

c) The departure diameter of vapor bubbles from a single rod in a bundle were almost equal to that from an isolated single rod, but increased with increase in the number of heated

rods in its neighbourhood. The additional heated rods in the bundle provided with a higher temperature fluid in the ambience of the observed rod, facilitating the growth of the bubble both at the base and the cap with an effectively thicker superheated layer on the heated rods.

d) The departure frequency from a single rod in a bundle was significantly higher compared to that from an isolated single rod. The frequency further increased with the number of heated rods in the bundle. The bundle geometry and additionally heated rods ensure that the liquid in the vicinity of the heated rods, that replaces the departed bubble is sat a higher temperature compared to that in a single rod in a channel (case 1), resulting in a lower waiting period, and hence, a significantly higher departure frequency.

5. Chapter 5

Semi-Empirical Model Development for Subcooled Boiling in Horizontal Rods and Rod Bundles

5.1. Introduction

In Chapter 1, we listed the models for bubble departure diameter and frequency in the pool boiling conditions from the open literature. Most of these correlations have been developed with saturated boiling data, hence, predicting subcooled boiling data using these correlations produces results with significant errors. Also, these correlations do not take into account the dependence of departure characteristics on heater surface characteristics, inclination angle and geometry. Further, there are no models for predicting the bubble departure diameter or frequency under cross flow boiling conditions on a single rod or rod bundle. In this chapter, we have compared the existing models with the data in the literature and with that generated in this study and found them lacking. Hence, we have developed new semi-empirical models for bubble departure diameter and frequency in subcooled pool boiling conditions on a horizontal heater. The models have been validated using the data generated in the experiments described in chapter 3 and that existing in the open literature. These models have then been extended to take the cross flow boiling in a single rod into account, and finally, for cross flow boiling in the rod bundle.

5.2. Current Status

Figure 5.1 shows the parity plots for the bubble departure diameter models available in the literature. The first correlation for departure diameter was derived by Fritz (1935) by carrying out a force balance between the buoyancy and surface tension forces acting on a bubble. This correlation included the contact angle term to account for the surface properties,

but Cole (1967) found that for most of the commonly used metals, the contact angle for water can be approximated by 50° ± 20%. Since, in this model, the bubble departure diameter is only a function of liquid properties and the dependence of the diameter on the experimental conditions is not taken into account, the agreement with different data sets is quite bad, as seen in the figure. However, it formed the basic length scale for the future models, which used empirical functions of operating parameters along with the "*Fritz diameter*". The dependence of the departure diameter on the wall superheat was taken into account by Ruckenstein (1961), Cole and Rohsenow (1969) by including Jakob number (Ja), but the developed correlations are not able to predict the experimental data well. Kutateladze and Gogonin (1979) introduced a factor to account for the fraction of the heater surface, a departing bubble influences (K_l). The bubble departure diameter calculated using this factor was later used by Jensen and Memmel (1986) and Stephan (1992). As seen in *Figure 5.1*, the Stephan (1992) model is an improvement over its predecessors. Kocamustafaogullari (1983) studied the pressure variation of bubble departure diameter and proposed a model to account for pressure variations in terms of the density ratio of the liquid and vapor. However, again not being able to account for operating conditions, the agreement between the model and the experimental data is not good. Kim and Kim (2006) non-dimensionalised the bubble radius in terms of a characteristic radius obtained by assuming bubble growth to be a function of only wall superheat in saturated boiling. They obtained that their dimensionless departure radius under all conditions was about 25, however, it does not agree with rest of the experimental database well. Hamzekhani *et al.* (2014) proposed empirical model for departure diameter in terms of non-dimensional groups, like Archimedes number (Ar), Capillary number (Ca), Bond number (Bo) and Jakob number (Ja). Their model is an improvement over the earlier ones, but still the average error is about 300%. Bovard *et al.* (2017) proposed a model similar to Hamzekhani *et al.* (2014) and the average error came down to about 61%. Hence, after a careful assessment of the existing models and

the parametric behavior of the bubble departure diameter with the various operating parameters like, heat flux, wall superheat, liquid subcooling, heater characteristics and inclination angle; we understand that major factors affecting the bubble departure diameter have not been considered in these models. Some of the models account for the wall superheat (Ja) and the liquid-surface interaction (Ca), but the effect of liquid subcooling and surface roughness has not been considered so far.
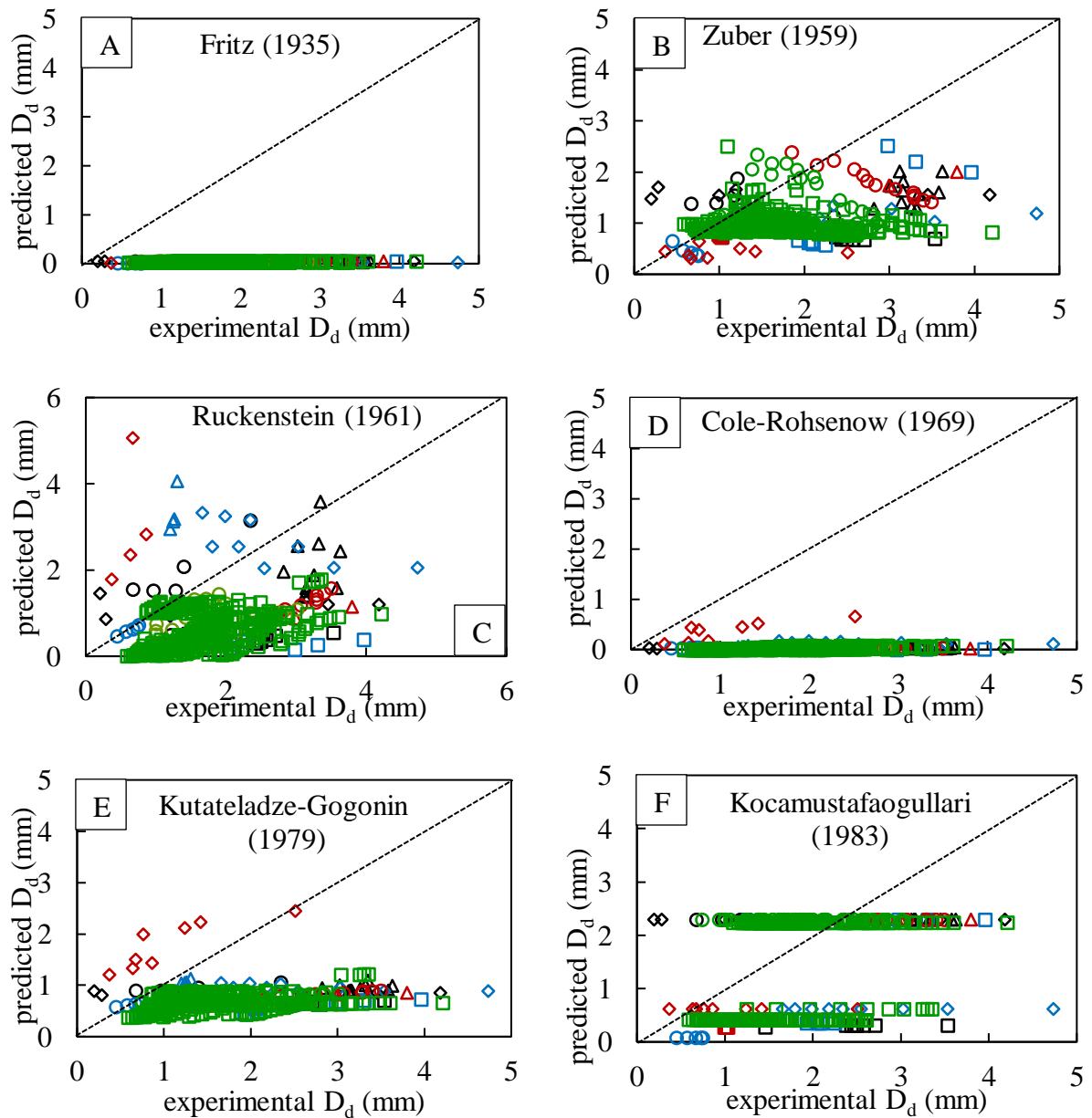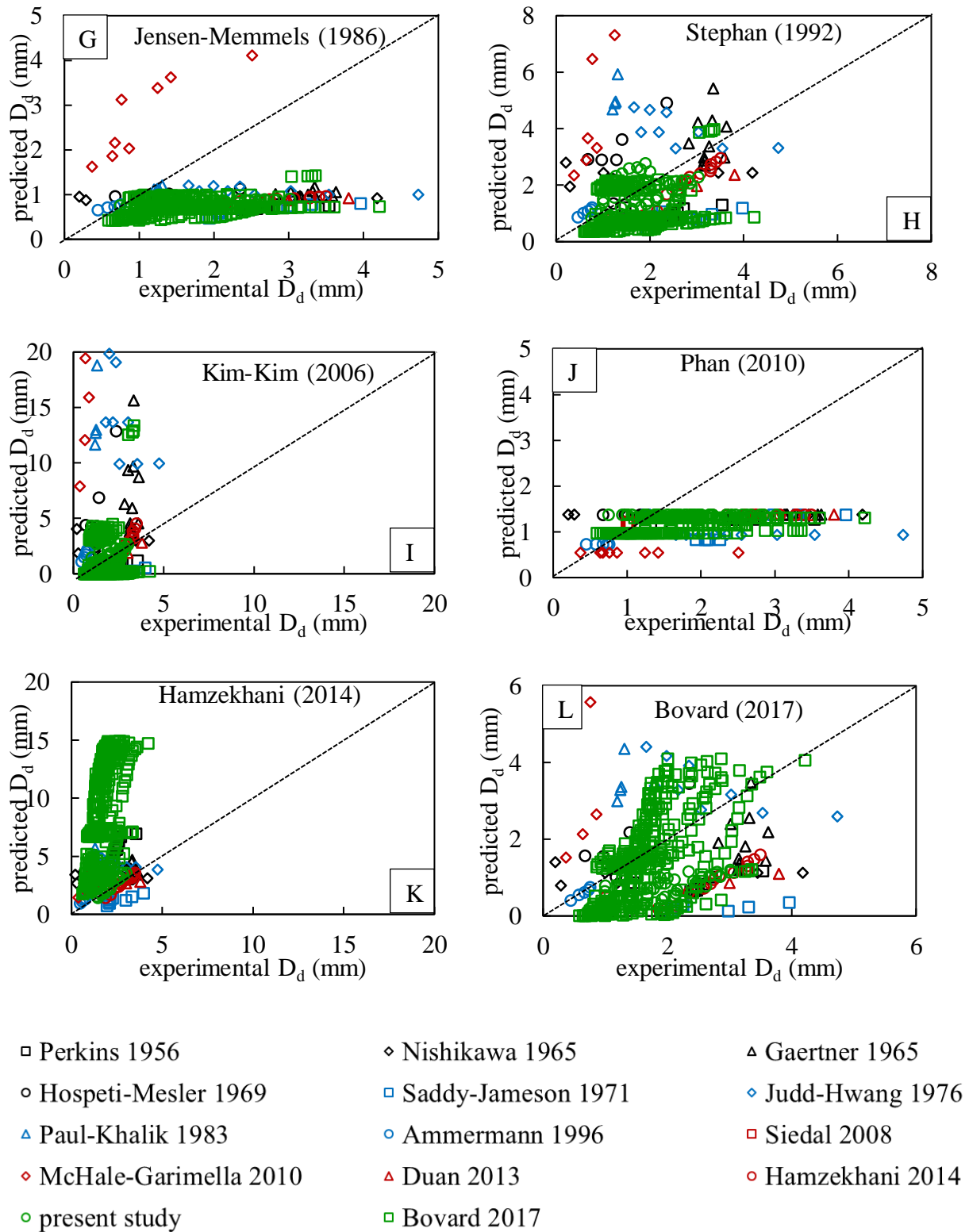
Figure 5.1 Comparison of experimental data for bubble departure diameter in pool boiling with models of (A)Fritz (1935), (B)Zuber (1959), (C)Ruckenstein (1961), (D)Cole and Rohsenow (1969), (E)Kutateladze and Gogonin (1979), (F)Kocamustafaogullari (1983), (G)Jensen and

Memmel (1986), (H)Stephan (1992), (I)Kim and Kim (2006), (J)Phan *et al.* (2010), (K)Hamzekhani, Maniavi Falahieh and Akbari (2014), and (L)Bovard *et al.* (2017).

Further, as observed in the literature and from our own experiments, f, D_d and hence, the product $f.D_d$ are increasing functions of the applied heat flux or wall superheat. However, most of the empirical models consider the product $f.D_d$ to be independent of wall superheat. *Figure 5.2* shows the parity plots comparing the data from the literature and that obtained in the present study with the frequency models available in the open literature. The bubble departure frequency has been observed to be strongly dependent on the departure diameter, which has been reflected in the models proposed over the years. Almost all the models are of the form $fD_d^a = constant$, where the constant is usually in terms of the liquid properties. These models have been tabulated in Chapter 1. Cole (1960) and McFadden and Grassmann (1962) found the constant to be dependent on the liquid densities and the acceleration due to gravity respectively. Ivey (1967) showed that the correlations can be either hydrodynamic (force balance derived) which are applicable for large bubble diameter data or thermodynamic (liquid thermo-physical properties dependent) which are applicable for the small diameter - low frequency data, with a transition region in between. It can be seen from *Figure 5.2* that the large diameter data (Cole (1960)) is well fitted with the correlation of the first kind, while the small diameter – low frequency data (Hsu and Graham (1961), Siedel *et al.* (2008)) can be fitted by the second kind. From the foregoing discussion, we can see that none of these models account for the frequency dependence on the operating conditions like heat flux, wall superheat or liquid subcooling. Hence, they are unable to predict the departure frequency under a wide range of conditions and have significant scatter.
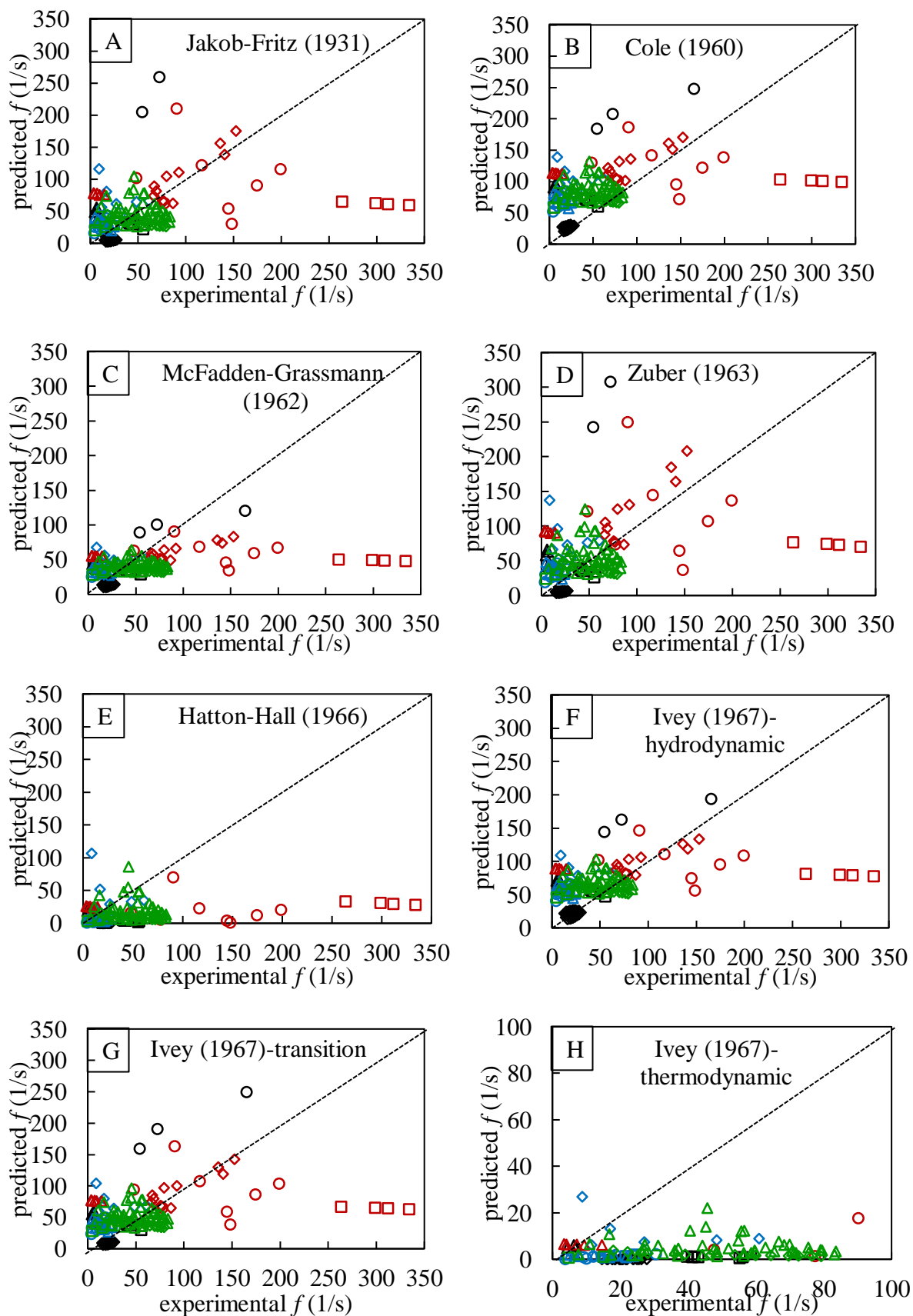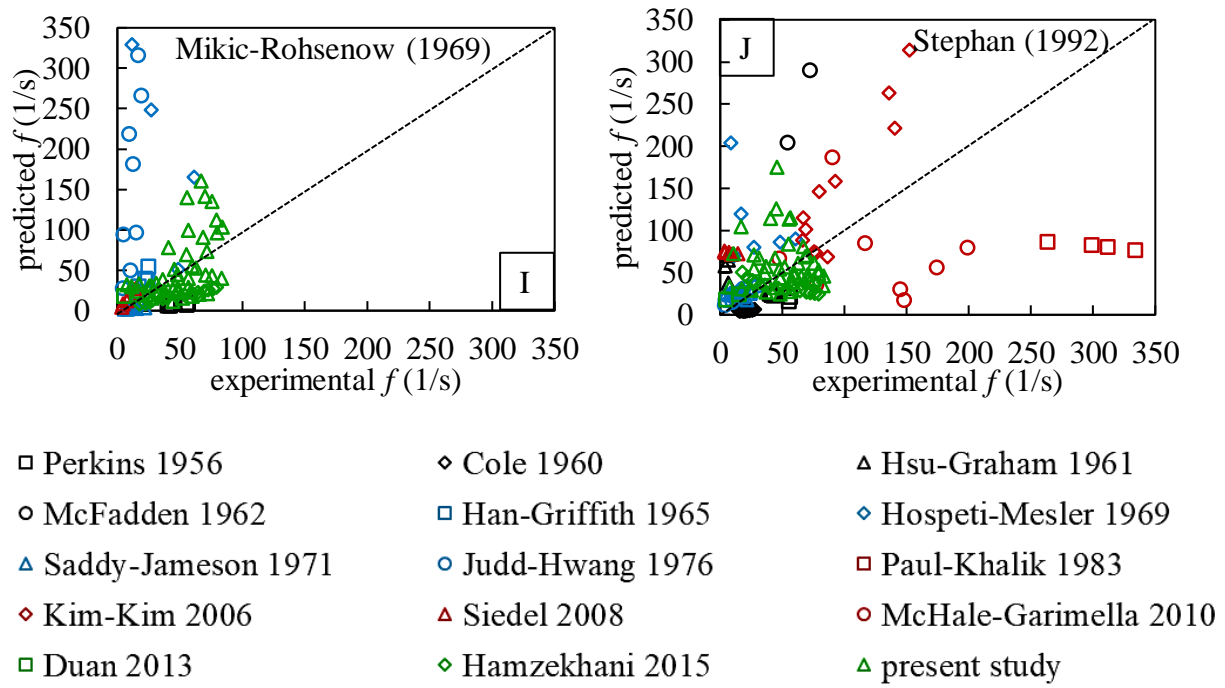
Figure 5.2 Comparison of experimental data for bubble departure frequency in pool boiling with the models of (A)Jakob and Fritz (1931), (B)Cole (1960), (C)McFadden and Grassmann (1962), (D)Zuber (1963), (E)Hatton and Hall (1966), (F-H)Ivey (1967), (I)Mikic and Rohsenow (1969), and (J)Stephan (1992).

5.3. Departure diameter

5.3.1. Subcooled Pool Boiling in single heater

From the parametric study of the behavior of bubble departure diameter with various operating variables described in chapter 3, we understand that a bubble departure diameter would be a function of – (1) wall superheat, (2) liquid subcooling, (3) working liquid – heater surface combination, (4) heater surface roughness, and (5) heater size. Hence, empirically, departure diameter can be expressed in terms of non-dimensional numbers as

$$Bo = m(\gamma - 1)^a \left(\frac{R_a}{L_c}\right)^b \left(\frac{D_h}{L_c}\right)^c Ja^d Pr^e \vartheta^f \tag{5.1}$$

where Bond number (Bo) is the measure of the importance of body forces compared to the surface tension forces. It implicitly contains the "*Fritz diameter*" in its definition, and is calculated as

$$Bo = \frac{gD_d^2(\rho_l - \rho_v)}{\sigma} \tag{5.2}$$

Jakob number (Ja) represents the ratio of the sensible heat to the latent heat absorbed in the process, and subcooling number (ϑ) is the ratio of the temperature difference between heater wall and bulk liquid to the wall superheat. γ is the surface-liquid interaction parameter (first defined by Sernas and Hooper (1969), in calculating the microlayer heat transfer from wall to the bubble), and Prandtl number (Pr) accounts for the liquid properties. The heater surface roughness (R_a) and the heater size accounted for in terms of the heater hydraulic diameter (D_h), have been non-dimensionalised using the length scale Laplace length (L_c) calculated as

$$L_c = \sqrt{\frac{\sigma}{g(\rho_l - \rho_v)}} \tag{5.3}$$

The transport properties used in the evaluation of the dimensionless groups have been taken from the National Institute of Standards and Technology (NIST) webbook (webbook.nist.gov/chemistry/fluid). Using curve fitting, the values of the coefficients in equation (5.1) were found to be: $m = 0.003$, $a = 1.78$, $b = 0.01$, $c = -0.8$, $d = 1.85$, $e = -2.5$ and $f = -0.6$. *Figure 5.3* shows the fitting of this correlation with pool boiling data from literature and our own data from chapter 3 and 4, and it can be seen that most of the data falls within $\pm 30\%$ limits with an R^2 value of 0.88.

The details of the datasets from literature used for the parity plots and model validation are presented in *Table 5.1*, and the average percentage errors for all the models with each dataset is summarized in *Table 5.2*. It can be clearly seen that the present model performs better than the previous models, over a wide range of conditions.
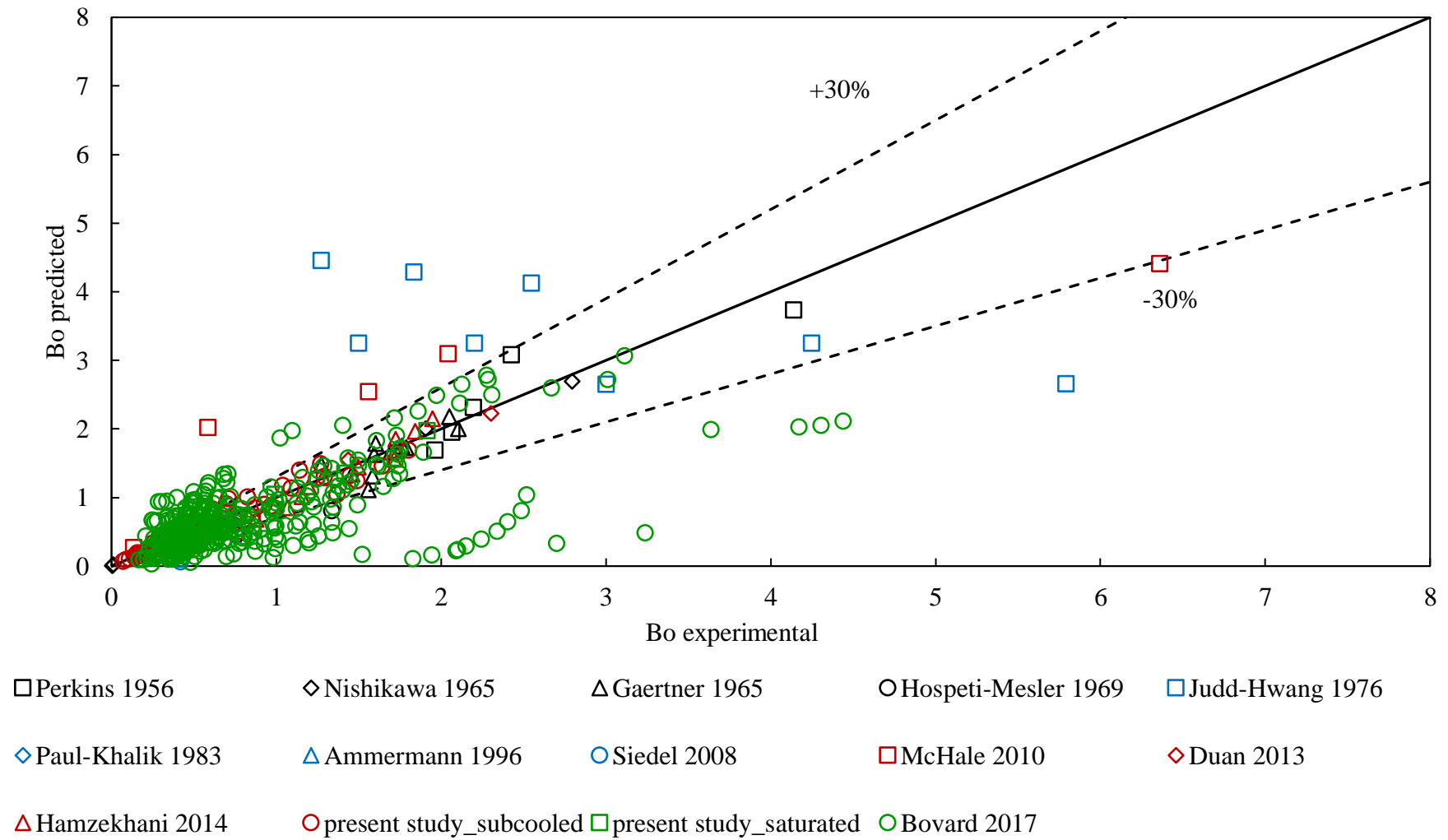
Figure 5.3 Comparison of experimental and predicted Bo for single heater in pool boiling.

Table 5.1 Details of the experimental data used to compare departure diameter models.

Reference	Working liquid	Heater element	Heat flux q'' (kW/m^2)	Wall superheat ΔT_{sat} (K)	Liquid subcooling ΔT_{sub} (K)	No. of data points
Perkins and Westwater (1956)	Methanol	Copper tube	190.12-348.66	21-33	0	7
Nishikawa *et al.* (1965)	Water	Brass plate	38.2-63.96	7-9.3	2.14-6.19	3
		Platinum wire	43.69-87.57	7.7-10.8	3.47-8.57	3
Gaertner (1965)	Water	Copper plate	32.91-205.34	10.3-16.74	0	8
		Platinum plate	49.6-143.75	15.86-21.26	0	3
Hospeti and Mesler (1969)	Water	Chromel strip	18.59-344.14	4.8-19.3	0	7
Saddy and Jameson (1971)	Acetic acid	Glass tube	11.97-56	2-6	0	5
	Water		3.21-12.84	2-4	0	3
Judd and Hwang (1976)	Dichloromethane	Glass plate with stannic oxide coating	25.3-60.62	25.86-37.33	0-11.3	9

Reference	Working liquid	Heater element	Heat flux q'' (kW/m^2)	Wall superheat ΔT_{sat} (K)	Liquid subcooling ΔT_{sub} (K)	No. of data points
Paul and Abdel-Khalik (1983)	Water	Platinum wire	227.02-513.56	18.36-23.3	0	4
Ammerman et al. (1996)	FC-72	Platinum wire	18.98-150.51	19.93-27.87	0	5
Siedel et al. (2008)	Pentane	Copper plate	8.59-40.67	2-7.1	0	6
McHale and Garimella (2010)	FC-77	Aluminum block	20.6-113.4	6-25.3	0	8
Duan et al. (2013)	Water	ITO film	28.7-36	7.4-9	0	2
Hamzekhani et al. (2014)	Water	SS rod	5.08-103.48	2.7-11.45	0	13
Bovard et al. (2017)	Water	SS	0.21-123.66	0.8-41.2	0	318
	Ethanol	Copper				
	Acetone	Brass				
	Methanol	Aluminum				

Reference	Working liquid	Heater element	Heat flux q'' (kW/m^2)	Wall superheat ΔT_{sat} (K)	Liquid subcooling ΔT_{sub} (K)	No. of data points
Present study	Water	SS rods, ribbon	5-250	0-15	5-20	69

Table 5.2 Mean percentage errors between experimental and predicted bubble departure diameter.

Models → experiment ↓	Fritz (1935)	Zuber (1959)	Ruckenstein (1961)	Cole and Rohsenow (1969)	Kutateladze and Gogonin (1979)	Kocamustafaogullari (1983)	Jensen and Memmel (1986)	Stephan (1992)	Kim and Kim (2006)	Phan et al. (2010)	Hamzekhani et al. (2014)	Bovard et al. (2017)	Present model
Perkins and Westwater (1956)	98.5	66.9	82.9	98.9	72.8	87.3	71.1	55.3	67.2	47.1	138.9	65.6	12.2
Nishikawa et al. (1965)	93.1	241.4	168.1	93.9	130.5	422.9	136.9	505.8	195.8	213.9	470.3	160	24.5
Gaertner (1965)	98.4	50.4	38.2	98.8	70.5	28.7	68.5	20.7	114.6	57.2	18.4	41.4	9.1

Models → experiment	Fritz (1935)	Zuber (1959)	Ruckenstein (1961)	Cole and Rohsenow (1969)	Kutateladze and Gogonin (1979)	Kocamustafaogullari (1983)	Jensen and Memmel (1986)	Stephan (1992)	Kim and Kim (2006)	Phan et al. (2010)	Hamzekhani et al. (2014)	Bovard et al. (2017)	Present model
Hospeti and Mesler (1969)	954	43.6	51.6	97.4	31.7	101.6	28.9	147.9	304.4	32.8	201.9	56.7	21.9
Saddy and Jameson (1971)	98.8	70.5	90.3	99.5	74	57.3	72.1	64.1	80.3	59.9	50.4	92.5	-
Judd and Hwang (1976)	98.7	54	43.4	94	59.2	74.1	53.8	78.1	541.3	60.9	87.9	62.6	85.7

Models → experiment	Fritz (1935)	Zuber (1959)	Ruckenstein (1961)	Cole and Rohsenow (1969)	Kutateladze and Gogonin (1979)	Kocamustafaogullari (1983)	Jensen and Memmel (1986)	Stephan (1992)	Kim and Kim (2006)	Phan *et al.* (2010)	Hamzekhani *et al.* (2014)	Bovard *et al.* (2017)	Present model
Paul and Khalik (1983)	95.8	12.5	164.8	95	14.5	83.4	8.7	307.8	1015.7	10.1	310.2	178.4	0.59
Ammerman *et al.* (1996)	97	40	4.5	93.8	12.6	86.9	18.2	71.9	169.9	21.1	99.3	4.5	15.6
Siedel *et al.* (2008)	96.7	25.8	86.3	99.1	50.5	72.6	46.5	41.5	83.2	19.2	198.9	75.4	49.1
McHale and Garimella (2010)	97.5	51.3	479.2	64.2	102.3	38.8	198.5	451.9	4316.9	42.9	154.9	456.2	44.2

Models → experiment	Fritz (1935)	Zuber (1959)	Ruckenstein (1961)	Cole and Rohsenow (1969)	Kutateladze and Gogonin (1979)	Kocamustafaogullari (1983)	Jensen and Memmel (1986)	Stephan (1992)	Kim and Kim (2006)	Phan *et al.* (2010)	Hamzekhani *et al.* (2014)	Bovard *et al.* (2017)	Present model
Duan *et al.* (2013)	98.4	44.7	70.3	99.4	75.1	31.5	73.3	36	31.5	58.9	19.1	71.1	5.6
Hamzekhani *et al.* (2014)	98.1	36.6	65.8	99.3	70.1	21.3	67.9	25.6	28.9	49.9	5.85	66.9	8.9
Bovard *et al.* (2017)	97.3	38.5	66.4	98.2	57.12	47.9	52.9	54.3	104.9	27.6	449.1	48.1	41.5
Present study	96.8	35.4	35.4	99.1	51.7	46.2	47.9	27.5	46.6	28.5	71	54.3	11.1

5.3.2. Cross flow boiling in single heater rod

Here, the Reynolds number (Re) was introduced to take the effect of flow velocity under cross flow conditions and the obtained correlation is as follows:

$$Bo = 0.003(\gamma - 1)^{1.78} \left(\frac{R_a}{L_c}\right)^{0.01} \left(\frac{D_h}{L_c}\right)^{-0.8} Ja^{1.85} Pr^{-2.5} (1 + Re)^{-0.036} \vartheta^{-0.6} \quad (5.4)$$

This correlation has been validated only for the saturated cross flow boiling data obtained in present experiments and might be applicable only for the conditions of the present investigation. The comparison of the correlation and our experimental data is shown in *Figure 5.4*, and the model agrees with the data within $\pm 20\%$.
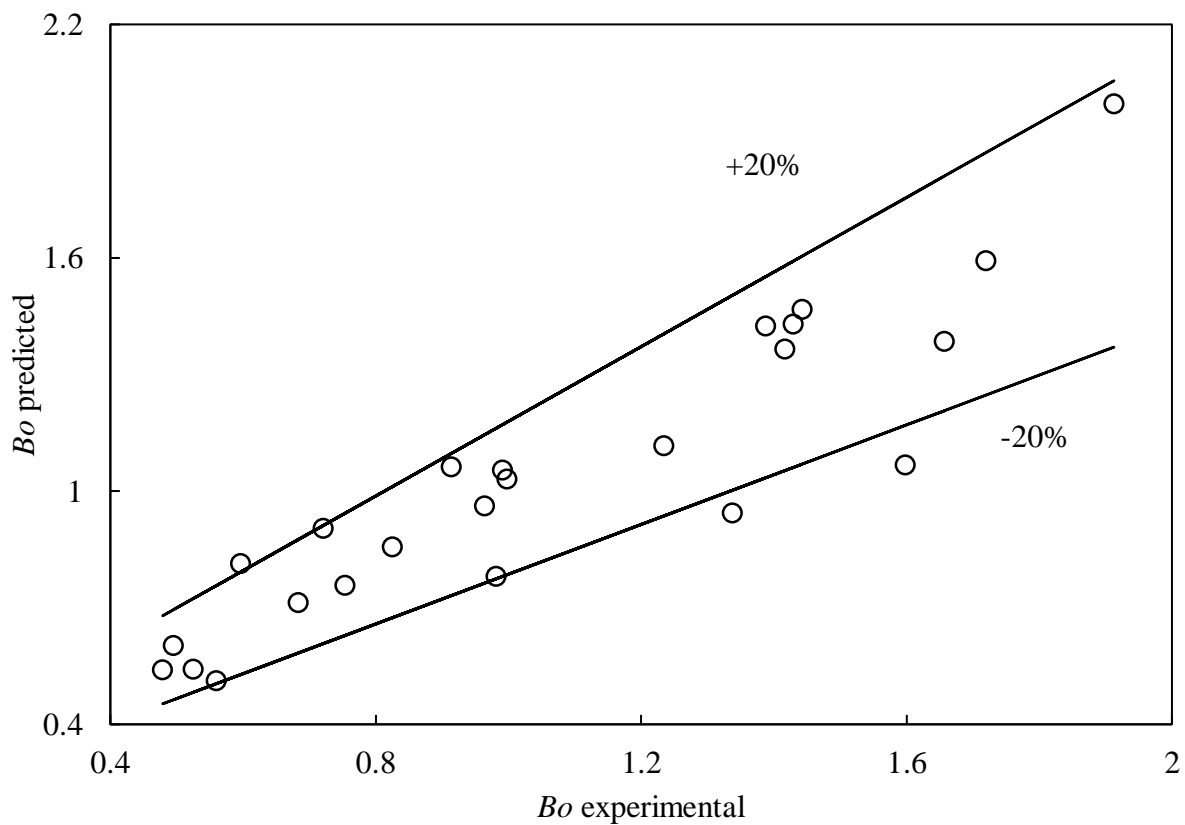
Figure 5.4 Comparison of experimental and predicted Bo for single rod in cross flow boiling.

5.3.3. Cross flow boiling in rod bundle

The departure characteristics of vapor bubbles from a heater rod in a bundle have not been studied so far. The vapor bubbles growing and departing from a heater rod surrounded by

other heated rods would be affected by their presence as discussed in chapter 4. We take this effect into account in terms of the number of heated rods (n) in the model for predicting the bubble departure diameter for the rod bundle cases. Also, as the wall temperatures and bubble departure diameter was observed to depend on the position of the observed rod with respect to the other heated rods, which means that the dependence of the factor n should change with the position of the observed rod in the bundle. Therefore, the Bond number correlation arrived at was:

$$Bo = 0.003(\gamma - 1)^{1.78} \left(\frac{R_a}{L_c}\right)^{0.01} \left(\frac{D_h}{L_c}\right)^{-0.8} n^q Ja^{1.85} Pr^{-2.5} (1 + Re)^{-0.036} \tag{5.5}$$

Where

$$q = \begin{cases} 0.75, top\ rod \\ 1.005, middle\ rod, \\ 0.255, bottom\ rod \end{cases} \tag{5.6}$$

and the condition refers to the position of the observed rod with respect to the other heated rods. The comparison of the model with the results obtained for rod no. 3 for the three cases (details were given in Table 4.1) have been shown in *Figure 5.5* and the data agreement with the model is within $\pm 30\%$. For the experiments conducted in the present study (as described in chapter 4), bubble dynamics were observed only for the rod 3, and so, it would be bottom rod for Case 2, top rod for case 3 and middle rod for Case 4. However, the model is expected to be applicable to any three rods of the bundle under the conditions within the range of those in present experiments.
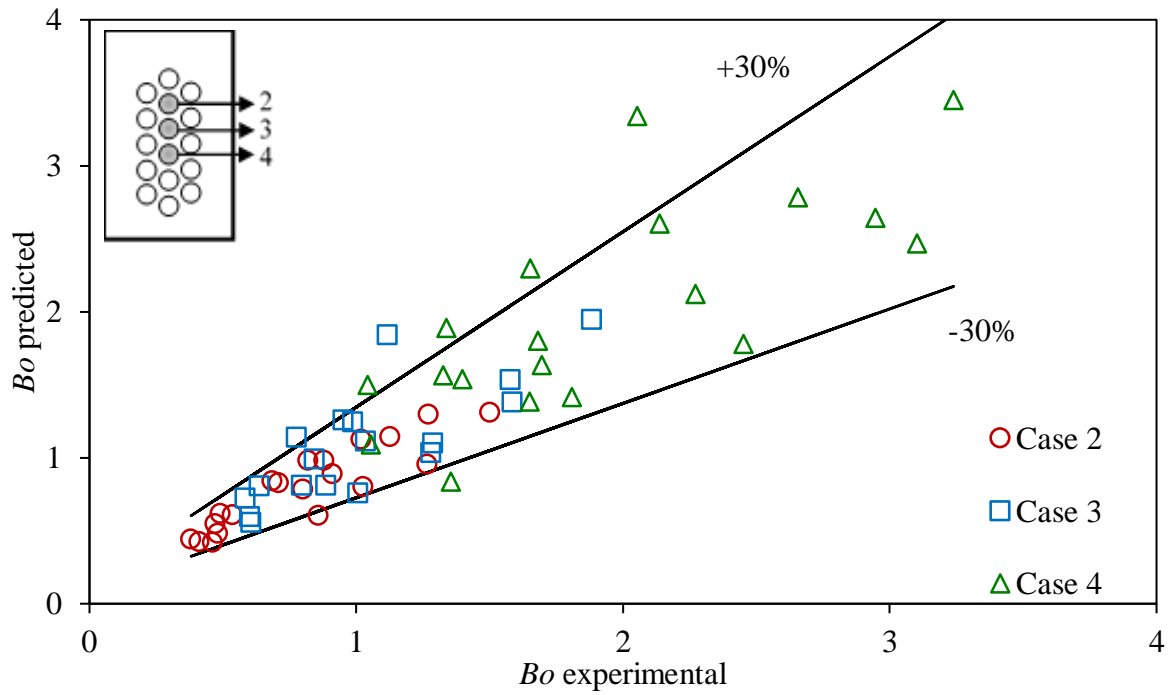
Figure 5.5 Comparison of experimental and predicted Bo (departure diameter) for rod bundle cases.

The range of conditions for which the presented bubble departure diameter model under cross flow conditions would be applicable are: $q^{"} = 8 - 28 \ kW/m^2$, $G = 120 - 303.5 \ kg/m^2 s$, water-stainless steel combination, cylindrical heater ($R_a = 0.5 \ \mu m$, $\theta = 60°$). The validity of the correlation can be extended to even higher number of heated rods subject to the condition that the tubes must have similar surface characteristics as those for which the correlation is developed. Also, the correlation is valid only for the range of heat flux and mass flux investigated in the present investigation. This is to note that the constant q of every row needs to be found out experimentally as the bubble interaction increases as one moves from bottom to top of the tube bundle.

5.4. Departure frequency

5.4.1. Subcooled pool boiling in single heater

The most widely used correlation for predicting bubble departure frequency is the one given by Cole (1960). He suggested that at heat fluxes near critical heat flux, when the

successive departing bubbles coalesce with each other, the product of departure diameter and frequency is equal to the bubble rise velocity. He carried out a force balance between buoyancy and drag forces on a freely rising bubble and gave the relation

$$f\sqrt{D_d} = \left(\frac{4g(\rho_l - \rho_v)}{3\rho_l}\right)^{\frac{1}{2}} \qquad (5.7)$$

But this equation over predicts the experimental data at lower heat fluxes where the successive bubbles leaving the surface do not coalesce and hence, the frequency is lower than that at heat flux close to CHF, due to a finite waiting period as shown in *Figure 5.2*. It has been seen in the experimental data that the waiting period itself is a function of the wall superheat, so we have incorporated a factor of wall superheat and heater surface to account for the differences between experiments and Cole's equation. Additional to the Jakob number, the subcooling number and the heater surface characteristics parameters are also considered to obtain the following equation

$$f\sqrt{D_d} = 0.01\gamma^a \left(\frac{R_a}{L_a}\right)^b \left(\frac{4g(\rho_l - \rho_v)}{3\rho_l}\right)^{\frac{1}{2}} Ja^c \vartheta^d \qquad (5.8)$$

Using curve fitting, the values of coefficients in equation (5.8) were found to be $a = 0.01$, $b = 0.22$, $c = 2.05$ and $d = 0.39$. *Figure 5.6* shows the comparison of the experimental data with the predicted data for the pool boiling condition of a single rod, for our experiments as well as the data from literature, where the correlation is able to predict the data within $\pm 25\%$ with an R^2 value of 0.97.

The details of the datasets from literature used for the parity plots and model validation are presented in *Table 5.3*, and the average percentage errors for all the models with each dataset is summarized in *Table 5.2*. It can be clearly seen that the presently proposed model performs better than the previous models, over a wide range of conditions.
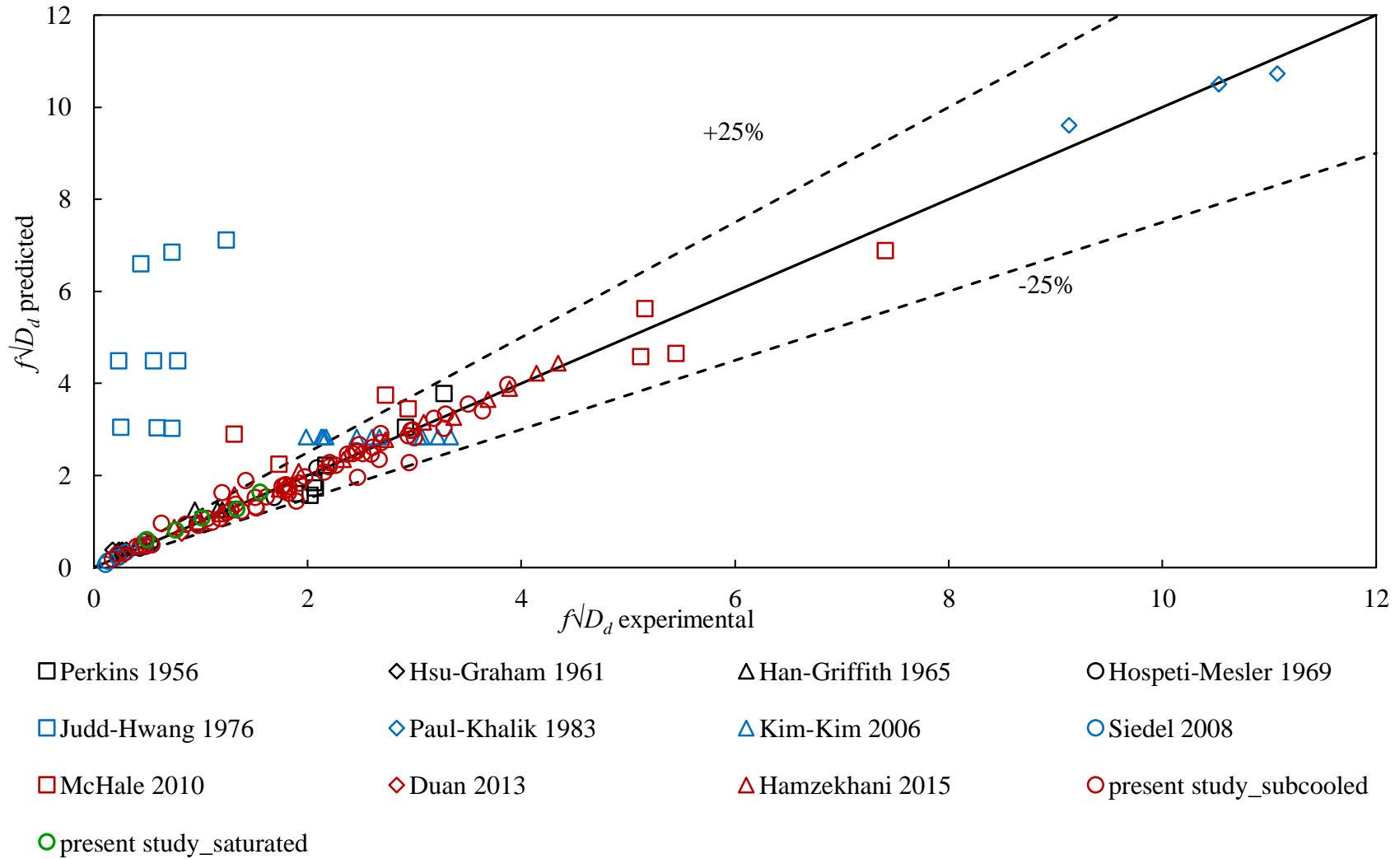
Figure 5.6 Comparison of experimental and predicted departure frequency for single heater in pool boiling.

5.4.2. Cross flow boiling in single heater rod

For the cross-flow conditions, taking the effect of Re into account, our experimental data could be fitted with the correlation given by

$$f\sqrt{D_d} = 0.01\gamma^{0.01}\left(\frac{R_a}{L_a}\right)^{0.22}\left(\frac{4g(\rho_l-\rho_v)}{3\rho_l}\right)^{\frac{1}{2}}Ja^{2.05}(1+Re)^{-0.031}\vartheta^{0.39} \qquad (5.9)$$

This model, similar to the departure diameter model, has been validated only for the saturated cross flow boiling data obtained in present experiments, and might be applicable only for the conditions of the present investigation.
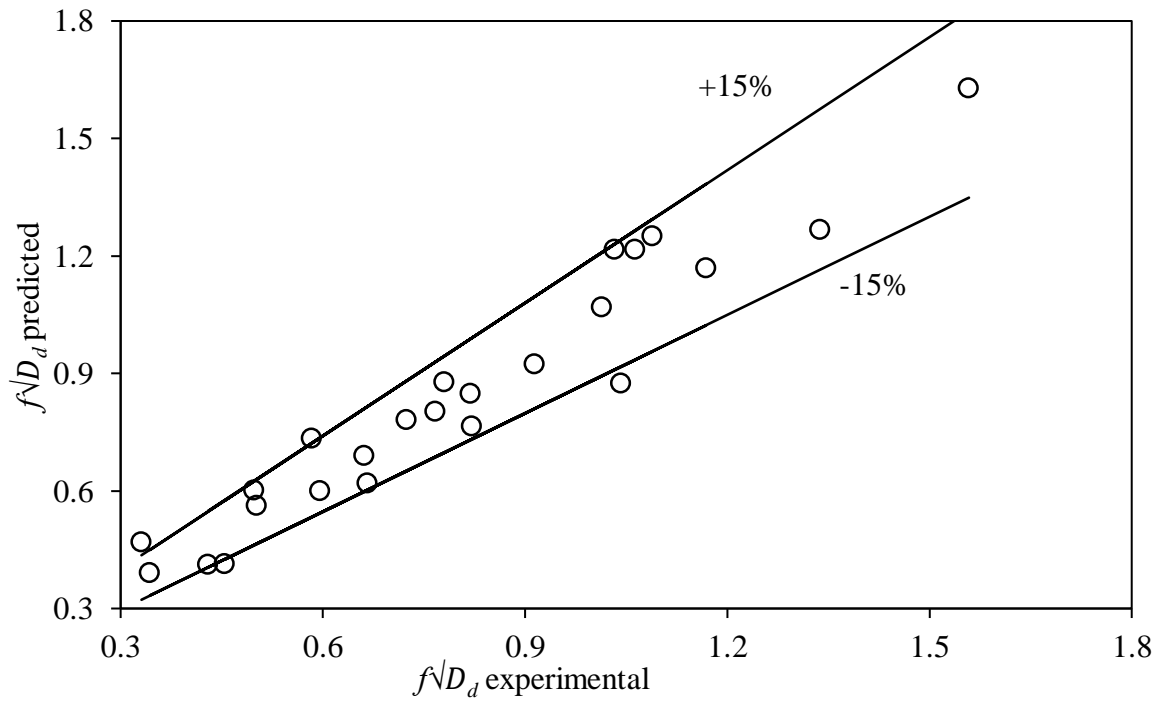
Figure 5.7 Comparison of experimental and predicted departure frequency for single rod in cross flow boiling.

Table 5.3 Details of the experimental data used to compare departure frequency models.

Reference	Working liquid	Heater element	Heat flux q'' (kW/m^2)	Wall superheat ΔT_{sat} (K)	Liquid subcooling ΔT_{sub} (K)	No. of data points
Perkins and Westwater (1956)	Methanol	Copper tube	190.12-348.66	21-33	0	7
Cole (1960)	Water	Zirconium ribbon	Near CHF	-	0	23
Hsu and Graham (1961)	Water	Chromel strip	15.76	32.68	0	4
McFadden and Grassmann (1962)	Nitrogen	-	-	-	0	3
Han and Griffith (1965)	Water	Copper cylinder with gold plating	-	9.99	0	4
Hospeti and Mesler (1969)	Water	Chromel strip	18.59-344.14	4.8-19.3	0	6

Reference	Working liquid	Heater element	Heat flux q'' (kW/m^2)	Wall superheat ΔT_{sat} (K)	Liquid subcooling ΔT_{sub} (K)	No. of data points
Saddy and Jameson (1971)	Acetic acid	Glass tube	11.97-56	2-6	0	5
	Water		3.21-12.84	2-4		3
Judd and Hwang (1976)	Dichloromethane	Glass plate with stannic oxide coating	25.3-60.62	25.86-37.33	0-11.3	9
Paul and Abdel-Khalik (1983)	Water	Platinum wire	227.02-513.56	18.36-23.3	0	4
Kim and Kim (2006)	R113	Microheater array	-	25	0	11
Siedel et al. (2008)	Pentane	Copper plate	8.59-40.67	2-7.1	0	5
McHale and Garimella (2010)	FC-77	Aluminum block	20.6-113.4	6-25.3	0	8
Duan et al. (2013)	Water	ITO film	28.7-36	7.4-9	0	2

Reference	Working liquid	Heater element	Heat flux q'' (kW/m^2)	Wall superheat ΔT_{sat} (K)	Liquid subcooling ΔT_{sub} (K)	No. of data points
Hamzekhani *et al.* (2015)	Water	SS rod	5.08-103.48	2.7-11.45	0	14
Present study	Water	SS rods, ribbon	5-250	0-15	5-20	69

Table 5.4 Mean percentage errors between experimental and predicted bubble departure diameter.

Models → experiment	Jakob and Fritz (1931)	Cole (1960)	McFadden and Grassmann (1962)	Zuber (1963)	Hatton and Hall (1966)	Ivey (1967) - Hydrodynamic	Ivey (1967) - transition	Ivey (1967) – Thermodynamics	Stephan (1992)	Mikic and Rohsenow (1969)	Present model
Perkins and Westwater (1956)	32.2	58.8	22.7	19.7	90.2	29.2	15.3	97.5	48.2	84.1	12.7
Cole (1960)	78.9	30.4	36.5	75.1	99.2	13.8	56.9	99.8	73.4	-	-
Hsu and Graham (1961)	737.5	1447.7	653.7	892.1	227.4	1111.3	835.2	22.3	898.6	-	67.1

Models → experiment	Jakob and Fritz (1931)	Cole (1960)	McFadden and Grassmann (1962)	Zuber (1963)	Hatton and Hall (1966)	Ivey (1967) - Hydrodynamic	Ivey (1967) - transition	Ivey (1967) – Thermodynamics	Stephan (1992)	Mikic and Rohsenow (1969)	Present model
McFadden and Grassmann (1962)	222.1	160.4	44.6	281.6	-	103.8	137.7	-	260.6	-	-
Han and Griffith (1965)	29.1	218.6	55.2	52.9	71.9	149.4	66.6	92.9	26.1	87.6	11.9
Hospeti and Mesler (1969)	358.3	543.1	218.6	442.9	252.2	403.3	344.9	86.1	609.4	-	3.7
Saddy and Jameson (1971)	227.3	614.9	248.2	284.9	53.1	459.5	295.7	84.9	133.9	70.1	-
Judd and Hwang (1976)	209.7	654.2	267.3	266.9	62.4	490.2	295.9	90.4	120.3	1345.8	83.9
Paul and Abdel-Khalik (1983)	79.2	66	83.4	75.3	89.7	73.4	78.1	97.4	72.5	173.3	2.8
Kim and Kim (2006)	18.4	41.8	30.9	30.5	-	18.9	14.5	-	53.7	-	19.1

Models → experiment	Jakob and Fritz (1931)	Cole (1960)	McFadden and Grassmann (1962)	Zuber (1963)	Hatton and Hall (1966)	Ivey (1967) - Hydrodynamic	Ivey (1967) - transition	Ivey (1967) – Thermodynamics	Stephan (1992)	Mikic and Rohsenow (1969)	Present model
Siedel *et al.* (2008)	1219.8	1834.1	841.8	1463.5	332.7	1413.6	1213.3	50.9	1164.2	69.6	13.9
McHale and Garimella (2010)	62.9	60.2	48.3	69.9	79.6	48.2	54.1	94.8	54.4	-	30.7
Duan *et al.* (2013)	205	740.4	309.2	261.3	46.8	557.7	316.1	86.5	184.4	157.5	7.1
Hamzekhani *et al.* (2015)	54.6	98.2	48.7	58.4	74.7	71.3	55.8	93.6	59.7	62.3	4.6
Present study	62.1	130.9	52.1	72.2	66.7	86.8	64.2	86.7	82.2	55.3	8.1

5.4.3. Cross flow boiling in rod bundle

Following a process similar to that with departure diameter, taking the effect of the number of heated rods into account, we obtained

$$f\sqrt{D_d} = 0.04\gamma^{0.01}\left(\frac{R_a}{L_a}\right)^{0.22} n^r \left(\frac{4g(\rho_l-\rho_v)}{3\rho_l}\right)^{\frac{1}{2}} Ja^{2.05}(1+Re)^{-0.031} \tag{5.10}$$

$$r = \begin{cases} 0.178, & top\ rod \\ 0.356, & middle\ rod \\ 0.178, & bottom\ rod \end{cases} \tag{5.11}$$

Here, the constant is higher than that obtained for the single rod case, which reflects the much higher frequency in the bundle cases compared to the isolated tube case. The comparison of the model with the data for the three bundle cases have been given in *Figure 5.8*, and the predictions were found to be within the acceptable limits. Again, the condition on r is based on the position of the observed rod (rod 3, here) in the bundle. The correlation, however, is expected to be applicable to any three rods of the bundle under the conditions within the range of the present experiments.
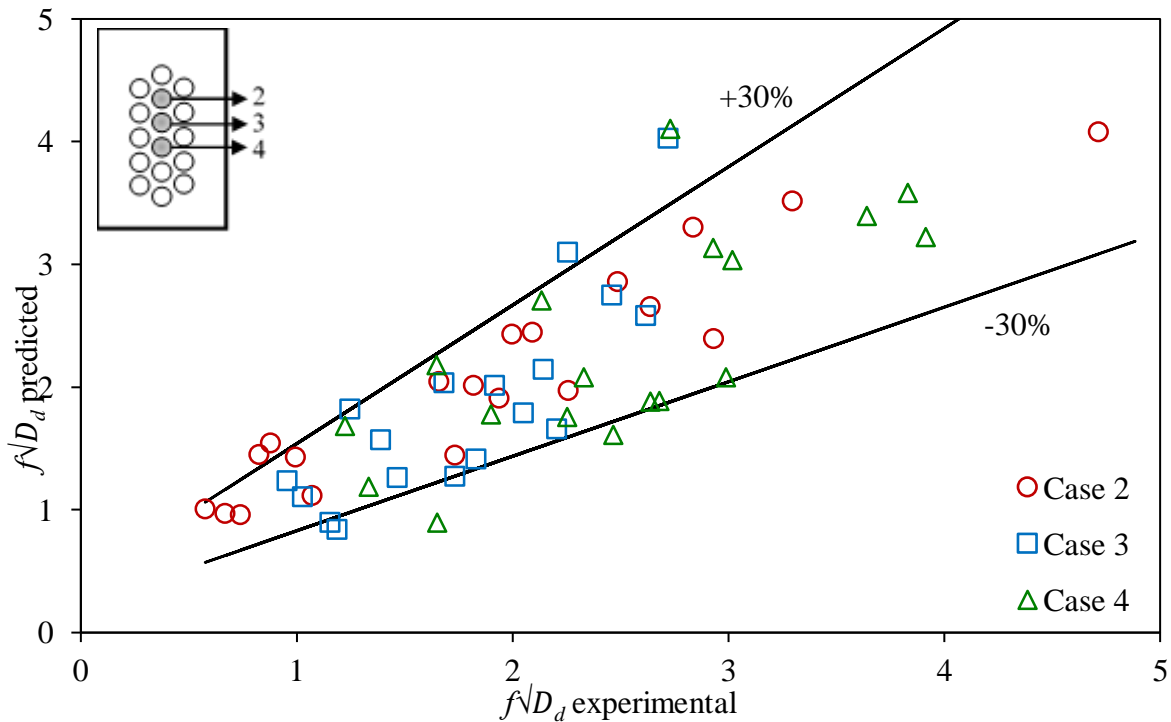
Figure 5.8 Comparison of experimental and predicted departure frequency for tube bundle cases.

The range of conditions for which the value the constant 0.04 has been obtained, and the model would be applicable are: $q^{"} = 8 - 28 \, kW/m^2$, $G = 120 - 303.5 \, kg/m^2s$, water-stainless steel combination, cylindrical heater ($R_a = 0.5 \, \mu m$, $\theta = 60°$). The validity of the model can be extended to even higher number of heated rods subject to the condition that the tubes must have similar surface characteristics as those for which the correlation is developed. Also, the correlation is valid only for the range of heat flux and mass flux investigated in the present investigation. This is to note that the constant r of every row needs to be found out experimentally as the bubble interaction increases as one moves from bottom to top of the tube bundle.

5.5. Closure

A number of existing models for bubble departure diameter and frequency in pool boiling conditions have been studied. The models for departure diameter have been developed on the basis of the saturated pool boiling data, and hence, are unable to predict the effects of liquid subcooling. They also do not account for the effects of heater surface characteristics and heater size, which play a significant role in bubble diameter as discussed in chapter 3. The prediction of departure frequency requires the information of departure diameter, and the limited number of models available in the literature do not take the operating conditions into account. After carefully studying the existing models and their scatter with the experimental data, new models for bubble departure diameter and frequency have been proposed for subcooled pool boiling and cross flow boiling for a single horizontal heater. Also, the models for bubble departure diameter and frequency in cross flow boiling in a horizontal rod bundle have been proposed for the first time.

6. Chapter 6

Study of Bubble Departure Characteristics in Vertical Forced Convective Subcooled Nucleate Boiling

6.1. Introduction

Forced convective subcooled nucleate boiling in channels or annuli with flow parallel to the axis of the channel or tube respectively, finds a number of applications in the industry due to its high heat transfer capabilities at relatively low wall temperatures. The most common applications being in heat exchangers, evaporators, reboilers, etc. The advancement of the modern electronics resulted in the requirement of cooling technologies in small scale devices, and flow boiling in micro-channels has been found to be an excellent option for the purpose. The rod bundle assemblies in a nuclear reactor also utilize the flow boiling heat transfer mechanism to generate power.

A large number of studies exist studying the heat transfer and bubble dynamics in channels or annuli, for high heat and mass flux conditions, as discussed in chapter 1. However, few studies have been carried out in the low heat and mass flux ranges. Such conditions occur during the start-up of AHWR or during accidental conditions in PHWRs for example, where passive systems provide coolant circulation. The typical mass flux in such conditions is of the order of 30 g/s or less, and the typical heat flux per fuel pin is $< 50\ kW/m^2$. There is no data and consequently no validation of the applicability of the existing models in such conditions. Further, the studies in mini- or micro-channels and rod bundles, mostly focus on the heat transfer measurements and no studies have been performed to study the effect of presence of neighboring heated rods on bubble dynamics to the best of author's knowledge. To this end, visualization experiments have been carried out to study the vapor bubble departure

characteristics under low heat and mass flux conditions in a conventional sized annulus, a narrow annulus and a four-rod bundle.

6.2. Experimental Description

6.2.1. Setup

A schematic of the experimental setup is shown in *Figure 6.1*. The setup is essentially a closed loop consisting of a reservoir, a centrifugal pump, a test section and a condenser. The reservoir was used to store the demineralized water and to collect the condensate from the condenser. Three test sections were used – two annuli of different hydraulic diameters and a four-rod bundle. All three test sections had the quartz glass tube as the outer tube and stainless steel (SS316) cartridge heaters as the inner rods. The heater rods had an outer diameter of 12 *mm*. The dimensional details of the three test sections are provided in *Table 6.1* below.

Table 6.1 Dimensional details of the test sections used.

Test Section	Glass tube I.D. (mm)	Total Length (mm)	Heated Length (mm)	Entry length (mm)	Exit Length (mm)	Hydraulic Diameter (mm)
Conventional Annulus	45	980	900	80	-	33
Narrow Annulus	16	1040	560	240	240	4
4-rod bundle	36	1040	560	240	240	8.57

Distilled water was fed to the test section via the centrifugal pump from the reservoir, which was fitted with an auxiliary preheater to heat the water to a desired degree of subcooling from inlet to the test section. The control valves were provided to control the flow rate through the test section. The heated water and water vapor outlet from the test section were passed

through a condenser and fed back to the reservoir to maintain a closed loop. The reservoir was provided with a chimney to release any excess steam and to maintain the atmospheric pressure in the loop. The heaters used were hollow rods having an average surface roughness of $0.5\ \mu m$, and a nichrome heating wire placed in the hollow space packed with magnesium oxide powder. The heater rods were powered by an AC power supply routed through a variac to control the amount of power given to the heater.

$D = 45\ mm$

$D = 12\ mm$

Conventional annulus

$D = 16\ mm$

$D = 12\ mm$

Narrow annulus

a= 2.2 mm

$D = 36mm$

$D = 12\ mm$

4-rod bundle

(B)
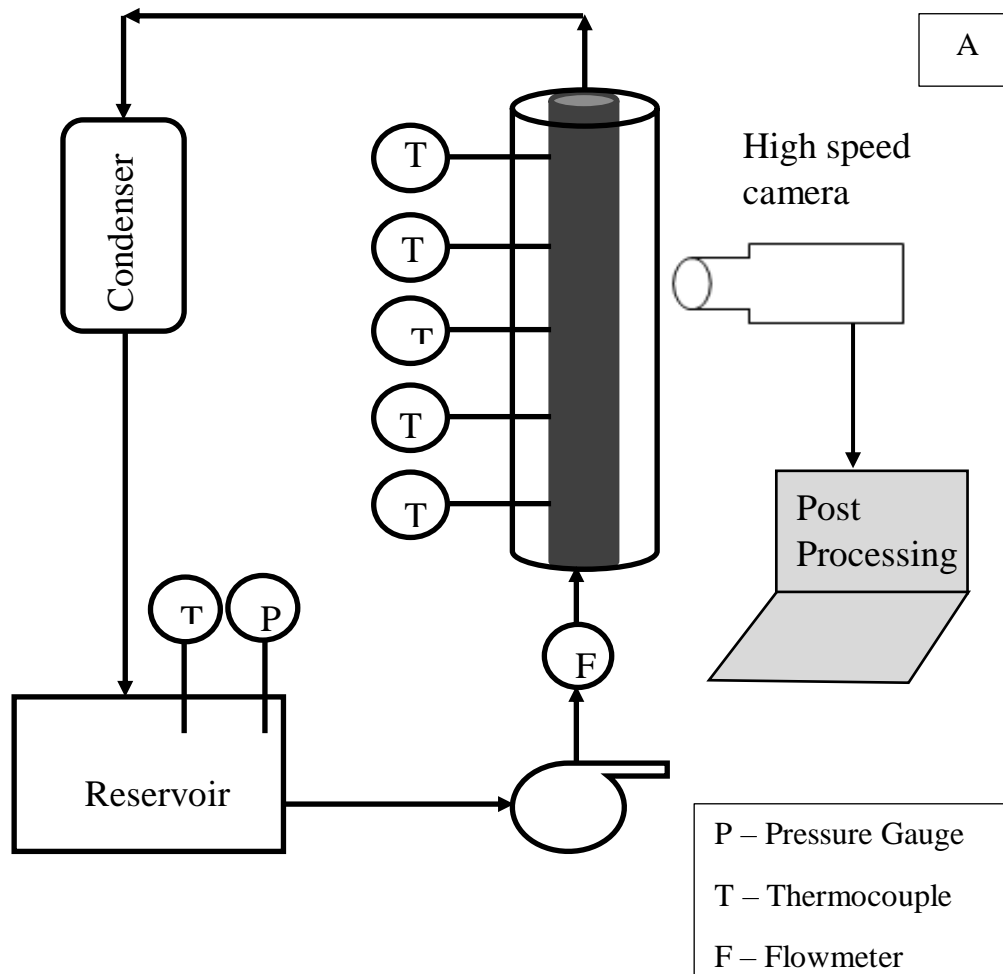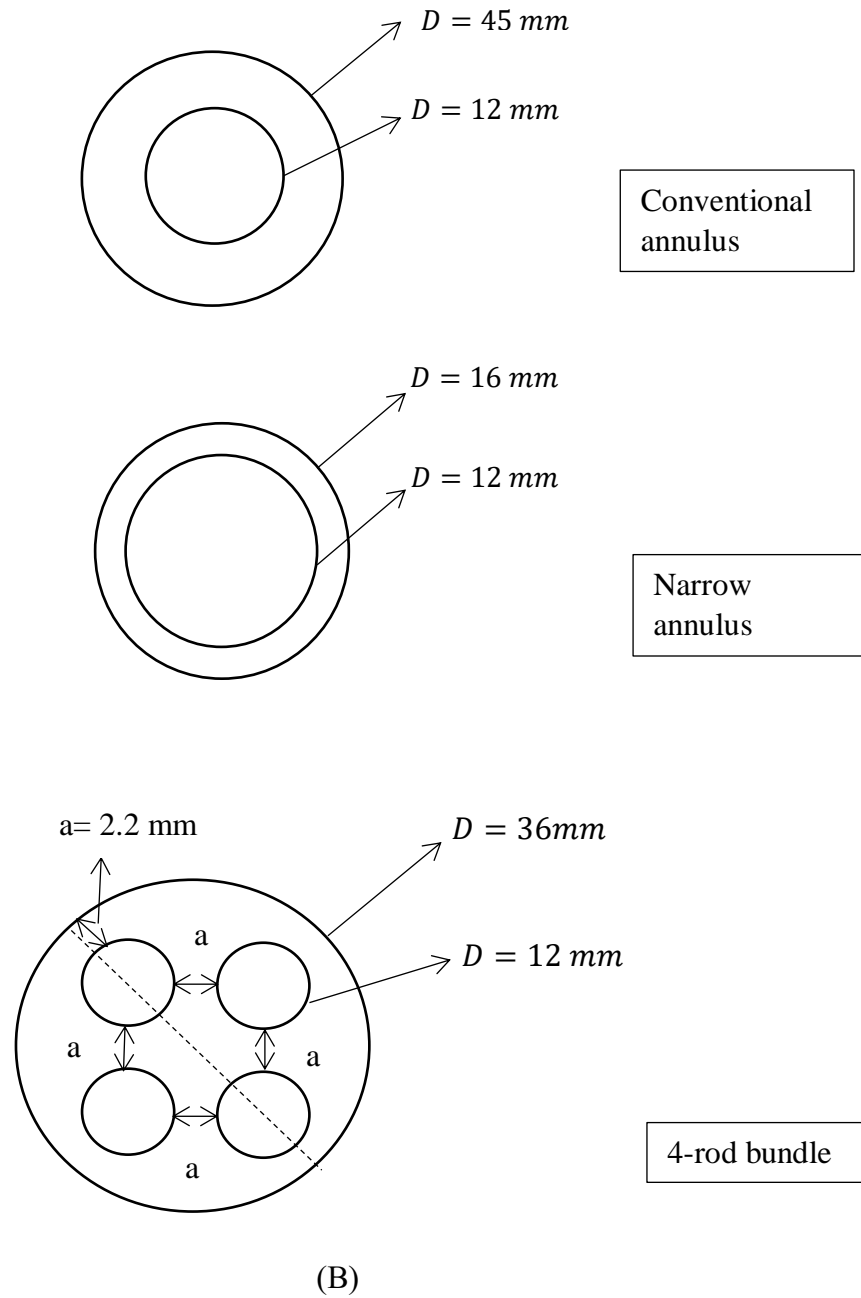
Figure 6.1 (A) Schematic diagram of experimental setup. (B) cross-sectional view of the three test sections.

K-type thermocouples were provided at five locations along the axis of all the annuli to measure the local heater surface temperature and the liquid bulk temperature, along with the inlet temperature from the reservoir. In case of the rod bundle, two thermocouples were connected to each heater rod to measure the wall temperature, while local bulk temperature measurements could not be made. An Omega FL-10 rotameter ($0 - 2000\ ml/min$) was used

to measure the inlet flow rate. A voltmeter and an ammeter were used to record the power applied to the cartridge heater. The heat flux applied to the heater was calculated by dividing the applied power by the effective surface area of the heater. The bubble dynamics were recorded using a Mikrotron Motion BLITZ Cube 4 high speed camera at a speed of $1700\ fps$ (time resolution of $0.6\ ms$) at a spatial resolution of 480×607 pixels. A zooming lens of $20 - 100\ mm$ focal length and a $1000\ W$ halogen light source was used for the camera as described in chapter 2 earlier.

6.2.2. Procedure

The distilled water in the reservoir was first heated to the desired liquid temperature. This heated water was then circulated in the loop at desired flow rate for about 30 minutes before the cartridge heater was powered on. Then the water was allowed to boil in the loop for about 2 hours to expel any trapped gases before starting the experiment. At that time, the auxiliary heater in the reservoir was switched off and the power to the cartridge heater was increased in small steps. The system was allowed to achieve a steady state, which took about 10-15 minutes and the bubble behavior was recorded for the natural sites. The experimental operating conditions for all three test sections are tabulated below in *Table 6.2*. These conditions were selected specifically to study the bubble characteristics in a natural convection BWR during startup conditions.

High speed recordings of the bubble dynamics lasting for about 3 seconds were made to estimate the bubble diameters and frequencies under various conditions. Recordings for several conditions were made 2-3 times to ensure the repeatability of the results. The image frames from the high-speed videos were manually analyzed using the ImageJ software as discussed in chapter 2. The time variation of the temperature measurements was also recorded simultaneously. Since, the temperature values fluctuated in each frame, the average values of the temperatures were used for the analysis for all conditions.

The measurement of voltage (V_o) and current (I) involve the least count errors of $\pm 0.01\ V$ and $\pm 1\ A$, respectively. The error in temperature gauging is $\pm 0.75\%$ of the measured value up to 400 °C, and that in flow rate measurement is $\pm 10\ ml/min$, which leads to an error of about $0.11\ kg/m^2 s$ in the conventional annulus, $1.84\ kg/m^2 s$ in the narrow annulus, and $0.29\ kg/m^2 s$ in the rod bundle in the measurement of mass flux. The known diameter of the heater rod ($12\ mm$) was used for the calibration of the length scale, which resulted in $1\ pixel = 0.024\ mm$. This amounts to an error of about $\pm 4.8\%$ for a bubble diameter of about $0.5\ mm$. The error in time measurement comes from the speed of the camera, and is nearly $590\ \mu s$. The frequency having been calculated as per equation (2.3) gave a maximum error of 9%. Since, the annular test sections were not insulated, the maximum heat loss from the glass walls to the ambient air was estimated to be ~2.5% for the conventional annulus, ~15% for the narrow annulus and ~20% for the bundle, and the evaporative heat loss from the reservoir was estimated to be ~7% of the applied power (Appendix C). Some other errors like change in refractive index of water with temperature, error due to test section curvature, camera zoom etc. might have occurred which cannot be quantified in this work.

Table 6.2 Experimental matrix for the three test sections.

Test section	Applied heat flux $q"\ (kW/m^2)$	Wall superheat $\Delta T_{sat}\ (K)$	Degree of subcooling $\Delta T_{sub}\ (K)$	Mass flow rate $\dot{m}\ (g/s)$	Mass flux G $(kg/m^2 s)$
Conventional annulus	40-95	0-6	10, 20, 30	10, 15, 20	6.78, 10, 13.33
Narrow annulus	1-30	0-6	5, 10	20, 30	227.27, 340.91
4-rod Bundle	1-30	0-6	5, 10	20, 30	35.37, 53.05

6.3. Results and Discussion

6.3.1. Heat transfer coefficient

The heat transfer coefficient was calculated as

$$h = \frac{q''}{T_w - T_{l,local}} = \frac{q''}{\Delta T_{sat} + \Delta T_{sub,local}} \tag{6.1}$$

The local bulk temperature has been measured in the conventional and the narrow annulus, and has been estimated for the rod bundle using heat balance. The boiling curves and the corresponding heat transfer coefficients for the conventional annulus are presented in *Figure 6.2* and *Figure 6.3* respectively. The dashed line separates the convective (on the left) and boiling regimes (right). The negative values of the wall superheat signify the wall temperatures below the saturation temperature of the liquid. It can be seen from *Figure 6.2*(A) that the boiling curves shift to the left as the inlet subcooling increases, meaning that with a decrease in bulk liquid temperature, the wall temperature achieved is a little less. It can be seen from the heat transfer coefficient curve (*Figure 6.3*(A)), that the h decreases as the degree of subcooling increases. For the single-phase region, as the local subcooling increases at any given heat flux, the ΔT_{sat} decreases slightly, resulting in a net decrease in the temperature difference, and hence, from equation (6.1), h decreases slightly. While in the boiling regime, an increased subcooling results in suppressed nucleation and delayed onset of nucleate boiling, and hence, any increase in the subcooling results in greater decrease in heat transfer coefficient.
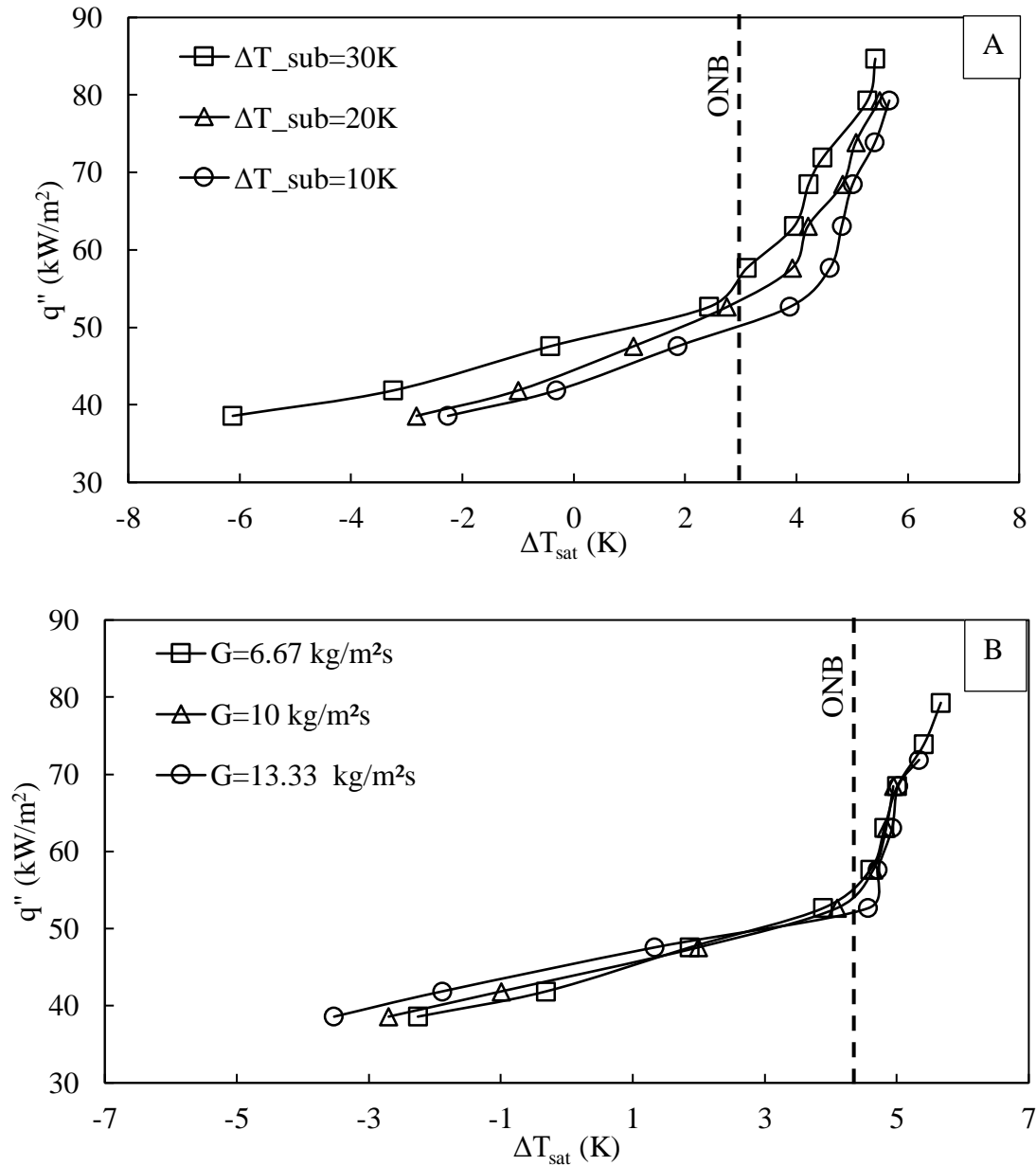
Figure 6.2 Boiling curves - Effect of (A) degree of subcooling ($G = 6.67 \; kg/m^2 s$), and (B) mass flux ($\Delta T_{sub} = 10 \; K$).

Further, as the liquid mass flux increases, the boiling curves shift to the left in the single-phase region but the curves tend to merge in the boiling regime, as shown in *Figure 6.2*(B). In the single-phase regime, an increase in flow velocity results in a faster heat removal from the heater surface giving a lower wall temperature and hence, a higher convective heat transfer coefficient (*Figure 6.3*(B)). Although, the boiling curves merge in the nucleate boiling regime, showing that the two-phase heat transfer is almost independent of the mass flux, indicating that

the nucleate boiling is the dominant mechanism. Similar results were obtained by Del Valle and Kenning (1985), Thorncroft *et al.* (1998) and Bang *et al.* (2004). The heat transfer coefficients estimated experimentally have also been compared with the predictions of two of the most widely used boiling heat transfer coefficient models. The Gungor and Winterton (1986) model is a modified version of the well-known Chen correlation and is given as

$$h_{TP} = (SS_2 + FF_2)h_{sp} \tag{6.2}$$

Where

$$h_{sp} = 0.023Re_l^{0.8}Pr_l^{0.4}(k_l/D) \tag{6.3}$$

$$S = 1 + 3000Bg^{0.86} \tag{6.4}$$

$$S_2 = \begin{cases} Fr_l^{(0.1-2Fr_l)}, & for\ horizontal, or\ Fr_l < 0.05 \\ 1, otherwise \end{cases} \tag{6.5}$$

$$F = 1.12\left(\frac{x}{1-x}\right)^{0.75}\left(\frac{\rho_l}{\rho_v}\right)^{0.41} \tag{6.6}$$

$$F_2 = \begin{cases} Fr_l^{1/2}, for\ horizontal\ or\ Fr_l < 0.05 \\ 1, otherwise \end{cases} \tag{6.7}$$

Here, the parameters S, S_2 are the suppression factors to account for the suppression of wall superheat and nucleation due to the forced convection, and F, F_2 are the enhancement factors that account for the enhanced convective heat transfer due to increase in velocities in two phase-flow, even at lowest of vapor qualities. Bg is the boiling number and Fr_l is the liquid Froude number defined as

$$Fr_l = \frac{G^2}{\rho_l^2 gD} \tag{6.8}$$

The second model used for comparison is the Kandlikar (1990) model, originally given for flow boiling inside a tube. The model divides the two-phase heat transfer regime into two parts based on the value of convection number (Co). For $Co < 0.65$,

$$h_{TP} = h_{sp}\left[1.136Co^{-0.9}(25Fr_l)^{0.3} + 667.2(Bg^{0.7}F_{fl})\right] \tag{6.9}$$

And for $Co > 0.65$

$$h_{TP} = h_{sp}\left[0.6683 Co^{-0.2}(25 Fr_l)^{0.3} + 1058(Bg^{0.7}F_{fl})\right] \tag{6.10}$$

Where

$$Co = \left(\frac{1-x}{x}\right)^{0.8}\left(\frac{\rho_v}{\rho_l}\right)^{0.5} \tag{6.11}$$

It can be seen from *Figure 6.3* that though the experimentally estimated values are in close range of the predicted values, the Gungor and Winterton (1986) model is unable to predict the influence of subcooling on the two-phase heat transfer as it does not account for it, and the effect of the velocity is also a little underpredicted. The Kandlikar (1990) model severely under predicts the data in both the cases, probably because it was not validated for the annular geometry.

(A)

(B)
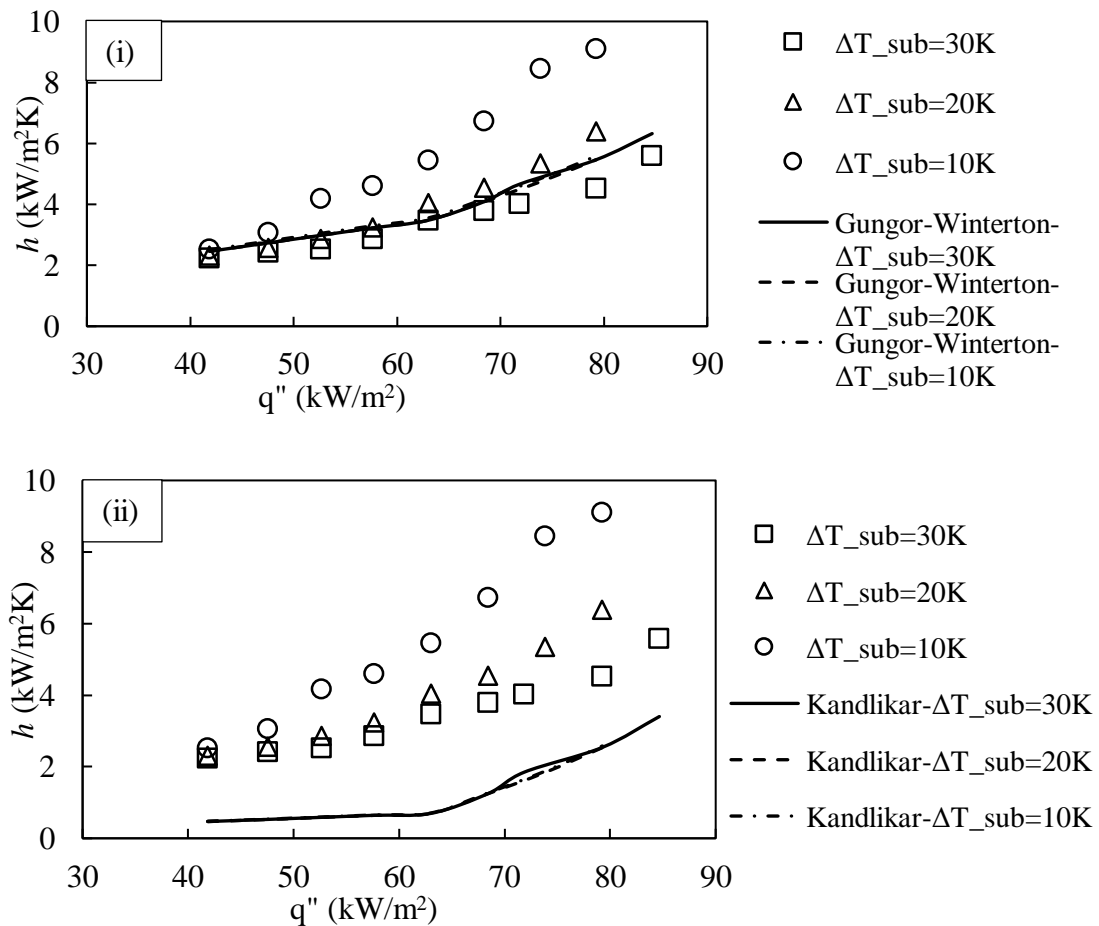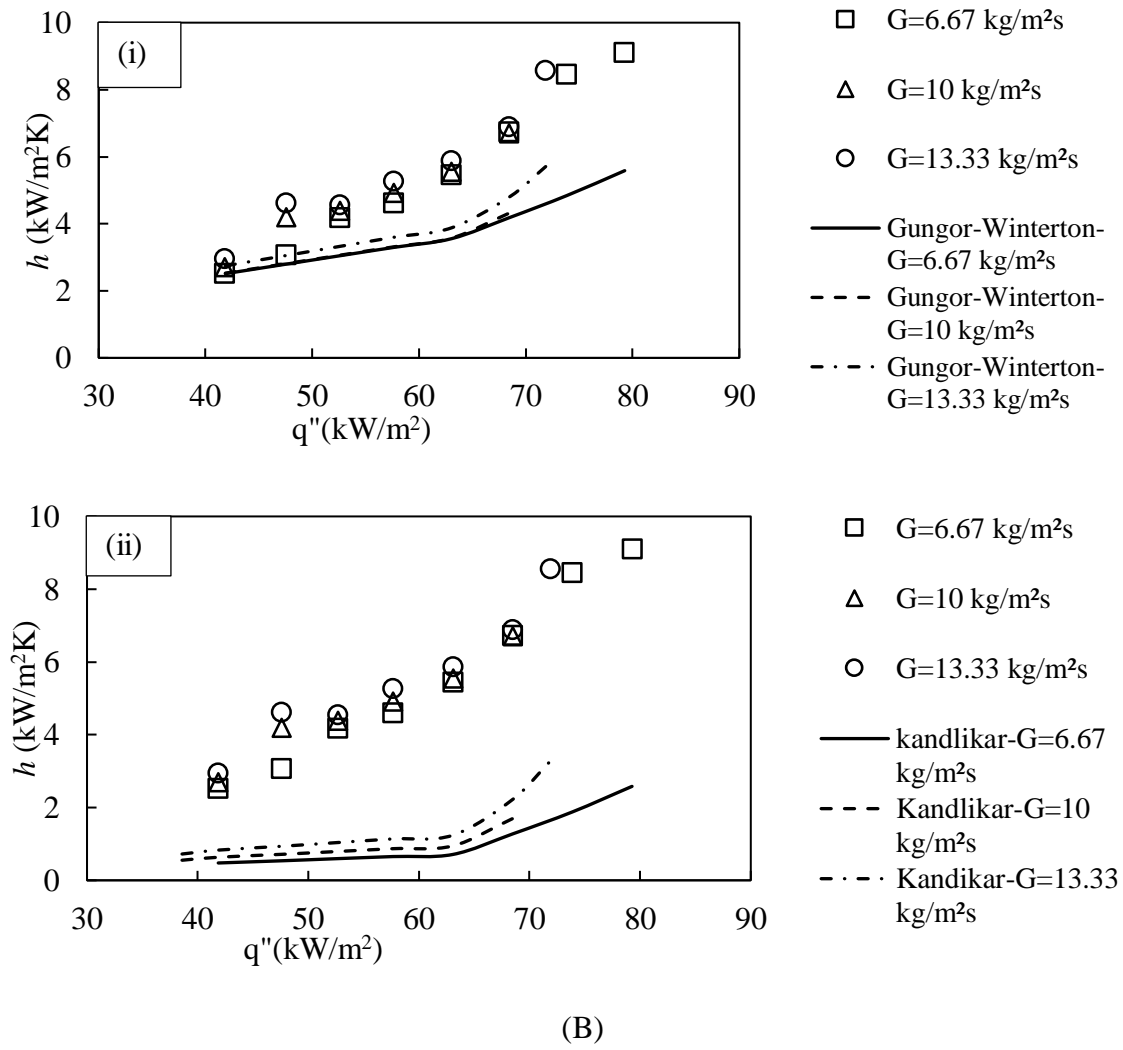
Figure 6.3 Heat transfer coefficient - Effect of (A) degree of subcooling ($G = 6.67\ kg/m^2 s$), and (B) mass flux ($\Delta T_{sub} = 10\ K$).

Next, the boiling curves and corresponding heat transfer coefficients for the narrow annulus and the rod bundle were studied. The boiling curves for the rod bundle presented here, are for only one rod in the bundle, which is heated. As seen in *Figure 6.4*, the boiling curves for the narrow annulus and bundle behave similar to that for conventional or wide annulus, with the degree of subcooling. The heat transfer coefficient decreases with an increase in the subcooling, however, for the same range of heat flux, the heat transfer coefficient for the confined cases (narrow annulus and the bundle) would be higher than that for the conventional annulus, as can be observed from the interpolations in *Figure 6.4*(B).
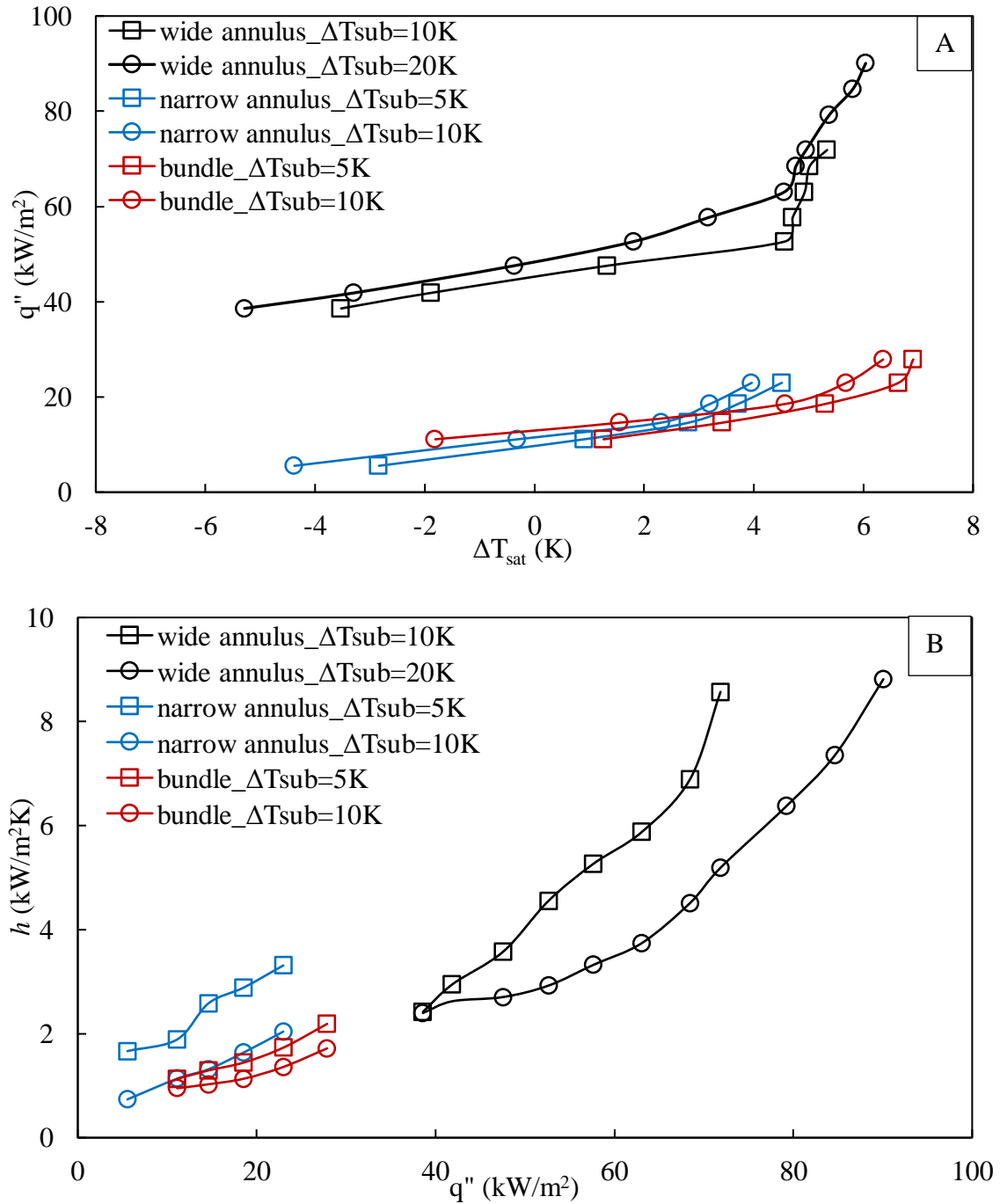
Figure 6.4 Effect of degree of subcooling on (A) boiling curves and (B) heat transfer

coefficient for the three test sections (20 *g/s*).

Again, from *Figure 6.5*, we see that the boiling curves shift to the left with an increase

in the mass flux in the single-phase region and tend to merge in the nucleate boiling region.

Hence, the heat transfer coefficient increases in the single-phase region with an increase in

flow velocity, but shows no significant change in the nucleate boiling regime. The heat transfer

coefficient for the wide annulus increase by about 20% in the single-phase region ($q'' <$ 60 kW/m^2), while the increase in heat transfer coefficient in the nucleate boiling regime is nearly 3-4%. The heat transfer coefficients in the narrow annulus and bundle would again be higher than those in the conventional annulus in the similar range of heat flux, though *Figure 6.5* shows that the influence on mass flux was less in the confined test sections compared to the wide annulus. The increase in heat transfer coefficient in the narrow annulus and the rod bundle being about 2% and 3.5%, respectively. This indicates that the forced convection effects are less important in the confined geometries in the observed range of conditions.
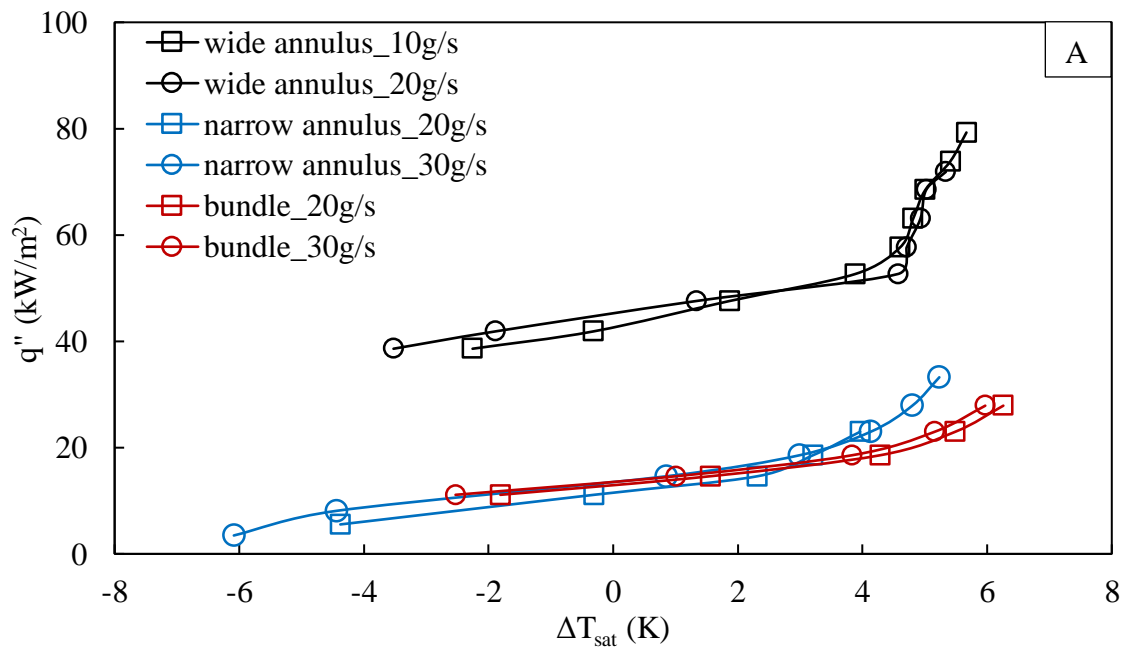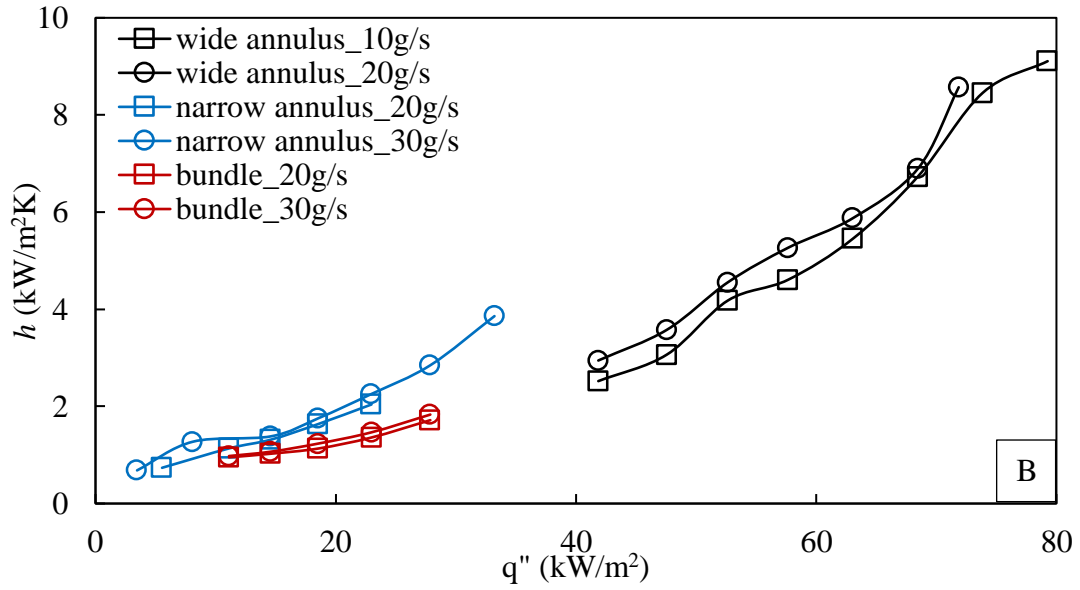
Figure 6.5 Effect of mass flux on (A) boiling curves and (B) heat transfer coefficient for the three test sections ($\Delta T_{sub} = 10K$).

Lastly, the heat transfer coefficient for the observed rod, with different number of rods heated in the bundle were studied. The total power to the bundle is supplied such that the heat flux on each heater remains the same as in case 1. As shown in *Figure 6.6*, as more number of rods are heated, the heat transfer coefficient of a single rod increases. This can be attributed to the higher local bulk temperature achieved due to multiple rods being heated, which would increase the convective heat transfer, and also hasten the nucleation process, increasing the total two phase heat transfer.
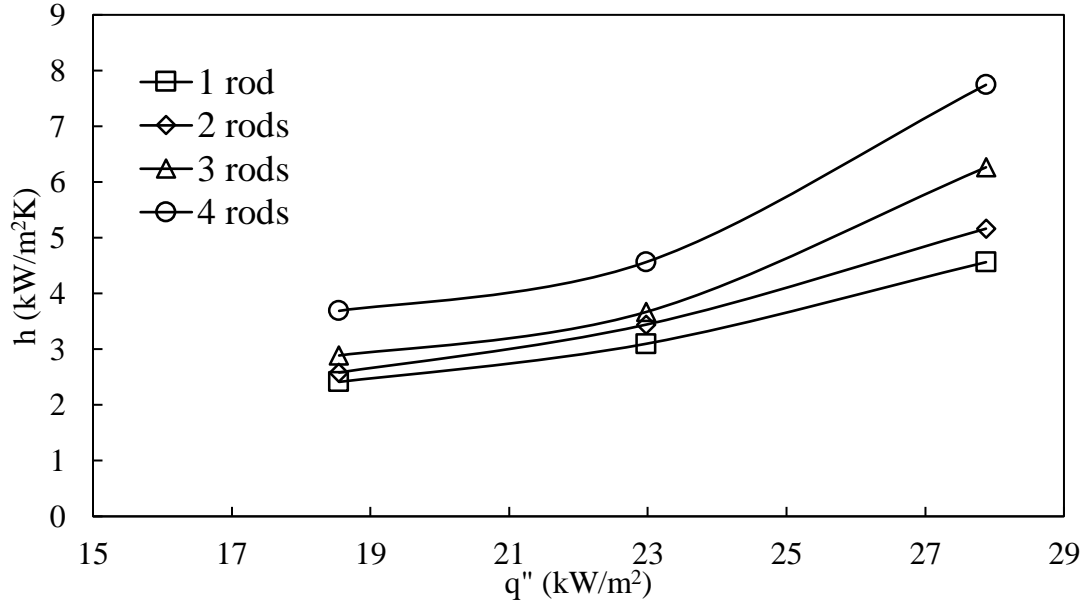
Figure 6.6 Heat transfer coefficient for the observed rod with different number of heated rods.

6.3.2. Bubble growth and condensation

The observation zone was set in the section of length 10 mm at a height of about 500 mm from the inlet in all three test sections. It was seen that the various bubbles growing at different nucleation sites on the heater surface have different sizes. *Figure 6.7* shows the growth curves of a typical vapor bubble in three test sections, where the bubbles depart from their nucleation sites, a few milliseconds after their inception and grow while sliding on the heater surface. The data points highlighted in black, red and green reflect the departure, maximum and the lift-off points, respectively. The bubbles grow because of evaporation in the superheated thermal boundary layer at the surface and the microlayer beneath the bubbles. As the bubble grows, the temperature of the superheated layer and heater surface decreases, and hence, we see a fall in growth rate after some time. Further, with increase in bubble size, their cap comes in contact with the subcooled liquid where the condensation begins. Thus, there is a competition between evaporation at the heater wall in superheated layer and the condensation at the bubble cap. So, the bubbles grow to achieve a maximum size when the rate of evaporation becomes equal to the rate of condensation, and beyond this point the condensation starts to

dominate. After some time, the bubble leaves the heater surface and gets ejected into the bulk liquid where it quickly condenses completely. *Figure 6.8* presents the growth and condensation of a typical bubble in the conventional annulus, which can be seen to go through each of the above described process.
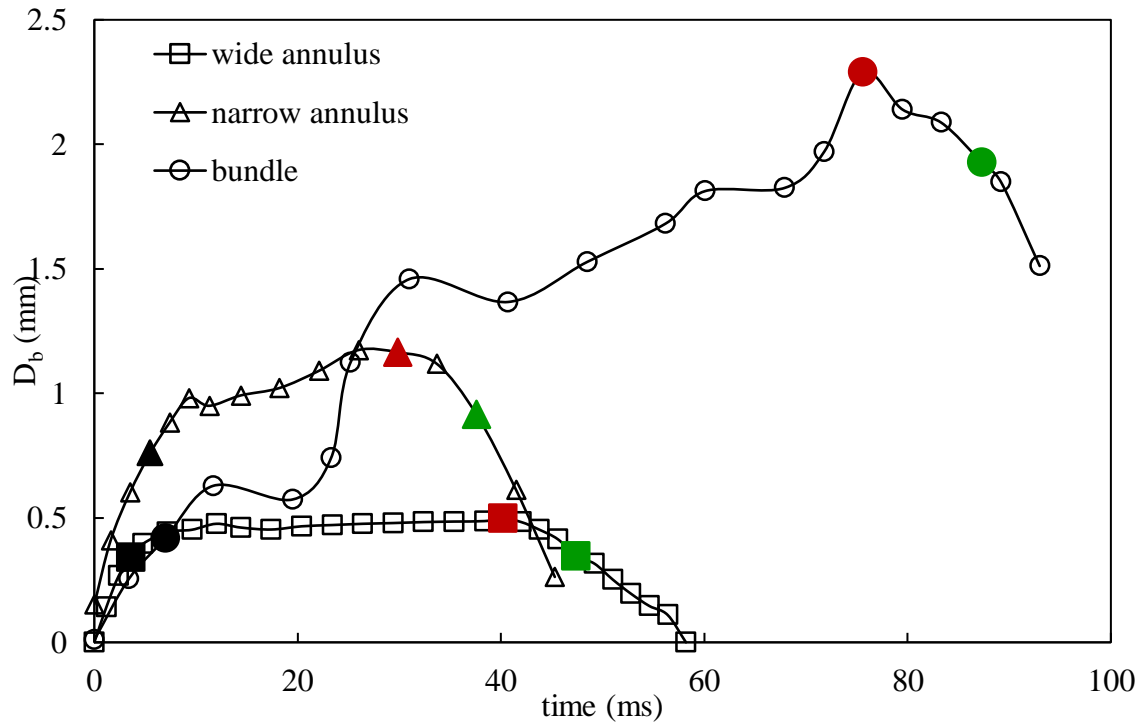
Figure 6.7 Growth and condensation curve of a typical vapor bubble (solid black points show departure; red points show maximum size and green points show lift-off).
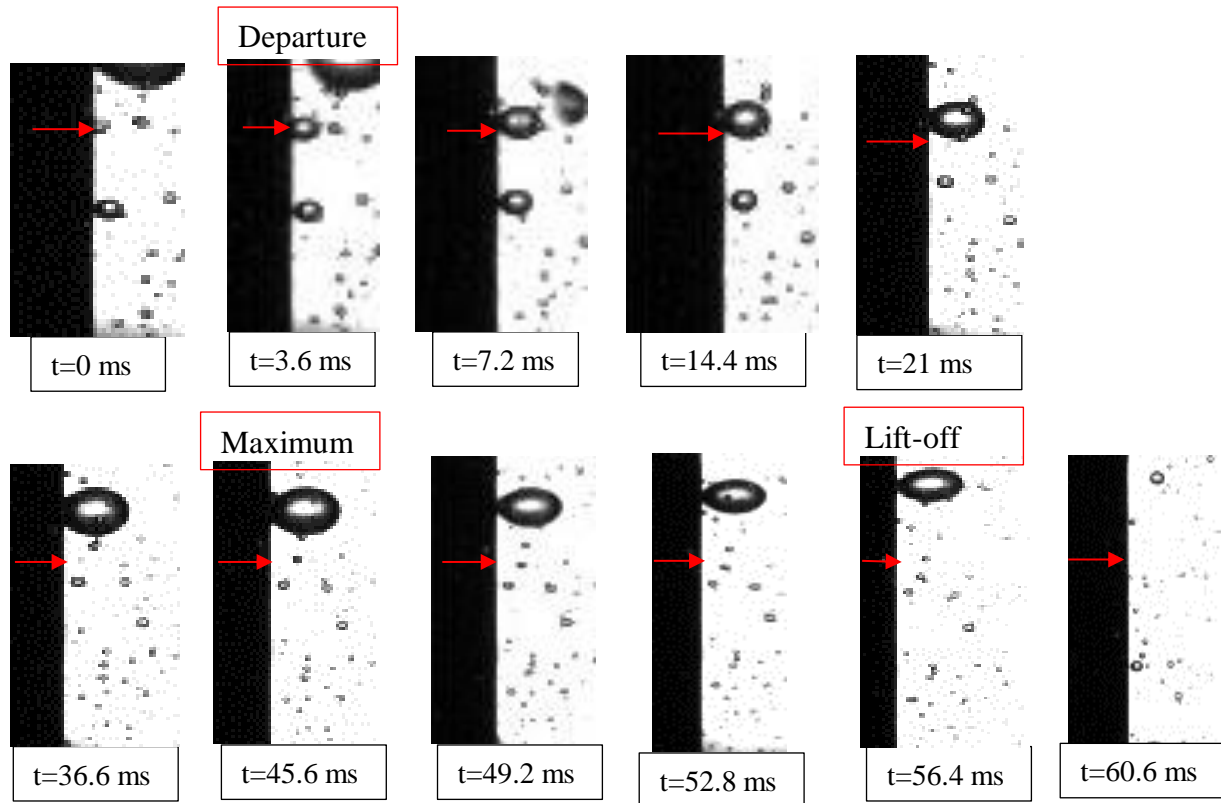
Figure 6.8 Growth and collapse of a typical bubble in wide annulus ($q'' = 68.46\ kW/m^2, \Delta T_{sub} = 10\ K, G = 10\ kg/m^2\ s$).

In addition to the basic growth behavior described above, three different kinds of bubble growths could be observed in the narrow annulus. First, were the *individual bubbles*, that have life cycle similar to the ones observed in the wide annulus. Second, were the *merged bubbles* - bubbles that nucleated close to each other, and merged to form a single bubble in the early periods of their growth cycles, and then slid and lifted as a single entity. Third, were the *confined bubbles* – due to the smaller gap between the heater and the glass tube, some bubbles grew to touch the glass surface. These bubbles then elongated rather than growing radially. The bubble growth in both the cases, was observed to be faster than the growth rate in the conventional annulus, and major growth of the bubbles occurred during the sliding phase. Three kinds of bubble growth patterns are presented in *Figure 6.9*, where the red arrows mark the nucleation sites of the concerned bubbles.

(A)

(B)

| 0 ms | 4 ms | 8 ms | 12 ms | 16 ms |

| 20 ms | 24 ms | 28 ms | 32 ms |
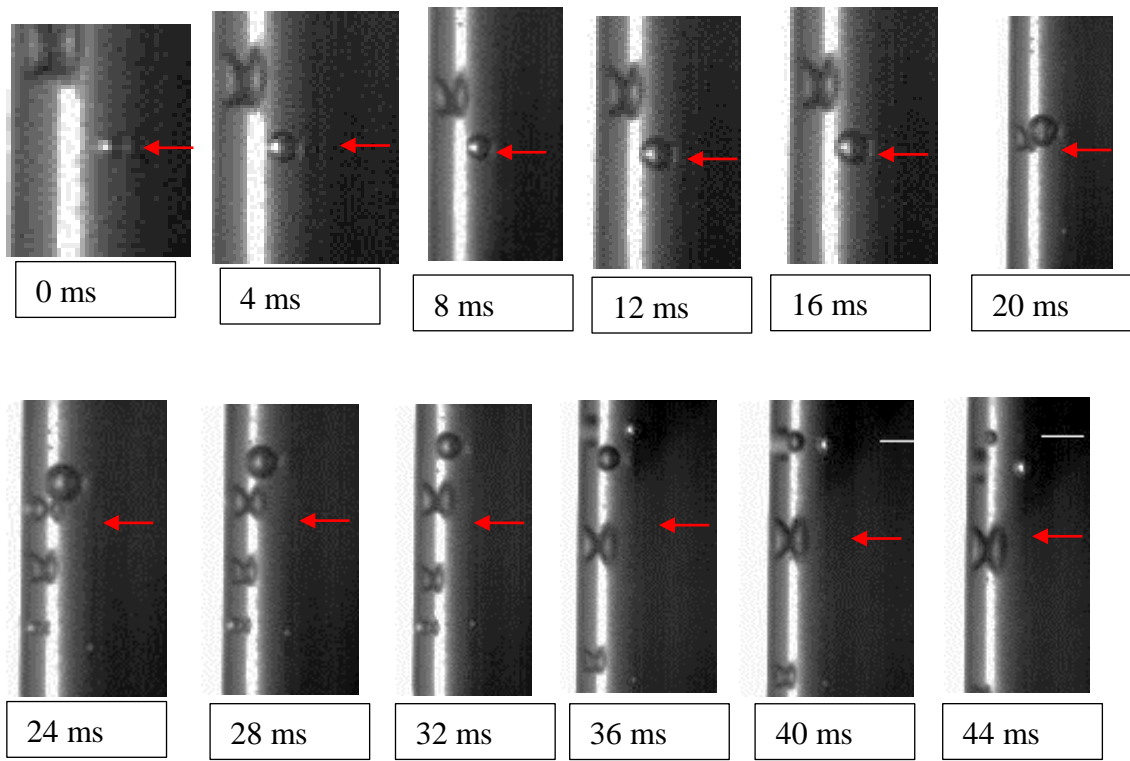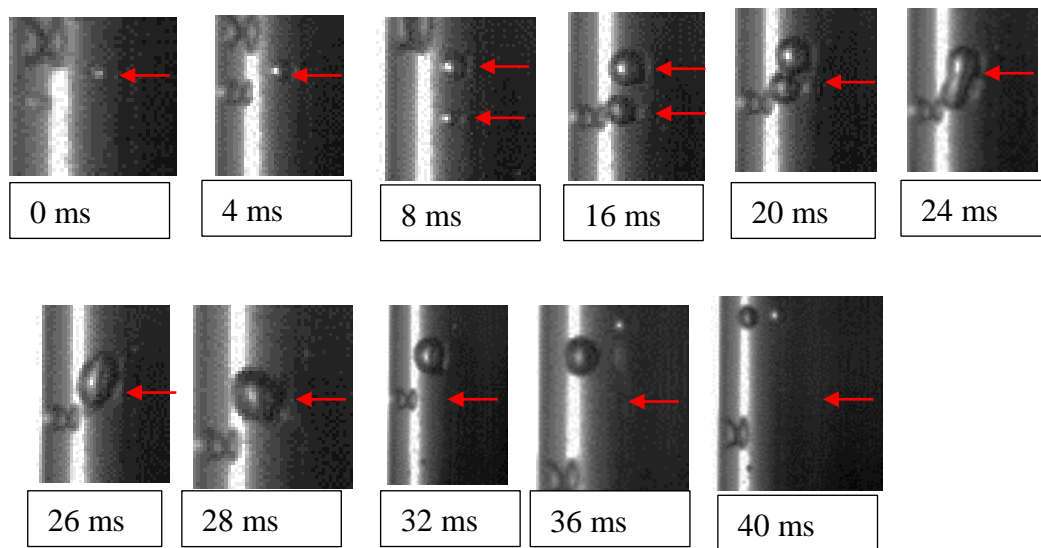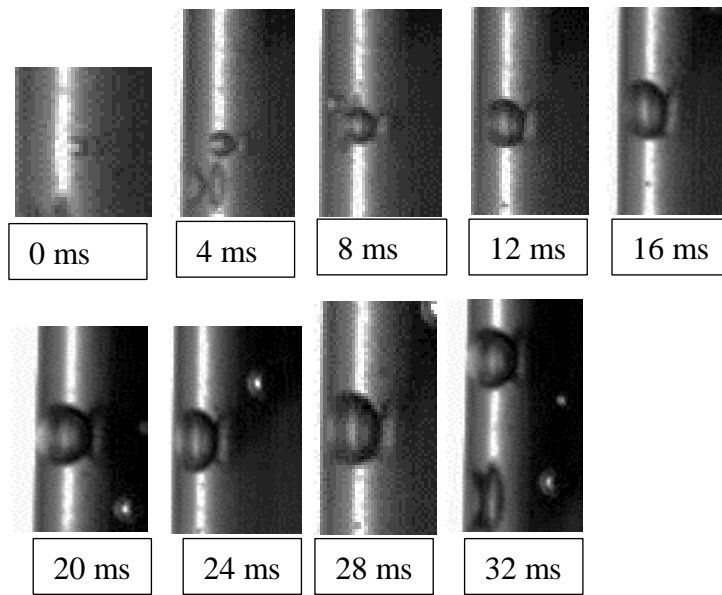
(C)

Figure 6.9 Growth cycle of bubbles in narrow annulus- (A) isolated bubbles, (B) merging bubbles, (C) confined bubbles.

Finally, it was observed that the heater rods had a large number of nucleation sites in the bundle, under the presently used operating conditions. The bubbles nucleated at their sites, grew to a size, then departed from their nucleation site to merge with a nearby bubble. The coalesced bubble then started sliding, where it oscillated between growing and condensing, merged with another bubble encountered in its sliding path, till it achieved a maximum size; after which it started to condense and lifted off soon after to collapse in the bulk liquid. It can be seen in *Figure 6.10*, that the two closely nucleated bubbles (marked by red arrows) coalesce at about $16\ ms$ to form a single bubble, this bubble then slides up and merges with another bubble in its vicinity at about $36\ ms$. Thus formed large bubble starts to slide along the heater surface, where it condenses a little because of exposure to the subcooled liquid, but then coalesces with another bubble at $60\ ms$. This bubble then slides up the heater surface, and starts to neck around $92\ ms$ and lifts from the surface around $96\ ms$.

| 0 ms | 8 ms | 12 ms | 16 ms | 24 ms |

| 36 ms | 48 ms | 56 ms | 60 ms | 68 ms |

| 76 ms | 84 ms | 92 ms | 96 ms |
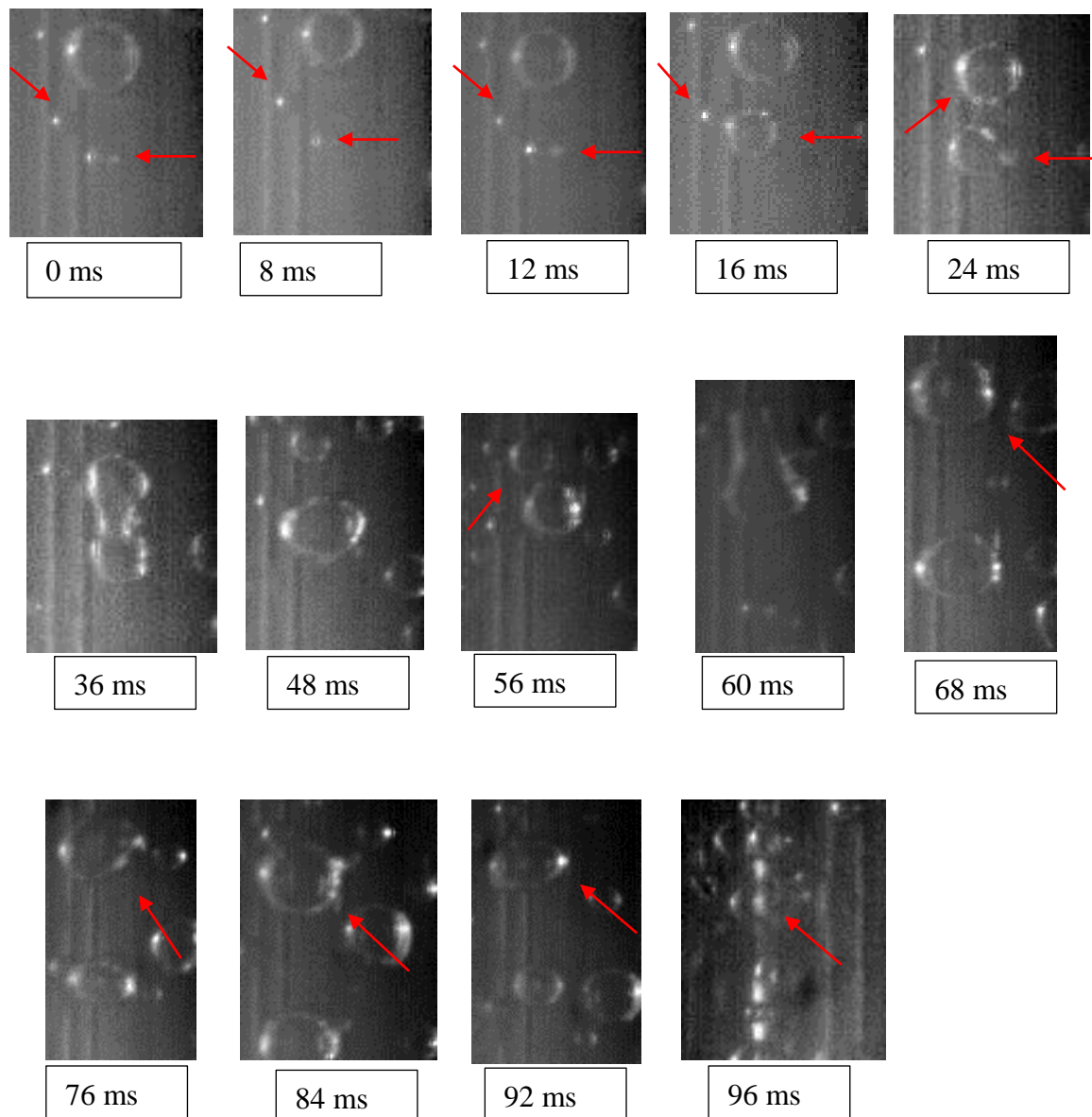
Figure 6.10 Growth pattern of a typical bubble in rod bundle.

Figure 6.11 demonstrates the growth and condensation curves of various bubbles under identical conditions. It can be seen that the growth rates are almost identical for all the bubbles nucleating under identical conditions, but the bubble maximum, departure and lift off diameters, and bubble lifetimes vary. This can be attributed to the local fluctuations in thermal and velocity fields.
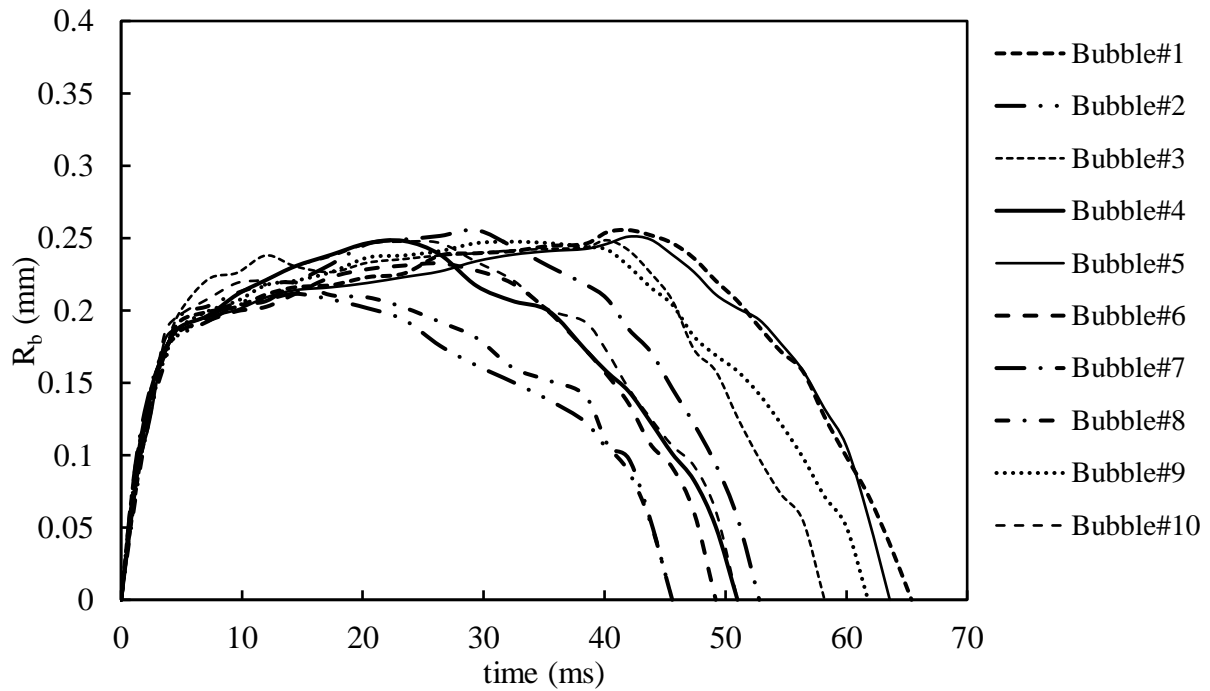
Figure 6.11 Bubble growth curves for various bubbles for wide annulus for $q'' = 63.06\ kW/m^2$, $\Delta T_{sub} = 20\ K$, $G = 10\ kg/m^2s$.

A bubble growing on a nucleation site is acted upon by various forces in the direction parallel and perpendicular to the flow. The bubble starts to slide along the heater surface, when the net forces (surface tension, buoyancy, drag and growth forces) in the x-direction become greater than zero, while the forces in the y-direction (surface tension, growth force, pressure forces and lift force) remain in equilibrium. As the bubble moves along the surface, it grows taking up heat from the superheated layer near the heater wall and the microlayer trapped between the bubble and the wall. Initially, as the bubble size increases, its contact diameter increases slightly, but as the microlayer beneath the bubble evaporates, the contact diameter shrinks and the bubble is observed to elongate as it grows, as shown in *Figure 6.12*. Further, the bubble was observed to start out slowly, but the velocity increased with the distance, quickly becoming higher than the bulk liquid velocity. The bubbles were seen to slide for about $4 - 12\ mm$ on an average growing on the heater surface in both the annuli. Thorncroft *et al.* (1998) obtained similar sliding behavior and suggested that due to the bubble leading the liquid

flow around it, the resulting shear causes the lift force to push the bubble against the wall, thereby causing long sliding distances. However, the sliding distances were observed to be significantly longer for the bubbles in the bundle due its coalescing pathway, under present experimental conditions.
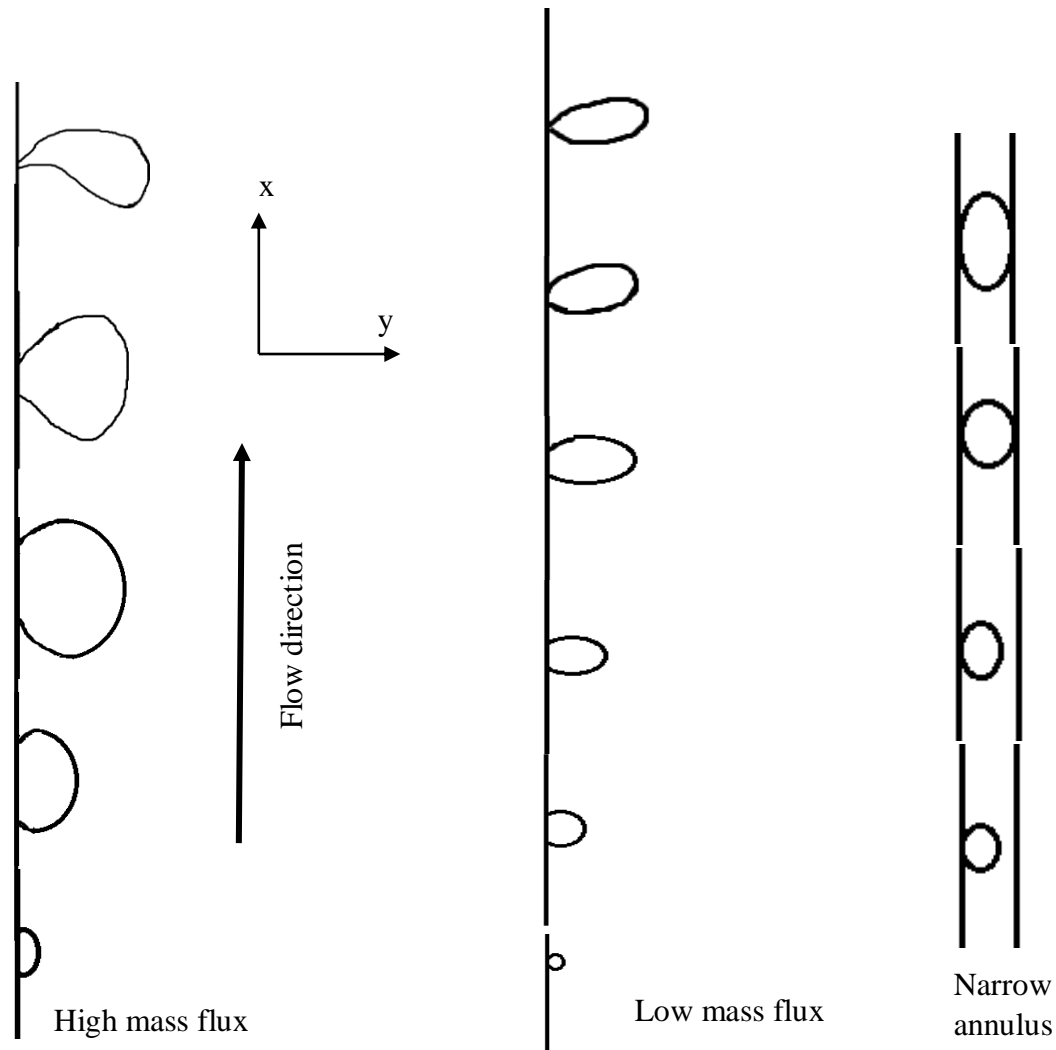
Figure 6.12 Bubble shapes during sliding motion

As reported in the literature for high liquid mass fluxes (Bibeau and Salcudean (1994), Ahmadi *et al.* (2012), Cao *et al.* (2016)), a sliding bubble significantly changes its shape as it grows while sliding on the heater surface. The tiny spherical bubble departed from the nucleation cavity, initially grows into a hemispherical shape with a large contact diameter. Then, the evaporation of the microlayer starts to cause necking, decreasing the contact

diameter. During this time, the shearing effect of the flow causes the deformation in the upstream side of the bubble, leading it to assume a so-called inverted pear like shape (*Figure 6.12*). The bubble lifts-off from the surface, when the net force in the y-direction become greater than zero. However, the present studies have all been carried out for very small mass flow rate values, where the shearing effect was not high enough to cause the above-mentioned deformation of the bubbles. Hence, necking with only elongation of the fairly symmetric bubbles was observed (*Figure 6.12*). Even though the velocities in the narrow annulus were fairly at the same mass flow rates due to the lower cross section area, the confinement of the bubbles did not allow for the bubble deformation, rather the bubbles either grew symmetrically or grew elongated being constrained between the heater and the glass wall.

6.3.3. Bubble departure characteristics

The vapor bubble diameters and frequencies were measured using the high-speed images. For each experimental case, few nucleating sites which were regular in their activity were selected. The bubbles departing from these sites were then observed for the departure, maximum and lift-off diameters and frequency. Such measurements were made for 40-50 bubbles per case. The statistical average of the diameter and frequency for a particular case, taking all the regular sites into account were used in the parametric studies. In case of the rod bundle, bubble measurements were made on one heater rod with different number of rods heated in the bundle. The obtained average values of maximum, departure and lift-off diameters and frequency for all three test sections are given in *Table 6.3* through *Table 6.5*. The standard deviation and 95% confidence intervals were calculated for each case population in addition to the mean values. For brevity, the values for all three measured diameters and frequency for some of the experimental cases are shown in *Table 6.6*.

Table 6.3 Bubble diameters and frequency measurements for flow boiling in the conventional annulus.

Expt. No.	Mass flux G (kg/m^2s)	Heat flux q'' (kW/m^2)	Inlet subcooling $\Delta T_{sub,in}$ (K)	Local subcooling $\Delta T_{sub,local}$ (K)	Wall superheat ΔT_{sat} (K)	Departure diameter D_d (mm)	Maximum diameter D_{max} (mm)	Lift-off diameter D_{lo} (mm)	Departure frequency f (s^{-1})
1.1a	6.67	57.658	10	7.9	4.6	0.382	0.734	0.526	15.8228
1.1b	6.67	63.059	10	6.7	4.8	0.416	0.816	0.658	18.9394
1.1c	6.67	68.461	10	5.2	5.0	0.455	0.922	0.769	23.9234
1.1d	6.67	71.863	10	3.3	5.4	0.531	1.036	0.962	32.5733
1.1e	6.67	79.265	10	3.0	5.7	0.586	1.227	1.07	40.9836
1.2a	6.67	57.658	20	10.9	3.9	0.355	0.506	0.35	13.2979
1.2b	6.67	63.059	20	10.4	4.7	0.394	0.625	0.514	16.2338
1.2c	6.67	68.461	20	9.2	4.8	0.432	0.715	0.663	20.5761
1.2d	6.67	71.863	20	8.8	5.1	0.468	0.907	0.703	27.3224
1.2e	6.67	79.265	20	6.9	5.5	0.504	1.026	0.901	34.9650
1.3a	6.67	63.059	30	14.2	4.5	0.339	0.496	0.316	11.7096
1.3b	6.67	68.461	30	13.8	4.7	0.392	0.582	0.491	13.4771

Expt. No.	Mass flux G (kg/m^2s)	Heat flux q'' (kW/m^2)	Inlet subcooling $\Delta T_{sub,in}$ (K)	Local subcooling $\Delta T_{sub,local}$ (K)	Wall superheat ΔT_{sat} (K)	Departure diameter D_d (mm)	Maximum diameter D_{max} (mm)	Lift-off diameter D_{lo} (mm)	Departure frequency f (s^{-1})
1.3c	6.67	71.863	30	13.4	4.9	0.425	0.755	0.614	15.9774
1.3d	6.67	79.265	30	12.2	5.3	0.452	0.874	0.795	20.1207
1.3e	6.67	84.667	30	9.7	5.4	0.476	0.988	0.88	26.5252
1.4a	10	52.648	10	7.9	4.1	0.318	0.601	0.416	11.6686
1.4b	10	57.658	10	6.9	4.6	0.379	0.665	0.498	12.85315
1.4c	10	63.059	10	6.1	4.8	0.407	0.792	0.583	15.015
1.4d	10	68.461	10	5.1	4.9	0.426	0.874	0.714	18.0832
1.5a	10	63.059	20	10.6	4.6	0.386	0.593	0.443	11.7509
1.5b	10	68.461	20	9.7	4.8	0.404	0.676	0.576	12.5945
1.5c	10	71.863	20	8.4	5.1	0.459	0.835	0.681	15.0602
1.5d	10	79.265	20	7.5	5.5	0.492	0.949	0.804	21.0084
1.5e	10	84.667	20	4.6	5.7	0.581	1.034	0.895	28.9017
1.5f	10	90.069	20	4.6	5.9	0.613	1.197	0.982	36.9004

Expt. No.	Mass flux G (kg/m^2s)	Heat flux q'' (kW/m^2)	Inlet subcooling $\Delta T_{sub,in}$ (K)	Local subcooling $\Delta T_{sub,local}$ (K)	Wall superheat ΔT_{sat} (K)	Departure diameter D_d (mm)	Maximum diameter D_{max} (mm)	Lift-off diameter D_{lo} (mm)	Departure frequency f (s^{-1})
1.6a	10	68.461	30	14.8	3.9	0.371	0.513	0.414	10.8814
1.6b	10	71.863	30	14.0	4.3	0.409	0.684	0.573	12.8535
1.6c	10	79.265	30	13.1	4.8	0.433	0.739	0.692	17.8891
1.6d	10	84.667	30	10.7	5.5	0.464	0.882	0.715	22.1729
1.6e	10	90.069	30	11.2	5.7	0.512	0.957	0.833	33.1126
1.7a	13.33	52.648	10	6.5	4.6	0.301	0.565	0.341	10.8578
1.7b	13.33	57.657	10	6.9	4.7	0.353	0.613	0.427	12.1655
1.7c	13.33	63.059	10	6.1	4.9	0.394	0.748	0.486	14.0252
1.7d	13.33	68.461	10	5.3	5.0	0.416	0.822	0.534	16.7504
1.7e	13.33	71.863	10	3.0	5.3	0.535	0.899	0.611	19.4553
1.8a	13.33	63.059	20	10.3	4.6	0.361	0.531	0.408	10.846
1.8b	13.33	68.461	20	9.4	4.8	0.401	0.627	0.484	11.7096
1.8c	13.33	71.863	20	8.9	4.9	0.437	0.786	0.565	13.7931

Expt. No.	Mass flux G (kg/m^2s)	Heat flux q'' (kW/m^2)	Inlet subcooling $\Delta T_{sub,in}$ (K)	Local subcooling $\Delta T_{sub,local}$ (K)	Wall superheat ΔT_{sat} (K)	Departure diameter D_d (mm)	Maximum diameter D_{max} (mm)	Lift-off diameter D_{lo} (mm)	Departure frequency f (s^{-1})
1.8d	13.33	79.265	20	7.0	5.4	0.482	0.865	0.623	17.5439
1.8e	13.33	84.667	20	4.7	5.8	0.544	0.972	0.681	21.5983
1.8f	13.33	90.069	20	4.2	6.0	0.603	1.085	0.749	29.5858
1.9a	13.33	68.461	30	18.2	4.1	0.304	0.497	0.374	10.4275
1.9b	13.33	71.863	30	17.6	4.6	0.318	0.568	0.439	12.0773
1.9c	13.33	79.265	30	16.2	4.9	0.354	0.661	0.497	15.7233
1.9d	13.33	84.667	30	12.0	5.3	0.399	0.784	0.555	20.6186
1.9e	13.33	90.069	30	14.1	5.6	0.427	0.842	0.616	27.8552
1.9f	13.33	95.471	30	13.8	6.3	0.554	0.911	0.702	36.7647

Table 6.4 Bubble diameters and frequency measurements for flow boiling in narrow annulus.

Expt. No.	Mass flux G $(kg/m^2 s)$	Heat flux q'' (kW/m^2)	Inlet subcooling $\Delta T_{sub,in}$ (K)	Local subcooling $\Delta T_{sub,local}$ (K)	Wall superheat ΔT_{sat} (K)	Departure diameter D_d (mm)	Maximum diameter D_{max} (mm)	Lift-off diameter D_{lo} (mm)	Departure frequency f (s^{-1})
2.1a	227.273	14.605	10.6	11.9	2.3	0.438	1.221	0.742	6.1543
2.1b	227.273	18.549	10.4	10.1	3.2	0.503	1.285	0.813	10.1679
2.1c	227.273	22.977	9.9	8.8	3.9	0.597	1.398	0.957	17.6548
2.2a	227.273	14.605	5.3	2.8	2.8	0.477	1.261	0.834	8.2677
2.2b	227.273	18.549	4.7	2.7	3.7	0.551	1.355	0.943	13.6574
2.2c	227.273	22.977	4.5	2.4	4.5	0.645	1.492	1.116	21.1655
2.3a	340.909	22.977	9.4	6.1	4.1	0.548	1.337	0.851	15.3897
2.3b	340.909	27.875	9.1	5.0	4.8	0.616	1.436	0.933	19.2676
2.3c	340.909	33.216	8.7	3.4	5.2	0.724	1.516	1.061	26.4871
2.4a	340.909	18.549	5.0	3.4	3.5	0.535	1.307	0.846	11.1657
2.4b	340.909	22.977	4.9	2.8	4.6	0.613	1.417	0.991	18.8599
2.4c	340.909	27.875	4.8	2.1	5.9	0.741	1.522	1.146	26.5947

Table 6.5 Bubble diameter and frequency measurements for flow boiling in rod bundle.

Expt. no.	No. of heated rods	Mass flux G $(kg/m^2 s)$	Heat flux q'' (kW/m^2)	Inlet subcooling $\Delta T_{sub,in}$ (K)	Wall superheat ΔT_{sat} (K)	Departure diameter D_d (mm)	Maximum diameter D_{max} (mm)	Lift-off diameter D_{lo} (mm)	Departure frequency f (s^{-1})
3.11a	1	35.368	18.549	10	4.3	0.796	2.313	1.597	2.413
3.11b		35.368	22.978	9.9	5.5	1.183	2.631	1.707	3.098
3.11c		35.368	27.876	9	6.3	1.322	2.846	1.895	4.562
3.12a	2	35.368	18.549	10.1	4.6	0.975	2.494	1.672	2.582
3.12b		35.368	22.978	9.8	5.6	1.544	2.775	1.867	3.442
3.2c		35.368	27.876	9.7	6.4	1.636	2.919	1.972	5.163
3.13a	3	35.368	18.549	10.3	4.6	1.165	2.643	1.743	2.887
3.13b		35.368	22.978	9.9	5.6	1.668	2.922	1.892	3.669
3.13c		35.368	27.876	9.6	5.6	1.892	3.133	2.006	6.264
3.14a	4	35.368	18.549	10.2	4.6	1.116	2.796	1.823	3.688
3.14b		35.368	22.978	9.8	5.7	1.826	3.065	1.934	4.564
3.14c		35.368	27.876	9.5	6.6	1.975	3.321	2.019	7.744

Expt. no.	No. of heated rods	Mass flux G (kg/m^2s)	Heat flux q'' (kW/m^2)	Inlet subcooling $\Delta T_{sub,in}$ (K)	Wall superheat ΔT_{sat} (K)	Departure diameter D_d (mm)	Maximum diameter D_{max} (mm)	Lift-off diameter D_{lo} (mm)	Departure frequency f (s^{-1})
3.21a	1	35.368	18.549	5.1	5.3	0.864	2.385	1.638	2.668
3.21b		35.368	22.978	4.6	6.6	1.235	2.713	1.853	3.245
3.21c		35.368	27.876	4.4	6.9	1.454	2.976	1.974	4.713
3.22a	2	35.368	18.549	5.2	5.4	1.135	2.537	1.749	2.864
3.22b		35.368	22.978	4.9	6.6	1.613	2.886	1.963	3.661
3.22c		35.368	27.876	4.7	7.1	1.732	3.034	2.165	5.513
3.23a	3	35.368	18.549	5.2	5.4	1.213	2.776	1.851	3.089
3.23b		35.368	22.978	4.8	6.6	1.753	3.064	2.113	3.864
3.23c		35.368	27.876	4.7	7.1	1.969	3.247	2.248	6.131
3.24a	4	35.368	18.549	5.3	5.4	1.435	2.913	1.964	3.846
3.24b		35.368	22.978	4.9	6.7	1.954	3.172	2.286	4.785
3.24c		35.368	27.876	4.7	7.2	2.115	3.438	2.442	7.924
3.31a	1	53.052	18.549	10.0	3.8	0.711	2.169	1.461	2.361

Expt. no.	No. of heated rods	Mass flux G $(kg/m^2 s)$	Heat flux q'' (kW/m^2)	Inlet subcooling $\Delta T_{sub,in}$ (K)	Wall superheat ΔT_{sat} (K)	Departure diameter D_d (mm)	Maximum diameter D_{max} (mm)	Lift-off diameter D_{lo} (mm)	Departure frequency f (s^{-1})
3.31b		53.052	22.978	9.9	5.2	1.054	2.488	1.583	2.995
3.31c		53.052	27.876	9.5	5.9	1.162	2.692	1.775	3.623
3.32a	2	53.052	18.549	10.1	3.9	0.847	2.341	1.559	2.473
3.32b		53.052	22.978	9.8	5.3	1.231	2.566	1.778	3.167
3.32c		53.052	27.876	9.6	6.0	1.463	2.823	1.892	4.302
3.33a	3	53.052	18.549	10.2	3.9	1.058	2.575	1.663	2.798
3.33b		53.052	22.978	9.7	5.5	1.542	2.781	1.869	3.432
3.33c		53.052	27.876	9.4	6.1	1.736	2.976	1.975	5.667
3.34a	4	53.052	18.549	10.1	4.0	1.102	2.658	1.736	3.614
3.34b		53.052	22.978	9.8	5.6	1.773	2.991	1.911	4.228
3.34c		53.052	27.876	9.6	6.2	1.893	3.143	2.003	6.712
3.41a	1	53.052	18.549	5.1	4.6	0.785	2.267	1.552	2.495
3.41b		53.052	22.978	4.6	5.8	1.116	2.533	1.726	3.162

Expt. no.	No. of heated rods	Mass flux G (kg/m^2s)	Heat flux q'' (kW/m^2)	Inlet subcooling $\Delta T_{sub,in}$ (K)	Wall superheat ΔT_{sat} (K)	Departure diameter D_d (mm)	Maximum diameter D_{max} (mm)	Lift-off diameter D_{lo} (mm)	Departure frequency f (s^{-1})
3.41c		53.052	27.876	4.4	6.3	1.315	2.761	1.851	4.228
3.42a	2	53.052	18.549	5.3	4.7	0.926	2.446	1.626	2.651
3.42b		53.052	22.978	4.9	5.9	1.462	2.714	1.848	3.385
3.42c		53.052	27.876	4.7	6.4	1.645	2.943	1.997	4.925
3.43a	3	53.052	18.549	5.2	4.7	1.115	2.634	1.773	2.866
3.43b		53.052	22.978	4.7	5.9	1.673	2.951	1.974	3.567
3.43c		53.052	27.876	4.6	6.4	1.852	3.144	2.163	5.823
3.44a	4	53.052	18.549	5.2	4.8	1.267	2.759	1.864	3.762
3.44b		53.052	22.978	4.8	6.0	1.824	3.073	2.136	4.459
3.44c		53.052	27.876	4.6	6.5	2.068	3.264	2.272	7.116

Table 6.6 Statistical analysis of experimental data.

Expt. No.		Mean	Standard deviation	95% confidence interval
1.1c	D_{dep}	0.455	0.0403	0.0256
	D_{max}	0.922	0.0235	0.0149
	D_{lo}	0.769	0.0318	0.0202
	f	23.923	0.0425	0.0416
2.2b	D_{dep}	0.551	0.0352	0.0244
	D_{max}	1.355	0.0288	0.0187
	D_{lo}	0.943	0.0391	0.0268
	f	13.657	0.0454	0.0439
3.3a	D_{dep}	1.058	0.0391	0.0264
	D_{max}	2.575	0.0314	0.0185
	D_{lo}	1.663	0.0292	0.0272
	f	2.798	0.0467	0.0413

The quantitative study of the bubble diameters show that the maximum diameter represents the upper limit on the bubble size and the departure diameter represents the lower limit, while the lift-off diameter lies somewhere between the two, as shown in *Figure 6.13*.
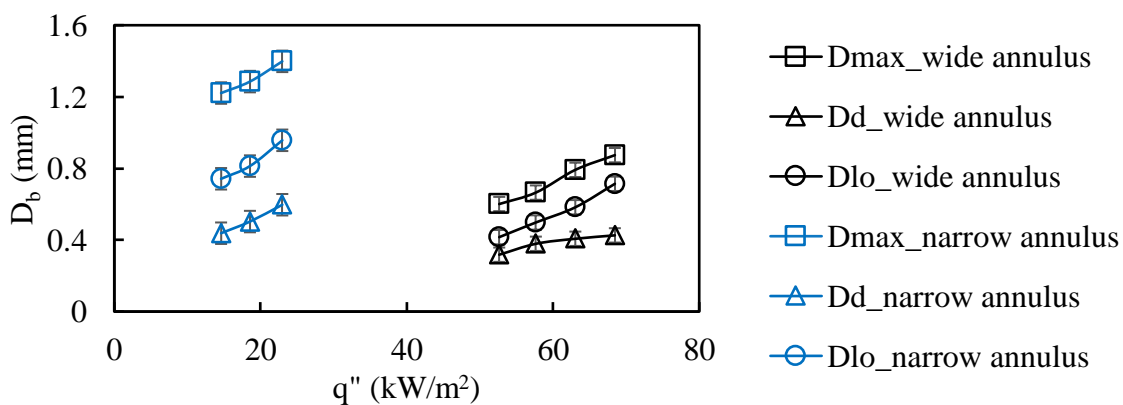

Figure 6.13 Quantitative comparison of maximum, departure and lift-off diameters.

6.3.3.1. Wide annulus

Parametrically, in the range of conditions considered here, all three bubble diameters show similar behavior, i.e. they increase with an increase in the heat flux or wall superheat, but decrease with an increase in the subcooling (*Figure 6.14*) and the mass flux (*Figure 6.15*). These results are in agreement with the studies in the literature which have been carried out for heat and mass fluxes much higher than those considered in this study. The increase in heat flux causes increase in wall superheat, which results in a higher evaporative heat transfer producing larger bubbles. The maximum diameter showed an increase of $\sim 60\%$, departure diameter of $\sim 30\%$, and lift-off diameter of $\sim 50\%$ as the heat flux increased from 60 to 80 kW/m^2. On the other hand, an increase in the liquid subcooling has a dual effect – (1) lowering of wall superheat, at the same value of applied heat flux causing reduction in evaporative heat transfer and (2) lower bulk liquid temperature, which causes enhanced condensation around the bubble cap. These two effects result in lower bubble sizes. Until bubble departure, the bubble size is small enough to be not affected by the bulk liquid temperature; while the maximum and lift-off diameters are affected by both lowered wall temperature and bulk temperature. This explains the observed fall in departure diameter of $\sim 15\%$ as the subcooling increased from $10\ K$ to $30\ K$, while the decrease in maximum and lift-off diameter for the same change in subcooling was $\sim 60\%$. Similarly, an increase in liquid flow velocity, causes increase in liquid shear making the superheated boundary layer thinner, resulting in reduced evaporation and hence, smaller bubble sizes. Also, increased mass flux means increased drag and lift forces, which cause the bubble to leave the nucleation site early, giving smaller departure and lift-off diameters respectively. Increased drag forces also increase the bubble sliding velocity, which results in smaller maximum diameters.
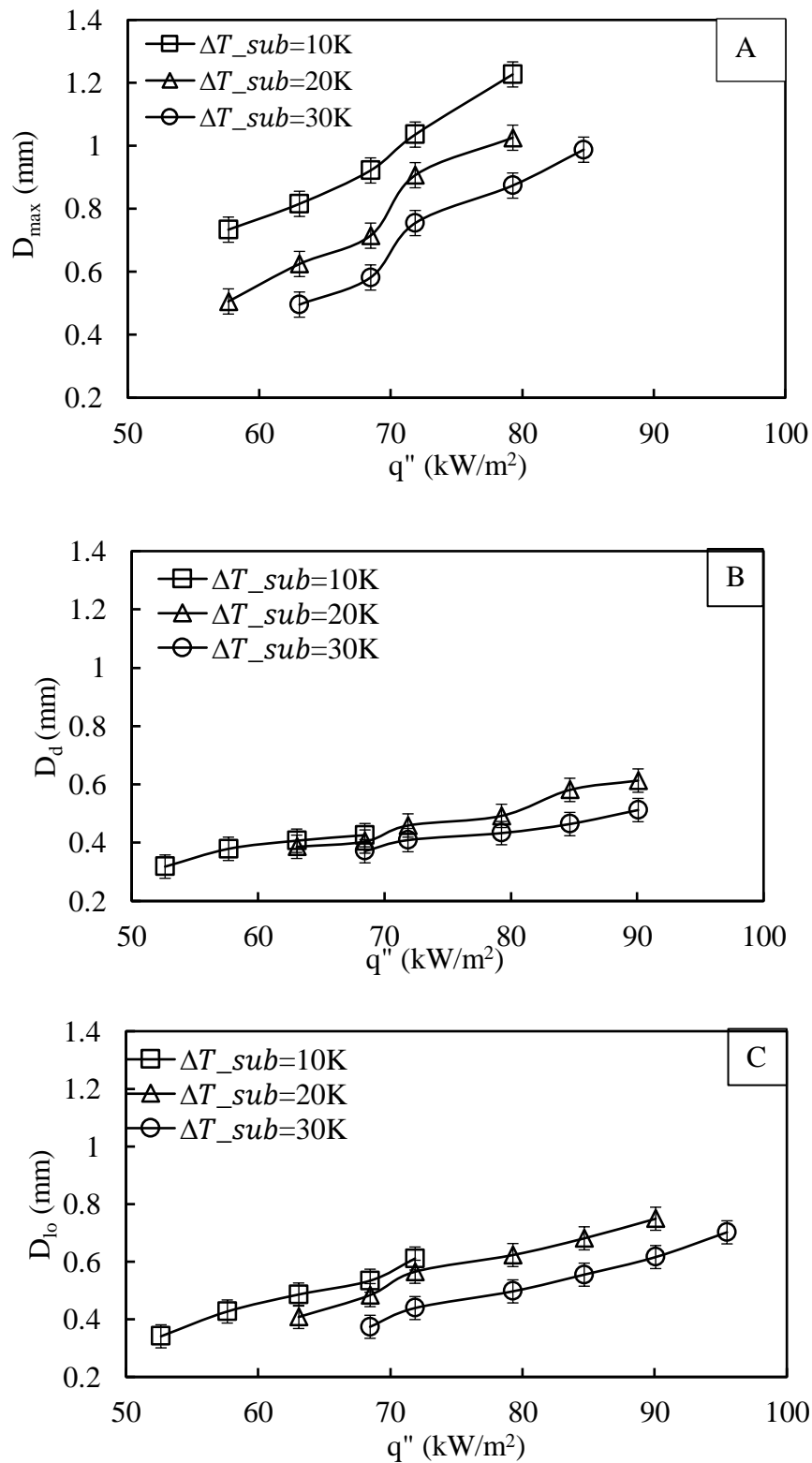
Figure 6.14 Effect of heat flux and degree of subcooling on (A) maximum ($G = 6.67\ kg/m^2 s$), (B) departure ($G = 10\ kg/m^2 s$) and (C) lift-off diameter ($G = 13.33\ kg/m^2 s$) in wide annulus.
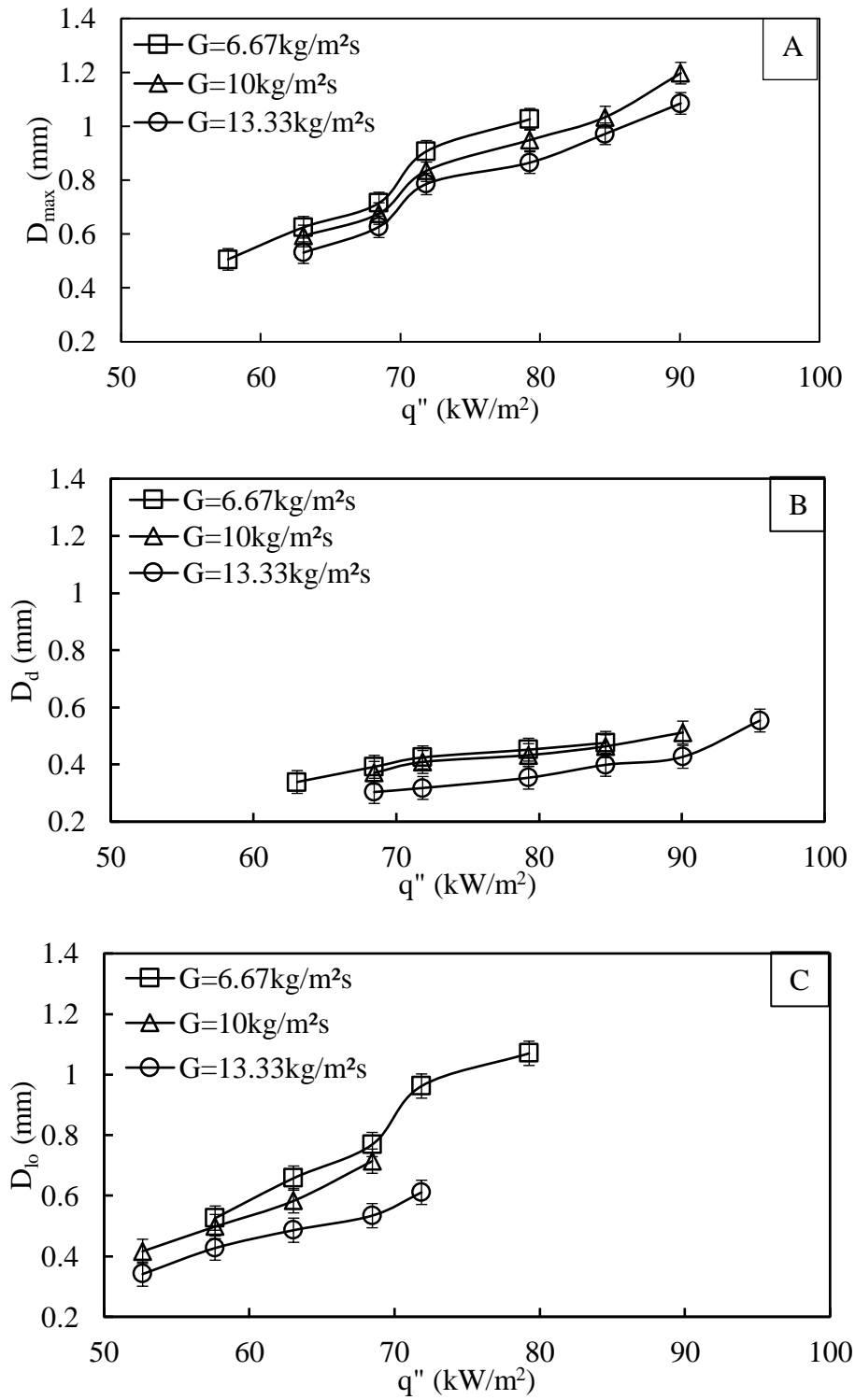
Figure 6.15 Effect of liquid mass flux on the (A) maximum ($\Delta T_{sub} = 20\ K$), (B) departure

($\Delta T_{sub} = 30\ K$) and (C) lift-off diameter ($\Delta T_{sub} = 10\ K$) in wide annulus.

As discussed in chapter 2, bubble departure frequency was calculated as the inverse of

time period between two consecutive bubbles from a given nucleation site. This time consists

of two parts – (1) bubble growth period (t_g), time for which the bubble grows at the nucleation site (up to departure), and (2) waiting period (t_w), time from departure of first bubble till a next bubble appears at the site. When a bubble departs from the site, the surrounding subcooled liquid rushes in to take its place, thereby causing the local destruction of the superheated boundary layer. The waiting period is essentially the time required by the boundary layer at the heater surface to regain its superheated temperature in the aftermath of the bubble departure. Thus, effectively,

$$f = \frac{1}{t_g + t_w} \tag{6.12}$$
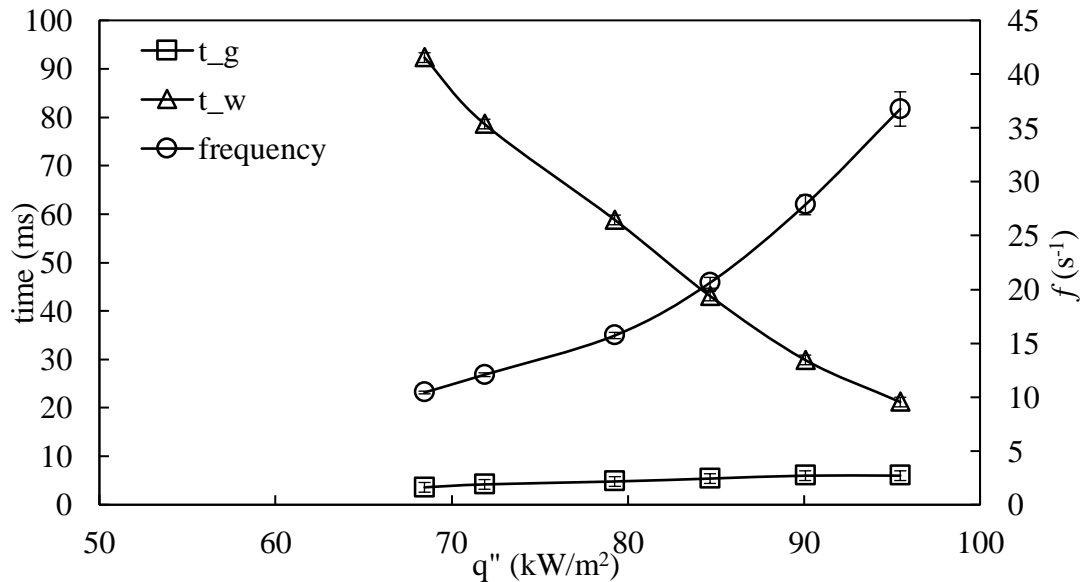
Figure 6.16 Effect of heat flux on growth time, waiting time and departure frequency

$(\Delta T_{sub} = 30\ K,\ G = 13.33\ kg/m^2 s)$.

It can be seen from *Figure 6.16* that the bubble growth time slightly increases with an increase in heat flux but waiting period significantly decreases with an increase in the heat flux, and hence, the departure frequency was observed to increase with an increase in the heat flux. As the heat flux increases, the evaporation rate increases increasing the bubble size, and a heavier bubble would take more time to depart. Higher heat flux at the surface means a higher temperature gradient ($T_w - T_l$), for a given bulk liquid temperature, which means a higher

convective heat transfer resulting in a faster recuperation of the superheated boundary layer, meaning a significant reduction in the waiting period. In effect, we see the number of bubbles departing per unit time increase with the heat flux. Hence, both bubble diameter and frequency increase with an increase in the heat flux, resulting in a higher heat transfer coefficient as previously seen in section 6.3.1. With an increase in the degree of subcooling, the growth time decreases a bit, since smaller bubbles depart from the nucleation site, at a given heat and mass flux; while the waiting period increases with an increase in the subcooling since it takes more time for the lower temperature liquid to reach the required level of superheat in the boundary layer. This effectively implies that the departure frequency decreases with an increase in liquid subcooling as shown in *Figure 6.17*. Lastly, the growth time slightly decreases with an increase in velocity, but waiting period significantly increases resulting in a lower departure frequency for a higher velocity as shown in *Figure 6.18*. This is because the increased fluid velocity results in continuous disruptions in the boundary layer increasing the waiting time.
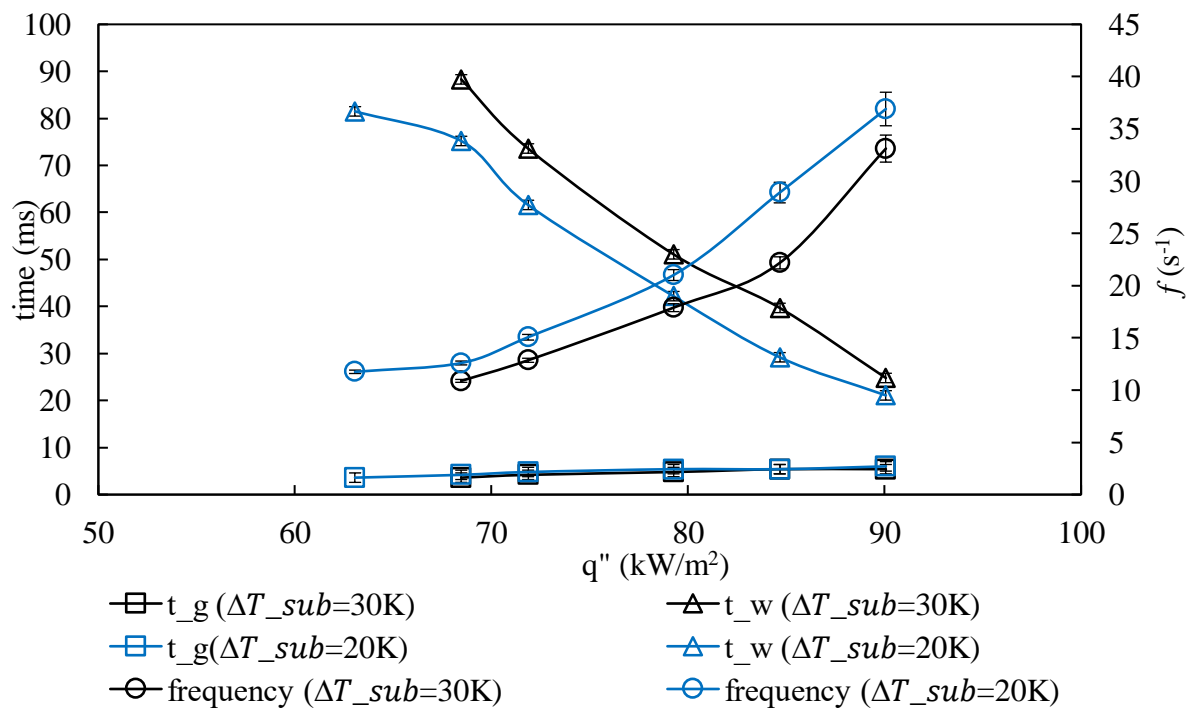
Figure 6.17 Effect of subcooling on growth time, waiting time and departure frequency ($G = 10 \; kg/m^2 s$).
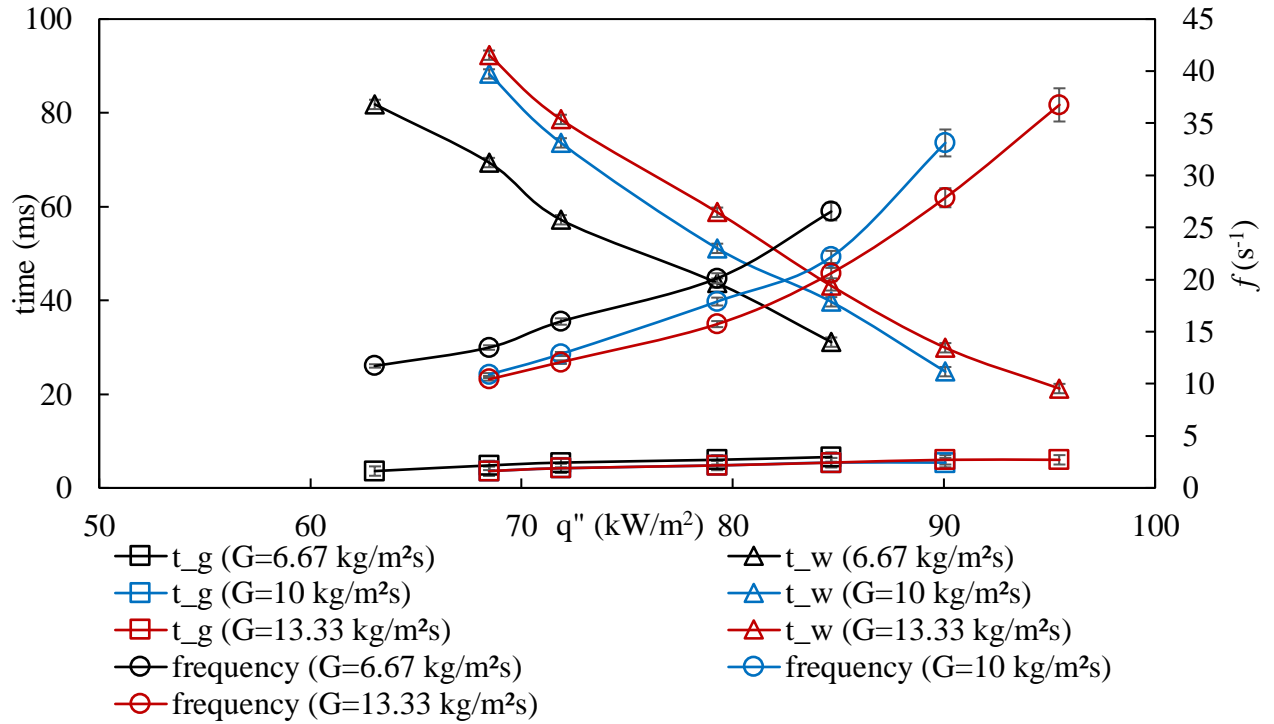
Figure 6.18 Effect of mass flux on growth time, waiting time and departure frequency

$$(\Delta T_{sub} = 30K).$$

6.3.3.2. *Narrow annulus and the rod bundle*

Kew and Cornwell (1997) proposed a non-dimensional number, called the confinement number (N_{conf}) to represent the restriction to the flow regimes and bubble growth caused by the small size of the annulus or channel.

$$N_{conf} = \frac{1}{D_h}\sqrt{\frac{\sigma}{g(\rho_l - \rho_v)}}$$ (6.13)

They suggested that the conventional heat transfer models could be applicable for geometries with $N_{conf} < 0.3$, beyond which the confinement effects would be significant. The confinement number in the present study changes from 0.078 for wide annulus to 0.65 for the narrow annulus, and to 0.31 for the bundle. Parametrically, the departure, maximum and lift-off diameter and the bubble departure frequency, all increase with an increase in heat flux or wall superheat, and decrease with an increase in liquid subcooling or mass flux in the narrow annulus and the bundle similar to that in wide annulus as shown in *Figure 6.19* and *Figure*

6.20. As discussed in the earlier section, three kinds of bubble growths were observed in the narrow annulus, and the average values used in the parametric study contains the diameter and frequency contributions from all three kinds of bubbles. It is clear from *Figure 6.19*, that bubble diameters in the narrow annulus would be larger than those in wide annulus in the same range of heat flux (extrapolation). This can be explained as follows: the coalescing and the confined bubbles have a higher rate of growth compared to the bubbles in the wide annulus, because these bubbles grow in an elongated manner by the evaporation of microlayer between the bubble and the surface. The elongated bubbles have higher contact area and hence, higher evaporation rate. Also, the narrow annular gap would lead to a lower local liquid subcooling to be achieved at the same value of applied heat flux, thereby reducing the degree of condensation of the bubbles.
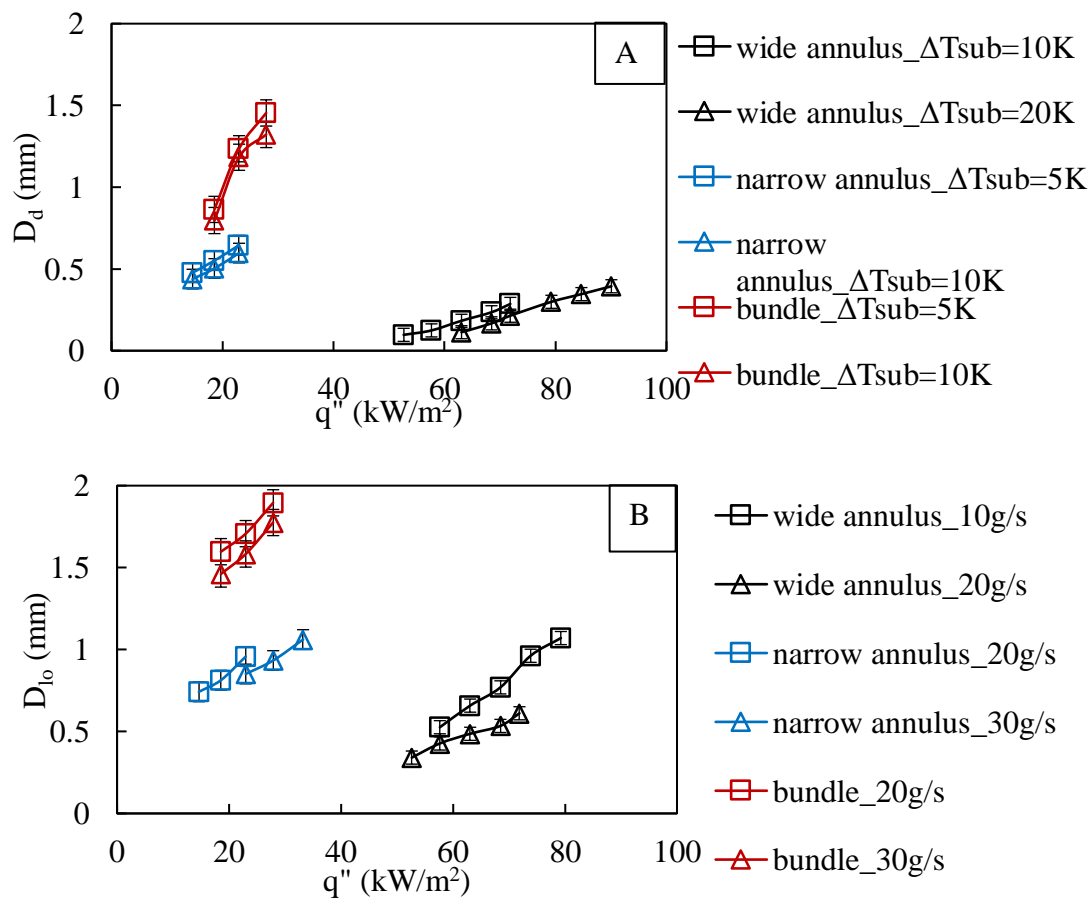
Figure 6.19 Effect of heat flux and (A) liquid subcooling (at $\dot{m} = 20 \ g/s$) and (B) mass flow rate ($\Delta T_{sub} = 10 \ K$) on bubble diameter in the three test sections.

In the bundle, the confinement as well as the lower local subcooling due to extra heated rods, lead to a large number of bubbles coalescing as discussed before. Hence, in the analysis, the departure diameter is considered to be the average size of the individual bubbles growing at their own sites, before they leave their site and merge with another bubble. The departure diameter for the rod bundle cases was observed to be in the range of $0.6 - 2.1\ mm$. The maximum diameter is the average size the coalesced bubble grows to before it starts condensing and necking, and lift-off diameter is the average size of the coalesced bubbles that lift from the heater surface. The observed range for bubble maximum diameter in rod bundle was $2.3 - 3.5\ mm$ and for the lift-off diameter was $1.6 - 2.4\ mm$. Hence, the coalesced bubbles would be larger than the bubbles in annuli for similar range of heat flux. The low annular gap in the narrow annulus and the bundle results in a higher effective velocity for same input mass flow rates, resulting in higher drag forces and more waiting time required for the recuperation of the superheated boundary layer. This results in significantly lower departure frequencies in the confined geometries as shown in *Figure 6.20*.
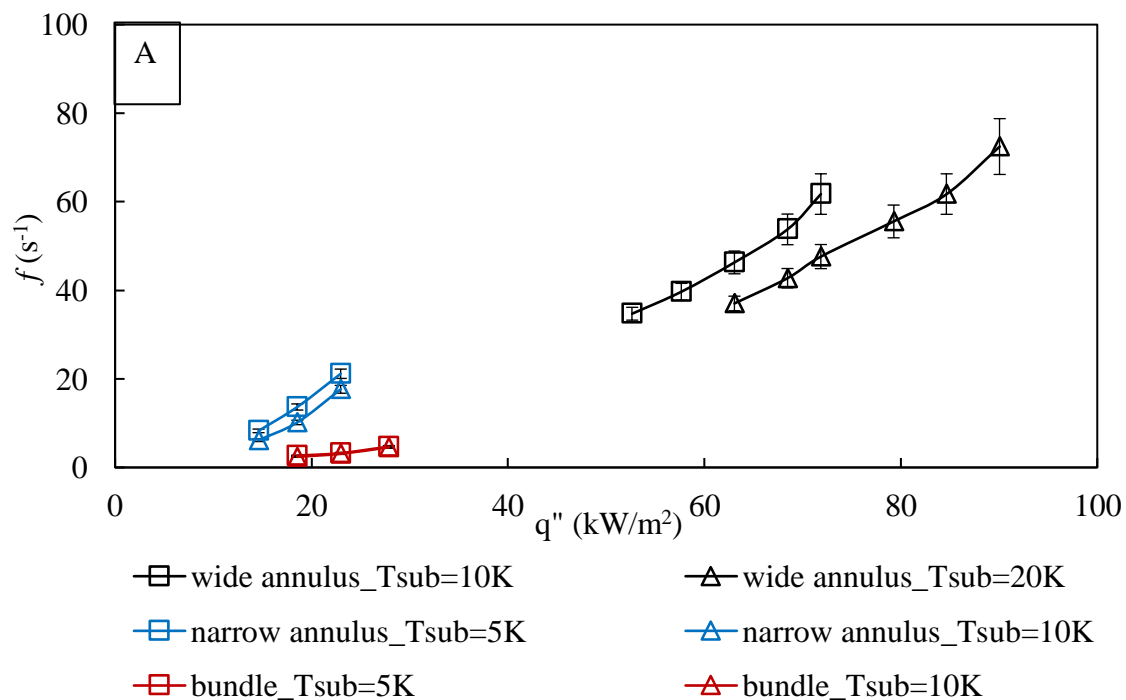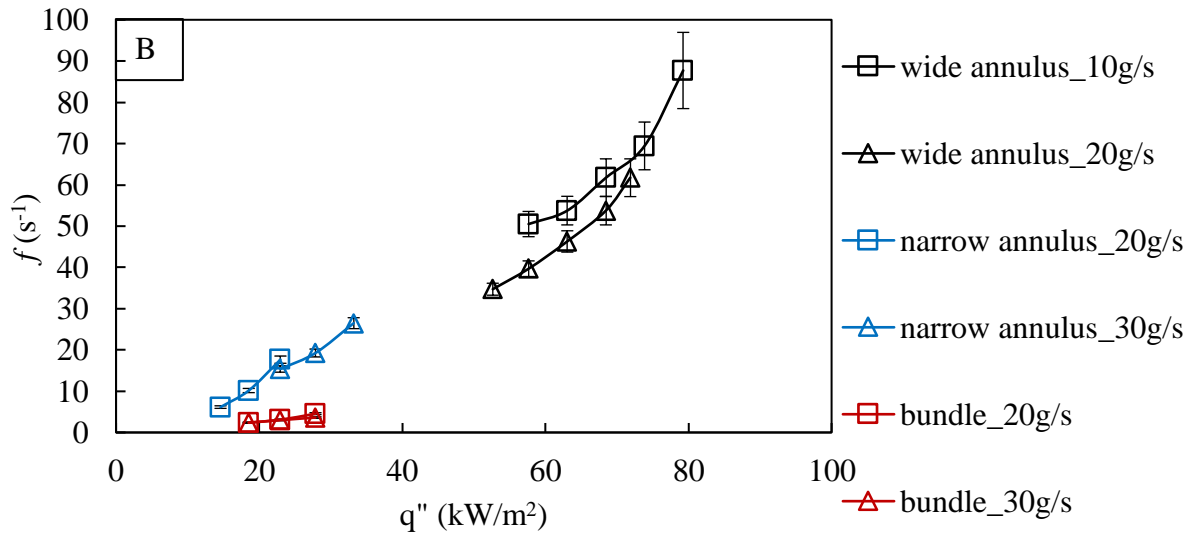
Figure 6.20 Effect of heat flux, (A) subcooling and (B) mass flow rate on bubble departure frequency in the three test sections.

Lastly, the effect of the neighboring heated rods on the departure characteristics was studied. As presented in *Figure 6.21*, the bubble diameters increase with increase in the number of heated rods in the bundle. However, the largest impact is observed on the departure diameter (about $\sim$54% from one heated rod to 4 heated rods), while the maximum and lift-off diameters increase about 14% in the same scenario. This is probably because the departure diameters recorded are of individual bubbles growing at their nucleation sites, and the effect can be clearly observed, while the effect is masked off in coalescence for the maximum and lift-off diameters. Similarly, the bubble departure frequency increased a maximum of 47% in going from one heated rod to four heated rods. Higher number of heated rods would result in (1) a lesser superheated boundary layer recuperation time, and (2) a speedy evaporation rate by providing higher temperature liquid in the growing bubbles vicinity reducing the bubble growth time as well. Both these factors would lead to a higher bubble departure frequency.
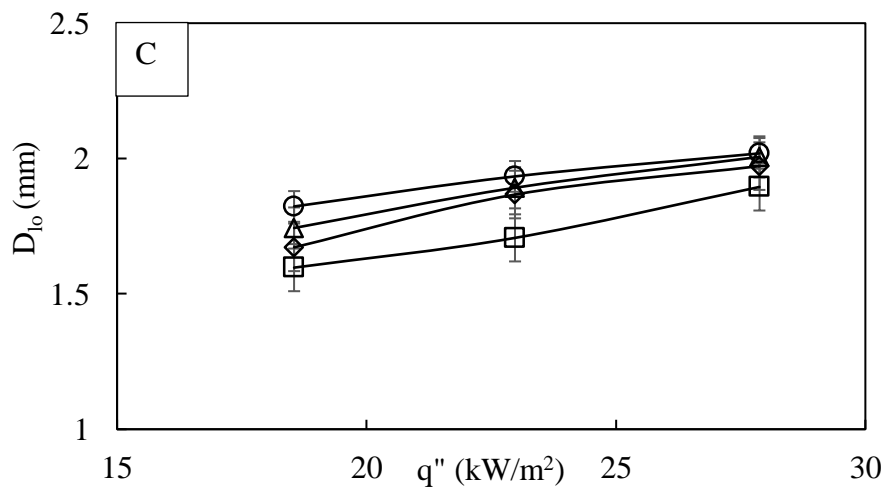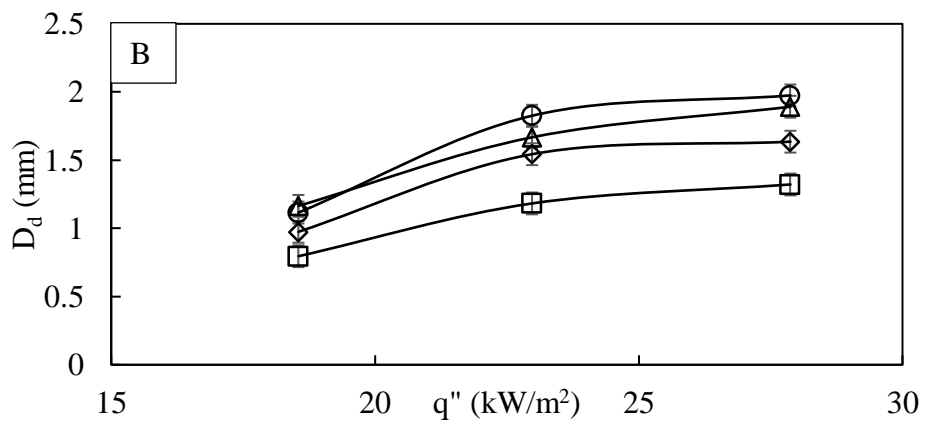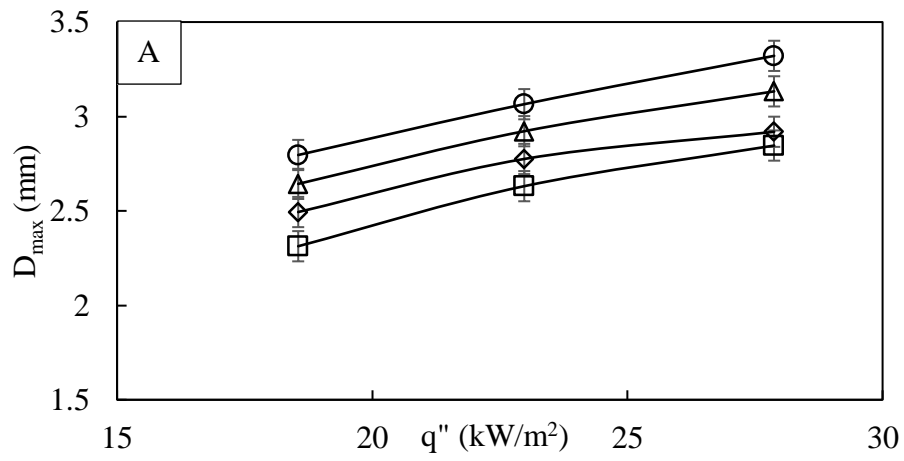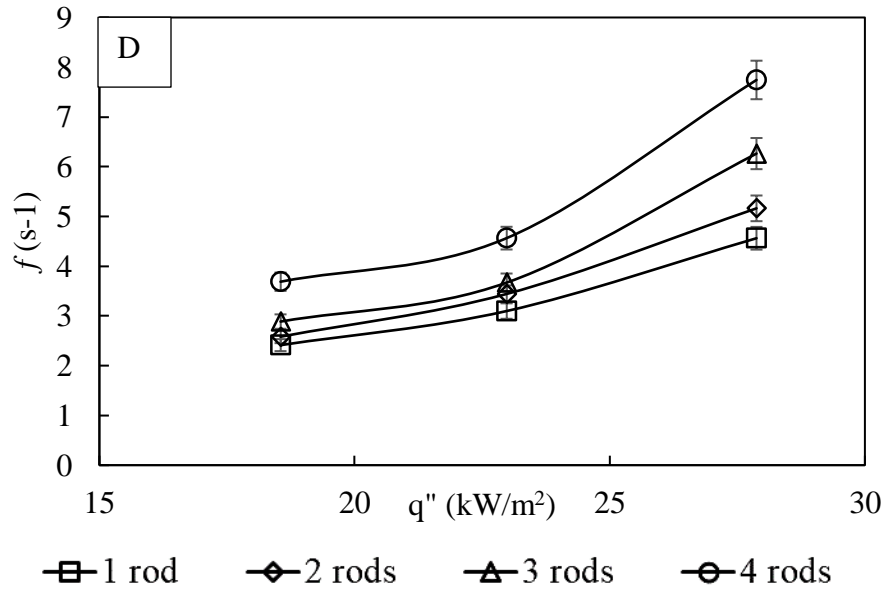
Figure 6.21 Effect of number of heated rods in the bundle on (A) maximum diameter, (B) departure diameter, (C) lift-off diameter and (D) frequency.

6.4. Conclusions

The bubble growth and departure characteristics were studied for subcooled convective boiling flow conditions under low heat flux ($q'' < 100 \ kW/m^2$) and mass flux ($G < 30 \ kg/m^2 s$) conditions, that would be typically encountered during a natural circulation Boiling Water Reactor (BWR), or in an accident scenario in a Pressurized Water Reactor (PWR), where the passive heat removal system takes over. The effect of varying operating conditions, like heat flux, wall superheat, liquid subcooling and mass flux, was studied on the bubble maximum, departure and lift-off diameters and departure frequencies. The studies were carried out using three different test sections – a conventional sized annulus, a narrow annulus and a four-rod bundle. The aim was to be able to understand the bubble behavior in a constricted space and in presence of the other heated rods. To the best of author's knowledge, the data in this range of conditions has not been reported in the literature, and can be used for model development and validation purposes.

a) The bubble ebullition studies show that for a conventional annulus, a bubble grows very fast at first, which causes cooling of superheated layer resulting in lowering of the growth rate. The bubble departs from the nucleation site early in its lifetime and slides along the heater surface growing and condensing and later ejecting into the bulk liquid. In the narrow annulus, apart from above described bubbles, coalescing and constricted bubbles could be observed. The bubbles nucleating in the bundle quickly grew at their sites and slid on to coalesce with the bubbles in their vicinity. They kept on condensing and coalescing with the bubbles in their path till they eventually lifted off the heater surface.

b) The heat transfer coefficient increases with an increase in the heat flux and a decrease in the liquid subcooling; while with an increase in mass flux, it increases for convective heat transfer but there is no effect of the flow velocity after nucleate boiling sets in. The heat transfer coefficient for similar values of applied heat flux, would be higher for the confined geometries, because of the higher local bulk temperatures. The effect of mass flux was also lesser in the case of narrow annulus and bundle, implying that convective heat transfer is not the dominant mechanism for these geometries under the presently studied conditions.

c) The increase in heat flux or wall superheat results in a higher evaporative heat transfer producing larger bubbles. On the other hand, an increase in liquid subcooling results in a lower wall superheat, at the same value of applied heat flux causing reduction in evaporative heat transfer and enhanced condensation on the bubble top. The two effects result in lower bubble sizes. Similarly, an increase in liquid flow velocity, results in a higher drag force which in turn reduces the bubble sizes.

d) For the departure frequency, the major factor is the bubble waiting period, which decreases as heat flux increases due to faster recuperation of the superheated boundary layer after the bubble departure, resulting in enhanced frequency. Whereas, an increase in liquid

subcooling or mass flux causes a rise in waiting period resulting in a reduced departure frequency.

e) The bubble departure diameter increases from wide annulus to narrow annulus and further in the bundle due to the confinement. The elongated bubble growth in the narrow annulus allows for the larger contact diameter, and hence, a higher evaporation rate coupled with the lower local subcooling due to lesser flow area, results in larger bubbles in the narrow annulus. The coalescence of bubbles in the bundle give further higher values of bubble sizes. However, the confinement results in higher effective velocities for same values of input mass flow rate, causing higher drag forces and more disruptions to the rebuilding of superheated boundary layer, and hence, resulting in lower frequencies.

f) The bubble diameters and frequency increase as the number of heated rods in the bundle increases. Higher number of heated rods would give a higher local bulk temperature, reducing the bubble condensation and a faster evaporation rate resulting in higher bubble sizes and departure rate.

7. Chapter 7

Model Development for Vertical Subcooled Flow

Boiling

7.1. Introduction

The models for heat transfer predictions in multiphase flows with wall boiling make use of the bubble departure characteristics as closure relations, to estimate the evaporation and quenching heat transfer components. Hence, they require accurate models for predicting bubble diameters and frequency. As discussed in chapter 1, a number of models have been proposed for the four parameters (three diameters, and frequency) over the years, but the error range is still quite large. The error in the diameter prediction needs to be small, because the value of diameter is cubed to represent the bubble volume, propagating any error in the bubble diameter three times its value. In this chapter, we first discuss the current status of the models for bubble departure characteristics, and then propose correlations for all four parameters based on the machine learning method – *random forest*.

7.2. Current status

We discussed the available models for bubble departure characteristics in chapter 1. The models for bubble diameters can mainly be divided in two categories – (1) force balance based analytical models, and (2) empirical correlations derived from experimental data. The first model for bubble departure diameter and lift-off diameter was proposed by Klausner *et al.* (1993) where they calculated the forces in the x-direction (direction parallel to the flow and the surface) and y-direction (direction perpendicular to the heater surface). The basic assumption was that the forces in both x- and y- direction are in equilibrium as the bubble grows on the surface, and so when $\sum F_x > 0$, the bubble departs and slides along the heater surface and when

$\sum F_y > 0$, the bubble lifts from the surface and moves into the bulk liquid. All the force balance models proposed thereafter are modifications of this first model, where the method of calculating instantaneous radius, or contact diameter or advancing and receding contact angles are modified. The parity plots for bubble departure and lift-off diameter calculated from the first model of Klausner *et al.* (1993) and the most recent model by Colombo and Fairweather (2015) are presented in *Figure 7.1* with ±50% bounds shown by red dotted lines. It can be seen that not much improvement over original Klausner *et al.* (1993) model has been achieved. It was seen that for the Klausner *et al.* (1993) model, about 38% and 42% data predictions for bubble departure diameter and lift-off diameter, respectively fall within the ±50% error bands; while for the Colombo and Fairweather (2015) model, 20% and 42% of the departure and lift-off diameter data respectively fall within the ±50% error bands. Recently, Mazzocco *et al.* (2018) studied the major force balance models in the literature and suggested that the physical representation of the individual forces acting on the bubble needs to be improved.
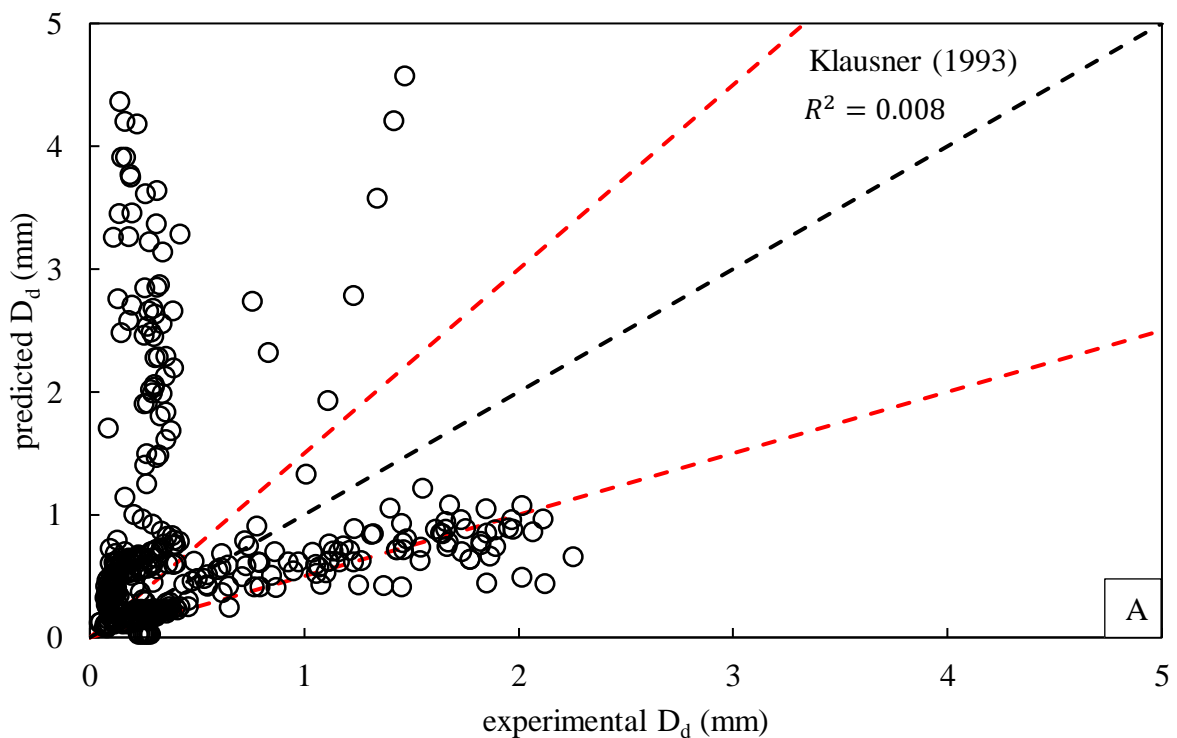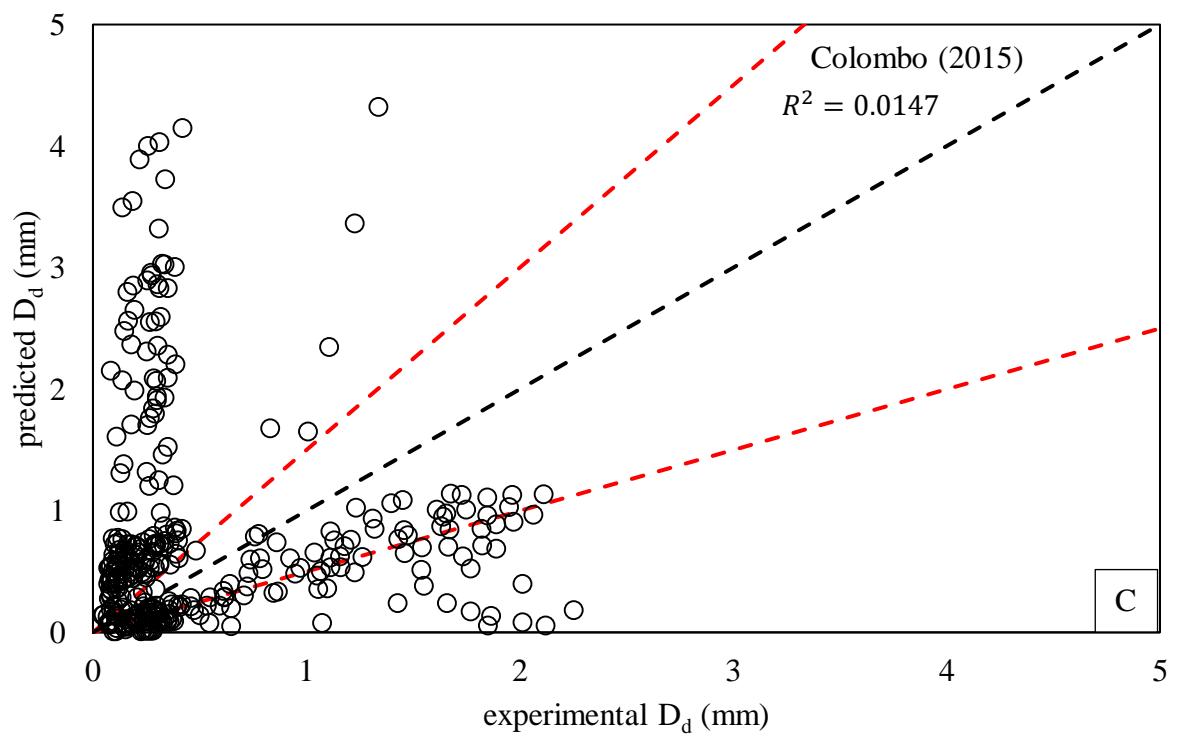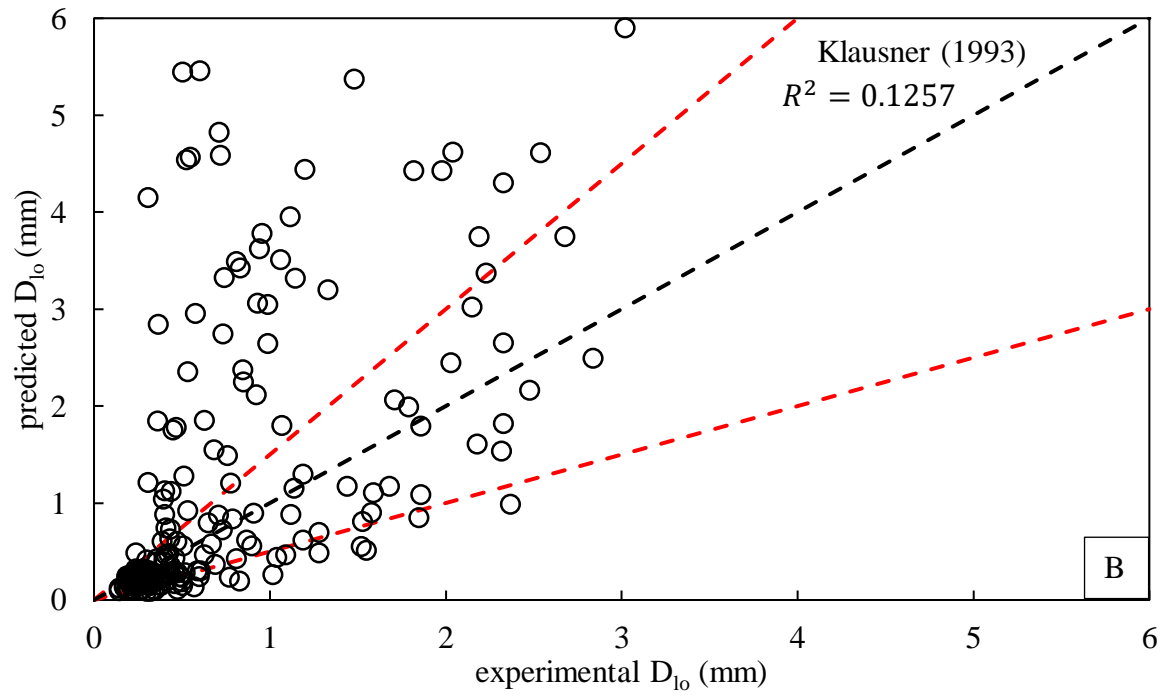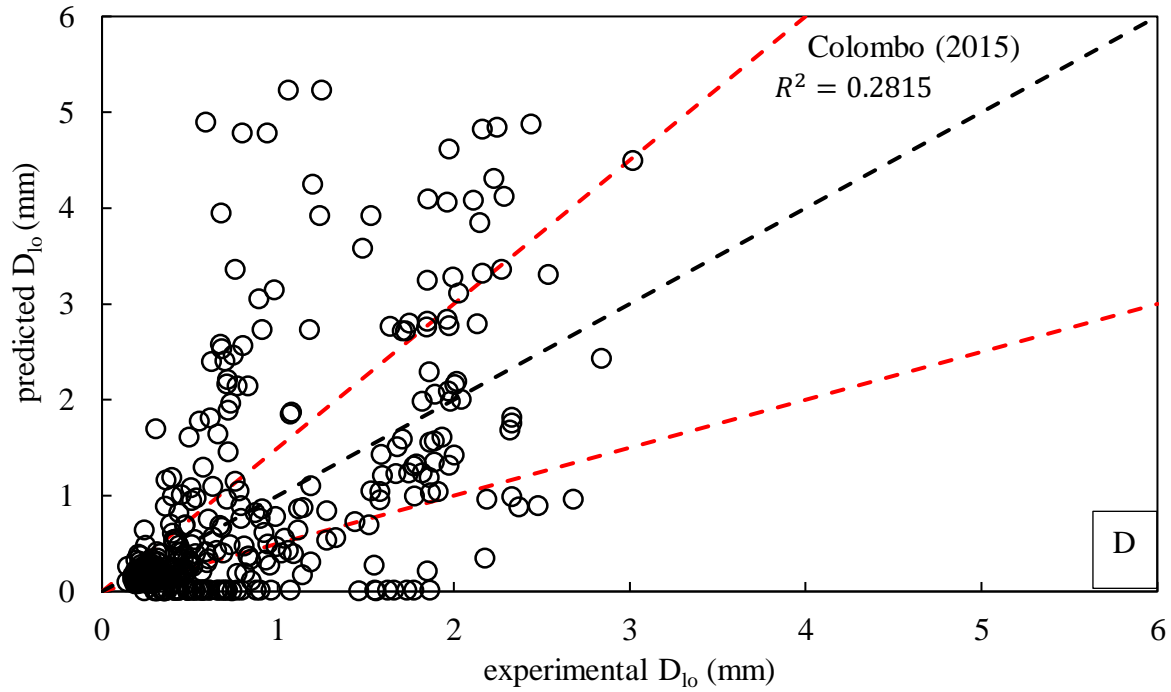
Figure 7.1 Parity plots for bubble departure diameter (A, C) and lift-off diameter (B, D) from

force balance models of Klausner *et al.* (1993) and Colombo and Fairweather (2015).

The empirical correlations are usually developed in terms of the non-dimensional numbers like, Jakob number (Ja), subcooling number (ϑ), Prandtl number (Pr), etc using the understanding developed from the parametric studies carried out in the experiments. These models are usually validated with selected sets of data, and hence, are unable to make accurate predictions over a wide range of conditions. The parity plots to show the large degree of scatter from the available models for all three kinds of bubble diameters are shown in *Figure 7.2* to *Figure 7.4* where the red dotted lines represent the $\pm 50\%$ error bands.
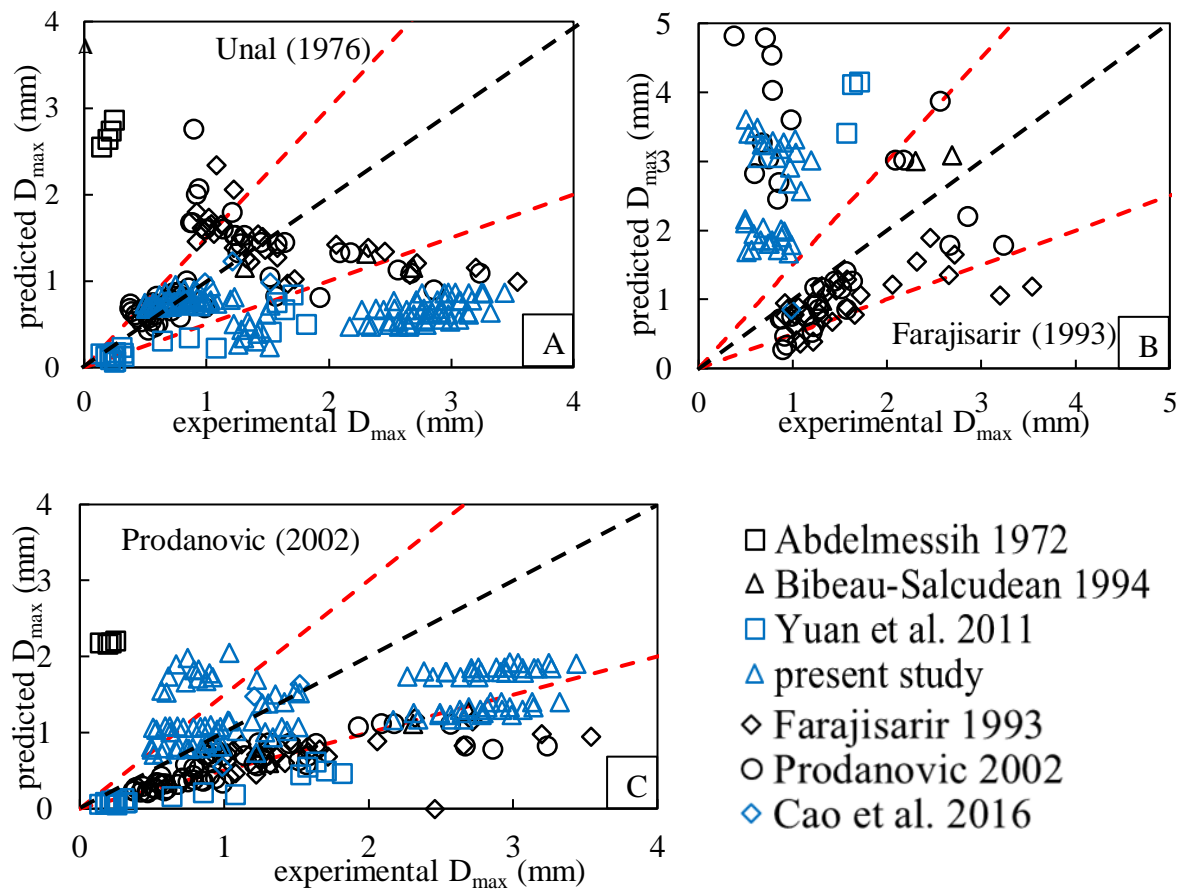
Figure 7.2 Comparison of experimental data for maximum diameter with models of (A)Ünal (1976), (B)Farajisarir (1993), and (C)Prodanovic *et al.* (2002).
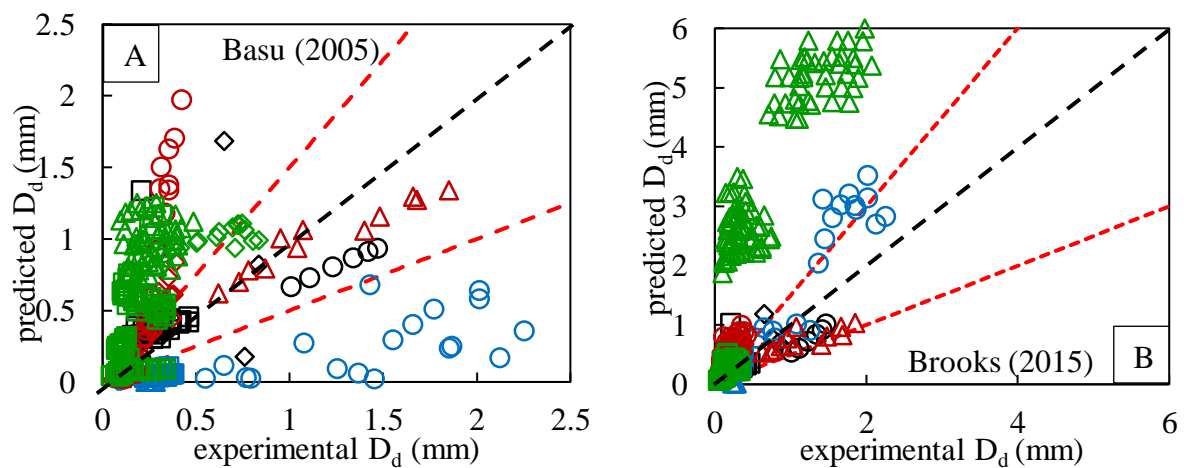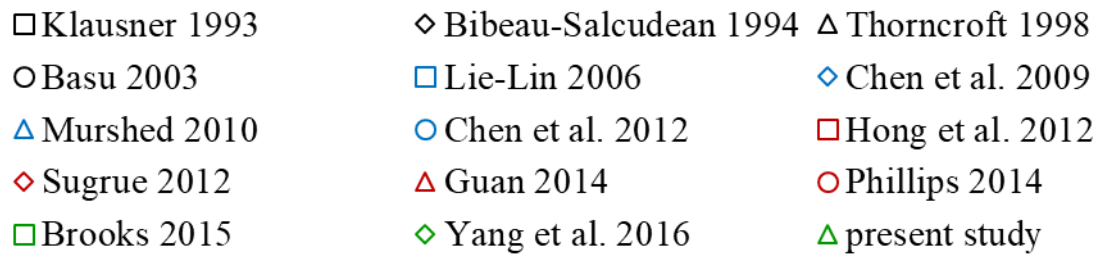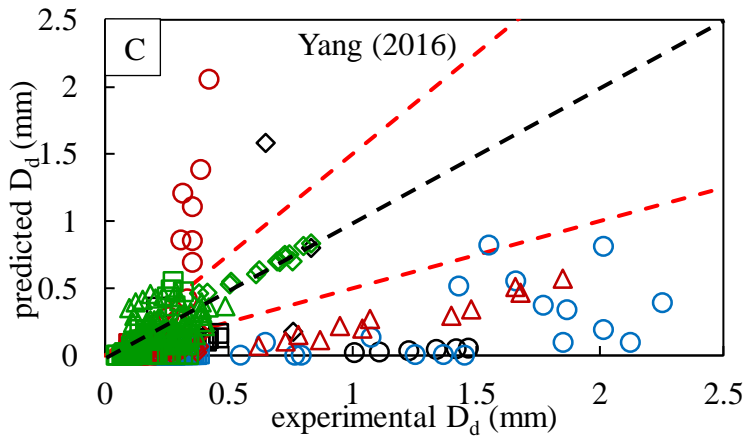
Figure 7.3 Comparison of experimental data for departure diameter with the models of

(A)Basu *et al.* (2005), (B)Brooks and Hibiki (2015) and (C)Yang *et al.* (2016).
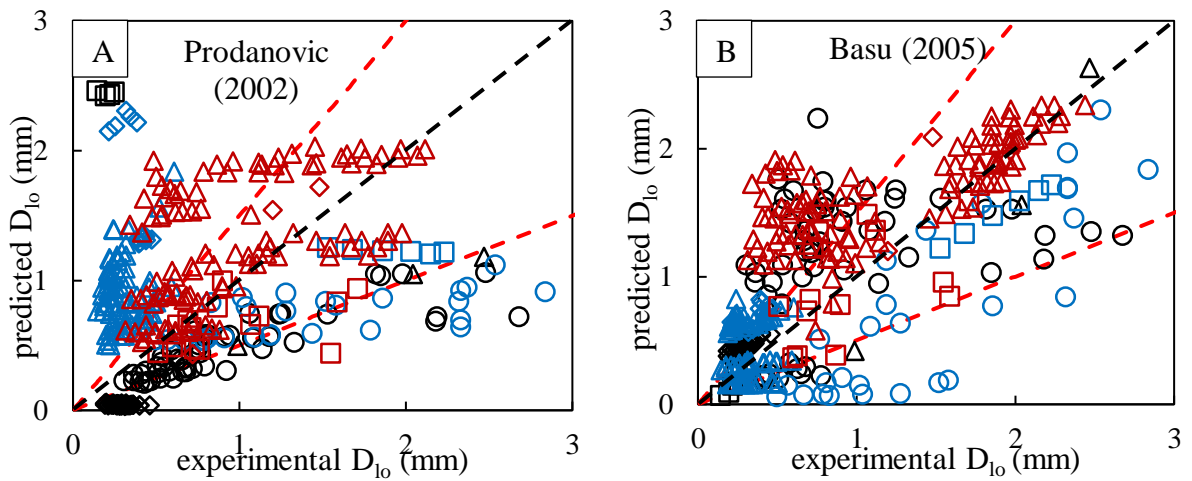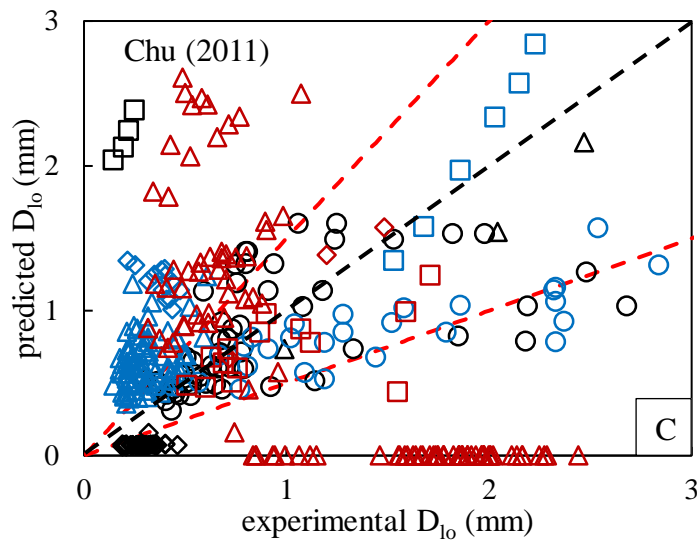
Figure 7.4 Comparison of experimental data for lift-off diameter with models of (A)Prodanovic *et al.* (2002), (B)Basu *et al.* (2005), and (C)Chu *et al.* (2011).

Further, as discussed in the literature review in chapter 1, studies have shown a strong dependence of departure frequency on the bubble departure diameter, and the few models that have been proposed for bubble departure frequency depend on the departure diameter values. However, limited data for simultaneous measurements of bubble departure diameter and frequency is available in the literature. The parity plots for the departure frequency for the models available in open literature are presented in *Figure 7.5* with the $\pm 50\%$ error bands. The semi-empirical Cole (1960) model, was developed for saturated pool boiling but is the most widely used model for estimating bubble departure frequency in the commercially available CFD modules, like ANSYS Fluent, STAR CCM+, etc. and it can be seen from the figure below that it severely over predicts the data in the low frequency range. It can be seen that some of the more recent correlations perform better, but the average error is still quite large ($\sim$300%).
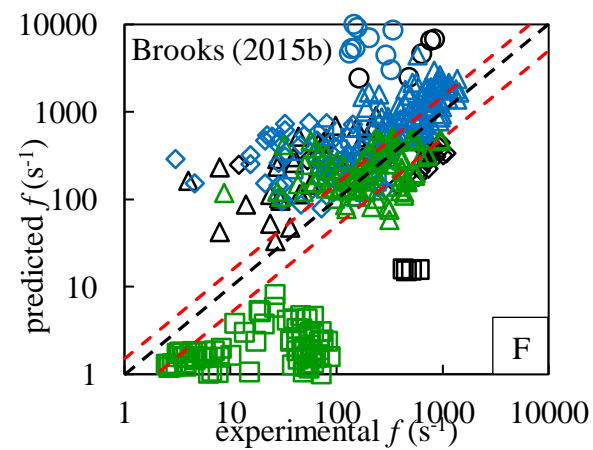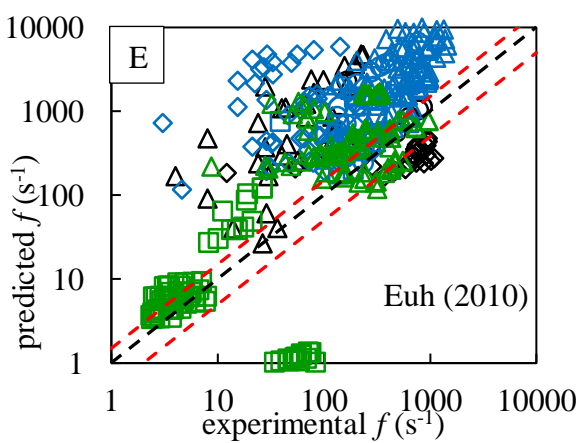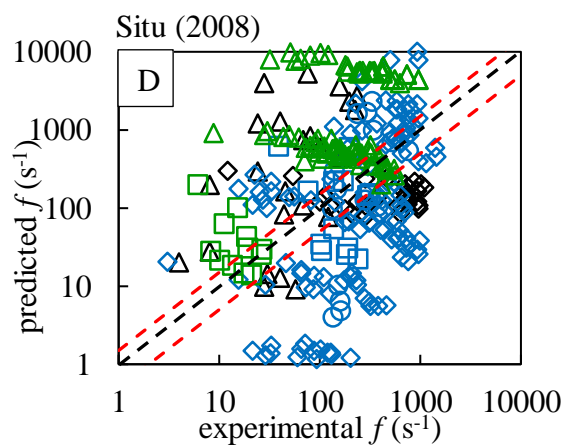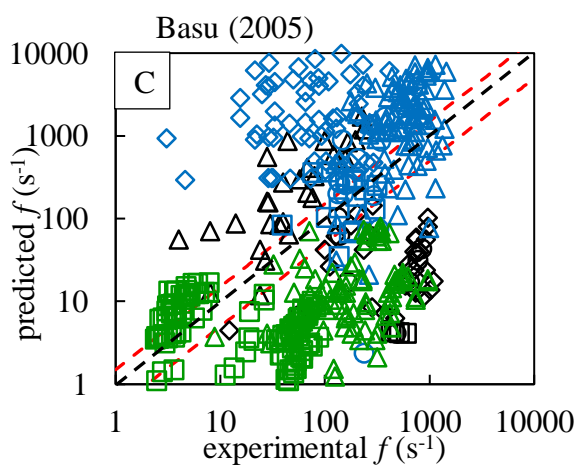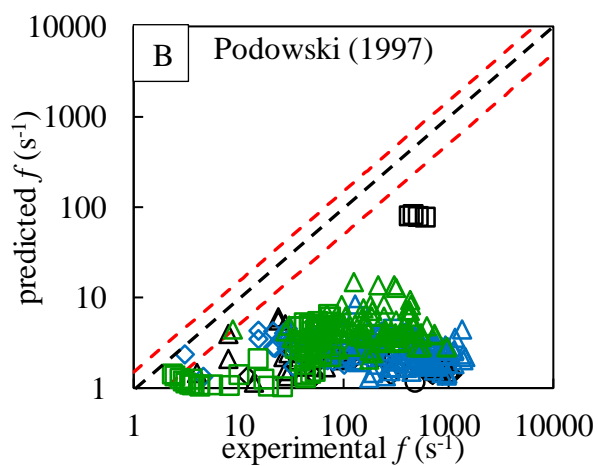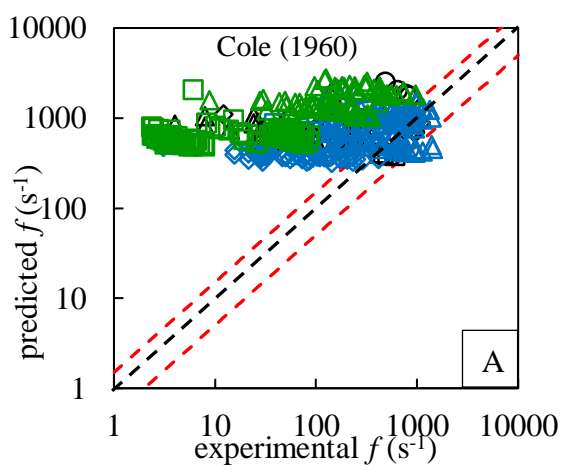
Figure 7.5 Comparison of experimental data for bubble departure frequency with the models of (A)Cole (1960), (B)Podowski *et al.* (1997), (C)Basu *et al.* (2005), (D)Situ *et al.* (2008), (E)Euh *et al.* (2010), and (F)Brooks and Hibiki (2015).

7.3. Development of correlation for bubble diameters and departure frequency

From the careful review of the literature and from the understanding developed from our own experiments, we understand that the bubble departure characteristics depend on a number of factors – (1) operating conditions, like applied heat flux, wall superheat, liquid subcooling, mass flow rate, and system pressure, (2) the heater characteristics, like surface material, surface roughness, contact angle, (3) the liquid and the vapor properties, (4) the liquid and heater material interaction, and (5) the flow area (hydraulic diameter). An empirical model would use the dimensionless numbers that represent all these parameters and relate them to the dimensionless bubble diameter or frequency using a structure of the following kind:

$$X^* = AJa^b\vartheta^c Bg^d Pr^c N_{conf}^d \left(\frac{\rho_l}{\rho_v}\right)^e \tag{7.1}$$

Here, X^* is the dimensionless bubble diameter or frequency, Ja is Jakob number which represents the effect of wall superheat, ϑ is subcooling number which accounts for the effect of liquid subcooling, Bg is boiling number and is the ratio of the effect of heat flux and mass flux, Pr is Prandtl number that represents the effects of liquid properties, N_{conf} is the confinement number which accounts for the effect of flow area, and $\frac{\rho_l}{\rho_v}$ is the ratio of liquid to vapor density which represents the effect of system pressure. We tried to find the coefficients A, b, c, d, e using regression methods using all the data available in the open literature and all

the combinations of the exponents obtained showed poor agreement with the entire collective data, similar to the parity plots presented before. This indicated that the process of arriving at the empirical models has limitations. For example, equation (7.1) would suggest that dimensionless parameter X is directly proportional to Ja^b, but in fact, the value of exponent on Ja depends on the values of other non-dimensional numbers in the equation. This point can be clarified by looking at *Figure 7.6*(A) to (C), which show that multiple values of bubble diameter or frequency exist for any given value of wall heat flux (q''), mass flux (G) and wall superheat (ΔT_{sat}), respectively. This means that the any value of bubble diameter or frequency depends on the simultaneous and combined effects of all the above discussed variables, and any type of dimensionless correlation is unable to result in a desirable level of accuracy. In view of this observation, it was thought desirable to implement the techniques of artificial intelligence (AI) to develop the platform which can predict the bubble departure characteristics over the entire range of conditions.
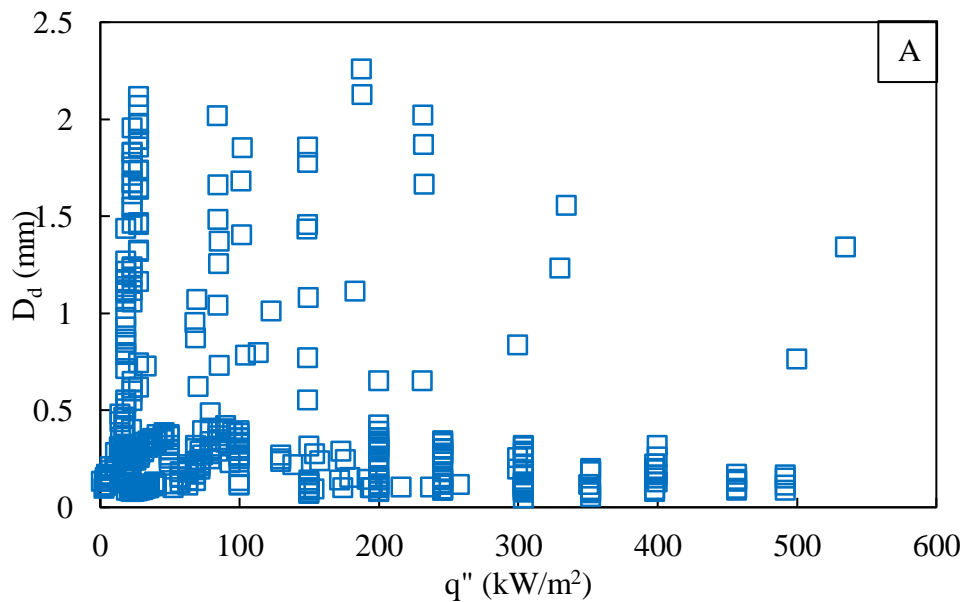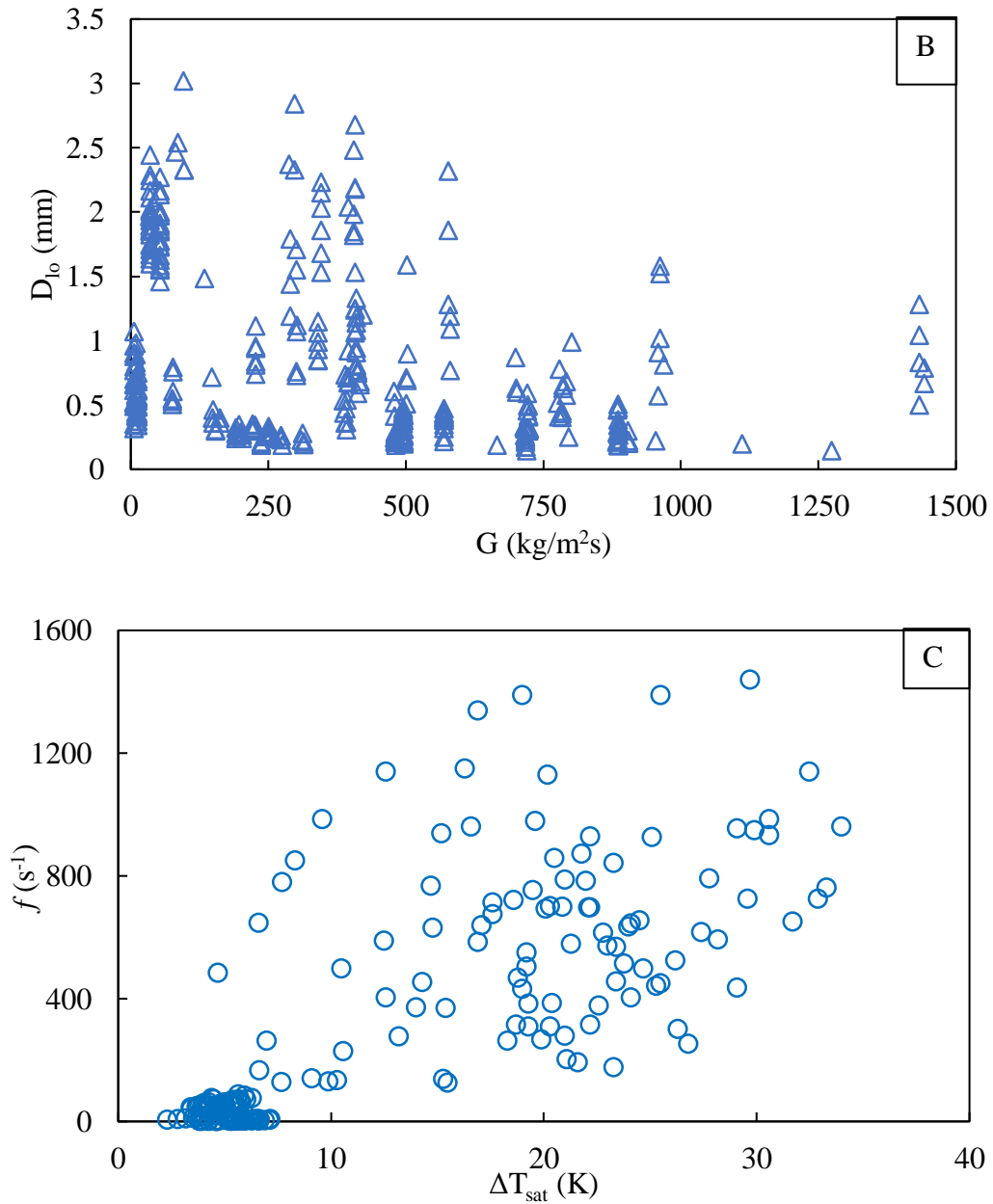
Figure 7.6 Parametric sensitivity study for (A) bubble departure diameter, (B) bubble lift-off diameter and (C) departure frequency.

7.4. Development of correlation based on data driven modelling

Data driven modelling employing artificial intelligence and machine learning techniques have been finding increasing relevance and application in the development of correlations for design parameters in the industry. The goal of the data driven modelling is t build a prototype that can adapt and learn from the practical data. The most popular data driven modelling techniques are artificial neural networks (ANN), support vector regression (SVR),

and random forests (RF). ANN is based on artificial intelligence, and uses empirical risk minimization to minimize the training data error. SVR and RF are machine learning methods that are based on rigorous statistical learning of the data. SVR uses structural risk minimizations, hence, accounts for model complexity as well as minimizes the training data error. The present work uses the random forests technique, which is an ensemble learning method for classification and regression of the data, by the process of constructing a multitude of the so-called classification or decision trees.

The ensemble model refers to the kind of models that use the average of the outputs from a large number of simple base models to arrive at a final prediction. In random forest, the base models are the decision trees. A *decision tree* is a flow chart like structure in which each node represents a decision on an attribute and each branch (called leaf) is a binary operation which represents the possible paths from one node to another as shown in *Figure 7.7*. It basically is a flow chart of questions relevant to the problem leading to a prediction. For any given problem in real life, we ask ourselves a series of questions, and based on the answers to those questions in combination with our previous life experiences arrive at a conclusion. A decision tree in machine learning also works similarly. A decision tree will take the input data, go through a series of questions, considering all the possible alternative responses to each question and arrive at a prediction.
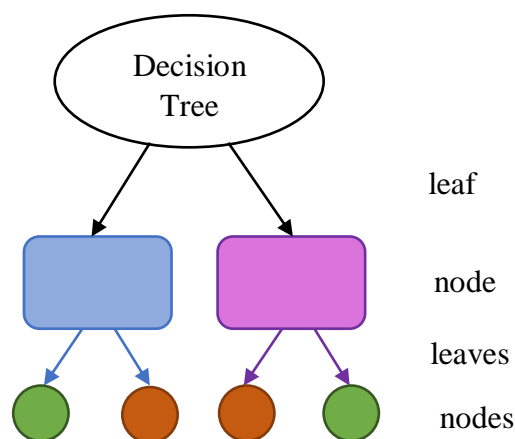
Figure 7.7 Schematic of a decision tree

The machine however, does not have the life experiences of a human, so it needs to be trained to translate the meaning of the responses of each question into reasonable predictions. This training phase of the random forest method is called *bootstrap aggregation* or *bagging*, which involves constructing each successive tree independently from the data set, such that the successive trees do not depend on the previous trees (*Figure 7.8*).
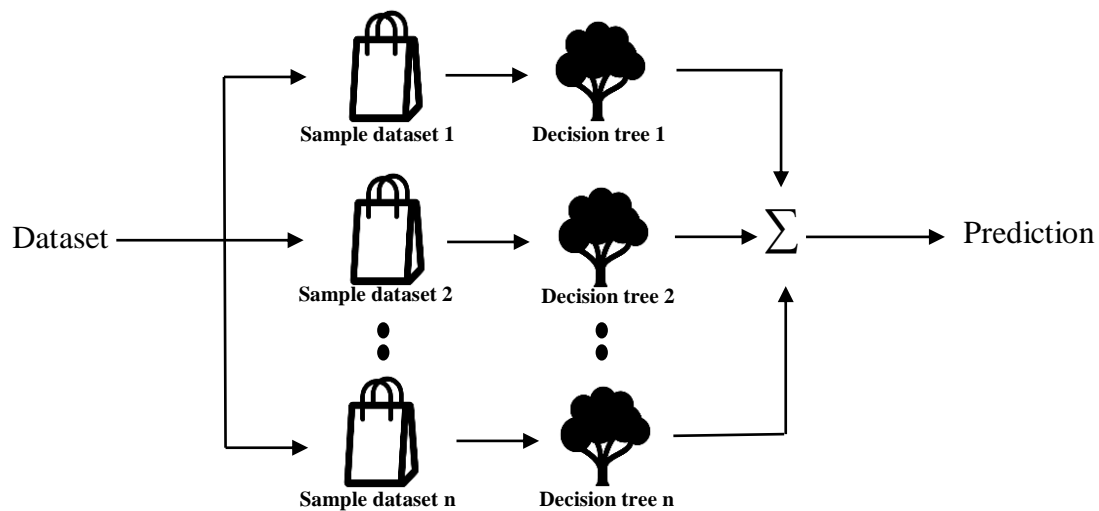
Figure 7.8 Schematic of the bagging method

Breiman (2001) proposed the concept of random forests, where he added an additional layer of randomness to bagging. In addition to constructing each tree using a different bootstrap sample of the data, random forests changes how the trees are constructed. In bagging, each node is split using the most important variable amongst all variables involved in the given problem, while random forest searches for the best variable among a random subset of the variables chosen at that node (*Figure 7.9*).

<div align="center">Bagging</div>

<div align="center">All M variables considered for node split</div>

<div align="center">Random Forests</div>

<div align="center">m<M variables considered for node split</div>
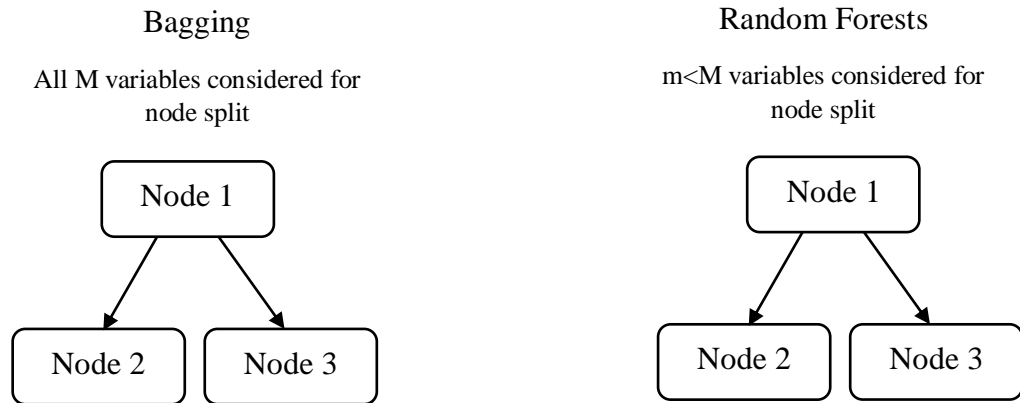
Figure 7.9 Bagging versus Random Forest training techniques

This somewhat counter-intuitive strategy results in a wide diversity that generally performs very well compared to many other classifiers and is robust against over fitting. In addition, it is very user-friendly in the sense that it has only two parameters (number of variables in the random subset at each node and the number of trees in the forests), and is usually not very sensitive to their values. The random forests algorithm for regression has following steps:

(1) Draw n bootstrap samples from the original data.

(2) For each of the bootstrap samples, grow an unpruned classification or regression tree by randomly sampling m of the total M predictors, and choosing the best split predictor from those m predictors. (Bagging can be thought of as the special case of random forests, when $m = M$).

(3) Predict new data by aggregating the predictions of the n trees (i.e. average for regression). This process is depicted in form of a flow chart in *Figure 7.10*.

The random forest package optionally produces two additional pieces of information: a measure of the importance of the predictor variables, and a measure of the internal structure of the data. The algorithm estimates the importance of a variable by looking at how much the prediction error increases when the out-of-bag (OOB) data for that variable is permuted while all others remain the same. The random forests are an effective tool in prediction, as they do not overfit because of the law of large numbers. Injecting the right kind of randomness makes

them accurate classifiers and regressors. Furthermore, the framework in terms of strength of the individual predictors and their correlations gives insight into the ability of the random forests to predict. Using an OOB estimation makes, the otherwise theoretical values of strength and correlation, concrete.

The forest consists of randomly selected inputs or combination of inputs at each node to grow each tree, giving a high degree of accuracy. This class of procedures has the following desirable characteristics: (1) high accuracy, (2) relatively robust to outliers and noise, (3) faster than bagging or boosting, (4) gives useful internal estimates of error, strength, correlation and variable importance, and (5) simple and easily parallelized.
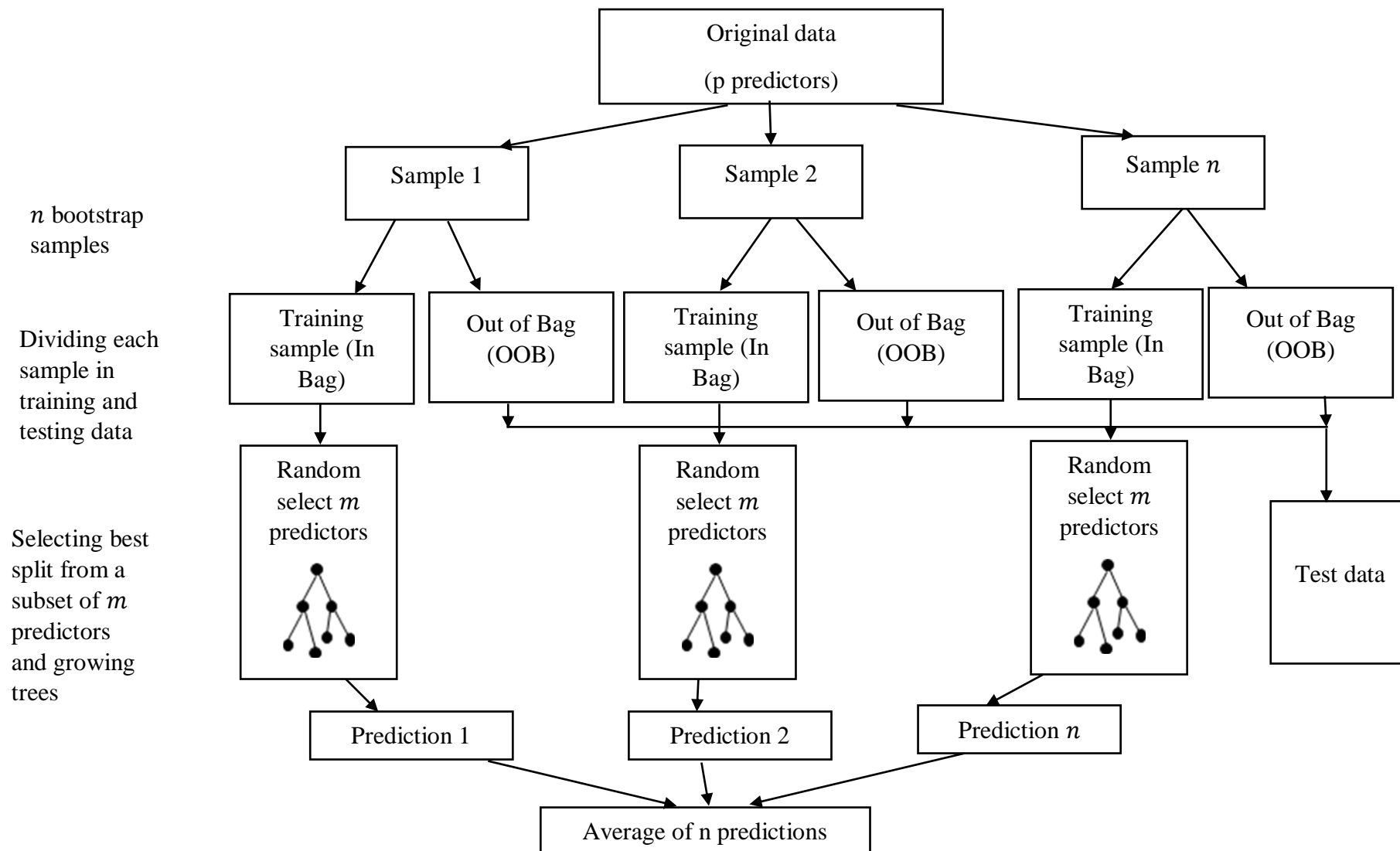
Figure 7.10 Flowchart for Random Forests regression algorithm.

The random forests code used in this study was developed by Dr. Aniruddha Joshi and was obtained by private communication. To develop random forest (RF) based correlations for bubble maximum, departure and lift-off diameter and bubble departure frequency, all available data in the open literature for flow boiling was considered, which meant 224 points for maximum diameter, 428 points for departure diameter, 362 points for lift-off diameter and 206 points for departure frequency, including the data collected in the present study. The data was input in form of the excel sheets as shown in *Figure 7.11*. All the independent variables are given in columns (D to J) along with the measured values of the bubble diameter or frequency (column C). The rows in column A are used to give the model a sense of the data, for example "relationship to output (-10 to +10)" row indicates the initial guess for the significance of each variable on the required output based on the user experience. Similarly, in other rows we specify the highest and lowest data points for each column, and possible highest and lowest values for each variable from user experience. The correlations were developed using 66% of the data points for training and 34% of the data for testing the models.

A	B	C	D	E	F	G	H	I	J
		Dd	P	q"	ΔT_sat	ΔT_sub	G	y	N_conf
		m	N/m^2	W/m^2	K	K	kg/m^2.s		
dimensionless (0 is input, 1 is formula, 2 is output)		2	0	0	0	0	0	0	0
relationship to output (-10 to +10)		1	-2	10	6	-3	-7	4	2
lowest (data)		0.000046	100000	1320	0.05	2.98	6.75676	0.125	0.0371
highest (data)		0.002255	899000	943000	43.3	49.32	1249.91	94.11	1.2823
lowest (practical)		0.00001	1000	50	0.01	0.01	1		
highest (practical)		0.004	8E+06	1E+06	60	90	2500		

Figure 7.11 Input sheet for Random Forests model

Parity plots generated after testing the data set are shown in *Figure 7.12* to *Figure 7.15* for bubble maximum, departure, lift-off diameter and frequency, respectively. The coefficient

of determination (R^2 value) for each model was estimated, and the values for all the data predicted with random forest were found to be 0.9272, 0.9123, 0.9219 and 0.8688 for maximum, departure, lift-off diameter and frequency, respectively. Comparing these plots with those shown in earlier sections, we can clearly see the effectiveness of the machine learning methods over the conventional regression methods.
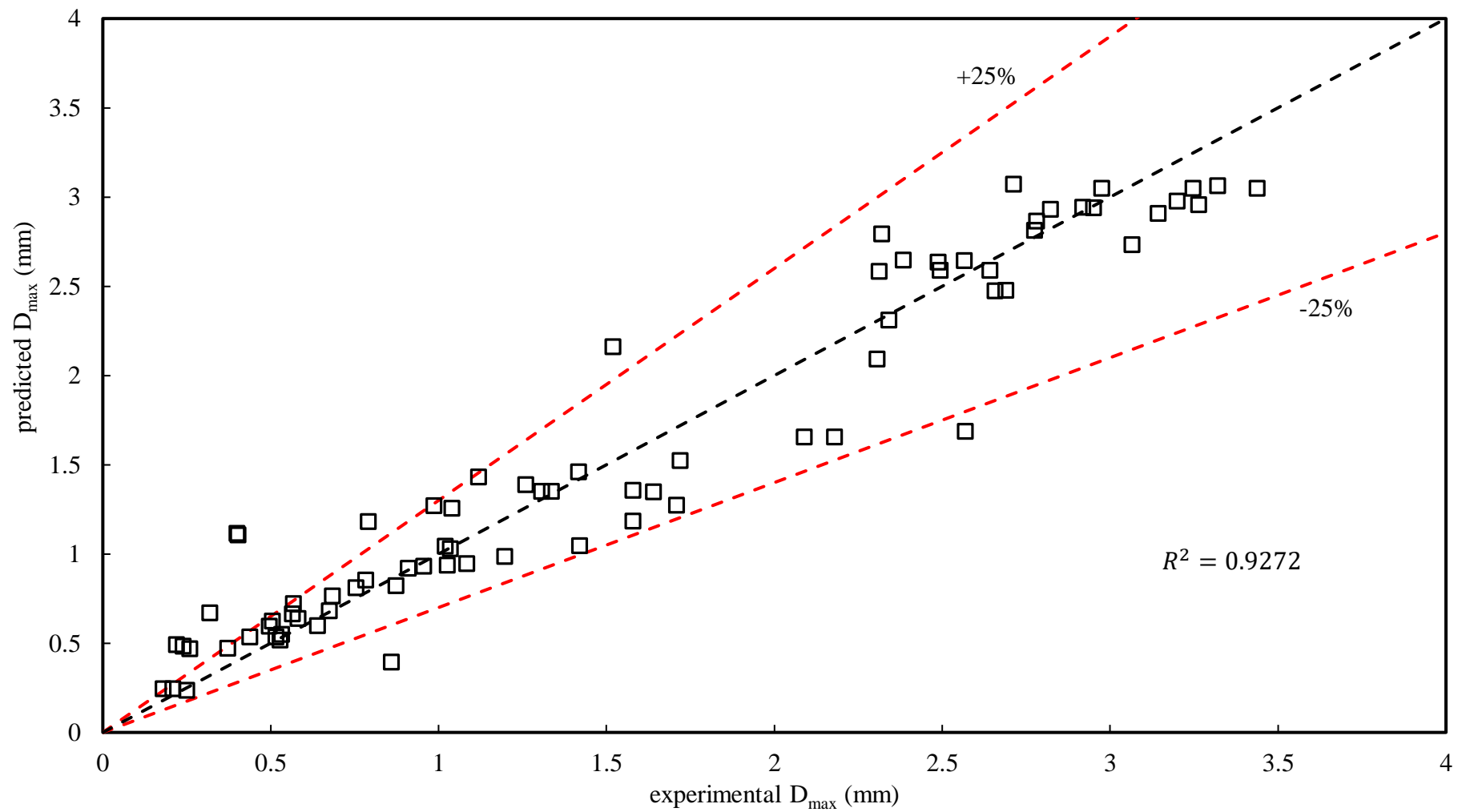
Figure 7.12 Parity plot for bubble maximum diameter.
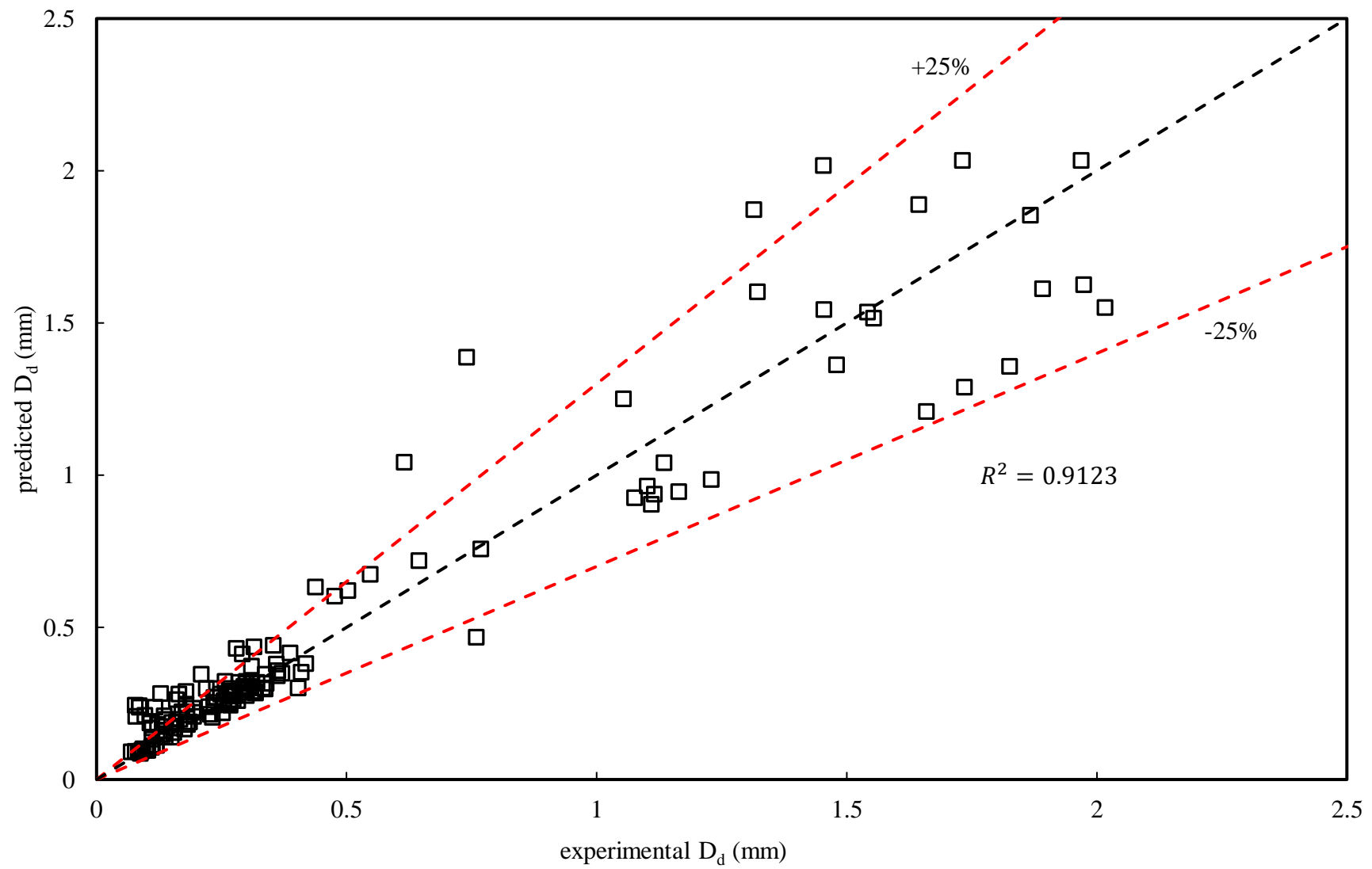
Figure 7.13 Parity plot for bubble departure diameter.
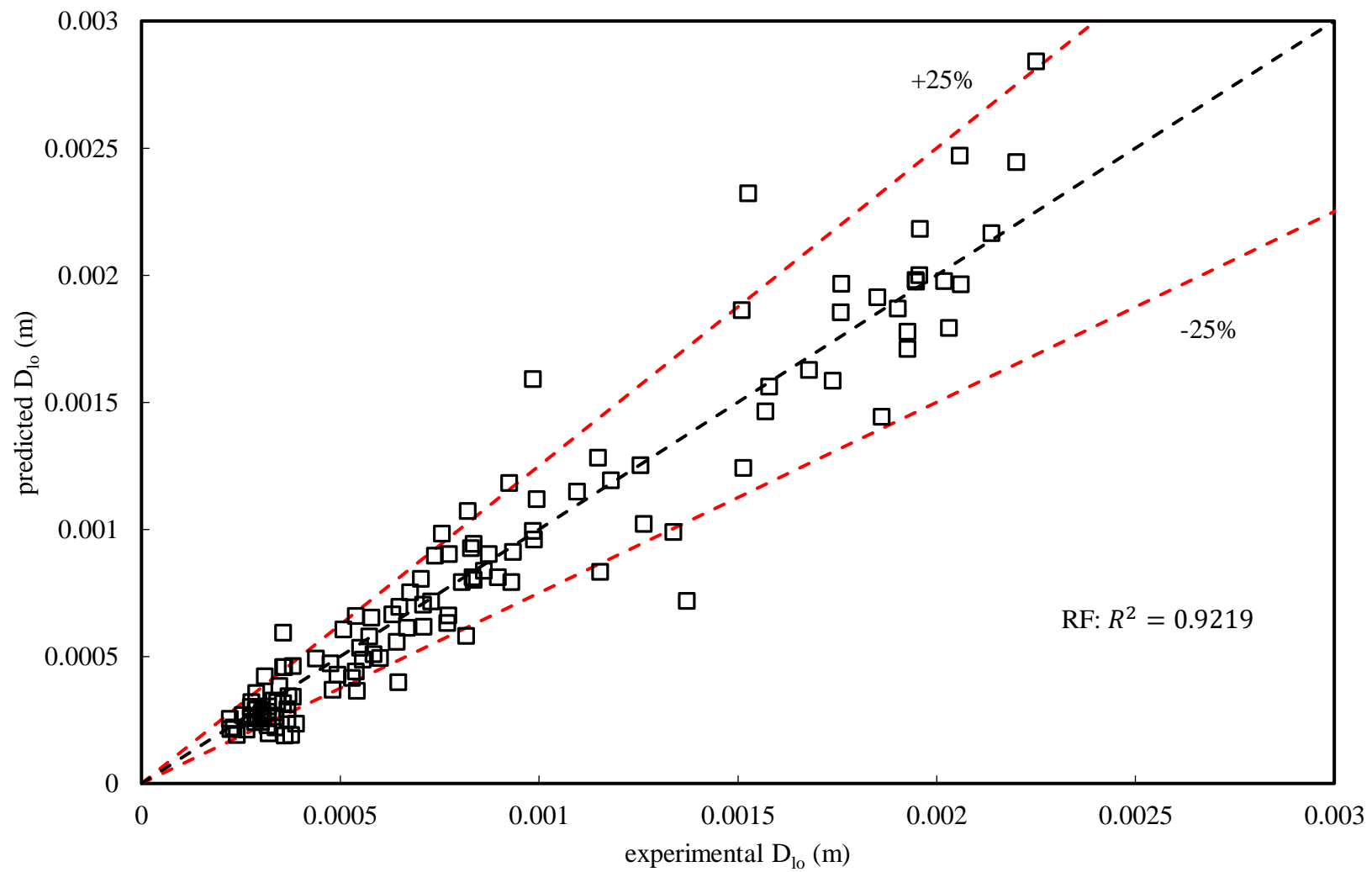
Figure 7.14 Parity plot for bubble lift-off diameter.
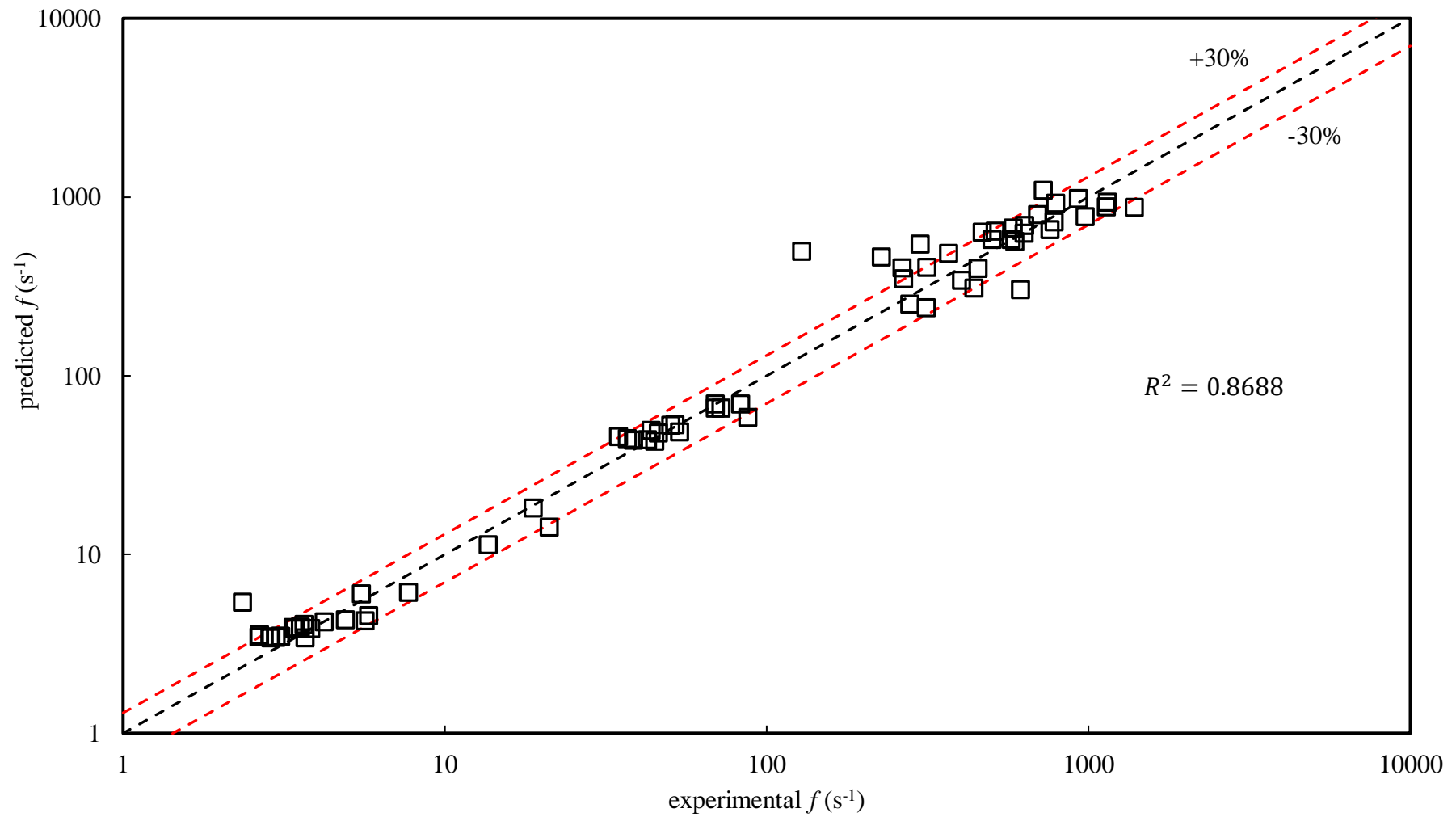
Figure 7.15 Parity plot for bubble departure frequency.

7.5. Closure

The models for bubble departure characteristics form the closure relations in the multiphase heat transfer models with wall boiling. They are important variables in the calculation of evaporation and quenching heat flux components in the total convective boiling heat transfer. The existing models for bubble departure characteristics in flow boiling conditions have been studied, and found to be incapable of providing the desired level of accuracy. Following the attempts made to develop empirical correlations for bubble diameters and departure frequency using conventional regression methods, it was observed that the parameters depend on the simultaneous and combined effects of a large number of variables. This led to the understanding that any empirical model with non-dimensional numbers would not be able to provide the anticipated accuracy, and artificial intelligence should be considered. Hence, machine learning methodology, called *random forest* (RF) has been used in the present work to obtain correlations for the bubble maximum, departure and lift-off diameter and departure frequency. The coefficient of determination for the correlations obtained from RF were found to be much superior as compared to all the other empirical models.

8. Chapter 8

Conclusions and Recommendations for Future Work

In the present work, extensive visualisation experiments have been carried out to study the bubble growth and departure characteristics on a single rod and rod bundles under various conditions relevant to the nuclear reactors. The bubble departure diameter and frequency were studied in pool boiling, cross flow and vertical flow boiling conditions, to gather information about their behaviour with various operating parameters like, applied heat flux, liquid subcooling, liquid mass flux, heater surface characteristics. The main aim was to understand the bubble departure behaviour to be able to recommend new empirical models for both departure diameter and frequency, that can be plugged in the multiphase CFD models for the prediction of two-phase heat transfer, to facilitate the safe design of multiphase heat transfer equipment, like nuclear reactors. Chapter 1 presented a detailed literature survey and listed the major unresolved issues in the literature, that helped to create a clear list of objectives of this study. The major conclusions from the present study and some recommendations for future work are highlighted below:

8.1. Effect of operating conditions, heater surface characteristics and geometry on bubble characteristics in pool boiling.

a) The heat transfer coefficients are substantially affected by the liquid subcooling, heater inclination, and the surface finish. The heat transfer coefficients increased with a decrease in the degree of liquid subcooling, decrease in surface roughness, and an increase in the heater inclination angle.

b) The departure diameter and frequency are increasing functions of the applied heat flux and wall superheat in both pool and cross flow boiling conditions. An increase in the wall heat

flux or wall superheat increases the evaporative heat transfer, and reduces the waiting period of the bubbles, resulting in higher bubble departure diameters and frequencies. This implies that $f.D_d$, which dimensionally represents the velocity of bubble rise in the liquid, is also an increasing function of heat flux. This would make sense, as the higher heat flux would cause more intense natural circulation giving the departing bubble a higher thrust.

c) The departure diameter decreased with an increase in the degree of subcooling due to higher condensation rate on the bubble cap. The bubble departure frequency is an increasing function of the degree of subcooling, but can decrease with subcooling for $\Delta T_{sub} < 5K$.

d) The departure diameter was found to decrease as the surface roughness of the heater increased, while the frequency increased with an increase in surface roughness, however only affected by the surface roughness for low superheats.

e) The diameter was observed to increase with increase in the heater surface area and the inclination angle of the heater element. While the departure frequency increased with increase in inclination angle, it decreased for a bigger heater surface.

8.2. The bubble dynamics in cross flow conditions in horizontal rod bundle in low liquid mass flux conditions, like those in LOCA or prolonged SBO in PHWR, where the passive coolant flow from bottom to top results in localised boiling with liquid cross flow.

a) In case of cross flow boiling, the heat transfer coefficient for the single rod in the channel was the lowest and increased as the number of heated rods in the bundle increased. The vapor rising from the lower heated rod increased the turbulence around the observed rod and bubble sliding decreased the average wall temperature leading to an enhanced heat transfer coefficient in case of heating a rod below the observed rod, compared to only the observed rod heated in the bundle. However, the heating of a rod above the observed rod did not have any effect on the observed heat transfer.

b)   The behaviour of bubble departure diameter and frequency with heat flux, wall superheat and liquid subcooling were identical to that in pool boiling. The departure diameter and frequency both were observed to decrease with an increase in mass flux for cross flow boiling. An increase in mass velocity caused larger drag forces causing the bubbles to detach earlier resulting in smaller departure diameters, and more disruptions in the thermal boundary layer leading to longer waiting periods, and lower departure frequencies.

c)   The departure diameter of vapor bubbles from a single rod in the non-heated bundle were almost equal to that from a single rod in the channel, but increased with increase in the number of heated rods in its neighbourhood. The departure frequency from a single rod in the non-heated bundle was significantly higher compared to that from a single rod in the channel. The frequency further increased with the number of heated rods in the bundle.

8.3.   Bubble characteristics in flow boiling under low heat and mass flux conditions in rod bundle like those during start-up of a natural circulation BWR.

a)   The bubble growth behavior is quite different in the three geometries. In the conventional sized annulus (hydraulic diameter > 4 mm), individual bubbles grow, slide and lift from the heater surface, but in the narrow annulus, coalescing and constricted bubbles could be observed other than a few individual bubbles. The bubbles nucleating in the bundle quickly grew at their sites and slid on to coalesce with the bubbles in their vicinity. They kept on condensing and coalescing with the bubbles in their path till they eventually lifted off the heater surface.

b)   The heat transfer coefficient increases with an increase in the heat flux and a decrease in the liquid subcooling, while with an increase in mass flux, it increases for convective heat transfer but there is no effect of the flow velocity after nucleate boiling sets in. The heat transfer coefficient for similar values of applied heat flux, would be higher for the confined geometries, because of the higher local bulk temperatures. The effect of mass flux was

also lesser in the case of narrow annulus and bundle, implying that convective heat transfer is not the dominant mechanism for these geometries under the presently studied conditions.

c) The bubble maximum, departure and lift-off diameters all showed similar behavior parametrically, i.e. they increased with an increase in heat flux or wall superheat but decrease with an increase in liquid subcooling or liquid flow rate. The departure frequency increased with an increase in heat flux, and decrease in subcooling or liquid flow rate.

d) The bubble departure diameter increased from wide annulus to narrow annulus and further in the bundle due to the confinement. The elongated bubble growth in the narrow annulus allows for the larger contact diameter, and hence, a higher evaporation rate coupled with the lower local subcooling due to lesser flow area, resulted in larger bubbles in the narrow annulus. The coalescence of bubbles in the bundle further gave higher values of bubble sizes. However, the confinement resulted in higher effective velocities for same values of input mass flow rate, causing higher drag forces and more disruptions to the rebuilding of superheated boundary layer, and hence, resulting in lower frequencies.

e) The bubble diameters and frequency increase as the number of heated rods in the bundle increases. Higher number of heated rods would give a higher local bulk temperature, reducing the bubble condensation and a faster evaporation rate resulting in higher bubble sizes and departure rate.

8.4. Development of models for bubble diameter and frequency in subcooled pool and flow boiling conditions.

a) The existing models for bubble departure diameter and frequency in pool boiling conditions were studied using parity plots, which clearly indicated the need for modified models with improved range of applicability and accuracy. Hence, empirical models for bubble departure diameter and frequency in subcooled pool boiling were developed, which

were then extended to cross flow boiling for single horizontal heater and for cross flow boiling in a horizontal rod bundle.

b) The mechanistic and empirical models for bubble maximum, departure and lift-off diameter and departure frequency were studied and were found to be lacking. The mechanistic models need closer physical representation of forces acting on a bubble growing on a surface. From the empirical models in the literature and our own attempts, it was concluded that any kind of empirical correlation relating bubble diameter or frequency with various affecting variables in non-dimensional form is unable to give high degree of accuracy over a wide range of conditions. Hence, correlations for all three bubble diameters and frequency were developed using the machine learning algorithm – random forest – which gave much superior results to all the previously available models.

8.5. Recommendations for future work

In the chapter 1, we listed the gap areas and scope of work to be done. In this study, gap areas have been addressed to some extent. However, as they say, the work is never finished, there is scope for future work on the subject. Some suggestions for future work path are as follows:

a) We carried out parametric studies for bubble departure characteristics in pool boiling for the effect of heater surface characteristics, like size, inclination, surface roughness. The results showed that these parameters have significant influence on the bubble dynamics. Hence, it would be interesting to conduct similar studies in cross flow and parallel- axis flow conditions, for simultaneous measurements of bubble diameters and frequency. It seems intuitive that surface finish and inclination angle would have noteworthy effects on the bubble sliding behaviour. Also, since *average surface roughness R_a* value depends on the process of surface preparation, a more universal parameter to express surface finish should be found.

264

b) The horizontal rod bundle cross flow has been studied for three central rods in a 5×3 bundle. This study shows promising results, and so it would be prudent to extend the study to more number of rods, and to understand the effect of side columns on the central rod bubble dynamics, and vice versa. It would also be interesting to study the bubble dynamics under different bundle geometries (in-line and staggered) for different P/D ratios so as to be able to define the influence of heater rods on bubble dynamics in terms of a more generalised parameter.

c) There is very limited data for bubble characteristics in narrow geometries (mini-or micro-channels or annuli). The conditions studied in this study were limited to low heat and mass fluxes, this range of conditions can be extended for a full range comparison in the bubble dynamics of conventional, mini- and micro- sized geometries. The study should also be conducted for different bundle sizes and packing, so as to vary the confinement number. It would be noteworthy to study the coupling effects of surface area, heat flux and temperature on the heat transfer over the entire boiling curve, starting from the convective region and progressing to the boiling regimes.

d) The empirical models for departure diameter and frequency for pool and cross flow boiling have been developed taking a lot of factors into account, that the previous models didn't consider. However, the empirical models can take us only so far, and looking at the success with the data driven model developed for vertical flow boiling, it would be pragmatic to look for avenues with mechanistic or AI based models for higher degree of accuracy. The mechanistic modelling approach can be used to come up with models with universal non-dimensional numbers for heat transfer and bubble parameters.

Appendix

1. Appendix A

The heat loss calculations in the pool boiling experimental setup.

The convective heat loss through the conducting walls of the tank was estimated as:

$$Ra = \frac{g\beta\Delta T L^3}{\nu\alpha}$$

$$Ra = \frac{9.8 \times 3.15 \times 10^{-3} \times (80-30) \times (0.2)^3}{18.42 \times 10^{-6} \times 2.58 \times 10^{-5}} = 2.6 \times 10^7$$

where the bulk liquid is considered at 80℃ and the ambient air temperature at 30℃ (as measured in experiment). The air thermal properties have been calculated at the film temperature $((80 + 30)/2 = 55℃)$.

$$Nu = \left[0.825 + \frac{0.387 Ra^{1/6}}{[1+\left(\frac{0.492}{Pr}\right)^{\frac{9}{16}}]^{8/27}}\right]^2$$

$$Nu = 40.99$$

$$h = \frac{Nuk}{L}$$

$$h = 3.327 \text{ W/m}^2\text{K}$$

$$Q = hA\Delta T = 38.43W$$

Also taking into account the 1000W power of the auxiliary heater, the percentage loss for an applied power of say, 18W comes out to be

$$\%loss = \frac{38.43}{18+1000} = 3.8\%$$

The maximum loss was observed for the case of bulk liquid 95℃, of ~7%.

The evaporative heat loss from the open top of the tank:

The experiments showed a loss of 1 cm of water height for the experimental run of 1 hour. So, the mass of water evaporated

$m_E = \rho V_E = 0.39\text{kg}$

$Q = m_E h_{fg}/3600\text{s}$

$Q = 246\text{ W}$

And using the same example as above, the percentage evaporative heat loss can be calculated as:

$\%\text{loss} = \dfrac{246}{1000+18} = 24\%$

2.   Appendix B

Referring to Figure 4.1(B), the heat flux is applied at the cartridge heater which is at the centre of the tube. The thermocouples are placed in the holes drilled in the heated rod in a circle of diameter 12 mm. So, the thermocouple measurements show the temperature of the heater rod 4 mm inside the rod surface. Hence, the temperature of the heater rod surface was estimated by correcting for the conduction losses within the stainless steel heated rod. Using the Fourier equation in cylindrical coordinates,

$T(r) = T_c - \dfrac{q''}{k_w} r_c \ln\left(\dfrac{r}{r_c}\right)$

Where T_c is the temperature measured by the thermocouple, q'' is the heat flux at the cartridge heater, k_w is the thermal conductivity of the stainless steel heater rod and r_c is the radius of the thermocouple location circle. The wall temperature thus obtained were used in the parametric studies.

267
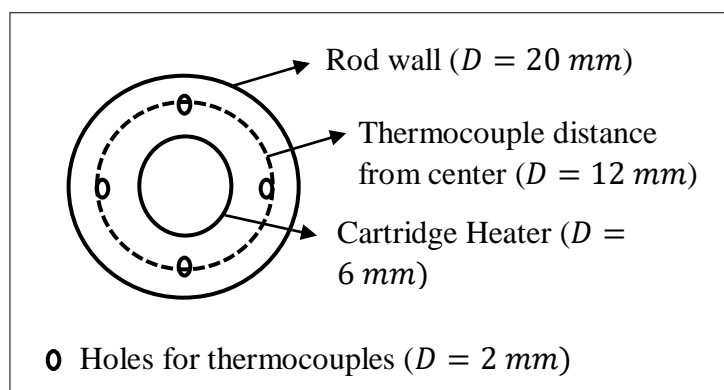
3. Appendix C

The heat loss calculations in the vertical axial flow boiling experimental setup:

To calculate the convective heat loss from glass walls to the ambient air, the natural convection heat transfer coefficient of the air was estimated using Churchill and Chu correlation as before in pool boiling case. For conventional annulus,

$$Ra = \frac{g\beta\Delta T L^3}{v\alpha}$$

$$Ra = \frac{9.8\times3.15\times10^{-3}\times(80-30)\times(0.9)^3}{18.42\times10^{-6}\times2.58\times10^{-5}} = 2.37\times10^9$$

where the bulk liquid is considered at 80℃ and the ambient air temperature at 30℃ (as measured in experiment), and characteristic length is the heated length of the annulus. The air thermal properties have been calculated at the film temperature $((80 + 30)/2 = 55℃)$.

$$Nu = \left[0.825 + \frac{0.387 Ra^{1/6}}{[1+\left(\frac{0.492}{Pr}\right)^{\frac{9}{16}}]^{8/27}}\right]^2$$

$$Nu = 160.183$$

$$h = \frac{Nuk}{L}$$

$$h = 4.33 \, W/m^2 K$$

$$Q = hA\Delta T = 30.63W$$

So, for an applied heat flux of say, 95.47 kW/m^2, the power comes out to be 3239.22 W, and hence, the percentage loss comes out to be

$$\%loss = \frac{30.63}{3239.22} = 1\%$$

The maximum loss was observed to be ~2.5%.

Similarly, for narrow annulus (outer diameter of the glass tube = 21 mm and heated length = 560 mm), the maximum percentage loss was calculated to be ~15%; and for the bundle (outer

diameter of the glass tube = 41 mm and heated length = 560 mm), the maximum percentage loss was estimated to be 20%.

These values have been corrected in the thesis.

The evaporative heat loss from the open top of the reservoir tank:

The experiments showed a loss of 1 cm of water height for the experimental run of 1 hour. So, the mass of water evaporated

$$m_E = \rho V_E = 0.27 kg$$

$$Q = m_E h_{fg}/3600s$$

$$Q = 169.275\ W$$

And using the same example as above, the percentage evaporative heat loss can be calculated as:

$$\%loss = \frac{169.275}{3239.22} = 5\%$$

And the maximum value was observed to be about 7%.

A_b	Bubble influenced area fraction
A_c	Minimum flow area (m^2)
a	gap size in the bundle
Ar	Archimedes number $\left(\frac{g\rho_l(\rho_l-\rho_v)}{\mu_l^2}\left(\frac{\sigma}{g(\rho_l-\rho_v)}\right)^{3/2}\right)$
B	Bubble diameter parallel to heater surface
Bo	Bond number $\left(\frac{gD_d^2(\rho_l-\rho_v)}{\sigma}\right)$
Bg	Boiling number $\left(\frac{q''}{Gh_{fg}}\right)$
C	Bubble diameter perpendicular to heater surface
Ca	Capillary number $\left(\frac{\mu_v v}{\sigma cos\theta}\right)$
C_D	Drag coefficient
C_f	Friction coefficient
CHF	Critical Heat Flux (kW/m^2)
C_L	Lift coefficient
C_p	Specific heat capacity at constant pressure $(kJ/kg.K)$
Co	Convection number $\left(\left(\frac{1-x}{x}\right)^{0.8}\left(\frac{\rho_v}{\rho_l}\right)^{0.5}\right)$
C_{sf}	Rohsenow constant
D	Diameter (mm)
D_h	Hydraulic diameter (mm)
d_w	Bubble contact diameter (mm)
f	Departure frequency $(Hz \; or \; s^{-1})$
F, F_2	Enhancement factor or Force (N)
F_{fl}	Fluid-surface parameter given by Kandlikar (1990)

Fr	Froude number $(G^2/\rho^2 gD)$
g	Acceleration due to gravity (m/s^2)
G	Mass flux $(kg/m^2 s)$
G_s	Dimensionless shear rate
h	Heat transfer coefficient $(kW/m^2 K)$
h_{fg}	Latent heat of vaporization (kJ/kg)
H	Height from start of heating zone (m)
I	Current (A)
Ja or Ja_{sup}	Superheat based Jakob number $\left(\frac{\rho_l C_p \Delta T_{sat}}{\rho_v h_{fg}}\right)$
Ja_{sub}	Subcooling based Jakob number $\left(\frac{\rho_l C_p \Delta T_{sub}}{\rho_v h_{fg}}\right)$
Ja_T	Overall temperature difference based Jakob number $\left(\frac{\rho_l C_p \Delta T}{\rho_v h_{fg}}\right)$
k	Thermal conductivity $(W/m.K)$
K_l	model parameter defined in *Table 1.5*
l	Length of the heater rod (mm)
L	Perimeter of heated rod (m)
L_c	Laplace length scale $\left(\sqrt{\frac{\sigma}{g(\rho_l - \rho_v)}}\right)$
$\dot{m}$	Mass flow rate (kg/s)
M	Molecular weight
n	Number of heated tubes in the bundle
N	row number from bottom in a horizontal bundle
N_a	Active nucleation site density
N_{conf}	Confinement number $\left(\frac{1}{D_h}\sqrt{\frac{\sigma}{g(\rho_l - \rho_v)}}\right)$

P	Pressure (bar)
p_r	Reduced pressure
ΔP	$P(T_w) - P(T_{sat})\ (N/m^2)$
P/D	Pitch to diameter ratio
Pe	Péclet number $(Re.Pr)$
Pr	Prandtl number $\left(\frac{C_p \mu}{k}\right)$
Q	Volumetric Flow rate (m^3/hr)
$q"$	Applied wall heat flux (kW/m^2)
r	Bubble nuclei radius
r_c	Nucleating cavity radius (mm)
R	Bubble radius (mm)
R_a or R_a	Average surface roughness value (μm)
Re	Reynolds number $\left(\frac{GD}{\nu}\right)$
Re_b	Bubble Reynolds number (defined in *Table 1.10*)
Re_B	Reynolds number for boiling, $\left(\frac{q"}{\mu h_{fg}} \sqrt{\frac{\sigma}{\rho_l - \rho_v}}\right)$
S, S_2	Suppression factors
t	time (ms)
t_g	Bubble growth time (ms)
t_w	Bubble waiting period (ms)
T	Temperature (K)
T_f	Bubble time period (s)
ΔT	$(T_w - T_l)\ (K)$
ΔT_{sat}	Degree of wall superheat (K)
ΔT_{sub}	Degree of subcooling (K)

U	Liquid velocity (m/s)
v	Vapor velocity (m/s)
v_{fg}	Specific density change of phase transition (m^3/kg)
V	Volume (m^3)
V_o	Voltage (V)
x	Vapor quality
Y_{IB}	Boiling intensity parameter in *Table 1.7*

Subscripts

b	bubble
d	departure
e	evaporative
in	inlet
l	liquid
lo	lift-off
loc	local
m	mean
max	maximum
mic	micro-convective or pool boiling
nb	nucleate boiling
q	quenching
sat	saturation
sp	single phase
sph	spheroid
su	vapor superficial
TP	Two-phase

v	vapor
w	wall
y	direction perpendicular to surface

Greek Symbols

α	Thermal diffusivity (m^2/s) or advancing contact angle (°)
β	Receding contact angle (°)
γ	Liquid-surface interaction parameter $\left(\sqrt{\frac{k_w C_w \rho_w}{k_l C_{p,l} \rho_l}}\right)$
δ	boundary layer thickness
θ	Contact angle (°)
ϑ	Subcooling number $\left(\frac{T_w - T_l}{T_w - T_{sat}}\right)$
λ	Friction factor
μ	Dynamic viscosity $(Pa.s)$
ν	Kinematic viscosity (m^2/s)
ρ	Density (kg/m^3)
σ	Surface tension (N/m)
τ	Shear stress
φ	Bubble inclination angle (°)
ϕ	Heater inclination angle (°)
ψ	Ratio of total to single phase heat transfer coefficient

Bibliography

Abdelmessih, A. H., Hooper, F. C. and Nangia, S. ((1972)) 'Flow effects on bubble growth and collapse in surface boiling', *International Journal of Heat and Mass Transfer*, 15(1), pp. 115–125. doi: 10.1016/0017-9310(72)90170-6.

Ahmadi, R. and Okawa, T. ((2015)) 'Influence of surface wettability on bubble behavior and void evolution in subcooled flow boiling', *International Journal of Thermal Sciences*, 97, pp. 114–125. doi: 10.1016/j.ijthermalsci.2015.06.012.

Ahmadi, R., Ueno, T. and Okawa, T. ((2012)) 'Bubble dynamics at boiling incipience in subcooled upward flow boiling', *International Journal of Heat and Mass Transfer*. Elsevier Ltd, 55(1–3), pp. 488–497. doi: 10.1016/j.ijheatmasstransfer.2011.09.050.

Ali, A. and Judd, R. L. ((1981)) 'An Analytical and Experimental Investigation of Bubble Waiting Time in Nucleate Boiling', *Journal of Heat Transfer-Transactions of the Asme*, 103(November), pp. 673–678.

Ammerman, C. N., You, S. M. and Hong, Y. S. ((1996)) 'Identification of Pool Boiling Heat Transfer Mechanisms From a Wire Immersed in Saturated FC-72 Using a Single-Photo/LDA Method', *Journal of Heat Transfer*, 118(1), pp. 117. doi: 10.1115/1.2824024.

Anklam, T. M. and Miller, R. F. ((1982)) 'Void fraction under high pressure, low flow conditions in rod bundle geometry', *Nuclear Engineering and Design*, 75, pp. 99–108. doi: 10.1016/0029-5493(83)90083-3.

Bang, I. C., Chang, S. H. and Baek, W. P. ((2004)) 'Visualization of the subcooled flow boiling of R-134a in a vertical rectangular channel with an electrically heated wall', *International Journal of Heat and Mass Transfer*, 47(19–20), pp. 4349–4363. doi: 10.1016/j.ijheatmasstransfer.2004.04.030.

Basu, N., Warrier, G. R. and Dhir, V. K. ((2005)a) 'Wall Heat Flux Partitioning During Subcooled Flow Boiling: Part 1—Model Development', *Journal of Heat Transfer*, 127(2), pp.

131-140. doi: 10.1115/1.1842784.

Basu, N., Warrier, G. R. and Dhir, V. K. ((2005)b) 'Wall Heat Flux Partitioning During Subcooled Flow Boiling: Part II—Model Validation', *Journal of Heat Transfer*, 127(2), pp. 141-148. doi: 10.1115/1.1842785.

Benjamin, R. J. and Balakrishnan, A. R. ((1997)) 'Nucleation Site Density in Pool Boiling of Saturated Pure Liquids: Effect of Surface Microroughness and Surface and Liquid Physical Properties', *Experimental Thermal and Fluid Science*, 15(1), pp. 32–42. doi: 10.1016/S0894-1777(96)00168-9.

Bergez, W. ((1995)) 'Nucleate boiling on a thin heating plate: heat transfer and bubbling activity of nucleation sites', *International Journal of Heat and Mass Transfer*, 38(10), pp. 1799–1811. doi: 10.1016/0017-9310(94)00296-8.

Bibeau, E. L. and Salcudean, M. ((1994)) 'A study of bubble ebullition in forced- convective subcooled nucleate boiling at low pressure', *International Journal of Heat and Mass Transfer*, 37(15), pp. 2245–2259.

Bovard, S. *et al.* ((2017)) 'Investigation and experimental analysis of the bubble departure diameter in pure liquids on horizontal cylindrical heater', *Heat and Mass Transfer/Waerme-und Stoffuebertragung*. Springer Berlin Heidelberg, 53(4), pp. 1199–1210. doi: 10.1007/s00231-016-1885-3.

Breiman, L. ((2001)) 'Random forests', *Machine Learning*, 45(1), pp. 5–32. doi: 10.1023/A:1010933404324.

Brooks, C. S. and Hibiki, T. ((2015)) 'Wall nucleation modeling in subcooled boiling flow', *International Journal of Heat and Mass Transfer*. Elsevier Ltd, 86, pp. 183–196. doi: 10.1016/j.ijheatmasstransfer.2015.03.005.

Cao, Y. *et al.* ((2016)) 'Visualization study on bubble dynamical behavior in subcooled flow boiling under various subcooling degree and flowrates', *International Journal of Heat and*

Mass Transfer. Elsevier Ltd, 93, pp. 839–852. doi: 10.1016/j.ijheatmasstransfer.2015.10.053.

Chen, C. A. *et al.* ((2009)) 'Subcooled flow boiling heat transfer of R-407C and associated bubble characteristics in a narrow annular duct', *International Journal of Heat and Mass Transfer*. Elsevier Ltd, 52, pp. 3147–3158. doi: 10.1016/j.ijheatmasstransfer.2009.01.027.

Chen, D.-Q. and Pan, L. M. ((2010)) 'Prediction Model for Bubble Contact Circle Diameter on Heating Wall', in *Proceedings of 18th International Conference on Nuclear Engineering ICONE18*. Xi'an, China, pp. 1–6. doi: 10.1115/ICONE18-30084.

Chen, D., Pan, L. M. and Ren, S. ((2012)) 'Prediction of bubble detachment diameter in flow boiling based on force analysis', *Nuclear Engineering and Design*, 243, pp. 263–271. doi: 10.1016/j.nucengdes.2011.11.022.

Chen, D. Q. *et al.* ((2011)) 'The nature of bubble growth under different system pressures in a narrow channel', *Nuclear Engineering and Design*. Elsevier B.V., 241(3), pp. 785–791. doi: 10.1016/j.nucengdes.2010.12.013.

Chen, J. C. ((1966)) 'Correlation for boiling heat transfer to saturated fluids in convective flow', *IIndustrial and Engineering Chemistry - Process Design and Development*, 5(3), pp. 322–329.

Chen, L.-T. and Chuang, W.-C. ((1979)) 'The Effect of Orientation on R-11 Bubble Frequencies in Nucleate Pool Boiling', *Letters in Heat and Mass Transfer*, 6, pp. 429–438.

Chi-Yeh, H. and Griffith, P. ((1965)) 'The mechanism of heat transfer in nucleate pool boiling-Part II. The heat flux-temperature difference relation', *International Journal of Heat and Mass Transfer*, 8(6), pp. 905–914. doi: 10.1016/0017-9310(65)90074-8.

Chu, I. C., No, H. C. and Song, C. H. ((2011)) 'Bubble lift-off diameter and nucleation frequency in vertical subcooled boiling flow', *Journal of Nuclear Science and Technology*, 48(6), pp. 936–949. doi: 10.1080/18811248.2011.9711780.

Cole, R. ((1960)) 'A photographic study of pool boiling in the region of the critical heat flux',

AIChE Journal, 6(4), pp. 533–538. doi: 10.1002/aic.690060405.

Cole, R. ((1967)) 'Bubble frequencies and departure volumes at subatmospheric pressures', *AIChE Journal*, 13(4), pp. 779–783. doi: 10.1002/aic.690130434.

Cole, R. and Rohsenow, W. M. ((1969)) 'Correlation of bubble departure diameters for boiling of saturated liquids', in *Chemical Engineering Progress Symposium Series 65*, pp. 211–213.

Cole, R. and Shulman, H. L. ((1966)) 'Bubble growth rates at high Jakob numbers', *International Journal of Heat and Mass Transfer*, 9(12), pp. 1377–1390. doi: 10.1016/0017-9310(66)90135-9.

Colombo, M. and Fairweather, M. ((2015)) 'Prediction of bubble departure in forced convection boiling: A mechanistic model', *International Journal of Heat and Mass Transfer*. Elsevier Ltd, 85, pp. 135–146. doi: 10.1016/j.ijheatmasstransfer.2015.01.103.

Cooper, M. G. ((1984)) 'Saturation nucleate pool boiling-a simple correlation', in *IchemE Symp. Ser.*, pp. 785–793. Available at: http://ci.nii.ac.jp/naid/10012447676/en/.

Cornwell, K. and Schuller, R. B. ((1982)) 'A study of boiling outside a tube bundle using high speed photography', *International Journal of Heat and Mass Transfer*, 25(5), pp. 683–690.

Plesset, M. S. and Zwick, S. A. ((1954)) 'The growth of vapor bubbles in superheated liquids', *Journal of Applied Physics*, 25(4), pp. 493–500. doi: 10.1063/1.1721668.

Demiray, F. and Kim, J. ((2004)) 'Microscale heat transfer measurements during pool boiling of FC-72: Effect of subcooling', *International Journal of Heat and Mass Transfer*, 47, pp. 3257–3268. doi: 10.1016/j.ijheatmasstransfer.2004.02.008.

Duan, X. *et al.* ((2013)) 'Synchronized high-speed video, infrared thermometry, and particle image velocimetry data for validation of interface-tracking simulations of nucleate boiling phenomena', *Experimental Heat Transfer*, 26(2–3), pp. 169–197. doi: 10.1080/08916152.2012.736837.

Duke, E. and Schrock, V. E. ((1961)) 'Void volume site density and bubble size for subcooled

nucleate pool boiling', in *Proceedings of the 1961 Heat Transfer and Fluid mechanics Institute*, pp. 130–145.

Eliceiri, K. *et al.* ((2012)) 'NIH Image to ImageJ : 25 years of image analysis HISTORICAL commentary NIH Image to ImageJ : 25 years of image analysis', *Nature Methods*, 9(7), pp. 671–675. doi: 10.1038/nmeth.2089.

Euh, D. *et al.* ((2010)) 'Characteristics of bubble departure frequency in a low-pressure subcooled boiling flow', *Journal of Nuclear Science and Technology*, 47(7), pp. 608–617. doi: 10.1080/18811248.2010.9720958.

Faneuff, C. E., McLean, E. A. and Scherrer, V. E. ((1958)) 'Some aspects of surface boiling', *Journal of Applied Physics*, 29(1), pp. 80–84. doi: 10.1063/1.1722950.

Plesset, M. S. and Zwick, S. A. ((1954)) 'The growth of vapor bubbles in superheated liquids', *Journal of Applied Physics*, 25(4), pp. 493–500. doi: 10.1063/1.1721668.

Forster, H. K. and Zuber, N. ((1955)) 'Dynamics of vapor bubbles and boiling heat transfer', *AIChE Journal*, 1(4), pp. 531–535. doi: 10.1002/aic.690010425.

Fritz, W. ((1935)) 'Berechnung des Maximalvolumes von Dampfblasen', *Physik. Zeitschr*, 36, pp. 379–384.

Gaertner, R. F. ((1965)) 'Photographic Study of Nucleate Pool Boiling on a Horizontal Surface', *Journal of Heat Transfer*, 87, pp. 17. doi: 10.1115/1.3689038.

Gerardi, C. *et al.* ((2010)) 'Study of bubble growth in water pool boiling through synchronized, infrared thermometry and high-speed video', *International Journal of Heat and Mass Transfer*, 53(19–20), pp. 4185–4192. doi: 10.1016/j.ijheatmasstransfer.2010.05.041.

Githinji, P. M. and Sabersky, R. H. ((1963)) 'Some Effects of the Orientation of the Heating Surface in Nucleate Boiling', *Journal of Heat Transfer*, 85(4), pp. 379. doi: 10.1115/1.3686129.

Guan, P. *et al.* ((2015)) 'Bubble departure size in flow boiling', *Heat and Mass Transfer*, 51(7),

pp. 921–930. doi: 10.1007/s00231-014-1461-7.

Guan, P. *et al.* ((2016)) 'Effect of Bubble Contact Diameter on Bubble Departure Size in Flow Boiling', *Experimental Heat Transfer*, 29(1), pp. 37–52. doi: 10.1080/08916152.2014.926433.

Gungor, K. E. and Winterton, R. H. S. ((1986)) 'A general correlation for flow boiling in tubes and annuli', *International Journal of Heat and Mass Transfer*, 29(3), pp. 351–358. doi: 10.1016/0017-9310(86)90205-X.

Gunther, F. C. ((1951)) 'Photographic study of surface boiling heat transfer to water with forced convection.', *ASME Journal of Heat Transfer*, 73, pp. 115–123.

Gupta, A. ((2005)) 'Enhancement of boiling heat transfer in a 5 × 3 tube bundle', *International Journal of Heat and Mass Transfer*, 48(18), pp. 3763–3772. doi: 10.1016/j.ijheatmasstransfer.2005.03.023.

Gupta, A., Kumar, R. and Kumar, V. ((2010)) 'Nucleate pool boiling heat transfer over a bundle of vertical tubes', *International Communications in Heat and Mass Transfer*. Elsevier Ltd, 37(2), pp. 178–181. doi: 10.1016/j.icheatmasstransfer.2009.06.023.

Gupta, A., Saini, J. S. and Varma, H. K. ((1995)) 'Boiling heat transfer in small horizontal tube bundles at low cross-flow velocities', *International Journal of Heat and Mass Transfer*, 38(4), pp. 599–605. doi: 10.1016/0017-9310(94)00282-Z.

Hamzekhani, S. *et al.* ((2015)) 'Experimental study on bubble departure frequency for pool boiling of water/NaCl solutions', *Heat and Mass Transfer/Waerme- und Stoffuebertragung*, 51(9), pp. 1313–1320. doi: 10.1007/s00231-015-1502-x.

Hamzekhani, S., Maniavi Falahieh, M. and Akbari, A. ((2014)) 'Bubble departure diameter in nucleate pool boiling at saturation: Pure liquids and binary mixtures', *International Journal of Refrigeration*. Elsevier Ltd and IIR, 46(256), pp. 50–58. doi: 10.1016/j.ijrefrig.2014.07.003.

Hatton, A. P. and Hall, I. S. ((1966)) 'Photographic study of boiling on prepared surfaces', in *3rd International Heat Transfer Conference, Chicago*, pp. 24–37.

Henry, C. D. and Kim, J. ((2004)) 'A study of the effects of heater size, subcooling, and gravity level on pool boiling heat transfer', *International Journal of Heat and Fluid Flow*, 25(2), pp. 262–273. doi: 10.1016/j.ijheatfluidflow.2003.11.019.

Hoang, N. H. *et al.* ((2016)) 'A mechanistic model for predicting the maximum diameter of vapor bubbles in a subcooled boiling flow', *International Journal of Heat and Mass Transfer*. Elsevier Ltd, 94, pp. 174–179. doi: 10.1016/j.ijheatmasstransfer.2015.11.051.

Holman, J. P. ((1968)) *Heat Transfer*.

Hong, G. *et al.* ((2012)) 'Bubble departure size in forced convective subcooled boiling flow under static and heaving conditions', *Nuclear Engineering and Design*. Elsevier B.V., 247, pp. 202–211. doi: 10.1016/j.nucengdes.2012.03.008.

Hospeti, N. B. and Mesler, R. B. ((1969)) 'Vaporization at the base of bubbles of different shape during nucleate boiling of water', *AIChE Journal*, 15(2), pp. 214–219. doi: 10.1002/aic.690150217.

Hsu, Y. Y. and Graham, R. W. ((1961)) *An analytical and experimental study of the thermal boundary layer and ebullition cycle in nucleate boiling*. Washington.

Hsu, Y. Y. ((1962)) 'On the Size Range of Active Nucleation Cavities on a Heating Surface', *Journal of Heat Transfer*, 84(3), pp. 207–213. doi: 10.1115/1.3684339.

Hutter, C. *et al.* ((2012)) 'Nucleation site interaction between artificial cavities during nucleate pool boiling on silicon with integrated micro-heater and temperature micro-sensors', *International Journal of Heat and Mass Transfer*. Elsevier Ltd, 55(11–12), pp. 2769–2778. doi: 10.1016/j.ijheatmasstransfer.2012.02.014.

Hwang, T. H. and Yao, S. C. ((1986)) 'Forced Convective Boiling in horizontal tube bundles', *International Journal of Heat and Mass Transfer*, 29(5), pp. 785–795.

Ibrahim, E. A. and Judd, R. L. ((1985)) 'An Experimental Investigation of the Effect of Suboooiing on Bubble Growth and Waiting Time in Nucleate Boiling', *Journal of Heat*

Transfer-Transactions of the Asme, 107(February), pp. 168–174.

Incropera, F. P. *et al.* ((2002)) *Fundamentals of Heat and Mass Transfer*. sixth edit. John Wiley & Sons.

Inoue, A. *et al.* ((1995)) 'Void fraction distribution in BWR fuel assembly and evaluation of subchannel code', *Journal of Nuclear Science and Technology*, 32(7), pp. 629–640. doi: 10.1080/18811248.1995.9731754.

Inoue, T., Kawae, N. and Monde, M. ((1998)) 'Effect of subcooling on critical heat flux during pool boiling on a horizontal heated wire', *Heat and Mass Transfer/Waerme- und Stoffuebertragung*, 33(5–6), pp. 481–488. doi: 10.1007/s002310050219.

Ivey, H. J. ((1967)) 'Relationships between bubble frequency, departure diameter and rise velocity in nucleate boiling', *International Journal of Heat and Mass Transfer*, 10(8), pp. 1023–1040. doi: 10.1016/0017-9310(67)90118-4.

Jakob, M. ((1949)) *Heat Transfer*. New York: John Wiley & Sons.

Jakob, M. and Fritz, W. ((1931)) 'Versuche uber den Verdampfungsvorgang', *Forsch. Ingenieurwes*, 2, pp. 435–447.

Jawurek, H. H. ((1969)) 'Simultaneous determination of microlayer geometry and bubble growth in nucleate boiling', *International Journal of Heat and Mass Transfer*, 12(8), pp. 843–848. doi: http://dx.doi.org/10.1016/0017-9310(69)90151-3.

Jensen, M. K. and Hsu, J. T. ((1988)) 'A Parametric Study of Boiling Heat Transfer in a Tube Bundle', *Journal of Heat Transfer*, 110(November 1988), pp. 976–981.

Jensen, M. K. and Memmel, G. J. ((1986)) 'Evaluation of bubble departure diameter correlations.', in *Proceedings of Eighth International Heat Transfer Conference, Vol. 4*, pp. 1907–1912.

Jones, B. J., McHale, J. P. and Garimella, S. V. ((2009)) 'The Influence of Surface Roughness on Nucleate Pool Boiling Heat Transfer', *Journal of Heat Transfer*, 131(12), pp. 121009. doi:

10.1115/1.3220144.

Judd, R. L. and Hwang, K. S. ((1976)) 'A Comprehensive Model for Nucleate Pool Boiling Heat Transfer Including Microlayer Evaporation', *Journal of Heat Transfer*, 98(4), pp. 623. doi: 10.1115/1.3450610.

Kandlikar, S. G. ((1990)) 'A General Correlation for Saturated Two-Phase Flow Boiling Heat Transfer Inside Horizontal and Vertical Tubes', *Journal of Heat Transfer*, 112(1), pp. 219. doi: 10.1115/1.2910348.

Kang, M.-G. ((2003)) 'Effects of Tube Inclination Angle on Nucleate Pool Boiling Heat Transfer', *Nuclear Engineering and Design*, 220, pp. 67–81. doi: 10.3795/KSME-B.2002.26.1.116.

Kew, P. A. and Cornwell, K. ((1997)) 'Correlations for the prediction of boiling heat transfer in small-diameter channels', *Applied Thermal Engineering*, 17(8–10), pp. 705–715. doi: 10.1016/S1359-4311(96)00071-3.

Khan, W. A., Culham, R. J. and Yovanovich, M. M. ((2006)) 'Analytical Model for Convection Heat Transfer from Tube Banks', *Journal of Thermophysics and Heat Transfer*, 20(4), pp. 720–727. doi: 10.2514/1.15453.

Kim, J. and Kim, M. H. ((2006)) 'On the departure behaviors of bubble at nucleate pool boiling', *International Journal of Multiphase Flow*, 32(10–11), pp. 1269–1286. doi: 10.1016/j.ijmultiphaseflow.2006.06.010.

Kim, J., Oh, B. Do and Kim, M. H. ((2006)) 'Experimental study of pool temperature effects on nucleate pool boiling', *International Journal of Multiphase Flow*, 32(2), pp. 208–231. doi: 10.1016/j.ijmultiphaseflow.2005.09.005.

Klausner, J. F. *et al.* ((1993)) 'Vapor bubble departure in forced convection boiling', *International Journal of Heat and Mass Transfer*, 36(3), pp. 651–662. doi: 10.1016/0017-9310(93)80041-R.

Kocamustafaogullari, G. ((1983)) 'Pressure dependence of bubble departure diameter for water', *International Communications in Heat and Mass Transfer*, 10(6), pp. 501–509. doi: 10.1016/0735-1933(83)90057-X.

Kumamaru, H. *et al.* ((1994)) 'Void-fraction distribution under high-pressure boil-off conditions in rod bundle geometry', *Nuclear Engineering and Design*, 150, pp. 95–105. doi: 10.1016/0029-5493(94)90054-X.

Kumar, A. *et al.* ((2015)) 'A review on the thermal hydraulic characteristics of the air-cooled heat exchangers in forced convection', *Indian Academy of Sciences*, 40(May), pp. 673–755. doi: 10.1007/s12046-015-0362-x.

Kumar, A. *et al.* ((2016)) '3D CFD simulations of air cooled condenser-III: Thermal-hydraulic characteristics and design optimization under forced convection conditions', *International Journal of Heat and Mass Transfer*. Elsevier Ltd, 93, pp. 1227–1247. doi: 10.1016/j.ijheatmasstransfer.2015.10.048.

Kumar, S., Mohanty, B. and Gupta, S. . ((2002)) 'Boiling heat transfer from a vertical row of horizontal tubes', *International Journal of Heat and Mass Transfer*, 45(18), pp. 3857–3864. doi: 10.1016/S0017-9310(01)00360-X.

Kurul, N. and Podowski, M. Z. ((1990)) 'Multidimensional effects in forced convection subcooled boiling', in *Proceedings of 9th International Heat Transfer Conference, Jerusalem, Israel*, pp. 21–26.

Kutateladze, S. S. and Gogonin, I. I. ((1979)) 'Growth rate and detachment diameter of a vapour bubble in free convection boiling of saturated liquids.', *High Temperature*, 17, pp. 667–671.

Lee, H. C. *et al.* ((2003)) 'Single bubble growth in saturated pool boiling on a constant wall temperature surface', *International Journal of Multiphase Flow*, 29(12), pp. 1857–1874. doi: 10.1016/j.ijmultiphaseflow.2003.09.003.

Lee, P. C., Tseng, F. G. and Pan, C. ((2004)) 'Bubble dynamics in microchannels. Part I: Single microchannel', *International Journal of Heat and Mass Transfer*, 47, pp. 5575–5589. doi: 10.1016/j.ijheatmasstransfer.2004.02.031.

Leong, L. S. and Cornwell, K. ((1979)) 'Flow boiling heat transfer coefficients in a kettle reboiler tube bundle.', *Chemical Engineering London*, 343, pp. 219.

Levy, S. ((1967)) 'Forced convection subcooled boiling-prediction of vapor volumetric fraction', *International Journal of Heat and Mass Transfer*, 10(7), pp. 951–965. doi: 10.1016/0017-9310(67)90071-3.

Lie, Y. M. and Lin, T. F. ((2006)) 'Subcooled flow boiling heat transfer and associated bubble characteristics of R-134a in a narrow annular duct', *International Journal of Heat and Mass Transfer*, 49(13–14), pp. 2077–2089. doi: 10.1016/j.ijheatmasstransfer.2005.11.032.

Lu, J. F. and Peng, X. F. ((2006)) 'Bubble leaping and slipping during subcooled boiling on thin wires', *International Journal of Thermal Sciences*, 45(9), pp. 908–916. doi: 10.1016/j.ijthermalsci.2005.12.003.

Marcus, B. D. and Dropkin, D. ((1963)) 'The Effect of Surface Configuration on Nucleate Boiling Heat Transfer', *International Journal of Heat and Fluid Flow*, 6, pp. 863–867.

Plesset, M. S. and Zwick, S. A. ((1954)) 'The growth of vapor bubbles in superheated liquids', *Journal of Applied Physics*, 25(4), pp. 493–500. doi: 10.1063/1.1721668.

McFadden, P. W. and Grassmann, P. ((1962)) 'The relation between bubble frequency and diameter during nucleate pool boiling', *International Journal of Heat and Mass Transfer*, 5, pp. 169–173.

McHale, J. P. and Garimella, S. V. ((2010)) 'Bubble nucleation characteristics in pool boiling of a wetting liquid on smooth and rough surfaces', *International Journal of Multiphase Flow*. Elsevier Ltd, 36(4), pp. 249–260. doi: 10.1016/j.ijmultiphaseflow.2009.12.004.

McHale, J. P. and Garimella, S. V. ((2013)) 'Nucleate boiling from smooth and rough surfaces

- Part 2: Analysis of surface roughness effects on nucleate boiling', *Experimental Thermal and Fluid Science*. Elsevier Inc., 44, pp. 439–455. doi: 10.1016/j.expthermflusci.2012.08.005.

Mikic, B. B. and Rohsenow, W. M. ((1969)) 'A New Correlation of Pool-Boiling Data Including the Effect of Heating Surface Characteristics', *Journal of Heat Transfer*, 91(2), pp. 245-250. doi: 10.1115/1.3580136.

Mitsutake, T. *et al.* ((1990)) 'Void fraction estimation within rod bundles based on three-fluid model and comparison with x-ray CT void data', *Nuclear Engineering and Design*, 120, pp. 203–212.

Murshed, S. M. S. *et al.* ((2010)) 'An experimental investigation of bubble nucleation of a refrigerant in pressurized boiling flows', *Energy*. Elsevier Ltd, 35(12), pp. 5143–5150. doi: 10.1016/j.energy.2010.07.052.

Nimkar, N. D., Bhavnani, S. H. and Jaeger, R. C. ((2006)) 'Effect of nucleation site spacing on the pool boiling characteristics of a structured surface', *International Journal of Heat and Mass Transfer*, 49(17–18), pp. 2829–2839. doi: 10.1016/j.ijheatmasstransfer.2006.02.018.

Nishikawa, K. *et al.* ((1984)) 'Effect of surface configuration on nucleate boiling heat transfer', *International Journal of Heat and Mass Transfer*, 27(9), pp. 1559–1571. doi: 10.1016/0017-9310(84)90268-0.

Nishikawa, K., Kusuda, H. and Yamasaki, K. ((1965)) 'Growth and Collapse of Bubbles in Nucleate Boiling', *Bulletin of Japan society of Mechanical Engineers*, 8(30), pp. 205–210.

Nukiyama, S. ((1934)) 'The maximum and minimum values of the heat Q transmitted from metal to boiling water under atmospheric pressure', *International Journal of Heat and Mass Transfer*, 9, pp. 1419–1433.

Okawa, T., Kubota, H. and Ishida, T. ((2007)) 'Simultaneous measurement of void fraction and fundamental bubble parameters in subcooled flow boiling', *Nuclear Engineering and Design*, 237(10), pp. 1016–1024. doi: 10.1016/j.nucengdes.2006.12.010.

Paul, D. D. and Abdel-Khalik, S. I. ((1983)) 'A statistical analysis of saturated nucleate boiling along a heated wire', *International Journal of Heat and Mass Transfer*, 26(4), pp. 509–519. doi: 10.1016/0017-9310(83)90002-9.

Peebles, F. N. and Garber, H. J. ((1953)) 'Studies on motion of gas bubbles in liquids', *Chemical Engineering Progress*, 49, pp. 88–97.

Perkins, A. S. and Westwater, J. W. ((1956)) 'Measurements of bubbles formed in boiling Methanol', *AIChE Journal*, 2(4), pp. 471–476. doi: 10.1002/aic.690020411.

Petkovsek, J. *et al.* ((2016)) 'IR thermographic investigation of nucleate pool boiling at high heat flux', *International Journal of Refrigeration*, 61, pp. 127–139. doi: 10.1016/j.ijrefrig.2015.10.018.

Phan, H. T. *et al.* ((2010)) 'A model to predict the effect of contact angle on the bubble departure diameter during heterogeneous boiling', *International Communications in Heat and Mass Transfer*. Elsevier Ltd, 37(8), pp. 964–969. doi: 10.1016/j.icheatmasstransfer.2010.06.024.

Phillips, B. A. ((2014)) *Experimental Investigation of Subcooled Flow Boiling Using Synchronized High Speed Video, Infrared Thermography, and Particle Image Velocimetry*. Massachusetts Institute of Technology.

Plesset, M. S. and Zwick, S. A. ((1954)) 'The growth of vapor bubbles in superheated liquids', *Journal of Applied Physics*, 25(4), pp. 493–500. doi: 10.1063/1.1721668.

Podowski, M. Z. and Podowski, R. M. ((2009)) 'Mechanistic multidimensional modeling of forced convection boiling heat transfer', *Science and Technology of Nuclear Installations*. doi: 10.1155/2009/387020.

Podowski, R. M. *et al.* ((1997)) 'A mechanistic model of the ebullition cycle in forced convection subcooled boiling.', in *Proceedings of 8th International Topical Meeting on Nuclear Reactor Thermal Hydraulics, NURETH-8, vol. 3*. Kyoto, Japan, pp. 1535–1542.

Prodanovic, V., Fraser, D. and Salcudean, M. ((2002)) 'On the transition from partial to fully developed subcooled flow boiling', *International Journal of Heat and Mass Transfer*, 45(24), pp. 4727–4738. doi: 10.1016/S0017-9310(02)00197-7.

Raad, T. E. D. and Myers, J. E. ((1971)) 'Nucleation Studies in Pool Boiling on Thin Plates Using Liquid Crystals', *AIChE Journal*, 17(5), pp. 1260–1261. doi: 10.1002/aic.690170543.

Ribatski, G., Saiz Jabardo, J. M. and da Silva, E. F. ((2008)) 'Modeling and experimental study of nucleate boiling on a vertical array of horizontal plain tubes', *Experimental Thermal and Fluid Science*, 32(8), pp. 1530–1537. doi: 10.1016/j.expthermflusci.2008.04.008.

Rohsenow, W. M. ((1952)) *A method of correlating heat transfer data for surface boiling of liquids*, Massachusetts Institute of Technology, Cambridge.

Rohsenow, W. M. ((1971)) 'Boiling', *Annual Reviews of Fluid Mechanics*, 3, pp. 211–236.

Ruckenstein, E. ((1961)) 'A physical model for nucleate boiling heat transfer from a horizontal surface.', *Bulletin of Institute Politehnica Bucuresti*, 23, pp. 79–88.

Saddy, M. and Jameson, G. J. ((1971)) 'Prediction of departure diameter and bubble frequency in nucleate boiling in uniformly superheated liquids', *International Journal of Heat and Mass Transfer*, 14(11), pp. 1771–1785. doi: 10.1016/0017-9310(71)90046-9.

Santo, M. De, Liguori, C. and Pietrosanto, A. ((2000)) 'Uncertainty Characterization in Image-Based Measurements : A Preliminary Discussion', *IEEE Transactions on Instrumentation and Measurement*, 49(5), pp. 1101–1107.

Sernas, V. and Hooper, F. C. ((1969)) 'The initial vapor bubble growth on a heated wall during nucleate boiling', *International Journal of Heat and Mass Transfer*, 12(12), pp. 1627–1639. doi: http://dx.doi.org/10.1016/0017-9310(69)90097-0.

Setoodeh, H. *et al.* ((2016)) 'Experimental Investigation of Subcooled Flow Boiling in an Inclined Channel with a Hot Spot', *Experimental Heat Transfer*, 29(6), pp. 741–758. doi: 10.1080/08916152.2015.1113214.

Sgheiza, J. E. and Myers, J. E. ((1985)) 'Behavior of nucleation sites in pool boiling', *AIChE Journal*, 31(10), pp. 1605–1613. doi: 10.1002/aic.690311004.

Shah, M. M. ((1984)) 'A correlation for heat transfer during subcooled boiling on a single tube with forced crossflow', *International Journal of Heat and Fluid Flow*, 5(1), pp. 13–20.

Shah, M. M. ((2005)) 'Improved General Correlation for Subcooled Boiling Heat Transfer During Flow Across Tubes and Tube Bundles', *HVAC&R Research*, 11(2), pp. 285–303.

Shah, M. M. ((2007)) 'A General Correlation for Heat Transfer During Saturated Boiling with Flow Across Tube Bundles', *HVAC&R Reseach*, 13(5), pp. 749–768.

Sheng, C. H. and Palm, B. ((2000)) 'The visualization of boiling in small diameter tubes', in *Proceedings of International Conference on Heat Transfer and Transport Phenomena in Microscale*. Banff, Canada, pp. 204–208.

Siedel, S., Cioulachtjian, S. and Bonjour, J. ((2008)) 'Experimental analysis of bubble growth, departure and interactions during pool boiling on artificial nucleation sites', *Experimental Thermal and Fluid Science*, 32(8), pp. 1504–1511. doi: 10.1016/j.expthermflusci.2008.04.004.

Singh, R. L., Saini, J. S. and Varma, H. K. ((1983)) 'Effect of crossflow in boiling heat transfer of water', *International Journal of Heat and Mass Transfer*, 26(12), pp. 1882–1885. doi: 10.1016/S0017-9310(83)80159-8.

Singh, R. L., Saini, J. S. and Varma, H. K. ((1985)) 'Effect of cross-flow on boiling heat transfer of refrigerant-12', *International Journal of Heat and Mass Transfer*, 28(2), pp. 512–514.

Situ, R. *et al.* ((2004)) 'Photographic study of bubble behaviors in forced convection subcooled boiling', *International Journal of Heat and Mass Transfer*, 47(17–18), pp. 3659–3667. doi: 10.1016/j.ijheatmasstransfer.2004.04.005.

Situ, R. *et al.* ((2005)) 'Bubble lift-off size in forced convective subcooled boiling flow', *International Journal of Heat and Mass Transfer*, 48(25–26), pp. 5536–5548. doi:

10.1016/j.ijheatmasstransfer.2005.06.031.

Situ, R. *et al.* ((2008)) 'Bubble departure frequency in forced convective subcooled boiling flow', *International Journal of Heat and Mass Transfer*. Elsevier Ltd, 51(25–26), pp. 6268–6282. doi: 10.1016/j.ijheatmasstransfer.2008.04.028.

Stephan, K. ((1992)) *Heat transfer in condensation and boiling*. Springer-Verlag, Berlin.

Sugrue, R. and Buongiorno, J. ((2016)) 'A modified force-balance model for prediction of bubble departure diameter in subcooled flow boiling', *Nuclear Engineering and Design*. Elsevier B.V., 305, pp. 717–722. doi: 10.1016/j.nucengdes.2016.04.017.

Sugrue, R. M. ((2012)) *The Effects of Orientation Angle , Subcooling , Heat Flux , Mass Flux, and Pressure on Bubble Growth and Detachment in Subcooled Flow Boiling*. Massachusetts Institute of Technology. doi: 10.1016/j.nucengdes.2014.08.009.

Sung-Ho, K. and El-Genk, M. S. ((1989)) 'Heat transfer experiments for low flow of water in rod bundles', *International Journal of Heat and Mass Transfer*, 32(7), pp. 1321–1336. doi: 10.1016/0017-9310(89)90032-X.

Sultan, M. and Judd, R. L. ((1983)) 'Interaction of the Nucleation Phenomena at Adjacent Sites in Nucleate Boiling', *Journal of Heat Transfer-Transactions of the Asme*, 105(February 1983), pp. 3–9.

Swain, A. and Das, M. K. ((2017)) 'Flow boiling of distilled water over plain tube bundle with uniform and varying heat flux along the height of the tube bundle', *Experimental Thermal and Fluid Science*. Elsevier Inc., 82, pp. 222–230. doi: 10.1016/j.expthermflusci.2016.11.022.

Thorncroft, G. E., Klausner, J. F. and Mei, R. ((1998)) 'An experimental investigation of bubble growth and detachment in vertical upflow and downflow boiling', *International Journal of Heat and Mass Transfer*, 41(23), pp. 3857–3871. doi: 10.1016/S0017-9310(98)00092-1.

Thorncroft, G. E., Klausner, J. F. and Mei, R. ((2001)) 'Bubble forces and detachment models', *Multiphase Science and Technology*, 13(3–4), pp. 35–76.

Tolubinsky, V. I. and Kostanchuk, D. M. ((1970)) 'Vapor bubbles growth rate and heat transfer intensity at subcooled water boiling', in *Fourth Internationa Heat Transfer Conference, Paris - Versailles*, p. B2.8.

Ünal, H. C. ((1976)) 'Maximum bubble diameter, maximum bubble-growth time and bubble-growth rate during the subcooled nucleate flow boiling of water up to 17.7 MN/m2', *International Journal of Heat and Mass Transfer*, 19(6), pp. 643–649. doi: 10.1016/0017-9310(76)90047-8.

Del Valle, V. H. and Kenning, D. B. R. ((1985)) 'Subcooled flow boiling at high heat flux', *International Journal of Heat and Mass Transfer*, 28(10), pp. 1907–1920. doi: 10.1016/0017-9310(85)90213-3.

Wang, H., Peng, X. F. and Christopher, D. M. ((2005)) 'Dynamic bubble behaviour during microscale subcooled boiling', *Chinese Physics Letters*, 22(11), pp. 2881–2884. doi: 10.1088/0256-307X/22/11/043.

Weisman, J. ((1959)) 'Heat Transfer to Water Flowing Parallel to Tube Bundles', *Nuclear Science and Engineering, Letters to the Editor*, (6), pp. 78–79.

Whitaker, S. ((1972)) 'Forced Convection Heat Transfer Correlations for Flow In Pipes, Past Flat Plates, Single Cylinders, Single Spheres, and for Flow in Packed Beds and Tube Bundles', *AIChE Journal*, 18(2), pp. 361–371.

Williams, D. D. and Mesler, R. B. ((1967)) 'The effect of surface orientation on delay time of bubbles from artificial sites during nucleate boiling', *AIChE Journal*, 13(5), pp. 1020–1024.

Yang, L. X., Guo, A. and Liu, D. ((2016)) 'Experimental Investigation of Subcooled Vertical Upward Flow Boiling in a Narrow Rectangular Channel', *Experimental Heat Transfer*, 29(2), pp. 221–243. doi: 10.1080/08916152.2014.973978.

Yeoh, G. H. *et al.* ((2011)) 'Modeling Vertical Subcooled Boiling Flows at Low Pressures', in *Journal of ASTM International*, JAI103374. doi: 10.1520/JAI103374.

Yeoh, G. H. and Tu, J. Y. ((2005)) 'A unified model considering force balances for departing vapour bubbles and population balance in subcooled boiling flow', *Nuclear Engineering and Design*, 235(10–12), pp. 1251–1265. doi: 10.1016/j.nucengdes.2005.02.015.

Yoo, J., Estrada-Perez, C. E. and Hassan, Y. A. ((2016)) 'Experimental study on bubble dynamics and wall heat transfer arising from a single nucleation site at subcooled flow boiling conditions - Part 2: Data analysis on sliding bubble characteristics and associated wall heat transfer', *International Journal of Multiphase Flow*. Elsevier Ltd, 84, pp. 292–314. doi: 10.1016/j.ijmultiphaseflow.2016.04.019.

Yuan, D. W. *et al.* ((2011)) 'Bubble behavior of high subcooling flow boiling at different system pressure in vertical narrow channel', *Applied Thermal Engineering*. Elsevier Ltd, 31(16), pp. 3512–3520. doi: 10.1016/j.applthermaleng.2011.07.004.

Yun, B. *et al.* ((2010)) 'Prediction of a subcooled boiling flow with mechanistic wall boiling and bubble size models', in *Proceedings of Computational Fluid dynamics for Nuclear Reactor Safety Applications CFD4NRS-3*. Bethesda, Maryland, USA.

Zeitoun, O. and Shoukri, M. ((1996)) 'Bubble behavior and mean diameter in subcooled flow boiling', *Journal of Heat Transfer*, 118(1), pp. 110–116. doi: 10.1115/1.2824023.

Zeng, L. Z., Klausner, J. F. and Mei, R. ((1993)) 'A unified model for the prediction of bubble detachment diameters in boiling systems—I. Pool boiling', *International Journal of Heat and Mass Transfer*, 36(9), pp. 2261–2270.

Zhang, K. *et al.* ((2017)) 'Experimental investigations on single-phase convection and steam-water two-phase flow boiling in a vertical rod bundle', *Experimental Thermal and Fluid Science*, 80, pp. 147–154. doi: 10.1016/j.expthermflusci.2016.08.018.

Zuber, N. ((1959)) *Hydrodynamic Aspects Of Boiling Heat Transfer*. University of California, Los Angeles, California. doi: 10.2172/4175511.

Zuber, N. ((1963)) 'Nucleate boiling. The region of isolated bubbles and the similarity with

natural convection', *International Journal of Heat and Mass Transfer*, 6(1), pp. 53–78. doi: 10.1016/0017-9310(63)90029-2.